ΕΘΝΙΚΟ ΜΕΤΣΟΒΙΟ ΠΟΛΥΤΕΧΝΕΙΟ

ΔΙΑΤΜΗΜΑΤΙΚΟ-ΔΙΕΠΙΣΤΗΜΟΝΙΚΟ
ΠΡΟΓΡΑΜΜΑ ΜΕΤΑΠΤΥΧΑΙΚΩΝ ΣΠΟΥΔΩΝ
«ΕΠΙΣΤΗΜΗ & ΤΕΧΝΟΛΟΓΙΑ ΥΔΑΤΙΚΩΝ ΠΟΡΩΝ»

ΜΑΘΗΜΑΤΙΚΗ ΠΡΟΣΟΜΟΙΩΣΗ ΤΗΣ ΣΥΜΠΕΡΙΦΟΡΑΣ ΠΕΤΡΕΛΑΙΟΚΗΛΙΔΩΝ

Γεωργία Σ. Παπαδονικολάκη

«ΕΠΙΣΤΗΜΗ & ΤΕΧΝΟΛΟΓΙΑ ΥΔΑΤΙΚΩΝ ΠΟΡΩΝ»

Επιβλέπων: Α. Ι. Στάμου, Καθηγητής Ε.Μ.Π.

Αθήνα, Δεκέμβριος 2013

NATIONAL TECHNICAL UNIVERSITY OF ATHENS

INTERDEPARTMENTAL PROGRAM OF
POSTGRADUATE STUDIES IN
«WATER RESOURCES SCIENCE & TECHNOLOGY»

MATHEMATICAL MODELING OF THE BEHAVIOUR OF OIL SPILLS

Georgia S. Papadonikolaki

«WATER RESOURCES SCIENCE & TECHNOLOGY »

Supervisor: A. I. Stamou, Professor N.T.U.A.

Athens, December 2013

CONTENTS

ACKNOWLEDGEMENTS

This work has been carried out at the Department of Water Resources and Environmental Engineering of the School of Civil Engineering of the National Technical University of Athens under the supervision of Professor Anastasios I. Stamou.

It is my pleasure to acknowledge my supervisor Professor Anastasios I. Stamou for giving me the opportunity to work on this topic as well as for his guidance and comments. Helpful discussions and comments by Professor George Christodoulou and Assistant Professor Vicky Tsoukala are gratefully acknowledged.

I would also like to thank my colleagues, Anthi Gkesouli, Panayiotis Makatounis and Yiannis Nikiforakis, for their useful discussions, support and precious help during the research period.

I offer very special debt of deep gratitude to my parents and brother for their unceasing sacrifices and encouragement.

The present study, which was carried out within the framework of the Program of Postgraduate Studies (IPPS) in Water Resources Science and Technology (WRST), was founded by the State Scholarship Foundation (I.K.Y.).

Η ολοκλήρωση της εργασίας αυτής έγινε στο πλαίσιο της υλοποίησης του μεταπτυχιακού προγράμματος το οποίο συγχρηματοδοτήθηκε μέσω της Πράξης "**Πρόγραμμα χορήγησης υποτροφιών Ι.Κ.Υ. με διαδικασία εξατομικευμένης αξιολόγησης ακαδ. έτους 2011-2012"** από πόρους του ΕΠ "Εκπαίδευση και Δια Βίου Μάθηση" του Ευρωπαϊκού Κοινωνικού Ταμείου (Ε.Κ.Τ.) και του ΕΣΠΑ, του 2007-2013".

ABSTRACT

Oil slicks have severe environmental and ecological impacts on sea and coastal ecosystems. When the oil is leaked into the seawater it spreads forming a spill and a series of physical, chemical and biological processes take place (weathering processes), such as transport, dispersion, dissolution, evaporation, emulsification, sedimentation, photo-oxidation and biodegradation. Various mathematical models have been developed in order to describe this behaviour and predict the oil spill trajectory after a sea accident, for operational actions to avoid or mitigate the pollution impacts.

In the present study, a physics-based hydrodynamic model (HYM) was employed to calculate the sea currents that determine the trajectory of an oil spill, the time needed to reach the coast and its mass evolution with time. An Oil Spill Model (OSM) was developed in order to predict the oil spill behaviour once an oil spill accident happens. Apart from advection, the weathering processes taken into account were dispersion, dissolution, evaporation and emulsification, employing empirical models frequently used in the literature. The particle tracking method was also employed to model the transport of the spill; the oil mass was divided into a large number of particles that moved individually in random directions.

The present methodology was applied in the case of Saronicos Gulf; the selection was based on the high navigational traffic of the gulf and the fact that it includes the biggest and busiest port in Greece, located in the vicinity of Athens, i.e. the Port of Piraeus. The four most probable accident locations in the gulf were chosen and 49 wind scenarios were examined, including eight wind directions, six wind magnitude categories and the calm condition.

Generally, the results of the OSM are reasonable; the areas most at risk are the coastal areas near Piraeus Port, the north-western coasts of the island of Aegina, and north-western end of the Gulf near the town of Isthmia. Indicative results of the time needed for a spill, occurred in the chosen accident locations, to reach the coast, show that in the most probable cases of a spill accident, retention of the impacts of the spill is feasible if the alarming is immediate.

ΕΚΤΕΤΑΜΕΝΗ ΠΕΡΙΛΗΨΗ

1. ΕΙΣΑΓΩΓΗ

Τα ατυχήματα πετρελαιοκηλίδων έχουν σοβαρές επιπτώσεις στο θαλάσσιο αλλά και το ανθρωπογενές περιβάλλον. Σε περίπτωση θαλάσσιου ατυχήματος διαρροής, το πετρέλαιο εξαπλώνεται διαμορφώνοντας μια κηλίδα ενώ στη συνέχεια ενεργοποιείται ένα πλήθος διεργασιών, φυσικών, χημικών και βιολογικών, οι οποίες συμβάλλουν στην "παλαίωση" του (weathering processes) και είναι καθοριστικές για την εξέλιξη της πετρελαιοκηλίδας. Τέτοιες διεργασίες είναι, εκτός από τη μεταφορά, η διασπορά, η διάλυση, η εξάτμιση, η γαλακτωματοποίηση, η καθίζηση, η οξείδωση και η βιοδιάσπαση. Κάποιες από αυτές τις διεργασίες συμβάλλουν στη συρρίκνωση της πετρελαιοκηλίδας ενώ κάποιες προκαλούν αύξηση του όγκου της.

Διάφορα μαθηματικά μοντέλα έχουν αναπτυχθεί προκειμένου να περιγράψουν τη συμπεριφορά και να προβλέψουν την τροχιά μιας πετρελαιοκηλίδας αλλά και τις πιθανές επιπτώσεις της σε περίπτωση ατυχήματος. Η πλειονότητα αυτών των μαθηματικών μοντέλων αναπτύσσεται για διαχειριστικούς λόγους, προκειμένου δηλαδή να παρέχουν τις απαραίτητες πληροφορίες στις αρμόδιες αρχές για τον έγκαιρο καθαρισμό της πετρελαιοκηλίδας σε περίπτωση διαρροής.

Στην παρούσα εργασία έγινε δόμηση ενός διδιάστατου (2D) μαθηματικού μοντέλου πρόβλεψης της συμπεριφοράς πετρελαιοκηλίδας (Oil Spill Model, OSM) σε γλώσσα προγραμματισμού FORTRAN. Για τον υπολογισμό του πεδίου ροής έγινε χρήση του υδροδυναμικού μοντέλου FLOW-3DL (Stamou et al., 1999; 2007a; 2007b) το οποίο τροποποιήθηκε κατάλληλα προκειμένου να εξαχθούν οι ταχύτητες των επιφανειακών ρευμάτων λόγω ανεμογενούς κυκλοφορίας. Τα δεδομένα αυτά εισήχθησαν στο OSM το οποίο αναπτύχθηκε για να υπολογίζει την τροχιά αλλά και την εξέλιξη της μάζας της πετρελαιοκηλίδας, λαμβάνοντας υπόψη τη μέθοδο παρακολούθησης της κίνησης των σωματιδίων (particle tracking method), για την πρόβλεψη της κίνησης της πετρελαιοκηλίδας, αλλά και τις διάφορες διεργασίες που επιδρούν στη μάζα της. Το παρόν OSM υπολογίζει επίσης το χρονικό διάστημα που απαιτείται προκειμένου η πετρελαιοκηλίδα να φτάσει στην ακτή. Τέλος, έγινε εφαρμογή των μοντέλων στην περίπτωση του Σαρωνικού Κόλπου, ο οποίος επελέγη καθώς περιλαμβάνει το πιο μεγάλο λιμάνι της χώρας, δηλαδή το Λιμάνι του Πειραιά.

2. ΜΕΘΟΔΟΛΟΓΙΑ

2.1. Εισαγωγικά

Τα μοντέλα πετρελαιοκηλίδας (Oil Spill Models, OSM) προβλέπουν τη συμπεριφορά μιας πετρελαιοκηλίδας (μεταφορά, διασπορά και φυσικές, βιολογικές και χημικές διεργασίες) χρησιμοποιώντας ως δεδομένα εισόδου μετεωρολογικά στοιχεία και υδροδυναμικούς υπολογισμούς ή δεδομένα. Συνήθως το υδροδυναμικό πεδίο αναπαράγεται από κάποιο υδροδυναμικό μοντέλο (hydrodynamic model, HYM) και εισάγεται στους υπολογισμούς του μοντέλου πρόβλεψης της συμπεριφοράς της πετρελαιοκηλίδας. Στην παρούσα εργασία, ο υπολογισμός των ταχυτήτων των θαλάσσιων ρευμάτων, λόγω ανεμογενούς κυκλοφορίας, έγινε με χρήση του υδροδυναμικού μοντέλου FLOW3DL (Stamou et al., 1999a; 1999b; 2007). Στην συνέχεια τα αποτελέσματα του HYM εισήχθησαν στο OSM προκειμένου να υπολογιστεί η τροχιά και η γενικότερη συμπεριφορά και "τύχη" της πετρελαιοκηλίδας.

2.2. Το υδροδυναμικό μοντέλο FLOW-3DL

2.2.1. Εισαγωγή

Το μαθηματικό μοντέλο FLOW-3DL (Stamou et al., 1999; 2007a; 2007b) έχει δομηθεί στο Υπολογιστικό Κέντρο του Εργαστηρίου Εφαρμοσμένης Υδραυλικής της Σχολής Πολιτικών Μηχανικών του ΕΜΠ με την επιστημονική ευθύνη του Καθηγητή Αναστάσιου Ι. Στάμου. Είναι ένας κώδικας γραμμένος σε γλώσσα προγραμματισμού FORTRAN και έχει τη δυνατότητα να προσομοιώνει την τρισδιάστατη υδροδυναμική συμπεριφορά και τις βασικές διεργασίες (μεταφορά, διάχυση, φυσικοχημικές και βιολογικές αντιδράσεις), οι οποίες καθορίζουν την ποιότητα των νερών στους υδάτινους αποδέκτες.

2.2.2. Διαφορικές εξισώσεις πεδίου ροής

Οι θεμελιώδεις εξισώσεις που επιλύει το μοντέλο FLOW-3DL για τον υπολογισμό του πεδίου ροής είναι οι τρισδιάστατες διαφορικές εξισώσεις συνέχειας και ποσότητας κίνησης σε μη μόνιμη κατάσταση, διατυπωμένες για στρώματα σταθερού πάχους, στα οποία διαιρείται το εξεταζόμενο πεδίο. Θεωρώντας σταθερές διαπερατές διεπιφάνειες μεταξύ των στρωμάτων, οι εξισώσεις του μοντέλου ολοκληρώνονται κατά την κατακόρυφη διεύθυνση στο βάθος h, που αντιστοιχεί σε ένα υπολογιστικό στρώμα με το ίδιο πάχος, και επιλύονται με τη μέθοδο των πεπερασμένων διαφορών.

Για την κατανομή της πίεσης γίνονται οι ακόλουθες παραδοχές:

(i) η κατανομή της πίεσης είναι υδροστατική,
(ii) ισχύει η προσέγγιση Boussinesq, και
(iii) η πίεση στην επιφάνεια είναι ίση με την ατμοσφαιρική (σχετική πίεση ίση με μηδέν).

Οι μεταβλητές του υδροδυναμικού μοντέλου είναι:

(i) οι μέσες κατά βάθος συνιστώσες της ταχύτητας u, v και w [L/T] κάθε στρώματος κατά τους άξονες x, y και z, αντίστοιχα, ενός καρτεσιανού συστήματος αξόνων, και
(ii) η ανύψωση της ελεύθερης επιφάνειας, ζ [L].

Ο άξονας z θεωρείται θετικός πάνω από τη στάθμη ηρεμίας της ελεύθερης επιφάνειας. Οι εξισώσεις συνέχειας και ποσότητας κίνησης γράφονται ως εξής:

Εξίσωση συνέχειας

$$\frac{\partial u}{\partial x}+\frac{\partial v}{\partial y}+\frac{\partial w}{\partial z}=0 \tag{1}$$

Εξισώσεις ποσότητας κίνησης

Κατά τη διεύθυνση x

$$\frac{\partial u}{\partial t}+u\frac{\partial u}{\partial x}+v\frac{\partial u}{\partial y}+w\frac{\partial u}{\partial z}=fv-\frac{1}{\rho}\frac{\partial p}{\partial x}+\frac{\partial}{\partial x}\left(\nu_h\frac{\partial u}{\partial x}\right)+\frac{\partial}{\partial y}\left(\nu_h\frac{\partial u}{\partial y}\right)+\frac{\partial}{\partial z}\left(\nu_v\frac{\partial u}{\partial z}\right) \tag{2}$$

Κατά τη διεύθυνση y

$$\frac{\partial v}{\partial t}+u\frac{\partial v}{\partial x}+v\frac{\partial v}{\partial y}+w\frac{\partial v}{\partial z}=-fu-\frac{1}{\rho}\frac{\partial p}{\partial y}+\frac{\partial}{\partial x}\left(\nu_h\frac{\partial v}{\partial x}\right)+\frac{\partial}{\partial y}\left(\nu_h\frac{\partial v}{\partial y}\right)+\frac{\partial}{\partial z}\left(\nu_v\frac{\partial v}{\partial z}\right) \tag{3}$$

Κατά τη διεύθυνση z

$$\frac{\partial p}{\partial z}=-\rho g \tag{4}$$

όπου: t [T] είναι ο χρόνος,
u, v και w [L/T] είναι οι συνιστώσες της ταχύτητας κατά τις διευθύνσεις x, y και z, αντίστοιχα,
p [F/A] είναι η πίεση,
v_h και v_v [L^2/T] είναι ο οριζόντιος και ο κατακόρυφος συντελεστής τυρβώδους συνεκτικότητας, αντίστοιχα,
f είναι η παράμετρος Coriolis,
g [L/T^2] είναι η επιτάχυνση της βαρύτητας και
ρ [M/L^3] είναι η πυκνότητα του νερού.

Η υπολογιστική διαδικασία είναι η ακόλουθη:
(i) Για δεδομένη κατά βάθος κατανομή της πυκνότητας, προσδιορίζεται η πίεση p χρησιμοποιώντας την εξίσωση (4).
(ii) Στη συνέχεια υπολογίζονται οι οριζόντιες συνιστώσες της ταχύτητας (u και v) από τις εξισώσεις (2) και (3).
(iii) Οι κάθετες ταχύτητες (w) υπολογίζονται από την εξίσωση συνέχειας (1) για κάθε στρώμα αρχίζοντας από τον πυθμένα, όπου ισχύει η οριακή συνθήκη w = 0.

Στην ελεύθερη επιφάνεια, η εξίσωση συνέχειας (1) γράφεται ως μια γραμμικοποιημένη οριακή κινηματική συνθήκη για τον προσδιορισμό της ανύψωσης της ελεύθερης επιφάνειας:

$$\frac{\partial \zeta}{\partial t} + \frac{\partial \zeta}{\partial t} u_\zeta + \frac{\partial \zeta}{\partial t} v_\zeta = w_\zeta \qquad (5)$$

όπου ο δείκτης «ζ» συμβολίζει τις τιμές των ταχυτήτων στην ελεύθερη επιφάνεια.

Στην παρούσα εργασία το υδροδυναμικό μοντέλο τροποποιήθηκε έτσι ώστε να εφαρμοστεί σε ένα μεμονωμένο στρώμα προκειμένου να γίνει ο υπολογισμός των μέσων κατά βάθος ταχυτήτων. Στη συνέχεια, οι οριζόντιες ταχύτητες των επιφανειακών ρευμάτων, στις διευθύνσεις x και y, υπολογίζονται από τις εξισώσεις (6) και (7) σύμφωνα με τον Koutitas (1985):

$$U_{surf} = 1.5\,u + 0.03\,U_{wx} \qquad (6)$$

$$V_{surf} = 1.5\,v + 0.03\,U_{wy} \qquad (7)$$

όπου
U_{surf} και V_{surf} είναι οι συνιστώσες της ταχύτητας των επιφανειακών ρευμάτων (m s^{-1}), κατά τις x και y κατευθύνσεις, αντίστοιχα, και
U_{wx} και U_{wy} είναι οι συνιστώσες της ταχύτητας του ανέμου (m s^{-1}), κατά τις x και y κατευθύνσεις, αντίστοιχα.

2.3. Το μοντέλο συμπεριφοράς πετρελαιοκηλίδας OSM

2.3.1. Εισαγωγή

Το παρόν μοντέλο συμπεριφοράς πετρελαιοκηλίδας (Oil Spill Model, OSM) αναπτύχθηκε για να προβλέπει τις κινήσεις των σωματιδίων του πετρελαίου, επομένως την τροχιά της πετρελαιοκηλίδας, στις δύο διαστάσεις (2D προσέγγιση), λαμβάνοντας υπόψη τις διεργασίες παλαίωσης του πετρελαίου (weathering processes) οι οποίες χρησιμοποιούνται από την πλειοψηφία των μαθηματικών μοντέλων συμπεριφοράς πετρελαιοκηλίδας που συναντώνται στη βιβλιογραφία (για παράδειγμα από τους Zadeh and Hejazi, 2012; Chao et al., 2001). Οι διεργασίες αυτές είναι η εξάπλωση, η εξάτμιση, η διασπορά, η διάλυση και η

γαλακτωματοποίηση και προσεγγίζονται με μαθηματικά μοντέλα που ελήφθησαν από τη βιβλιογραφία. Η μετάθεση και η διασπορά της πετρελαιοκηλίδας προσεγγίζονται με τη μέθοδο παρακολούθησης της κίνησης των σωματιδίων (particle tracking method). Η συνολική μάζα της πετρελαιοκηλίδας διαχωρίζεται σε συγκεκριμένο αριθμό σωματιδίων τα οποία μετατοπίζονται στο χώρο με τυχαίο τρόπο (random walk procedure) και ανεξάρτητα μεταξύ τους.

Η έκλυση του πετρελαίου θεωρείται στιγμιαία. Επιπλέον, οι υπολογισμοί αφορούν στο διάστημα που το κύριο σώμα της πετρελαιοκηλίδας βρίσκεται μέσα στο νερό, καθώς από τη στιγμή που το πετρέλαιο συσσωρεύεται στην ακτή πολλές από τις διεργασίες που το επηρεάζουν, όπως η εξάτμιση, διαφοροποιούνται. Για το λόγο αυτό, οι υπολογισμοί σταματούν μετά από χρόνο T*, ο οποίος αντιστοιχεί στη χρονική στιγμή που το 10% των σωματιδίων του πετρελαίου έχει φτάσει στην ακτή ή έχει εξέλθει από το ανοικτό όριο της περιοχής μελέτης. Το κριτήριο αυτό επιτρέπει την εκτίμηση των χρόνων εκείνων που είναι κρίσιμοι και πρέπει να είναι γνωστοί για την έγκαιρη αντιμετώπιση και πρόληψη των συνεπειών σε περίπτωση διαρροής πετρελαίου.

Τα δεδομένα εισόδου του μοντέλου είναι (i) η ποσότητα (όγκος) και οι ιδιότητες (πυκνότητα) του πετρελαίου που έχει διαρρεύσει, (ii) οι συνιστώσες της ταχύτητας των επιφανειακών ρευμάτων, (iii) τα ανεμολογικά χαρακτηριστικά, (iv) τα χαρακτηριστικά του θαλασσινού νερού (πυκνότητα και θερμοκρασία), και (v) οι θέσεις των ατυχημάτων.

2.3.2. Περιγραφή του μοντέλου OSM

Στο παρόν μοντέλο συμπεριφοράς πετρελαιοκηλίδας (OSM) οι υδροδυναμικοί υπολογισμοί, που πραγματοποιούνται με χρήση του μοντέλου FLOW-3DL, δε γίνονται παράλληλα αλλά προηγούνται των υπόλοιπων υπολογισμών. Αφού ολοκληρωθεί ο υπολογισμός των μόνιμων συνθηκών του πεδίου ροής για συγκεκριμένη πνοή ανέμου και υπολογιστούν οι μέσες κατά βάθος ταχύτητες, εξάγονται οι ταχύτητες των επιφανειακών ρευμάτων και εισάγονται στο OSM. Το OSM χρησιμοποιεί το ίδιο υπολογιστικό πλέγμα με το υδροδυναμικό μοντέλο. Κάθε κελί του πλέγματος χαρακτηρίζεται από έναν αριθμό, N_i, με χρήση του οποίο καταμετράται ο αριθμός σωματιδίων πετρελαίου που κινούνται στα όρια του, σε κάθε χρονικό βήμα. Η υπολογιστική διαδικασία είναι η ακόλουθη:

Βήμα 1: Εισάγονται οι περιβαλλοντικοί παράγοντες, δηλαδή (α) η ταχύτητα του ανέμου, (β) η θερμοκρασία του αέρα, (γ) η πυκνότητα και κινηματική συνεκτικότητα του θαλασσινού νερού. Εισάγονται επίσης, όπως προαναφέρθηκε, οι ταχύτητες των επιφανειακών θαλάσσιων ρευμάτων στις x και y διευθύνσεις, οι οποίες υπολογίζονται από τις εξισώσεις (6) και (7), αντίστοιχα.

Βήμα 2: Εισάγονται τα χαρακτηριστικά της αρχικής πετρελαιοκηλίδας, δηλαδή ο όγκος του πετρελαίου που διέρρευσε (V_o), η πυκνότητά του (ρ_o) και η θέση του ατυχήματος (X,Y). Στο βήμα αυτό επιλέγεται επίσης ο αριθμός, N, των σωματιδίων στον οποίο θα διαχωριστεί η πετρελαιοκηλίδα.

Βήμα 3: Γίνεται υπολογισμός του νέου όγκου , V_{oil}, της πετρελαιοκηλίδας και της πυκνότητας, ρ_{oil}, του πετρελαίου, λαμβάνοντας υπόψη τις διεργασίες της εξάπλωσης, της εξάτμισης, της διάλυσης και της γαλακτωματοποίησης, με την ακόλουθη σειρά:

- Υπολογίζεται η νέα επιφάνεια, A_s [m^2], της πετρελαιοκηλίδας με χρήση της εξίσωσης (8) των Lehr et al. (1984):

$$A_s = \frac{\pi}{4} l_{min}\, l_{max} \;\; \text{ή} \;\; A_s = 2270\left(\frac{\Delta\rho}{\rho_{oil}}\right)^{2/3} V_o^{2/3}\, t^{1/2} + 40\left(\frac{\Delta\rho}{\rho_{oil}}\right)^{1/3} V_o^{1/3}\, U_w^{4/3}\, t \qquad (8)$$

όπου $l_{min} = 53.76\left(\frac{\Delta\rho}{\rho_{oil}}\right)^{1/3} V_o^{1/3} t^{1/4}$ και $l_{max} = l_{min} + 0.95\, U_w^{4/3} t^{3/4}$ (9)

και
l_{min} και l_{max} είναι τα μήκη του μικρού και μεγάλου άξονα της πετρελαιοκηλίδας [m], αντίστοιχα,
$\Delta\rho = \rho_w - \rho_{oil}$, όπου ρ_w και ρ_{oil} είναι οι πυκνότητες του θαλασσινού νερού και του πετρελαίου, αντίστοιχα [kg m^{-3}],
V_o είναι ο αρχικός όγκος της πετρελαιοκηλίδας [barrels],
U_w είναι η ταχύτητα του ανέμου [knots] και
t είναι ο χρόνος [min].

- Υπολογίζεται το κλάσμα, F_e [-], του πετρελαίου που εξατμίζεται, με χρήση της εξίσωσης (10) του Mackay (1980):

$$F_e = \left(\frac{T}{BT_G}\right) \ln\left(\theta\left(\frac{BT_G}{T}\right)\exp\left(A - \frac{BT_o}{T}\right) + 1\right) \quad (10)$$

όπου
T είναι η θερμοκρασία του αέρα, [K],
A και B είναι σταθερές (Bobra, 1992),
T_o είναι το αρχικό σημείο βρασμού που αντιστοιχεί σε F_e=0, [K],
T_G είναι η κλίση της καμπύλης απόσταξης του πετρελαίου, [K],
θ είναι η έκθεση στην εξάτμιση, δηλαδή ο όγκος του εκτεθειμένου αέριου κλάσματος τη χρονική στιγμή t, ο οποίος υπολογίζεται από την εξίσωση (11):

$$\theta = \frac{K_2 A_S t}{V_o} \quad (11)$$

όπου
t είναι ο χρόνος, [s],
V_o είναι ο αρχικός όγκος της πετρελαιοκηλίδας, [m^3],
K_2 είναι ο συντελεστής μεταφοράς μάζας λόγω εξάτμισης [m s^{-1}] ο οποίος υπολογίζεται από την εξίσωση (12) (MacKay and Matsugu, 1973):

$$K_2 = 0.0107\, U_w^{0.78} D_s^{-0.11} S_c^{-0.67} \quad (12)$$

όπου
U_w είναι η ταχύτητα του ανέμου, [m s^{-1}],
D_s είναι η διάμετρος της κηλίδας, [m],
S_c είναι ο αριθμός Schmidt που αντιπροσωπεύει την επιφανειακή τραχύτητα και λαμβάνεται ίσος με 2.7, [-], (Zadeh and Hejazi, 2012).

- Υπολογίζεται ο ρυθμός διάλυσης, S_D, από την εξίσωση (13) των Cohen et al. (1980):

$$S_D = K_D A_s S \quad (13)$$

όπου
S_D είναι ο συνολικός ρυθμός διάλυσης της πετρελαιοκηλίδας [gr s^{-1}],
K_D είναι ο συντελεστής μεταφοράς μάζας λόγω διάλυσης, [συνήθως $3\cdot10^{-6}$ m s^{-1}],

S είναι η διαλυτότητα στο νερό που δίνεται από την εξίσωση (14) (Mackay, 1980):

$$S = S_o e^{-\alpha t} \tag{14}$$

όπου
S_o είναι η διαλυτότητα του φρέσκου αργού πετρελαίου, [gr s^{-1}],
α είναι ο συντελεστής φθοράς, [$days^{-1}$] και
t είναι ο χρόνος, [days].

- Υπολογίζεται το κλάσμα που, F_w, που έχει γαλακτωματοποιηθεί με χρήση της εξίσωσης (15) του Mackay (1980):

$$F_w = K_b \left(1 - \exp\left(\frac{-K_a}{K_b} (U_w + 1)^2 t \right) \right) \tag{15}$$

όπου
F_w είναι το κλάσμα του περιεχόμενου νερού, [-],
U_w είναι η ταχύτητα του ανέμου, [m s^{-1}],
t είναι ο χρόνος, [s],
K_a είναι σταθερά της οποία η τιμή εξαρτάται από την ταχύτητα του ανέμου,
K_b είναι η σταθερά ιξώδους του γαλακτώματος, [-], η οποία λαμβάνεται ίση με 0.7 για το αργό και βαρύ πετρέλαιο και 0.25 για το πετρέλαιο θέρμανσης (Zadeh and Hejazi, 2012).
Οι τιμές που χρησιμοποιήθηκαν στην παρούσα εργασία έχουν προταθεί από τον Reed (1989), δηλαδή K_a =2.0 10^{-6} sec^{-1} και K_b =0.7.

Ο νέος όγκος, V_{oil}, και η πυκνότητα, ρ_{oil}, του πετρελαίου υπολογίζονται σε κάθε χρονικό βήμα από τις εξισώσεις (16) και (17) των Buchanan και Hurford (1988) και Guo και Wang (2009), αντίστοιχα.

$$\rho_{oil} = \rho_w F_w + (1 - F_w)(\rho_o + K_b F_e) \tag{16}$$

$$V_{oil} = \frac{V_o (1 - (F_e + F_d))}{1 - F_w} \tag{17}$$

όπου
ρ_{oil} είναι η νέα πυκνότητα του πετρελαίου, [kg m^{-3}],
ρ_w είναι η πυκνότητα του θαλασσινού νερού, [kg m^{-3}],
ρ_o είναι η αρχική πυκνότητα του πετρελαίου που διέρρευσε, [kg m^{-3}],
V_o είναι ο αρχικός όγκος της πετρελαιοκηλίδας [m^3] και
F_d είναι το κλάσμα του πετρελαίου που έχει υποστεί διάλυση, [-].

Βήμα 4: Υπολογίζεται η νέα συνολική μάζα της πετρελαιοκηλίδας, M_{oil}, σε κάθε χρονικό βήμα με την εισαγωγή των ανανεωμένων τιμών του όγκου, V_{oil}, και της πυκνότητας, ρ_{oil}, του πετρελαίου στην εξίσωση (18):

$$M_{oil} = V_{oil} \cdot \rho_{oil} \tag{18}$$

Βήμα 5: Η νέα συνολική μάζα της πετρελαιοκηλίδας, M_{oil}, χωρίζεται σε N αριθμό σωματιδίων ίσης μάζας τα οποία μετακινούνται και διασπείρονται στο υγρό πεδίο ανεξάρτητα μεταξύ τους. Η μάζα κάθε σωματιδίου, M_l, μεταβάλλεται στο χρόνο λόγω της επίδρασης των διεργασιών παλαίωσης του πετρελαίου. Ο αριθμός σωματιδίων θεωρείται σταθερός κατά τη διάρκεια της υπολογιστικής διαδικασίας. Στη συγκεκριμένη εργασία ελήφθη ίσος

με N=10,000 σωματίδια. Η μάζα κάθε σωματιδίου, σε κάθε χρονικό βήμα, υπολογίζεται από την εξίσωση (19):

$$M_i = M_{oil} / N \tag{19}$$

Βήμα 6: Υπολογίζεται, από την εξίσωση (20), η μετατόπιση κάθε σωματιδίου (DS_X και DS_Y), σε κάθε χρονικό βήμα, ως το άθροισμα των αποστάσεων που διανύει το καθένα λόγω μεταφοράς ($DS_{X,adv}$ και $DS_{Y,adv}$) και διασποράς ($DS_{X,disp}$ και $DS_{Y,disp}$):

και
$$\begin{aligned} DS_X &= DS_{X,adv} + DS_{X,disp} = U_{surf}\, Dt + DS\cos\varphi \\ DS_Y &= DS_{Y,adv} + DS_{Y,disp} = V_{surf}\, Dt + DS\sin\varphi \end{aligned} \tag{20}$$

όπου
DS [m] είναι η απόσταση που διανύει κάθε σωματίδιο λόγω οριζόντιας διασποράς και
φ είναι μία γωνία, [rad], μέσω της οποίας εισάγεται η τυχαιότητα της κατεύθυνσης κάθε σωματιδίου, σε κάθε χρονικό βήμα, λόγω της διασποράς. Η απόσταση DS και η γωνία φ υπολογίζονται από τις εξισώσεις (21) και (22), αντίστοιχα:

$$DS = \left[R\right]_0^1 \sqrt{12 D_h\, Dt} \tag{21}$$

$$\varphi = 2\pi \left[R\right]_0^1 \tag{22}$$

όπου
D_h είναι ο συντελεστής οριζόντιας διασποράς, [$m^2\ s^{-1}$],
Dt είναι το επιλεγμένο χρονικό βήμα, [s],
$\left[R\right]_0^1$ είναι ένας τυχαίος αριθμός στο διάστημα [0,1] ο οποίος εισάγει το στοχαστικό παράγοντα στις εξισώσεις.

Στη συνέχεια, υπολογίζεται η νέα θέση (X,Y) κάθε σωματιδίου στο τέλος κάθε χρονικού βήματος από την εξίσωση (23):

$$X = X^o + DS_X \text{ και } Y = Y^o + DS_Y \tag{23}$$

όπου X^o, Y^o είναι οι συντεταγμένες της θέσης κάθε σωματιδίου σε κάθε χρονικό βήμα.

Βήμα 7: Στη συνέχεια προσδιορίζεται ο συνολικός αριθμός σωματιδίων, N_i, που περιλαμβάνονται σε κάθε κελί του υπολογιστικού πλέγματος. Τα σωματίδια που φτάνουν στην ακτή «αποθηκεύονται» στα αντίστοιχα κελιά ενώ τα σωματίδια που εξέρχονται από το την περιοχή μελέτης μέσω του ανοικτού ορίου δε λαμβάνονται περεταίρω υπόψη στους υπολογισμούς. Υπολογίζεται τελικά η παραμένουσα μάζα της πετρελαιοκηλίδας, M, σε κάθε κελί με χρήση της εξίσωσης (24):

$$M = M_i \cdot N_i \tag{24}$$

Τα βήματα 3 με 7 επαναλαμβάνονται μέχρις ότου ικανοποιηθεί το κριτήριο τερματισμού, δηλαδή μέχρις ότου το 10% των σωματιδίων του πετρελαίου εγκαταλείψει το πεδίο υπολογισμού είτε φτάνοντας στην ακτή είτε εξερχόμενο από την περιοχή μελέτης μέσω του ανοικτού ορίου. Η χρονική αυτή στιγμή συμβολίζεται με T* και αποθηκεύεται, ενώ στη συνέχεια οι υπολογισμοί επαναλαμβάνονται μέχρι το χρόνο T* προκειμένου να γίνει παρακολούθηση της τροχιάς. Συγκεκριμένα γίνεται αποθήκευση των αποτελεσμάτων στις χρονικές στιγμές T*/8, T*/4, T*/2 και

T*, οι οποίες θεωρήθηκαν αντιπροσωπευτικές για την αναπαράσταση της τροχιάς της πετρελαιοκηλίδας. Στο Σχήμα 1 παρουσιάζεται το διάγραμμα ροής του υπολογιστικού κώδικα.

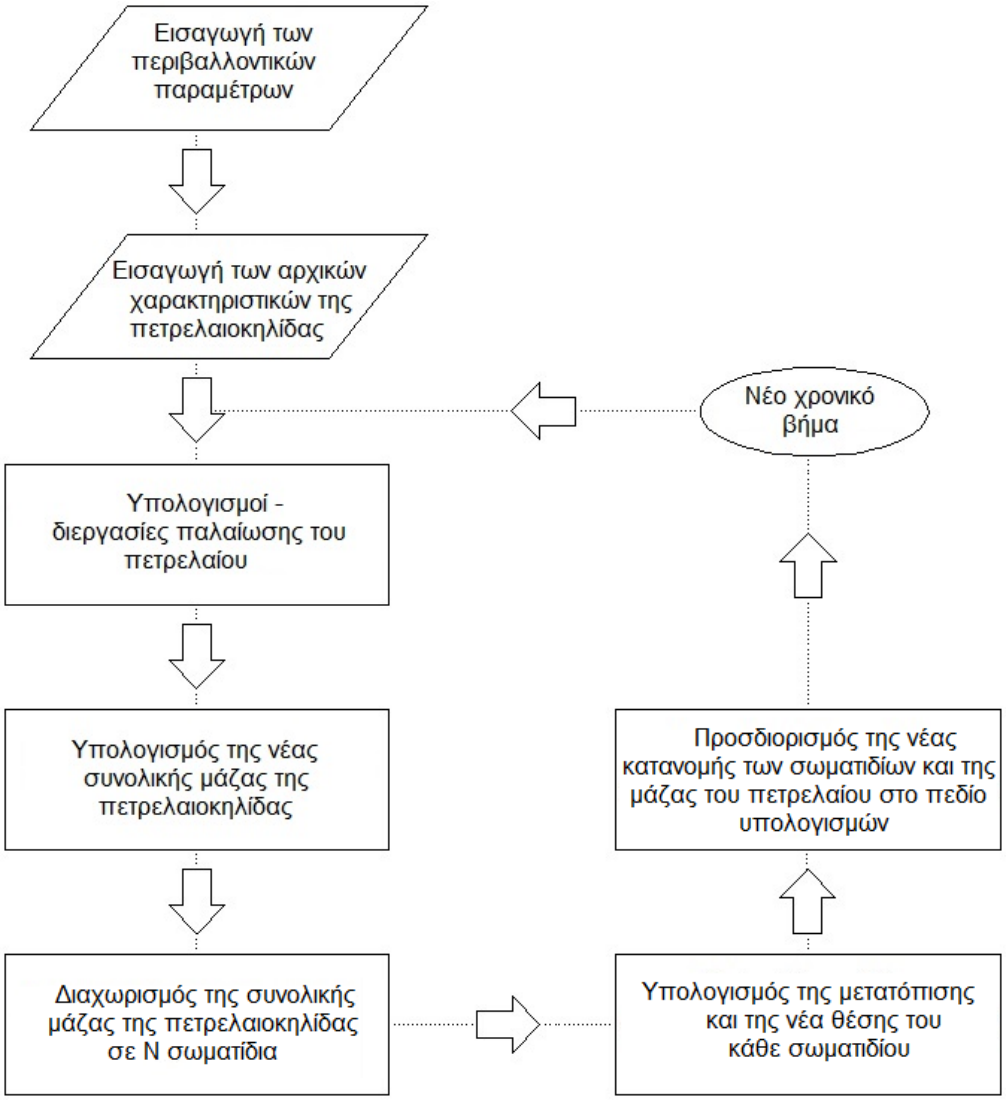

Σχήμα 1. Διάγραμμα ροής του υπολογιστικού κώδικα του OSM

3. ΕΦΑΡΜΟΓΗ ΤΩΝ ΜΑΘΗΜΑΤΙΚΩΝ ΜΟΝΤΕΛΩΝ

3.1. Χαρακτηριστικά της περιοχής εφαρμογής

Ο κόλπος του Σαρωνικού βρίσκεται στην κεντρική Ελλάδα και οριοθετείται από τις ακτές της Αττικής και της Πελοποννήσου, αλλά και τη νοητή γραμμή Πόρου-Σουνίου μήκους περίπου 40 km. Στα δυτικά, ο Σαρωνικός Κόλπος συνδέεται με τον Κορινθιακό μέσω του Ισθμού της Κορίνθου. Η γεωμετρία του κόλπου είναι αρκετά σύνθετη καθώς περιλαμβάνονται σε αυτόν μικρότεροι κόλποι, όπως ο κόλπος της Ελευσίνας, αλλά και πολλά νησιά, τα μεγαλύτερα των οποίων είναι η Αίγινα, η Σαλαμίνα, ο Πόρος και το Αγκίστρι. Περιλαμβάνονται επίσης πάνω από 30 λιμάνια διαφορετικών χρήσεων, το πιο σημαντικό των οποίων είναι ο Λιμένας του Πειραιά, ο οποίος είναι το μεγαλύτερο λιμάνι της Ευρώπης και ένα από τα μεγαλύτερα στον κόσμο ως προς την επιβατική κίνηση. Ο Λιμένας του Πειραιά γειτνιάζει με την Αθήνα, την πρωτεύουσα της

Ελλάδας, συμβάλλοντας σημαντικά στην οικονομική ζωή της χώρας. Στο Σχήμα 2 παρουσιάζεται άνω όψη του κόλπου του Σαρωνικού (http://www.google.com/earth/).

Σχήμα 2. Άνω όψη του Σαρωνικού Κόλπου
(Πηγή: http://www.google.com/earth/)

Στην παρούσα εργασία, επελέγη να γίνει εφαρμογή του κώδικα που αναπτύχθηκε στο Σαρωνικό Κόλπο, λόγω της υψηλής του σημασίας για τη χώρα αλλά και λόγω της αυξημένης πιθανότητας θαλάσσιου ατυχήματος πετρελαιοκηλίδας στην περιοχή λόγω της υψηλής ναυτιλιακής κίνησης. Επιπρόσθετα, ένα ατύχημα διαρροής πετρελαιοκηλίδας στα νερά του Σαρωνικού θα είχε σοβαρές περιβαλλοντικές επιπτώσεις στην περιοχή καθώς περιλαμβάνει μεγάλο αριθμό προστατευόμενων περιοχών και παραλιών κατά μήκος των ακτών του. Συνεπώς, η παρούσα εργασία θα μπορούσε να αποτελέσει βασικό εργαλείο για διαχειριστικούς σκοπούς και την κατασκευή Χαρτών Επικινδυνότητας ατυχημάτων πετρελαιοκηλίδας στα ύδατα του Σαρωνικού Κόλπου.

Αρχικά έγινε υπολογισμός των επιφανειακών ρευμάτων του κόλπου, με χρήση του υδροδυναμικού μοντέλου FLOW-3DL (Stamou et al., 1999; 2007a; 2007b), προκειμένου να εισαχθούν ως δεδομένο στο μοντέλο πρόβλεψης της συμπεριφοράς της πετρελαιοκηλίδας (Oil Spill Model, OSM) που αναπτύχθηκε στην παρούσα εργασία. Από την εφαρμογή του OSM έγινε υπολογισμός της τροχιάς της πετρελαιοκηλίδας, της εξέλιξης στο χρόνο της μάζας της και ο απαραίτητος χρόνος προκειμένου να φτάσει στην ακτή ή το ανοικτό όριο του κόλπου.

Η περιοχή εφαρμογής (βλ. Chapter 5, Figure 5.1-1) έχει έκταση 80.0 km X 60.0 km ενώ το υπολογιστικό πλέγμα που χρησιμοποιήθηκε και από τα δύο μοντέλα ήταν ορθογωνικό με διαστάσεις κελιού 2.5 km X 2.5 km και περιελάμβανε (α) όρια ξηράς (στερεά όρια), όπου οι εγκάρσιες προς τα στερεά όρια συνιστώσες της ταχύτητας τέθηκαν ίσες με μηδέν, και (β) ένα ανοικτό όριο, όπου χρησιμοποιήθηκε η συνθήκη ελεύθερης (χωρίς ανάκλαση) διάβασης (για τις εγκάρσιες στα όρια ανοικτής θάλασσας συνιστώσες της ταχύτητας) (Krestenitis, 1987). Τα μεγαλύτερα νησιά του Σαρωνικού Κόλπου, δηλαδή η Σαλαμίνα, η Αίγινα, ο Πόρος, το Αγκίστρι και οι Διάποροι Νήσοι συμπεριλαμβάνονται στο υπολογιστικό πεδίο, ενώ ο κόλπος της Ελευσίνας αγνοήθηκε καθώς αντικείμενο μελέτης της παρούσας εργασίας ήταν η - μεγαλύτερης κλίμακας - ευρύτερη περιοχή του Σαρωνικού Κόλπου. Το υπολογιστικό πλέγμα στράφηκε κατά 15° προκειμένου το ανοικτό όριο να είναι παράλληλο με τον άξονα x, διευκολύνοντας τους

υπολογισμούς. Στο Σχήμα 3 παρουσιάζεται η ευρύτερη περιοχή μελέτης και το υπολογιστικό πλέγμα που χρησιμοποιήθηκε.

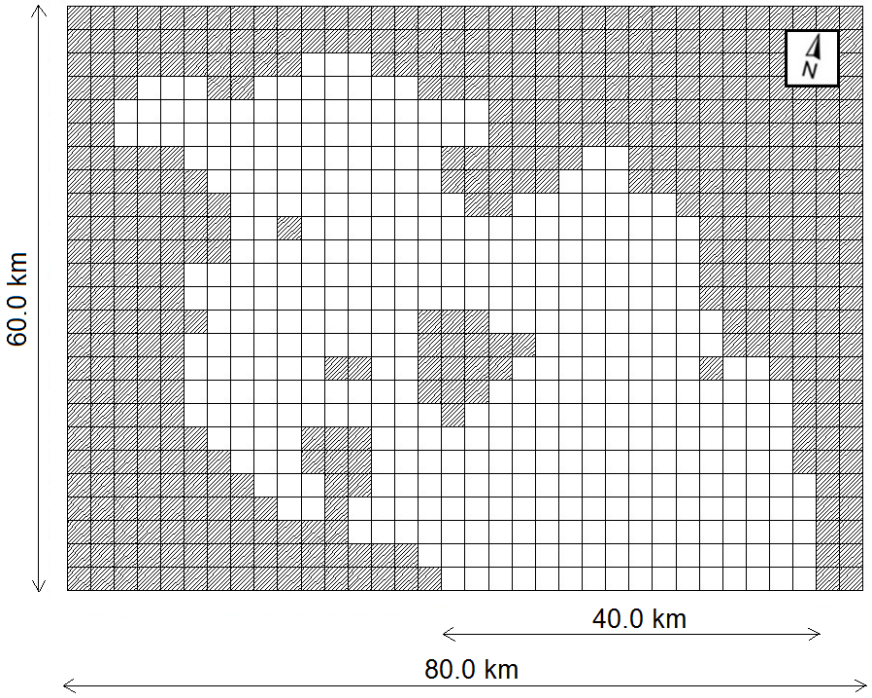

Σχήμα 3. Το υπολογιστικό πλέγμα και η περιοχή μελέτης

3.2. Εφαρμογή του υδροδυναμικού μοντέλου - Αποτελέσματα

Το υδροδυναμικό μοντέλο FLOW-3DL (Stamou et al., 1999; 2007a; 2007b) τροποποιήθηκε στην παρούσα εργασία προκειμένου να γίνει εφαρμογή του σε μία στρώση για τον υπολογισμό των ανεμογενών ρευμάτων στο Σαρωνικό Κόλπο. Τα απαραίτητα δεδομένα εισόδου ήταν:

(i) Το υπολογιστικό πλέγμα και οι οριακές συνθήκες (βλ. Παράγραφο 3.1 και Σχήμα 3).
(ii) Η βαθυμετρία του κόλπου (βλ. Figure 5.2-2), η οποία χαρακτηρίζεται από έντονη ανομοιομορφία καθώς στο δυτικό τμήμα τα βάθη φτάνουν μέχρι τα 400 m ενώ στον κόλπο περιλαμβάνονται και ρηχά νερά, κυρίως ανάμεσα στα νησιά (30-50 m βάθος).
(iii) Τα σενάρια ανέμου. Στην παρούσα μελέτη εξετάστηκαν 49 σενάρια ανέμου, έντασης που κυμαινόταν μεταξύ 1 έως 6 Beaufort. Συγκεκριμένα, οι 8 γεωγραφικοί τομείς {N, NE, E, SE, S, SW, W, NW}, οι 6 κατηγορίες ανέμου {1 to 6 bf} μαζί με το σενάριο της νηνεμίας οδήγησαν σε 49 σενάρια για τους υδροδυναμικούς υπολογισμούς.
(iv) Τα χαρακτηριστικά του θαλασσινού νερού, δηλαδή (α) η πυκνότητα του θαλασσινού νερού, ρ_w=1026 kg m^{-3}, (β) η κινηματική συνεκτικότητα, ν_w=1.1·10^{-6} m^2 s^{-1}, (γ) ο συντελεστής οριζόντιας διασποράς D_h =100.0 m^2 s^{-1} (Koutitas, 1989), και (δ) η παράμετρος Coriolis, f=2ω sinφ, η οποία εξαρτάται από το γεωγραφικό πλάτος, φ, το οποίο ελήφθη ίσο με φ=37.70 για την περίπτωση του Σαρωνικού Κόλπου (ω είναι η γωνιακή ταχύτητα της Γης η οποία ελήφθη ίση με 7.2921 · 10^{-5} rad s^{-1}).

Ενδεικτικά αποτελέσματα του υδροδυναμικού μοντέλου (HYM) για τα δύο πιο πιθανά σενάρια ανέμου, δηλαδή οι ταχύτητες των επιφανειακών ρευμάτων για άνεμους N - 3 και 4 bf (βλ. Table 4.3-1), παρουσιάζονται στο Σχήμα 4. Τα αποτελέσματα του HYM για τα 49 σενάρια ανέμου που εξετάστηκαν περιλαμβάνονται στο Παράρτημα Α (Appendix A).

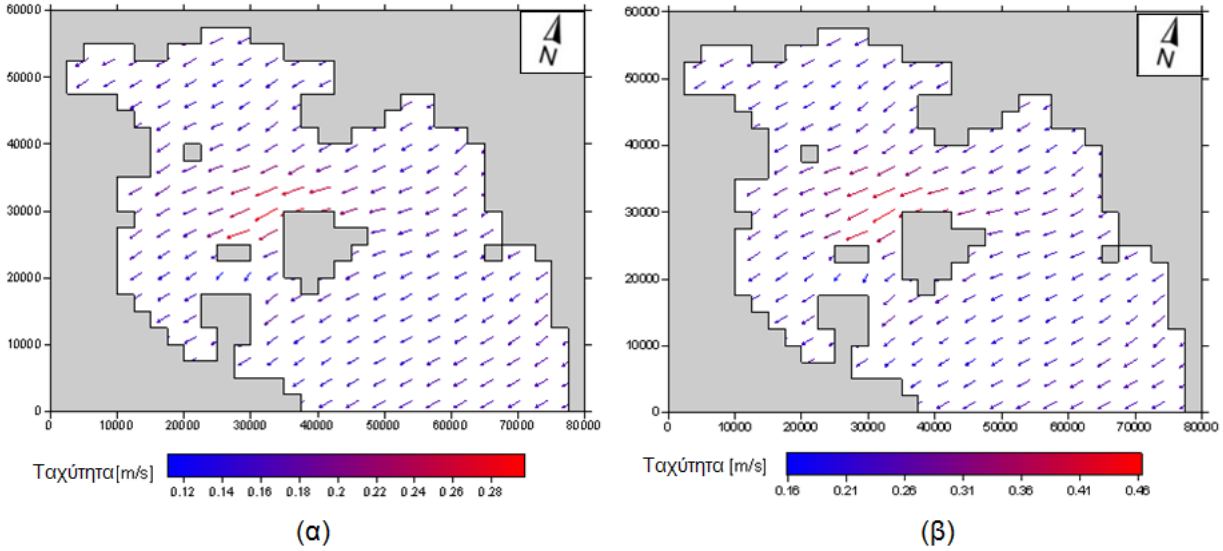

Σχήμα 4. Επιφανειακά ρεύματα για την περίπτωση βόρειου ανέμου έντασης (α) 3 bf και (β) 4 bf

3.3. Εφαρμογή του μοντέλου συμπεριφοράς πετρελαιοκηλίδας - Αποτελέσματα

3.3.1. Δεδομένα εισόδου του μοντέλου

Μετά την ολοκλήρωση τω υδροδυναμικών υπολογισμών έγινε η εφαρμογή του μοντέλου πρόβλεψης της συμπεριφοράς της πετρελαιοκηλίδας (OSM) στην περίπτωση του Σαρωνικού Κόλπου. Κάθε κελί του υπολογιστικού πλέγματος χαρακτηρίστηκε από έναν αριθμό , N_i, με χρήση του οποίου γινόταν μέτρηση του πλήθους των σωματιδίων που κινούνταν στα χωρικά του όρια, σε κάθε χρονικό βήμα. Τα στοιχεία που εισήχθησαν στο OSM για την περίπτωση του Σαρωνικού ήταν τα ακόλουθα:

(i) Οι θέσεις των ατυχημάτων. Προσδιορίστηκαν 4 πιθανές θέσεις ατυχημάτων, η επιλογή των οποίων βασίστηκε κυρίως στην υψηλή ναυτιλιακή κίνηση των περιοχών λόγω της γειτνίασής τους με τα μεγαλύτερα λιμάνια του κόλπου.

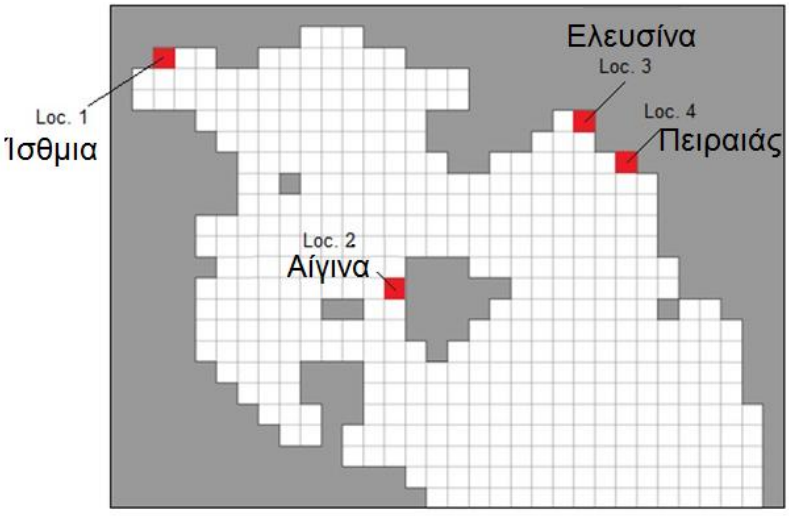

Σχήμα 5. Οι θέσεις ατυχημάτων που εξετάσθηκαν

Οι 4 αυτές θέσεις παρουσιάζονται στο Σχήμα 5 και είναι (α) η περιοχή των Ισθμίων, (β) το λιμάνι της Αίγινας, στην περιοχή ανάμεσα στα νησιά Αίγινα και Αγκίστρι όπου παρατηρούνται ρηχά νερά και άρα υπάρχει υψηλός κίνδυνος ατυχήματος, (γ) η έξοδος του κόλπου της Ελευσίνας, όπου υπάρχει και ιστορικό ατυχημάτων πετρελαιοκηλίδων που συνδέεται με τις βιομηχανικές δραστηριότητες στην περιοχή και (δ) η περιοχή του Λιμένα του Πειραιά που δέχεται τους μεγαλύτερους φόρτους ναυτιλιακής κίνησης στην Ελλάδα. Η επιλογή των θέσεων βασίστηκε επίσης στο ιστορικό ατυχημάτων στα ύδατα του Σαρωνικού Κόλπου (βλ. Figure 4.5-1).

(ii) Τα αρχικά χαρακτηριστικά της πετρελαιοκηλίδας. Ο αρχικός όγκος του πετρελαίου που θεωρήθηκε ότι διέρρευσε ήταν ίσο με V_o =1500 barrels =197 tons, με πυκνότητα ρ_o = 827 kg m^{-3}. Για τις διάφορες παραμέτρους που εισάγονται στις εξισώσεις υπολογισμού των διεργασιών παλαίωσης του πετρελαίου (weathering processes) χρησιμοποιήθηκαν τυπικές τιμές (βλ. Table 3.3-1 για την περίπτωση του πετρελαίου Diesel, T_o =517 K, T_G =139.8 K, A = 20.274 και B = 18.052).

(iii) Τα ανεμολογικά στοιχεία. Η ένταση του ανέμου, U_w, είναι απαραίτητο δεδομένο εισόδου για τους υπολογισμούς του OSM (49 σενάρια ανέμου).

(iv) Τα υδροδυναμικά χαρακτηριστικά του κόλπου. Για τα 49 σενάρια ανέμου που εξετάσθηκαν έγινε υπολογισμός των ταχυτήτων των επιφανειακών ρευμάτων με χρήση του HYM.

(v) Τα χαρακτηριστικά του θαλασσινού νερού και θερμοκρασία του αέρα. Τα χαρακτηριστικά του θαλασσινού νερού που προσδιορίζονται ως δεδομένα εισόδου του HYM εισάγονται και στο OSM (βλ. Παράγραφο 3.2). Επιπλέον, προσδιορίζεται η θερμοκρασία του αέρα η οποία στην συγκεκριμένη εφαρμογή ελήφθη ίση με 15 °C.

3.3.2. Αποτελέσματα

Τα 49 σενάρια ανέμου εξετάστηκαν για κάθε μία από τις 4 πιθανές θέσης ατυχήματος (βλ. Σχήμα 5). Ενδεικτικά αποτελέσματα του μοντέλου πρόβλεψης της συμπεριφοράς πετρελαιοκηλίδας (OSM) για τα δύο πιο πιθανά σενάρια ανέμου, δηλαδή η τροχιά της πετρελαιοκηλίδας και η εξέλιξη της μάζας της για άνεμους N - 3 και 4 bf (βλ. Table 4.3-1) παρουσιάζονται στα Σχήματα 6 και 7 αντίστοιχα. Τα αποτελέσματα του OSM για τα 49x4=196 σενάρια που εξετάστηκαν περιλαμβάνονται στο Παράρτημα Β (Appendix B).

Σχετικά με τη θέση ατυχήματος 1, κοντά στα Ίσθμια, παρατηρήθηκε ότι γίνεται παγίδευση της πετρελαιοκηλίδας στην περιοχή λόγω της μορφολογίας των ακτών για τα περισσότερα σενάρια ανέμου εκτός των βόρειων ανέμων λόγω των οποίων η πετρελαιοκηλίδα οδηγείται προς τις ακτές τις Πελοποννήσου (Αλμυρή και Κατακάλιον). Σχετικά με τη θέση ατυχήματος 2 (βλ. Σχήμα 5), στα περισσότερα σενάρια ανέμου που εξετάσθηκαν, η πετρελαιοκηλίδα παγιδεύεται μεταξύ των νησιών Αίγινα και Αγκίστρι και τα Μέθανα. Τόσο η χερσόνησος των Μεθάνων όσο και το Αγκίστρι έχουν χαρακτηριστεί ως περιοχές ιδιαίτερου φυσικού κάλους, ενώ στην περιοχή των Ισθμίων υπάρχουν παραλίες που έχουν χαρακτηριστεί με "γαλάζια σημαία". Συνεπώς ένα ατύχημα πετρελαιοκηλίδας στην περιοχή θα είχε σημαντικές επιπτώσεις τόσο στο περιβάλλον όσο και στις ανθρώπινες δραστηριότητες. Τέλος, για τα πιο πιθανά σενάρια ανέμων, δηλαδή τους βόρειους και τους βορειοδυτικούς, η πετρελαιοκηλίδα εξέρχεται από τον Σαρωνικό Κόλπο σε περίπτωση ατυχήματος στις θέσεις 3 και 4, οι οποίες γειτνιάζουν με τον Λιμένα του Πειραιά. Στα στενά μεταξύ της Σαλαμίνας, της εισόδου του κόλπου της Ελευσίνας και των ακτών της Αττικής, δηλαδή στην περιοχή της θέσης ατυχήματος 3, γίνεται επίσης εγκλωβισμός της πετρελαιοκηλίδας για τα περισσότερα σενάρια ανέμου. Οι περιοχές που πλήγονται στα περισσότερα εξεταζόμενα σενάρια είναι οι ακτές γύρω από τον Λιμένα του Πειραιά και την είσοδο του κόλπου της Ελευσίνας, οι βορειοδυτικές ακτές της Αίγινας και η περιοχή των Ισθμίων και Αγίων Θεοδώρων, λόγω της γειτνίασής τους με τις θέσεις ατυχημάτων και τη μορφολογία των ακτών του κόλπου.

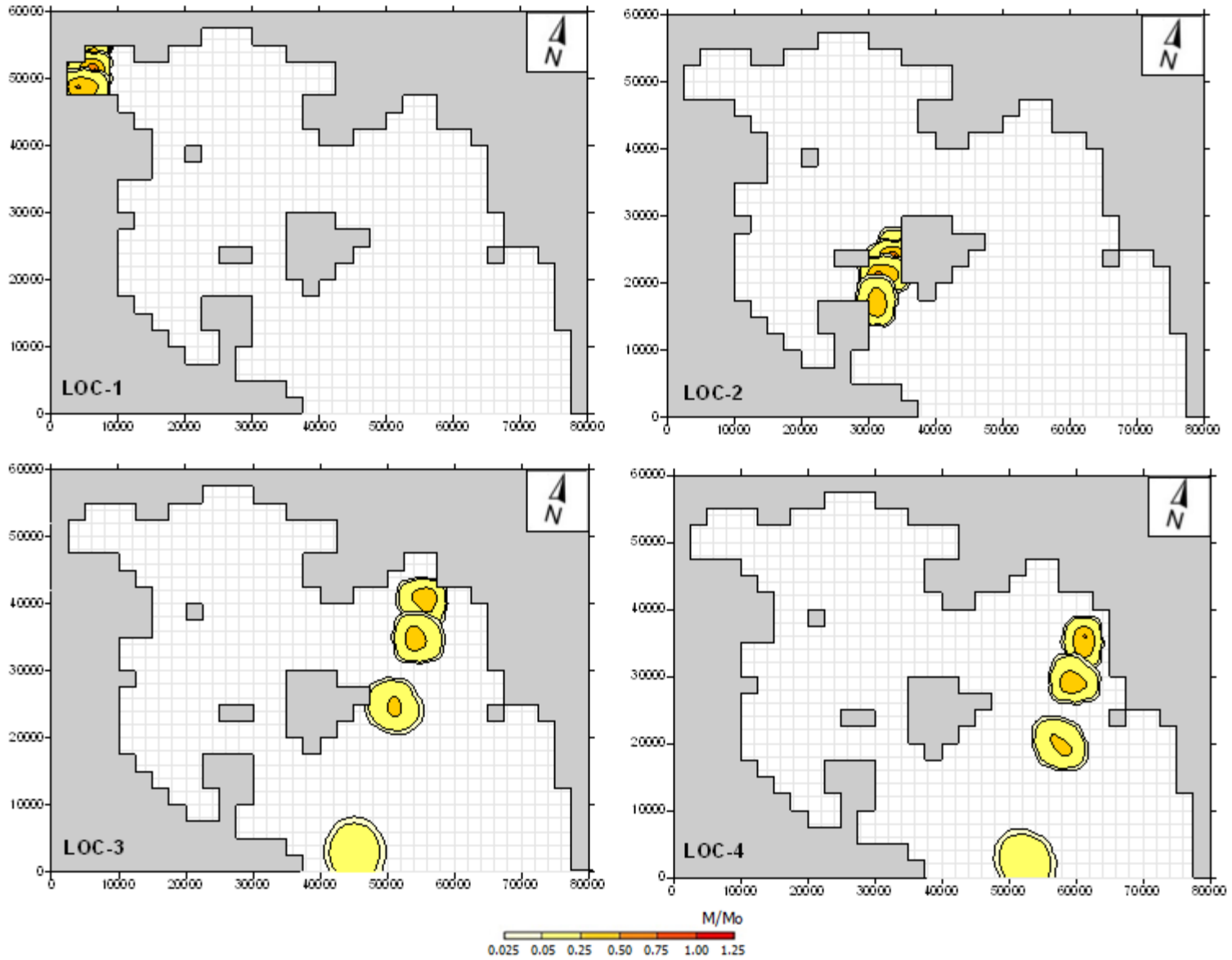

Σχήμα 6. Τροχιά και εξέλιξη της μάζας της πετρελαιοκηλίδας για τις 4 θέσεις ατυχήματος που εξετάστηκαν - Βόρειος άνεμος - 3 bf

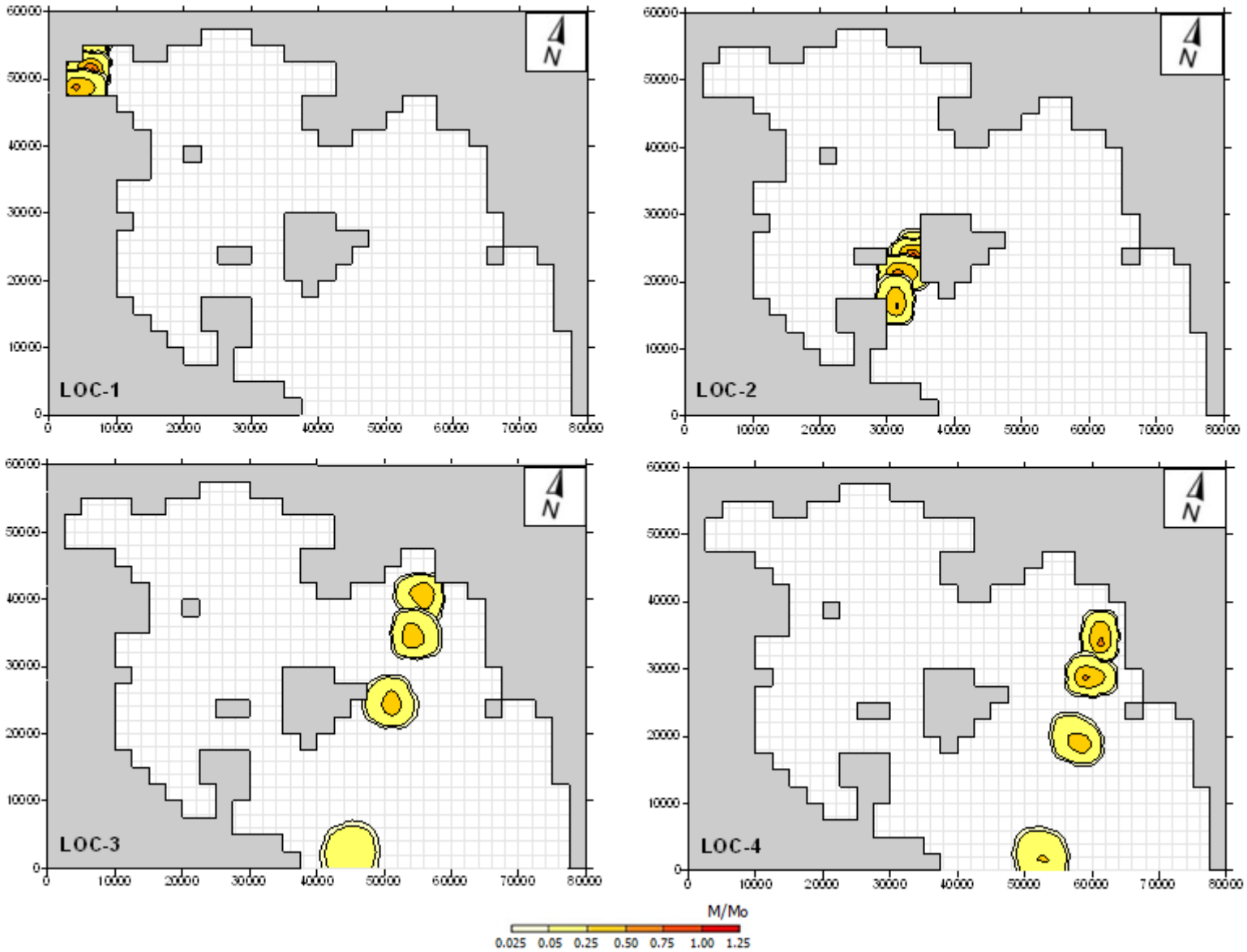

Σχήμα 7. Τροχιά και εξέλιξη της μάζας της πετρελαιοκηλίδας για τις 4 θέσεις ατυχήματος που εξετάστηκαν - Βόρειος άνεμος - 4 bf

Όσον αφορά στους χρόνους T* που υπολογίστηκαν κατά της εφαρμογή του OSM (βλ. Table 5.3-1), στις 11 από τις 196 περιπτώσεις που εξετάστηκαν η πετρελαιοκηλίδα εξέρχεται από τον κόλπο σε διάστημα μάλιστα μεγαλύτερο της μίας ημέρας. Συνεπώς, στην περίπτωση αυτή δεν υπάρχουν επιπτώσεις στις ακτές του Σαρωνικού ενώ το διάστημα αυτό κρίνεται επαρκές προκειμένου να ειδοποιηθούν και να λάβουν μέτρα αντιμετώπισης οι αρμόδιες αρχές.

Στην περίπτωση των βόρειων ανέμων χρειάζονται τουλάχιστον 3.5 ώρες προκειμένου η πετρελαιοκηλίδα να φτάσει στην ακτή, για ένταση ανέμου ίση με 6 bf. Για το πιο πιθανό σενάριο ανέμου, δηλαδή τον βόρειο άνεμο έντασης 3 bf, η πετρελαιοκηλίδα χρειάζεται τουλάχιστον 9.0 ώρες προκειμένου να φτάσει στην ακτή. Στις πιο δυσμενείς περιπτώσεις, όπου ο άνεμος πνέει με κατεύθυνση την ξηρά και η πετρελαιοκηλίδα φτάνει πιο γρήγορα στην ακτή, ο χρόνος T* είναι ίσος περίπου με 30 λεπτά της ώρα. Στην περίπτωση αυτή η παρεμπόδιση της πετρελαιοκηλίδας από το να φτάσει στην ακτή δεν είναι δυνατή. Ωστόσο, το σενάριο αυτό έχει μικρή πιθανότητα εμφάνισης θεωρώντας ότι η πιθανότητα πνοής των συγκεκριμένων ανέμων είναι καθοριστική.

4. ΣΥΜΠΕΡΑΣΜΑΤΑ - ΠΡΟΤΑΣΕΙΣ

Στην παρούσα εργασία αναπτύχθηκε ένα διδιάστατο (2D) μαθηματικό μοντέλο πρόβλεψης της συμπεριφοράς και της τροχιάς μιας πετρελαιοκηλίδας, σε περίπτωση θαλάσσιου ατυχήματος (Oil Spill Model, OSM). Το παρόν μοντέλο λαμβάνει υπόψη τις διεργασίες της μεταφοράς, της διασποράς, αλλά και της παλαίωσης του πετρελαίου (εξάπλωση, εξάτμιση, διάλυση και γαλακτωματοποίηση). Επιπλέον έγινε χρήση της μεθόδου παρακολούθησης της κίνησης των σωματιδίων (particle tracking method) για την πρόβλεψη της κίνησης των σωματιδίων του πετρελαίου, λαμβάνοντας υπόψη την τυχαιότητα που εισάγεται στην κίνηση κυρίως λόγω της διασποράς. Με την εφαρμογή του μοντέλου είναι δυνατός ο υπολογισμός της τροχιάς της πετρελαιοκηλίδας, της εξέλιξης της μάζας της στο χρόνο, καθώς και του απαιτούμενου χρόνου προκειμένου να φτάσει στην ακτή. Τα στοιχεία αυτά θα πρέπει να είναι γνωστά για την έγκαιρη αντιμετώπιση ενός τέτοιου ατυχήματος καθώς δίνουν τη δυνατότητα εκτίμησης του διαθέσιμου χρόνου για δράση αλλά και των ακτών που θα πληγούν. Η εφαρμογή του μοντέλου στην περίπτωση του Σαρωνικού Κόλπου, που περιλαμβάνει το μεγαλύτερο λιμάνι της Ελλάδας και συνεπώς δέχεται την πιο μεγάλη ναυτιλιακή κίνηση στη χώρα, έδειξε ότι οι ακτές που κινδυνεύουν περισσότερο βρίσκονται κοντά στο Λιμένα του Πειραιά και την είσοδο του κόλπου της Ελευσίνας, στο βορειοδυτικό τμήμα της Αίγινας και στην περιοχή των Ισθμίων.

Βασική παραδοχή του μαθηματικού μοντέλου είναι ότι όλοι οι υπολογισμοί λαμβάνουν χώρα κατά τη διάρκεια που η πετρελαιοκηλίδα κινείται μέσα στο υδάτινο στοιχείο και σταματούν όταν αυτή φτάσει στην ακτή, καθώς, από τη στιγμή που αρχίζει να συσσωρεύεται στην ξηρά, οι διεργασίες που επηρεάζουν τις φυσικοχημικές ιδιότητες του πετρελαίου αρχίζουν να τροποποιούνται. Προτείνεται λοιπόν η εξέλιξη του υπολογιστικού κώδικα προκειμένου να λαμβάνεται υπόψη η συσσώρευση των σωματιδίων του πετρελαίου στην ακτή. Επιπλέον, προτείνεται η εξέλιξη του μαθηματικού μοντέλου σε τρισδιάστατο (3D) προκειμένου να ληφθούν υπόψη και οι υπόλοιπες διεργασίες παλαίωσης του πετρελαίου, όπως η καθίζηση, καθώς η δράση των κυματισμών. Τέλος, δεδομένης της δυσκολίας πρόβλεψης ενός ατυχήματος πετρελαιοκηλίδας αλλά και της αβεβαιότητας που υπεισέρχεται στον προσδιορισμό των καιρικών συνθηκών, συνίσταται στοχαστική προσέγγιση του προβλήματος.

CHAPTER 1: INTRODUCTION

1.1. General

Oil spills occur due to accidents in sea and coastal waters. Oil leaked into the seawater creates a spill which spreads in a rate proportional to the oil density and conversely proportional to its kinematic viscosity. The behavior of the generated oil spill is affected by physical, chemical and biological processes, such as transport, dispersion, evaporation, emulsification, settling and biological decay. Experience from occurred oil spill accidents has shown that the environmental and ecological impacts on individual organisms and ecosystems are of high significance. For this reason, mathematical models have been developed and presented in the international literature.

The majority of the oil spill models are developed for operational purposes; that is to calculate the oil spill behaviour including the oil spill trajectory; thus, they provide information regarding the operation area for the retention-purification of oil spill to the proper services aiming at the avoidance-mitigation of pollution impacts. It is noted that, the utility of the above mentioned operational models is limited to the specific conditions of the examined case, without providing the capability of general applications.

1.2. Objectives of the present study

In the present study, a 2D physics-based mathematical model was developed for the prediction of the behaviour of an oil spill (oil spill model, OSM) in case of a sea accident. For the calculation of the flow field the hydrodynamic model FLOW-3DL (Stamou et al., 1999; 2007a; 2007b) was employed and modified accordingly; the sea surface currents were reproduced and inserted in the OSM to account for the process of advection. Empirical models (Mackay, 1980; MacKay and Matsugu, 1973 for example) were also used to account for the physical, chemical and biological processes that also contribute to the disappearance or persistence of the spilled oil. The Saronicos Gulf, which includes the busiest port of Greece, i.e. the Port of Piraeus, was chosen as a pilot area to apply the model that was developed.

1.3. Outline of the study

The present Masters of Science thesis consists of 7 Chapters.

- In the **1st Chapter** the contents and objectives of the present study are introduced.
- In the **2nd Chapter** the main processes that affect the oil spill behaviour are presented together with the governing equations and models used in the literature to predict it.
- In the **3rd Chapter** the mathematical models used for the calculation of the hydrodynamics (Hydrodynamic Model, HYM) and the oil spill behaviour (Oil Spill Model, OSM) are presented.
- In the **4th Chapter** the characteristics of the application site are presented; the model is applied to the case of Saronicos Gulf.
- In the **5th Chapter** the methodology, the application and results of the model are presented and discussed.
- In the **6th Chapter** conclusions are extracted and future work is proposed regarding the presented mathematical model.
- The **7th Chapter** includes the literature used in the study.
- Two Appendices are also included; **Appendix A** and **B** include the results of the hydrodynamic and oil spill models respectively.

CHAPTER 2: DESCRIPTION AND MODELING APPROACHES OF THE MAIN PROCESSES

2.1. General

The two main mechanisms that act on an oil spill governing its fate are advection and weathering. The advection, i.e. the transport of the main body of the oil spill, is driven by the wind and flow field. The weathering is the combination of the processes by which the spilled oil changes both physically and chemically. Some of those processes contribute to the disappearance of the oil whereas the others cause the increase of its mass, both by affecting its density and volume. The most important weathering processes, which are shown in Figure 2.1-1, are the spreading, evaporation, dispersion, emulsification, dissolution, sedimentation, photo-oxidation and biodegradation.

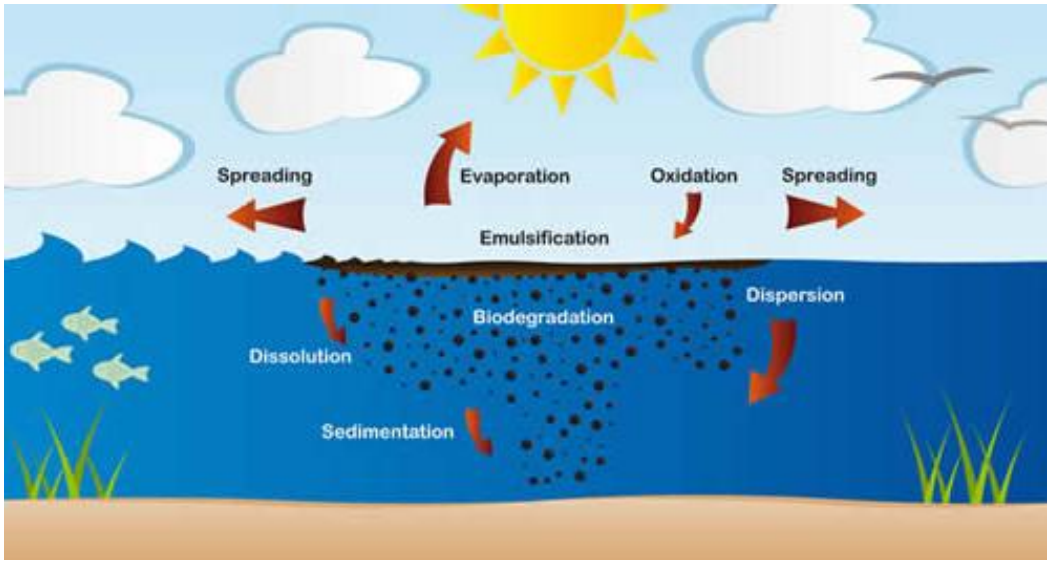

Figure 2.1-1. Major weathering processes for oil slicks
(Obtained from: http://www.itopf.com/marine-spills/fate/weathering-process/)

The factors that determine the transport and weathering of the spilled oil are the oil properties, hydrodynamic conditions and environmental conditions (temperature, wind speed etc). The most widely used modeling approaches of each process are reported in this chapter, together with the characteristic equations that govern oil properties and the most important environmental factors that affect oil spill behaviour.

2.2. Environmental factors

2.2.1. Wind

In the present study, the wind speed at 10 m above water surface was used as a reference height which is common in most oil weathering models. Provided that the measured height of the wind is less than 20 m, a common formula to adjust the available measurements to the reference height is equation 2.2-1 (Brutsaert and Yeh, 1970):

$$U_{10} = U_z \left(\frac{10}{z} \right)^{1/7} \qquad (2.2\text{-}1)$$

where
z is the height at which wind speed measurements are available, [m],
U_{10} is the reference wind speed at 10 m height from the sea surface, [m s^{-1}],
U_z is the measured wind speed at height z from the sea surface, [m s^{-1}].

Since the wind field is spatially varying, corrections have to be made if the measurement location is considerably far from the spill location or if the topography makes it necessary. Stolzenbach et al. (1977) suggested an interpolating technique and several oil spill models incorporate this capability (Lehr, 2001). However, in the present study, the wind field was assumed to be constant which is also very common in oil spill modeling.

2.2.2. Waves

The significant wave height, H_s, and wave period, t_p, are often obtained by simple formulas that express wave characteristics as functions of wind speed, fetch, and wind duration. Breaking waves significantly affect weathering processes such as dispersion and emulsification due to the intensive turbulence they generate (Lehr, 2001). However, in the present study the acting of waves is not taken into account since only wind driven flow is reproduced.

2.3. Advection

Once an amount of oil is spilled into the sea, most of the oil remains on the sea surface forming a thin film which moves horizontally, driven mainly by the winds and surface currents. The net transport rate and direction of the spill is determined by the act and interaction of the winds, waves, surface currents and oceanic turbulent diffusion. The thin film of an oil spill moves mainly horizontally forced by wind and sea surface currents, with most of the oil remaining mainly on the sea surface. However, the dispersive wave mechanism of breaking contributes to the vertical motion of oil at sea in the form of droplets of various sizes. Biodegradation, sedimentation and dissolution also contribute to the vertical motion of oil particles but their effect is minor compared to the contribution of turbulent diffusion and dispersion.

Advective currents can be computed from current atlases (static approximations), live meteorologic observations, buoys trajectory or hydrodynamic modeling (dynamic approximations) (Novelli, 2011). Moreover, so far, both two-dimensional (2D) and three-dimensional (3D) modeling approaches have been developed for the calculation of the sea currents and thus the prediction of the transport of an oil spill. In the present study, the hydrodynamic model FLOW-3DL (Stamou et al., 1999; 2007a; 2007) was employed for the prediction of the sea currents (see chapter 3.3). The model solves the 3D non-steady state shallow water (continuity and momentum) equations expressed in layer formulation. Thus, the layer averaged flow field was reproduced and the horizontal surface current velocities in the x and y directions were then extracted (see Chapter 3.3); in this study, the motion of the spilled oil was assumed to be two-dimensional.

In the present study, the displacement of each oil particle in the x and y directions, in each time step, due to advection by the surface currents, was calculated by equation 2.3-1:

$$DS_{X,adv} = U_{surf}\, Dt \qquad \text{and} \qquad DS_{Y,adv} = V_{surf}\, Dt \tag{2.3-1}$$

where
U_{surf} and V_{surf} are the horizontal surface current velocities in the x and y directions, respectively, [m s^{-1}], and
Dt is the time step, [s].

2.4. The weathering processes and oil properties

Since oil is a mixture of different organic compounds and not a pure chemical, its properties change during the lifetime of the slick. As already mentioned in Chapter 2.1, the interrelated physical, chemical and biochemical processes that affect the oil properties with time are called "the weathering". The most important weathering processes, which are also shown in Figure 2.4-2, are described in this chapter.

Determinant factors for the evolution of oil properties, and thus the weathering, are the environmental factors. The most determinant for the fate of the oil spill are the environmental temperature, wind speed and wave conditions. Also important environmental factors, depending upon the circumstance of the spill incident, are solar radiation, air temperature, water density and salinity, ice cover, and sediment loading in the water (Lehr, 2001). Moreover, the contribution of each process to the weathering differs in magnitude and time; the relative importance of each process is shown in Figure 2.4-1.

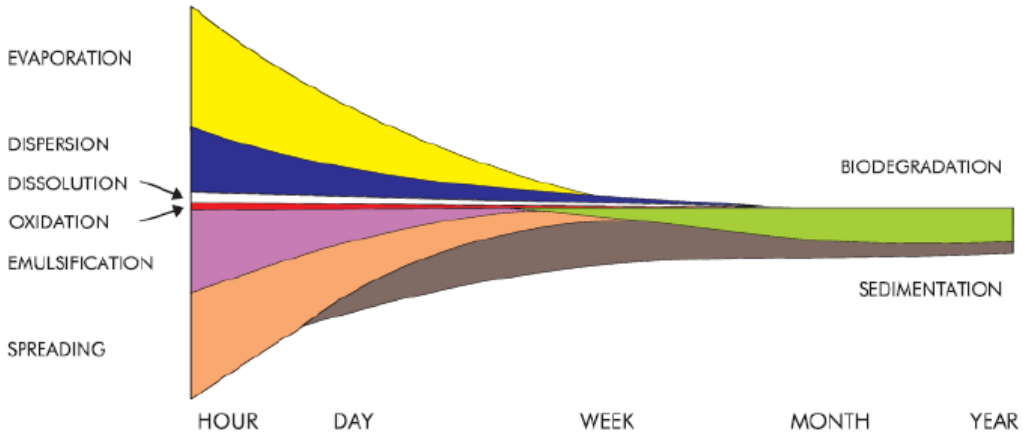

(a)

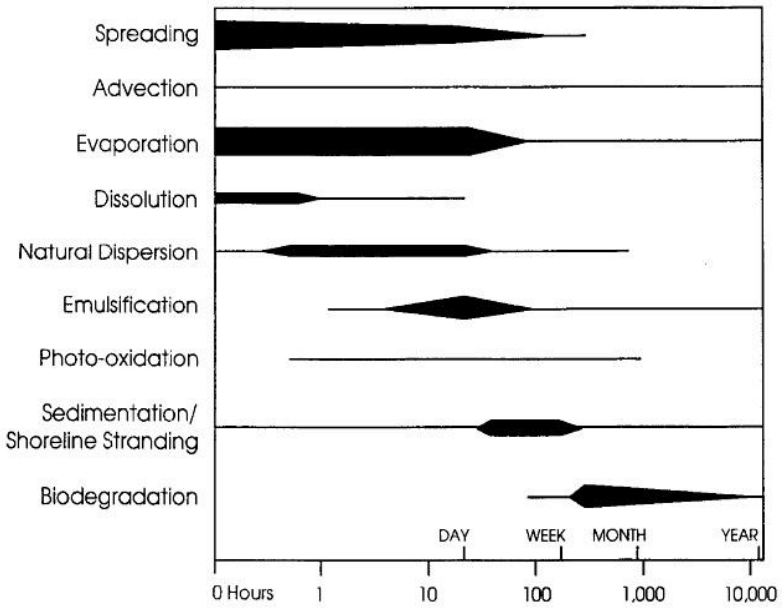

(b)

Figure 2.4-1. The relative importance of weathering processes with time (Obtained by (a) ITOPF, 2010 and (b) Exxon, 1985)

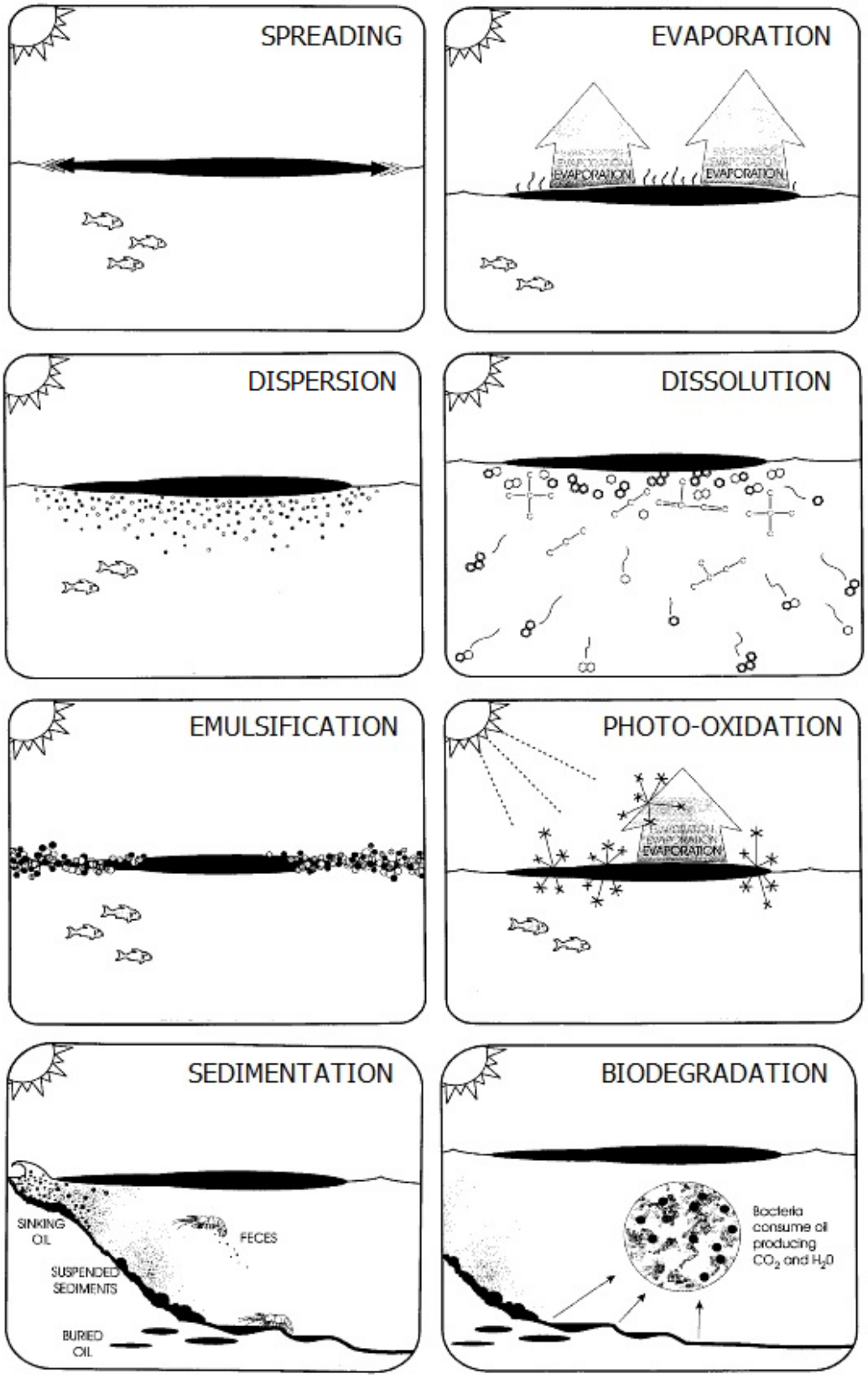

Figure 2.4-2. Depiction of the most important weathering processes (Obtained by: Boyd et al., 2001)

2.4.1. Spreading

Spreading is the horizontal expansion of an oil slick over the sea surface due to the forces of gravity, inertia, viscosity, interfacial tension and turbulent diffusion. When the oil is spilled, it initially forms a single slick with a speed which depends on the viscosity of the oil. The spreading is usually not uniform whereas after a few hours the slick begins to break up and, because of winds, wave action and, generally, turbulence, it forms narrow bands or windrows parallel to the wind direction (see Figure 2.4-4). The rate at which the oil spreads is also determined by the prevailing conditions such as temperature, water currents, tidal streams and wind speeds. The more severe the conditions, the more rapid the spreading and breaking up of the oil. (http://www.itopf.com/marine-spills/fate/weathering-process/).

Figure 2.4-3. Release of oil in the Gulf of Mexico, 2005
(Obtained from: http://www.noaanews.noaa.gov)

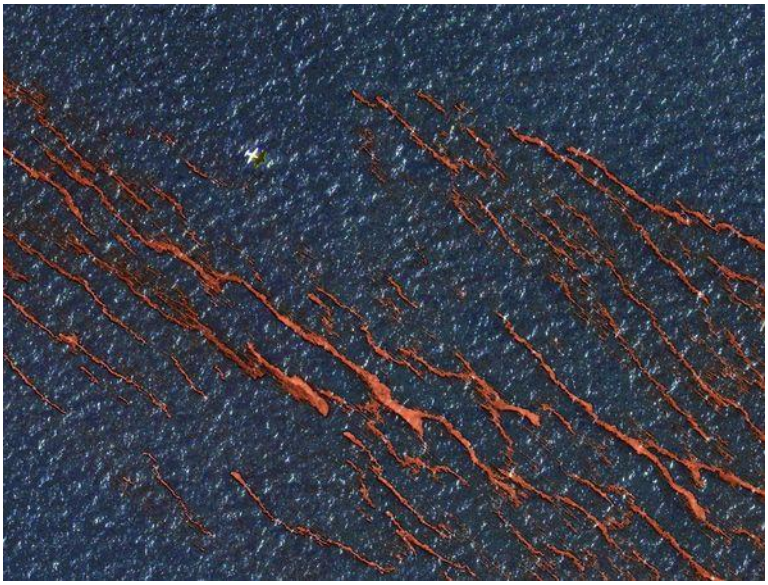

Figure 2.4-4. Forming of narrow bands
(Obtained from: http://www.oilspillsolutions.org/evaluation.htm)

The spreading of the oil spill is governed by gravity, momentum and viscous forces and, according to Lehr et al. (1984) it can be described by equation 2.4-1:

$$A_s = \frac{\pi}{4} l_{min}\, l_{max} \quad \text{or} \quad A_s = 2270\left(\frac{\Delta\rho}{\rho_{oil}}\right)^{2/3} V_o^{2/3}\, t^{1/2} + 40\left(\frac{\Delta\rho}{\rho_{oil}}\right)^{1/3} V_o^{1/3}\, U_w^{4/3}\, t \qquad (2.4\text{-}1)$$

$$\text{where } l_{min} = 53.76\left(\frac{\Delta\rho}{\rho_{oil}}\right)^{1/3} V_o^{1/3}\, t^{1/4} \quad \text{and} \quad l_{max} = l_{min} + 0.95\, U_w^{4/3}\, t^{3/4} \qquad (2.4\text{-}2)$$

A_s is the slick area [m^2],
l_{min} and l_{max} are the lengths of the minor and major axes of the spill [m], respectively,
$\Delta\rho = \rho_w - \rho_{oil}$, where ρ_w and ρ_{oil} are the densities of water and oil, respectively [kg m^{-3}],
V_o is the volume of the spilled oil [barrels],
U_w is the wind speed [knots] and
t is the time [min].

2.4.2. Evaporation

Since oil is not a pure chemical, the process of oil evaporation has not been clearly understood. It is though generally confirmed that it is the major mechanism of oil removal as it can result to 20-40% loss of oil in the first few hours (Gundlach and Boehm, 1981). It also changes the chemical mixture of the slick as the lighter components evaporate more quickly than the heavier hydrocarbons; thus it causes an increase in the viscosity and density of the oil residue. An oil with a large percentage of light and volatile compounds will evaporate more than one with a larger amount of heavier compounds. For example, petrol, kerosene and diesel oils, all light products, tend to evaporate almost completely in a few days whilst little evaporation will occur from a heavy fuel oil. In general, in temperate conditions, those components of the oil with a boiling point under 200ºC tend to evaporate within the first 24 hours. Evaporation can increase as the oil spreads, since the surface area of the slick increases. Rougher seas, high wind speeds and high temperatures also tend to increase the rate of the evaporation process (http://www.itopf.com/marine-spills/fate/weathering-process/).

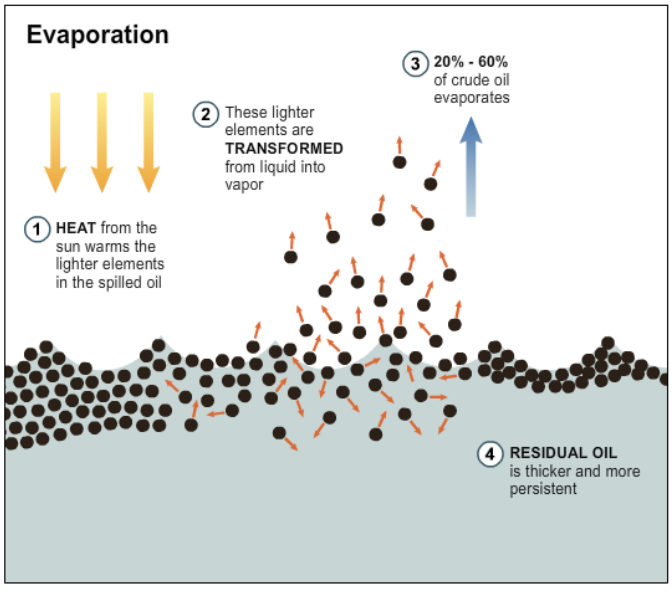

Figure 2.4-5. Evaporation of oil
(Obtained from: http://www.fastcompany.com/1659822/infographic-day-physics-oil-spills)

Evaporation is affected by the surface area and thickness of the spill, the oil vapor pressure, the solar radiation, the wind speed, the temperature, the sea conditions, volatility and diffusion characteristics (MacKay and Matsugu, 1973). The numerical models that have been developed over the past years either include the majority of those factors or derive from simplifying assumptions since the conversion from the liquid state to vapor is a complex process.

There are three modeling approaches regarding the evaporation process (Vos, 2005):
(1) Assuming a first order law for the decay process.
(2) Employing a one-fraction model.
(3) Employing a multi-component model.

When assuming a first order law for the decay process effects of varying temperature, vapor pressure, molecular weight or wind speed in the environment are not taken into account (Vos, 2005). It is the most simplified modeling technique to quantify the rate of evaporation, assuming a fixed decay constant, K_e [T^{-1}] and is expressed by equation 2.4-3:

$$\frac{dm_s}{dt} = m_s(t) F_e \exp(-K_e t) \qquad (2.4\text{-}3)$$

where
m_s is the oil mass, [kg],
t is the time, [days],
$m_s(t)$ is the total floating oil mass at time t, [kg],
F_e is the vaporizable fraction of the floating oil, [-],
K_e is the decay constant, i.e. the evaporation rate, [$days^{-1}$].

Mackay (1980) proposed an analytical method, which employs the semi-empirical distillation theory regarding multi-component liquids, to compute the rate of oil evaporation considering that the vaporizable fraction of the floating oil, F_e, [-], is considered not to be constant. This is the most frequently used method for estimating evaporation rates and is expressed by equation 2.4-4:

$$F_e = \left(\frac{T}{BT_G}\right) \ln\left(\theta\left(\frac{BT_G}{T}\right)\exp\left(A - \frac{BT_o}{T}\right) + 1\right) \qquad (2.4\text{-}4)$$

where
T is environmental temperature [K],
A and B are constants that derive from distillation data (Bobra, 1992);
T_o is the initial boiling point at F_e=0 [K],
T_G is the gradient of the distillation curve [K],
θ is the evaporation exposure, i.e. the volume of the exposed vapor at time t versus the initial spill volume, and is calculated by equation 2.4-5:

$$\theta = \frac{K_2 A_S t}{V_o} \qquad (2.4\text{-}5)$$

where
t is the time, [s],
V_o is the initial volume of the oil spill [m^3],
K_2 is the mass transfer coefficient for evaporation [m s^{-1}], defined by equation (2.4-6) (MacKay and Matsugu, 1973):

$$K_2 = 0.0107\, U_w^{0.78}\, D_s^{-0.11}\, S_c^{-0.67} \qquad (2.4\text{-}6)$$

where
U_w is the wind speed [m s^{-1}],
D_s is the oil slick diameter [m],
S_c is the Schmidt number which represents the surface roughness and is taken equal to 2.7, [-], (Zadeh and Hejazi, 2012).

In the multi-component approach each oil fraction evaporates in a different rat; thus the term dm_s/dt varies accordingly and is expressed by the mass balance equation:

$$\frac{dm_s}{dt} = -Q_e \sum_{i=1}^{n} \frac{x_i p_i M_i}{RT} \qquad (2.4\text{-}7)$$

where
x_i is the the molar fraction of the i component, [-],
p_i is the the vapor pressure of the i component, [atm],
M_i is the (average) molecular weight of the i component, [g mol^{-1}],
R is the ideal gas constant [8.206E-5 atm m^3 mol^{-1} K],
T is the temperature, [K],
Q_e is the evaporation rate, [kg m^{-2} sec^{-1}].

Hence, a set of equations is formed expressing the mass balance for each component and n mol-balance equations must be solved for all n fractions in the liquid (Reinhart and Rose, 1982; Jones 1997). In the present study, the one-fraction modeling approach of Mackay (1980) is empolyed to account for the weathering process of evaporation.

2.4.3. Dispersion

The floating oil slick breaks up into fragments and droplets of varying sizes because of the turbulence induced by the act of wind and waves. The droplets mix with water; the smaller ones tend to mix with sea water whereas the larger ones tend to return to the sea surface and probably attach with other droplets to reform a slick. The droplets that remain suspended in the sea water body are more easily subjected to other processes such as dissolution, biodegradation and sedimentation. This is a natural mechanism that contributes to the disappearance of the oil slick while addition of chemical dispersants can accelerate this process. Except the rough wind and wave conditions, low oil viscosity also accelerates dispersion (http://www.itopf.com/marine-spills/fate/weathering-process/).

Figure 2.4-6. Entrainment due to the act of the waves
(Obtained from: http://abbeydufoe.wordpress.com/2013/04/23/earth-week-2013-bp-oil-spill-update/)

Delvigne and Sweeney (1988) conducted a series of experiments to extract empirical relations for the natural dispersion of oils in the sea and then applied those relations in mathematical models. In the present study the turbulent dispersive transport of the oil particles was simulated by employing the particle tracking method where the displacement of each oil particle included a stochastic part. The distance DS [m] that each particle travelled due to horizontal dispersion at each time-step was calculated by equation 2.4-8 (Al-Rabeh et al., 1989; Chao et al., 2001):

$$DS = [R]_0^1 \sqrt{12 D_h Dt} \tag{2.4-8}$$

where
D_h is the horizontal dispersion coefficient [$m^2\ s^{-1}$],
Dt is the chosen time step for the calculations, [s],
$[R]_0^1$ is a random number in the interval [0,1] to include the stochastic factor and
φ is an angle [rad] that denoted the randomness of the direction of each particle, at each time-step, due to dispersion and was calculated by equation 2-4-9:

$$\varphi = 2\pi [R]_0^1 \tag{2.4-9}$$

Thus, the displacement of each oil particle in the X and Y directions, in each time step, due to dispersion was equal to:

$$DS_{X,disp} = DS \cos\varphi \quad \text{and} \quad DS_{Y,disp} = DS \sin\varphi \tag{2.4-10}$$

or

$$DS_{X,disp} = [R]_0^1 \sqrt{12 D_h Dt}\ \cos\left(2\pi [R]_0^1\right) \ \text{and} \ DS_{Y,disp} = [R]_0^1 \sqrt{12 D_h Dt}\ \sin\left(2\pi [R]_0^1\right) \tag{2.4-11}$$

2.4.4. Dissolution

Dissolution contributes to the disappearance of the oil spill but accounts for much less oil loss than evaporation and is generally two or more orders of magnitude smaller (Harrison et al., 1975), although exact measurements are difficult to obtain even in the laboratory. It is most active shortly after a spill and affects some of the same hydrocarbon fractions as evaporation. Oil composition and interfacial area significantly determine the dissolution process; entrainment of oil droplets enhance dissolution by increasing interfacial area between the water and the oil droplets. According to Novelli (2011) it is a process relatively unimportant in determining mass balance; this is attributed to the fact that only a few crude oil components are soluble in water to an appreciable degree. However, dissolution is very important in terms of potential biological impacts since the diluted components can have toxic effects on marine organisms.

In the present study, the multi-component theory developed by Cohen et al. (1980), for the calculation of the rate of mass loss from the oil slick due to dissolution, was used:

$$S_D = K_D A_s S \tag{2.4-12}$$

where
S_D is the total dissolution rate of the oil slick [$gr\ s^{-1}$],
K_D is the dissolution mass transfer coefficient, [usually $3 \cdot 10^{-6}\ m\ s^{-1}$],
S is the oil solubility in water which is given by equation (2.4-13) (Mackay, 1980):

$$S = S_o e^{-\alpha t} \tag{2.4-13}$$

where S_o is the solubility of fresh crude oil [gr s^{-1}],
α is a decay constant [$days^{-1}$] and
t is the time, [days].

2.4.5. Emulsification

Emulsification is the process of mixing water droplets into oil, forming a water-in-oil emulsion. It is the weathering process that plays the most important role in the persistence of the spilled oil on the sea surface; the oil can take up until 80% of water, changing drastically the density of the mixture which volume can expand up to five times the original volume. It increases also dramatically the viscosity (Jokuty et al., 2000; Xie et al., 2007). The emulsion formed is usually very viscous and more persistent than the original oil. This slows and delays other processes which would allow the oil to be dissipated.

The mechanism by which the water droplets penetrate the spill is still questionable. Water turns into a thick sticky mixture, forming a mousse of increased viscosity and volume, which is often referred to as “chocolate mousse” because of its appearance. Emulsification is affected by the wind and wave conditions as well as by temperature and spill characteristics (local thickness, degree of weathering etc). Oils with asphaltene content greater than 0.5% tend to form stable emulsions which may persist for many months after the initial spill has occurred. Those oils containing a lower percentage of asphaltenes are less likely to form emulsions and are more likely to disperse. Emulsions may separate into oil and water again if heated by sunlight under calm conditions or when stranded on shorelines (http://www.itopf.com/marine-spills/fate/weathering-process/).

Figure 2.4-7. Emulsified oil and detail of the “mousse”
(Obtained by: http://forbesindia.com/article/on-assignment/who-do-oil-companies-turn-to-when-theres-a-spill/17352/1, http://www.oilspillsolutions.org/evaluation.htm)

The modeling approach of Mackay (1980) to calculate the rate of water-in-oil emulsification, which was used in the present study, is expressed by equation 2.4-14:

$$F_w = K_b\left(1-\exp\left(\frac{-K_a}{K_b}(U_w+1)^2\, t\right)\right) \qquad (2.4\text{-}14)$$

where

F_w is the fractional water content, [-],
U_w is the wind speed, [m s^{-1}],
t is time [s],
K_a is a curve fitting constant that varies with wind speed,
K_b is the mousse viscosity constant, [-],which is taken equal to 0.7 for crude oils and heavy fuel oil, and 0.25 for home heating oil (Zadeh and Hejazi, 2012).

The values used in the present study have been proposed by Reed (1989); K_a =2.0 10^{-6} sec^{-1} and K_b =0.7.

2.4.6. Photo-oxidation

Crude oils are generally dark-colored and can absorb UV radiation from the sun. In some oils, in very sunny conditions, this can cause significant changes in the chemical composition and this can affect emulsification properties. Photo-oxidation is the process by which oil undergoes oxidation with energy from sunlight and polar, water soluble, oxygenated products are generated (Payne and Phillips, 1985). Photo oxidation is unimportant over the first few days of a spill but may become noticeable after a week or more. This process does not affect the mass balance; however, its products may be more toxic than those in the parent material (Lacaze and Villedon de Naide, 1976).

Photo-oxidation also plays an important role in the removal of dissolved petroleum hydrocarbons. Aliphatic and aromatic fractions of petroleum are oxidized photochemically in sunlight to more polar ketones, aldehydes, carboxylic acids, and esters. Because these products are more soluble in seawater, photo oxidation enhances the overall solubilization of intact petroleum. These dissolved products can undergo further oxidative processes by either direct or indirect photolysis. As weathering proceeds, individual components of the petroleum hydrocarbon mixture degrade by photo oxidation at different rates and to different products, further altering the spectral environment.

Modeling the photo-oxidation of petroleum hydrocarbons is complex because the surface film alters the intensity and spectrum of the incident sunlight. Various researchers have attempted to calculate the rate of photo-oxidation; Huang et al. (1982) proposed equation 2.4-15 for the estimation of photo-oxidation:

$$\frac{dP}{dt} = \left(\frac{B_{sr}}{70}\right)\left(1 - C_c\right) Y \qquad (2.4\text{-}15)$$

where
dP/dt is the photo-oxidation rate, [-],
B_{sr} is the angle of solar radiation, [^{o}],
C_c is the fractional cloud cover, [-],
Y is a coefficient which varies with the thickness of the oil spill, [-].

Most models of oil spill behaviour do not include the effect of photo-oxidation due to its complexity and since, as it has already been referred, it does not affect the mass equilibrium. In the present study, the effect of photo-oxidation was also not taken into account.

2.4.7. Sedimentation

Sedimentation is the adhesion of oil to solid particles which are suspended in the water column or sediment at the bottom. It usually occurs with the heavy-weight components of the oil which do not dissolve in the water. In general, oil adheres to detrital particles (particles which are mixtures of organic matter, bacteria, and small clay particles). Sedimentation also occurs when marine organisms ingest naturally dispersed oil droplets in the water column. The oil droplets

pass through the organism undigested and eliminate as part of the fecal matter. Sedimentation can also occur when oil is stranded on shore and then becomes incorporated with sediments and subsequently transported to subtidal environments. Very heavy or weathered oil can sink directly to the bottom without sorption onto sediments first; this process is enhanced as the density of the water is lowered by the influx of fresh water (ITOPF, 1987; Neff, 1990).

In very few spills of oil that is heavier than water, the oil sinks directly to the bottom, and these kinds of spills occur only in sheltered settings. In contrast, buoyant oil can pick up enough sediment, either after stranding onshore or mixing with sediment suspended by wave action, to become an oil-sediment mixture that is denser than sea water. If the sediment separates from the oil mass, the still-buoyant oil can then re-float.

The oil and sediment volume concentration, the wave heigth and water density are factors that affect this process. Many researchers dealt with the modeling of sedimentation to determine the rate of loss of free oil droplets due to collision and adherence to suspended particulate material (SPM). Lehr (2001) proposed equation 2.4-16 for calculating sedimentation rate:

$$Q_{sed} = k_{sed} \sqrt{\frac{D_{ba}\, f_{bw}}{H_{rms}\, \rho_w\, v_w}}\, C_o\, C_{sed} \qquad (2.4\text{-}16)$$

where
C_o is the entrained oil volume concentration, [mg l^{-1}],
C_{sed} is the suspended sediment volume concentration, [mg l^{-1}],
k_{sed} is a parameter which depends on the type and size of the pieces of sediment, [s],
D_{ba} is the dissipation of wave energy per unit surface area, [J m^{-2}],
F_{bw} is the breaking wave fraction, [-],
v_w is the kinetic viscosity of the water, [m^2 s^{-1}],
ρ_w is the water density, [kg m^{-3}],
H_{rms} is the root-mean-square wave height, [m].

Due to the complexity of the phenomenon, its effect is often neglected in oil spill modeling, especially in 2D modeling; in the present study the contribution of sedimentation was not taken into account to since the approach was two-dimensional .

2.4.8. Biodegradation

Biodegradation is the process where microbes (bacteria and fungi) consume hydrocarbons to use them as a food source and excrete carbon dioxide and water as waste products. This weathering process occurs on the water surface (see Figure 2.4-8), in the water column, in sediments and on shore (Atlas, 1981). Microbes which can utilize hydrocarbons are found naturally in the marine habitats; however, they grow and multiply after an oil spill occurs because additional food sources (carbon) become available following a spill. Biodegradation may continue for years after a spill occurs, and is affected by a variety of organisms. These micro-organisms exist in low concentrations and biodegrade naturally occurring oils in the sea that are liberated when marine flora and fauna die and decompose.

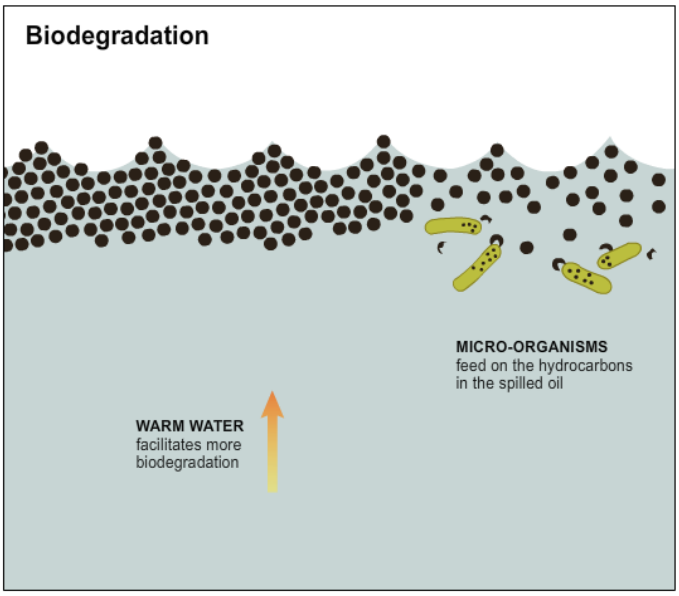

Figure 2.4-8. Biodegradation of oil
(Obtained by: http://www.fastcompany.com/1659822/infographic-day-physics-oil-spills)

The rate of such biodegradation depends upon the availability of nitrogen- and phosphorus-containing nutrients in thc water, as well as the surface exposure of the oil to the organisms (Lehr, 2001). Venosa et al. (1996) developed a first-order relationship for calculating the biodegradation rates of resolvable alkanes, from field data:

$$\left(\frac{A}{H}\right) = \left(\frac{A}{H}\right)_o e^{-K_{bd} t} \qquad (2.4\text{-}17)$$

where
t is the time, [s],
(A/H) is the time-varying hopane-normalized concentration of an analyte, [-],
$(A/H)_0$ is the time-varying hopane-normalized concentration of an analyte at time zero, [-],
K_{bd} is the first-order biodegradation rate constant for an analyte, [s^{-1}].

However, actual 1st-order biodegradation rates are not constant. Instead, they are a function of the residual nutrient concentration according to equation 2.4-18:

$$k_{obs} = k_{max}\left(\frac{N}{K_n + N}\right) \qquad (2.4\text{-}18)$$

where
k_{obs} and k_{max} are the observed and maximum first-order hydrocarbon biodegradation rates, respectively, [s^{-1}],
K_n is the half-saturation concentration for a specific nutrient, [kg m^{-3}],
N is the interstitial pore water residual nutrient concentration, [kg m^{-3}].

Biodegradation is frequently taken into account in oil spill modeling; Wang et al. (2008) who developed a 3D model for predicting oil spill behaviour, investigating the vertical motion of the spilled oil slick, accounted for biodegradation. In the present study, vertical motions and biodegradation are not considered.

2.5. Oil properties

The weathering mechanisms in combination with the environmental factors modify the oil properties with time. These properties are the temperature, the viscosity and density of the oil, the water content of the floating oil, the evaporated oil fraction, the thickness of the evaporating spill surface, the pour and flash points and solubility in water. The most significant of them are also described below.

2.5.1. Oil viscosity

Oil viscosity, μ, is mainly a function of temperature, T, the evaporation fraction, F_e, and the water component of the spill, F_w. Evaporation and emulsification cause its increase in viscosity, according to equation 2.5-1 by Mackay et al. (1980):

$$\mu = \mu_o \exp\left[K_c F_e\right] \exp\left[\frac{2.5 F_w}{\left(1 - K_b F_w\right)}\right] \quad (2.5\text{-}1)$$

where
K_c is oil dependent constant that varies between 1 and 10 (Mackay et al., 1980),
K_b is the mousse viscosity constant, [-], which is taken equal to 0.7 for crude oils and heavy fuel oil, and 0.25 for home heating oil (Zadeh and Hejazi, 2012),
F_w is the fractional water content, [-],
F_e is the volume fraction of the oil evaporated, [-],
μ_o is the parent oil viscosity, [cp], which is calculated by equation 2.5-2:

$$\mu_o = 224\, A_c^{1/2} \quad (2.5\text{-}2)$$

where A_c is the percentage Asphaltene (Zadeh and Hejazi, 2012).

2.5.2. Oil density

The oil density changes over time due to the weathering. Evaporation and emulsification also lead to its increase making the oil less buoyant; to account for the effect of these processes, most weathering models use the approach of Buchanan and Hurford (1988) to estimate the change of oil density with time:

$$\rho_{oil} = \rho_w F_w + \left(1 - F_w\right)\left(\rho_o + K_b F_e\right) \quad (2.5\text{-}3)$$

where
ρ_{oil} is the density of the remaining oil, [kg m^{-3}],
ρ_w is the water density, [kg m^{-3}],
ρ_o is the initial density of the spilled oil, [kg m^{-3}].

According to Lehr (2001) the oil floats under normal weathering processes unless sediment is mixed into it; this usually happens in the surf zone, close to the shore, where sediments are suspended due to wave breaking. Moreover, Lehr (2001) mentions that as the slick ages, it often turns into tar balls; these tar balls are dispersed by the breaking waves and, although they may seem to be sinking, they resurface if the sea surface turns calm since they are buoyant. In Figure 2.5-1 the evolution of an oil slick over time is depicted.

Figure 2.5-1. Evolution of an oil slick over time
(Obtained by Lehr, 2001)

In the present study the approach of Buchanan and Hurford (1988) has also been used (see Chapter 3.3). The oil is assumed to be buoyant, floating on the sea surface.

2.5.3. Oil volume

The evaporation process, together with dissolution and emulsification, leads to an increase in the oil volume. According to Guo and Wang (2009) the volume of the oil spill changes with time, due to the effect of the weathering, according to equation 2.5-4:

$$V_{oil} = \frac{V_o\left(1-\left(F_e + F_d\right)\right)}{1-F_w} \qquad (2.5\text{-}4)$$

where
V_o is the initial volume of the spilled oil [m^3],
F_d is the oil fraction dissolved, [-].

CHAPTER 3: PRESENTATION OF THE MATHEMATICAL MODEL

3.1. Introduction

An oil spill model (OSM) calculates the behaviour (transport, dispersion and physical, biological and chemical processes) of the oil slick using as input meteorological and hydrodynamic data. Although, meteorological data can be easily obtained from historical records and data, bounding the necessity of employing a weather forecasting model, the hydrodynamic field has to be reproduced by hydrodynamic models (HYM); current atlases and live meteorologic observations are not usually available or sufficient.

There are types of OSM; (a) the Coupled or integrated OSM (COSM) and (b) the Composite or single OSM (SOSM). COSM run the OSM and the HYM simultaneously, ideally in real time (dynamic mode). SOSM provides the OSM with weather data and hydrodynamic variables that have been estimated from observations or previous HYM calculations. COSM are more complex and usually require a physical oceanographer to deal with the wind and current input to the HYM, but perform better in predicting the evolution of the spill. However, since they require more information it is easier to get wrong results if the inputs are incorrect. SOSM are easier to handle and less prone to errors, but are less accurate.

The reproduction of the flow field is determinant for defining oil spill behaviour since it provides the necessary information for predicting the related transport and turbulent processes; these processes also affect the biological and physicochemical processes that also take place. In the present study the hydrodynamic model FLOW3DL (Stamou et al., 1999a; 1999b; 2007) has been employed for the calculation of the flow dynamics; the steady state depth averaged wind-induced currents were reproduced whereas the reduction to surface currents was achieved according to Koutitas (1985). The results of the HYM were inserted in the OSM as an input for the calculation of the oil spill trajectory and behaviour; thus the OSM , which was developed in the present study is a SOSM. In this chapter, the governing equations and methodology of the HYM and OSM used are described.

3.2. The hydrodynamic model FLOW-3DL

3.2.1. Introduction

The mathematical model FLOW-3DL (Stamou et al., 1999; 2007a; 2007b) was developed in the Computational Center of the Laboratory of Applied Hydraulics of the School of Civil Engineering of the NTUA supervised by Professor Anastasios I. Stamou. FLOW-3DL is a code written in FORTRAN language environment and can simulate the three-dimensional hydrodynamics and the fundamental processes (advection, diffusion, physicochemical and biological processes) that determine the quality of water bodies. It comprises of subroutines (main.FOR, boundaries.FOR, fishes.FOR, main.FOR, print.FOR, rest.FOR, sand.FOR, tempe.FOR etc) which are accesible by the user and can be modified by them according to the case study. In the present study, the subroutine osm.FOR was added for the prediction of oil spill behaviour (see Chapter 3.3.4).

3.2.2. Govering equations of the flow field

For the calculation of the flow field, model FLOW-3DL involves the 3D non-steady state continuity and momentum equations, expressed in layer formulation. Using fixed permeable interfaces between layers, the equations of the model are vertically integrated over a depth range h, corresponding to a computational layer of that thickness.

The following assumptions are made:
(i) the distribution of the pressure (p) is hydrostatic,
(ii) the Boussinesq approximation is valid, and
(iii) p at the surface is set equal to the atmospheric (zero).

The variables of the equations are:
(i) the layer-averaged velocity components, U, V and W [L/T], along axes x, y and z, respectively, of a Cartesian coordinate system, and
(ii) the free surface elevation, ζ.

Axis z is taken as positive upward from the sea surface.

The mass continuity and momentum equations are written as follows:

Mass continuity

$$\frac{\partial u}{\partial x}+\frac{\partial v}{\partial y}+\frac{\partial w}{\partial z}=0 \qquad (3.2\text{-}1)$$

Momentum equations

In the x direction

$$\frac{\partial u}{\partial t}+u\frac{\partial u}{\partial x}+v\frac{\partial u}{\partial y}+w\frac{\partial u}{\partial z}=fv-\frac{1}{\rho}\frac{\partial p}{\partial x}+\frac{\partial}{\partial x}\left(\nu_h\frac{\partial u}{\partial x}\right)+\frac{\partial}{\partial y}\left(\nu_h\frac{\partial u}{\partial y}\right)+\frac{\partial}{\partial z}\left(\nu_v\frac{\partial u}{\partial z}\right) \qquad (3.2\text{-}2)$$

In the y direction

$$\frac{\partial v}{\partial t}+u\frac{\partial v}{\partial x}+v\frac{\partial v}{\partial y}+w\frac{\partial v}{\partial z}=-fu-\frac{1}{\rho}\frac{\partial p}{\partial y}+\frac{\partial}{\partial x}\left(\nu_h\frac{\partial v}{\partial x}\right)+\frac{\partial}{\partial y}\left(\nu_h\frac{\partial v}{\partial y}\right)+\frac{\partial}{\partial z}\left(\nu_v\frac{\partial v}{\partial z}\right) \qquad (3.2\text{-}3)$$

In the z direction

$$\frac{\partial p}{\partial z}=-\rho g \qquad (3.2\text{-}4)$$

where
t is the time, [T],
u, v and w [L/T] are the variables of the equations are the layer-averaged velocity components, along axes x, y and z, respectively, of a Cartesian coordinate system,
v_h and v_v are the horizontal and vertical eddy viscosity coefficients, [L^2 T^{-1}], respectively,
p [F/A] is the pressure,
f is the Coriolis parameter, [-],
g is the gravitational acceleration, [L/T^2, 9.81 m s^{-2}],
ρ_w is the water density, [M/L^3].

The solution procedure is as follows:

(i) For a given vertical density variation, the pressure p is determined using equation 3.2-4.
(ii) The horizontal velocity components (u and v) are calculated next by equations 3.2-2 και 3.2-3.
(iii) The vertical velocity (w) is calculated via the continuity equation 3.2-1 for each layer, starting from the bottom where the boundary condition w=0 is valid.

In the free surface, the continuity equation 3.2-1 is written as a linearized kinematic boundary condition, whereby the surface elevation can be deduced:

$$\frac{\partial \zeta}{\partial t} + \frac{\partial \zeta}{\partial t} u_\zeta + \frac{\partial \zeta}{\partial t} v_\zeta = w_\zeta \qquad (3.2\text{-}5)$$

where the subscript 'ζ ' denotes values at the surface layer.

In FLOW-3DL the eddy viscosity coefficients can be set constant or be calculated from simple mathematical expressions; for example, the horizontal eddy viscosity coefficient can be derived by Smagorinsky (1963), while the vertical eddy viscosity coefficient for non-buoyant wind-induced flows can be determined using the distribution proposed by Koutitas and O'Connor (1980).

3.2.3. Boundary conditions

3.2.3.1. General

For the solution of the hydrodynamic equations the boundary conditions at the following boundaries have to be defined first:

(i) at the free surface,
(ii) at the bottom,
(iii) at the coasts, and
(iv) at the open sea boundaries.

3.2.3.2. Free surface

For the wind driven model, it is assumed that wind action at the free surface produces horizontal shear stresses τ_{sx} and τ_{sy}, [M L^{-1} T^{-2}], acting along axes x and y, respectively. These can be calculated by the following equations:

$$\frac{\tau_{sx}}{\rho} = \nu_v \left.\frac{\vartheta u}{\vartheta z}\right|_{z=-\zeta} = C_s\, u_{10} \sqrt{u_{10}^2 + v_{10}^2} \qquad (3.2\text{-}6)$$

$$\frac{\tau_{sy}}{\rho} = \nu_v \left.\frac{\vartheta v}{\vartheta z}\right|_{z=-\zeta} = C_s v_{10} \sqrt{u_{10}^2 + v_{10}^2} \qquad (3.2\text{-}7)$$

where
u_{10} and v_{10} x are the wind velocity components at 10m height from the surface along axes x and y, [L T^{-1}], respectively,
v_h and v_v are the horizontal and vertical eddy viscosity coefficients, [L^2 T^{-1}], respectively,
ρ_w is the water density, [M L^{-3}],
C_s is the shear stress coefficient at the free surface, in general varying with wind speed. In this study C_s is taken constant equal to $3.05 \cdot 10^{-6}$, [-], (Smagorinsky, 1963).

3.2.3.3. Bottom

At the sea bed the shear stress is given by the following equations:

$$\frac{\tau_{bx}}{\rho} = \nu_v \left.\frac{\vartheta u}{\vartheta z}\right|_{z=H} = C_b\, u_b \sqrt{u_b^2 + v_b^2} \qquad (3.2\text{-}8)$$

$$\frac{\tau_{by}}{\rho} = \nu_v \left.\frac{\vartheta v}{\vartheta z}\right|_{z=H} = C_b\, v_b \sqrt{u_b^2 + v_b^2} \qquad (3.2\text{-}9)$$

where
τ_{bx} and τ_{by} [M/LT^2] are the horizontal components of the shear stresses acting at the bottom along axes x and y, respectively,
C_b is the shear stress coefficient at the bottom, [-],
u_b and v_b the velocity components at the bottom along axes x and y, [$m\ s^{-1}$],respectively,
H is the water depth, [m].

In this study, C_b is calculated by equation 3.2-10 using a value for the Manning's friction coefficient to $n=0.03\ m^{-1/3}s^{1/2}$.

$$C_b = \frac{2 \cdot g \cdot n^2}{R_{hr}^{1/3}} \tag{3.2-10}$$

where
g is the gravitational acceleration, [$9.81\ m\ s^{-2}$],
R_{hr} is the hydraulic radius, [m].

3.2.3.4. Interfaces between the layers

The shear stress on the interfaces between the horizontal layers is calculated as follows:

$$\frac{\tau_{ix}}{\rho} = \nu_v \left.\frac{\vartheta u}{\vartheta z}\right|_{z=h_i} = C_i (u_u - u_d)\sqrt{(u_u - u_d)^2 + (v_u - v_d)^2} \tag{3.2-11}$$

$$\frac{\tau_{iy}}{\rho} = \nu_v \left.\frac{\vartheta v}{\vartheta z}\right|_{z=h_i} = C_i (v_u - v_d)\sqrt{(u_u - u_d)^2 + (v_u - v_d)^2} \tag{3.2-12}$$

where
τ_{ix} and τ_{iy} are the horizontal components of the shear stresses in the x and y directions, respectively, at the layer interfaces,
C_i is the (non-dimensional) shear stress coefficient of the interface,
u_u and v_u are the horizontal velocity components at the upper layer in the x and y directions, respectively,
u_d and v_d are the horizontal velocity components at the lower layer in the x and y directions, respectively, και
h_i is the depth of the layer.

3.2.3.5. Wall boundaries

The velocity components normal to the coastal (wall) boundaries are set equal to zero.

3.2.3.6. Open sea boundaries

The following boundary conditions can be used:
(a) Open sea boundary (no-reflection condition for the velocity normal to the boundary)
(b) Known water elevation variation with time (for example for the tidal driven conditions).
(c) Specified parameter values (e.g. water elevation, velocity components etc) from measurement field data.

3.2.4. Numerical solution of the equations of the flow field and quality variables behaviour

3.2.4.1. General

The differential equations that describe the flow field or the behaviour of a quality variable, that were described in Chapter 3.2.2 can be written as follows:

$$\frac{\partial}{\partial t}(\rho\Phi) + \mathrm{div}(\rho U\Phi) = \mathrm{div}(\Gamma \mathrm{grad}\Phi) + S_{\Phi} \qquad (3.2\text{-}13)$$

Setting
1) Φ=1 the continuity equation is derived,
2) Φ =u, v or w the momentum equations are derived and
3) Φ=T or S the advection-diffusion equation of a quality variable of concentration C is derived.

In most of the practical applications the differential equations formed like equation 3.2-13 cannot be analytically solved. Their solution is achieved by using numerical methods; the most prominent are the following:

1) The method of finite differences or finite volumes.
2) The method of finite elements.
3) The boundary elements method.

In the model FLOW-3DL the method of finite differences or finite volumes is used. In this method the computational domain is replaced by small regions that are called «control volumes (c.v.)». The differential equations are then integrated over each control volume and the numerical equations are derived; the numerical equations are then directly solved using an explicit solution scheme.

It is noted that the numerical equations are not as accurate as the differential equations since (a) the definition of the mode of variation the variables and their derivatives between control volumes (differencing scheme) and (b) the approximations made for some terms of the differential equations induce computational errors.

3.2.4.2. Discretization of the flow field

In FLOW-3DL discretization of the flow field in the horizontal and vertical dimensions is made, using an orthogonal grid of Dx, Dy and Dz dimensions, respectively, for the numerical solution of the equations.

The boundaries of the coasts and the open sea boundary are segmentally simulated by the sides of the c.v., which are parallel to the Ox or Oy directions.

The grid employed by FLOW-3DL is staggered. The velocities (u, v and w) and the scalar quantities (surface elevation, ζ, and quality parameters, Φ) are calculated in characteristic locations of the staggered computational grid. Specifically:

1) velocities u, v and w are determined at the faces of the control volumes, which are parallel to the Ox, Oy or Oz directions, respectively, whereas
2) the elevation of the water surface ζ and the quality variables Φ are determined at the centers of the control volumes.

Moreover, they are characterized by subscripts of exhibitors that correspond to the values of x, y, z and t variables:

1) the subscript i refers to the x-coordinate Ox ($x_i=i\Delta x$),
2) the subscript j refers to the y-coordinate Oy ($y_i=j\Delta y$),
3) the subscript k refers to the z-coordinate Oz ($x_k=k\Delta z$), and
4) the exhibitor n refers to time ($t^n=n\Delta t$).

The locations of the Cartesian coordinate system Oxyz, where u, v, w and ζ are calculated, together with their subscripts are shown in Figure 3.2-1. The symbols n, s, w and e are used to denote the north, south, western and eastern sides of the control volumes, respectively.

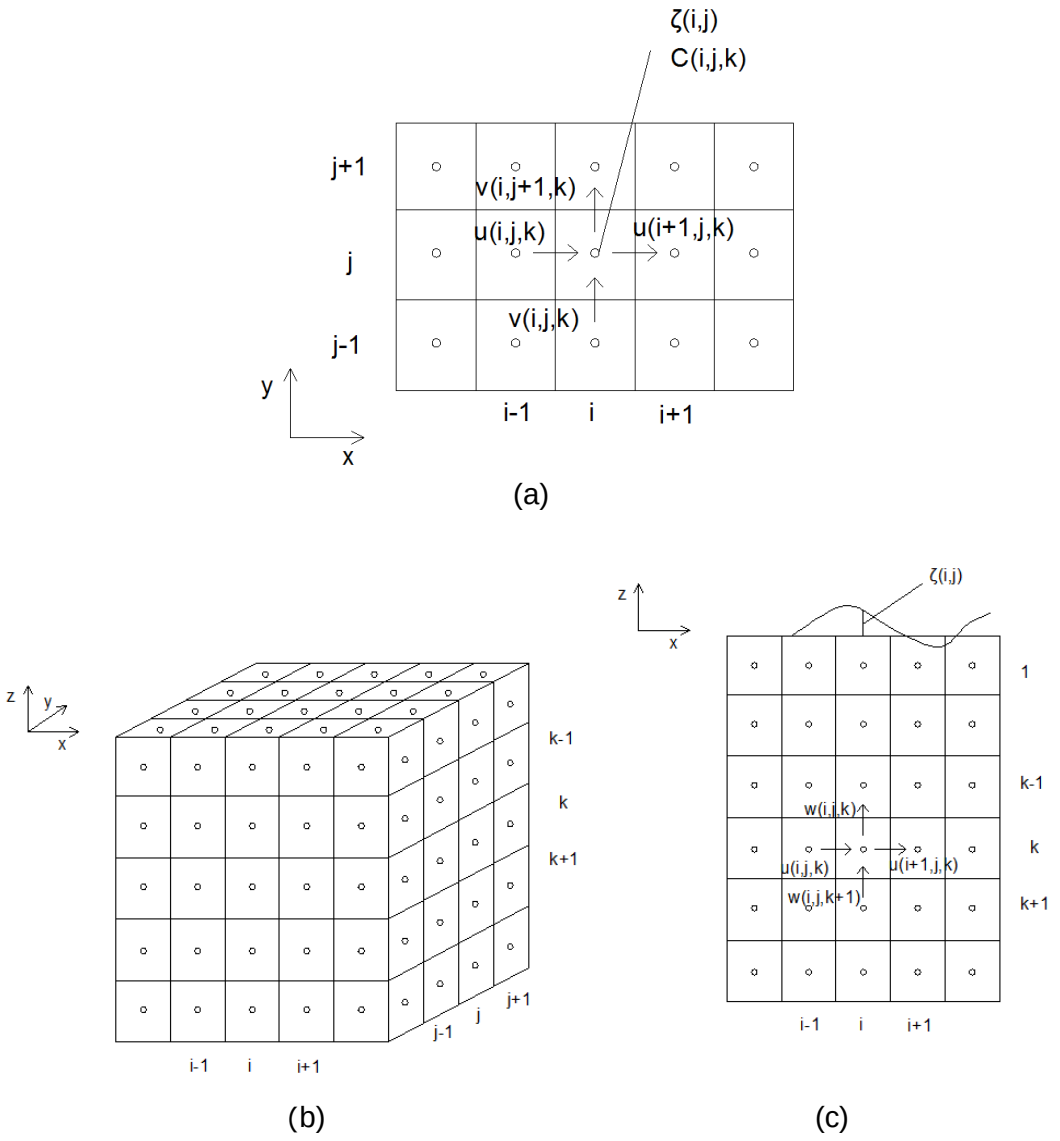

Figure 3.2-1. Sketch of the computational grid for the spatial discretization of the differential equations in (a) upper, (b) 3D and (c) side view.

3.2.5. Present modifications

The following modifications have been performed in the existing computer code to permit its use in the present study:

1) The depth average equations for one layer (k=1), were modified to calculate the average flow velocities.
2) The code was extended to calculate the velocities of the surface coastal currents. Since the main body of oil slick moves on the sea surface, the horizontal surface velocity components (U_{surf}, V_{surf}) were used in the calculations (see Chapter 3.3.2-2).

3.3. The Oil Spill model

3.3.1. Introduction

The present Oil Spill Model (OSM) was developed to predict the behaviour of an oil slick accounting for the two-dimensional motions of the oil particles and the most frequently used in the literature(for example Zadeh and Hejazi, 2012; Chao et al., 2001) weathering processes that are also the most important, compared to the others; these processes are the spreading, evaporation, dissolution and emulsification, which were modeled by the use of classical empirical methods (see Chapter 2). The advection and dispersion processes are also taken into account via the use of the random walk procedure of the particle tracking method; the oil mass was divided in a number of particles that moved separately, driven by the surface currents and a stochastic factor to include the effect of dispersion. The framework of the OSM is described next.

3.3.2. Input data

In this chapter the necessary input data, that have to be collected before applying the Oil Spill Model (OSM), are described. Figure 3.3-1 summarizes these data which are the following:

- the quantity and the properties of the spilled oil; see Chapter 3.3.2.1,
- the hydrodynamic data, i.e. surface currents velocity components; see Chapter 3.3.2.2,
- the wind characteristics (magnitude and direction); see Chapter 3.3.2.3,
- the sea characteristics (density and temperature); see Chapter 3.3.2.4, and
- the locations of the sea accidents; see Chapter 3.3.2.5.

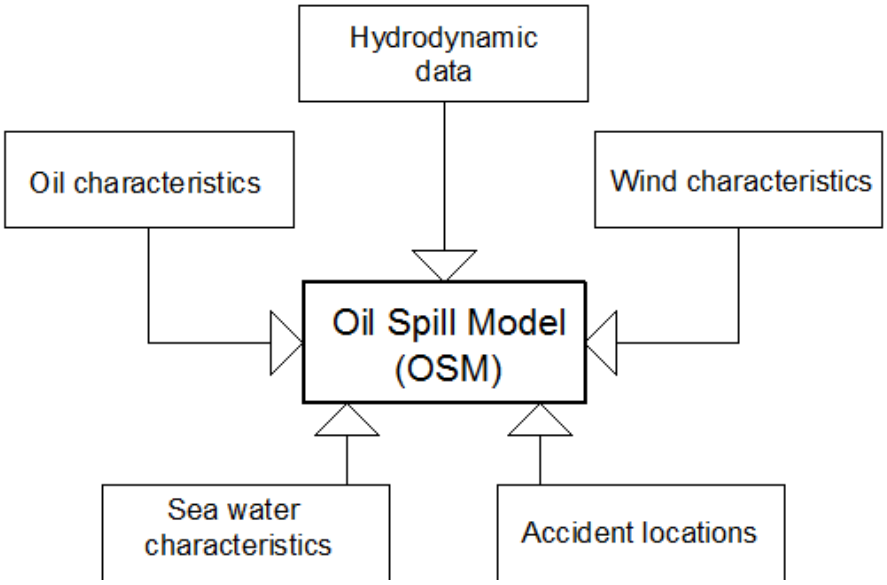

Figure 3.3-1. Necessary inputs for the OSM

3.3.2.1. Oil characteristics

The type of the spilled determines the behaviour of the slick which goes through the weathering; these are the initial oil viscosity (μ_o) and density (ρ_o), the initial boiling point at F_e=0 (T_o) and the gradient of the distillation curve (T_G). Moreover, the empirical models, which are employed by the OSM for modeling the weathering processes, require as an input parameters that derive from distillation data; for example the constants A and B that are inserted in equation 2.4-4 (Mackay, 1980) for modeling emulsification. For undefined crudes the A, B constants are taken equal to 6.3 and 10.3, respectively, according to Zadeh and Hejazi (2012) who also present Table 3.3-1, including oil properties data from the evaporation experiments conducted by Bobra (1992).

Table 3.3-1. Data from the Bobra (1992) evaporation experiments (Obtained by Zadeh and Hejazi, 2012)

Oil	T_o (K)	T_G (K)	A	B	Density (g/mL) 15°C	Viscosity (cp) 15°C
Adgo	551	195.4	24.278	20.535	0.953	61.6
ASMB	397	539.1	8.133	11.594	0.839	9.2
Amauligak	471	370	12.074	14.485	0.8896	14
Bent Horn	406	484	11.408	13.834	0.8181	24
Diesel	517	139.8	20.274	18.052	0.827	2.7
Endicott	453.7	1400	−0.815	7.107	0.9149	84
North Slope	430.6	722	4.452	10.137	0.8936	23
Panuke	268.1	367.8	7.174	11.437	0.7757	1.1

3.3.2.2. Hydrodynamic data

As already mentioned, the present OSM is characterized as a single OSM (SOSM) since the hydrodynamic data are provided from previous HYM calculations; the hydrodynamic model FLOW-3DL (Stamou et al., 1999; 2007a; 2007b) has to be applied first in order to reproduce the hydrodynamic field. In the present study, the Shallow Water Equations (SWE), i.e. depth average equations for one layer, were used to calculate the average flow velocities; thus, after applying the HYM, the horizontal depth averaged velocity components were extracted (U, V). However, since oil forms a thin film that mainly moves on the sea surface, the velocity of surface currents (U_{surf}, V_{surf}) had to be calculated. Koutitas (1985) proposed the following equations for the calculation of the horizontal surface current velocities in the x and y directions:

$$U_{surf} = 1.5\,U + 0.03\,U_{wx} \quad (3.3\text{-}1)$$

$$V_{surf} = 1.5\,V + 0.03\,U_{wy} \quad (3.3\text{-}2)$$

where

U and V are the depth averaged flow velocity components [m s^{-1}], in the x and y directions, respectively, which have been calculated by the HYM, and

U_{wx} and U_{wy} are the wind velocity components [m s^{-1}], in the x and y directions, respectively.

3.3.2.3. Wind characteristics

As already referred in Chapter 3.2, the wind characteristics, i.e. the wind direction and magnitude, are necessary inputs for the HYM. However, since the wind magnitude affects the weathering it also has to be inserted as an input in the OSM. Moreover, the wind direction is a necessary parameter for determining the magnitude of the sea surface currents (equations 3.3-1, 3.3-2). Wind data can be collected from meteorological stations to be statistically analyzed; the most probable wind scenarios should give the most probable oil slick trajectories in case of a sea accident. The environmental temperature (K) is also required as an input.

3.3.2.4. Sea water characteristics

The sea water density (ρ_w) is a necessary input for the modeling of the weathering processes (for example the spreading of the oil spill).

3.3.2.5. Accident locations

The determination of the sea accident locations, i.e. the locations of accidental release of oil into the sea, first of all, depend on the type of the accident. The main types of oil spill accidents are the following:

(a) Oil drilling accidents: hydrocarbon spills and blowouts during drilling operations due to equipment failure, human mistakes and extreme natural impacts (seismic activity, ice fields, hurricanes etc) (http://www.offshore-environment.com/accidents.html).

(b) Oil transportation and storage accidents: Tankers are the main way of delivering oil. The main causes of tanker accidents include running aground and into shore reefs, collisions with other vessels, and fires and explosions of the cargo. Moreover, underwater reservoirs for storing liquid hydrocarbons are often either built near platform foundations or anchored in the area of developments and near the onshore terminals. Thus, there is accident risk during tanker loading operations and under severe weather conditions. (http://www.offshore-environment.com/accidents.html).

(c) Generally ship accidents: Oil can be released into the sea due to various types of ship accidents which are also shown in Figure 3.3-2 (collision, fire, explosion, foundering, mechanical failure, grounding and ramming); in case of tankers the oil quantity released is the greatest.

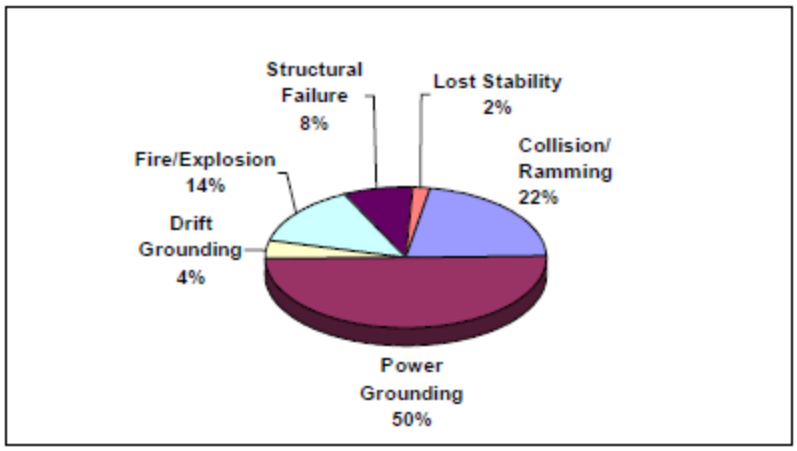

Figure 3.3-2. Main causes of oil spill accidents
(Obtained by Triantafyllou and Vergetis, 2004)

Thus, in case of a drilling or storage accident, the accident location can be easily defined. However, in the case of ship accidents, the prediction of the most probable accident locations requires accident frequency analysis which takes into account marine traffic and navigation data, ship characteristics, weather conditions and sea currents, hydrographic data, coastal facilities, statistics of previous accidents etc. In the present study, accident frequency analysis was not conducted; however, the accident locations were defined in the vicinity of the busiest ports in the application area and the shallowest waters of the gulf (see Chapter 4).

3.3.3. Objectives and assumptions

The present study is a preliminary but fundamental attempt to predict the behaviour of an oil spill in case of a sea accident. The objective is to estimate the trajectory of the oil spill that will be formed and the evolution of its volume and mass with time, while it moves in the fluid sea environment. Once the oil spill reaches the coast and oil starts to concentrate on the coast, the rate and evolution of most of the weathering processes is modified or stopped; for example, while oil reaches the coast the thickness of the deposited oil layer increases and , as a result, the evaporation rate decreases. Thus, most of the empirical models of the weathering processes are not valid if the oil is deposited on the coast.

The present OSM accounts for the weathering processes that are documented in the literature (see for example ITOPF, 2010; Exxon, 1985) to be the most determinant for the fate of an oil slick during the first days or weeks after the accident; these are the spreading, evaporation, dissolution and emulsification (see Figure 2.4-1). Advection and dispersion are also taken into account as the most decisive processes for the transport of the slick. The particle tracking method is employed to predict the oil slick motion and distribution of oil particle concentrations in the coastal waters, which has also been widely used in oil spill modeling (for example Wang et al., 2008; Chao, 2001). It is also assumed that the release of oil particles is instantaneous.

Since in the present version the OSM accounts only for the behaviour of the oil spill in the water body, an assumption had to be made regarding the "stopping criterion" for the track of the oil particles; calculations were stopped at time T*, when the 10% of the particles reached the coast (or the open boundary). This allowed the estimation of the time (T*) that the spill needed to reach the boundaries; this information is very important and critical for the operational actions that have to be taken for the retention and purification of an oil spill, once a sea casualty happens, aiming at the avoidance and mitigation of pollution impacts.

3.3.4. Description of the OSM

3.3.4.1. Methodology

The Oil Spill Model (OSM) that was developed in the present study is a part of the series FLOW-3DL. It is characterized as a Composite or Single OSM (SOSM) (see Chapter 3.1) since it is provided with hydrodynamic data from previous calculations by the HYM FLOW-3DL.

The Oil Spill Model (OSM) employs the computational grid constructed for the calculation of the flow field by the HYM. A random walk procedure is used for calculating the turbulent diffusive transport of the oil spill; the oil mass is divided into small particles mass which advect and disperse individually. Each grid cell is characterized by a number, N_i, which counts the number of oil particles that move within its boundaries, at the end of each time step. The procedure of the OSM calculations, which is also described in Figure 3.3-3, is as follows:

Step 1: Insertion of the environmental factors

Before any OSM calculations the following data are defined: (i) the wind speed, (ii) the environmental temperature, (iii) the density and (iv) the viscosity of the sea water. The hydrodynamic field, i.e. the results of the HYM model, are also inserted and the horizontal surface current velocities in the x and y directions are calculated by equations 3.3-1 and 3.3-2 (see Chapter 3.3.2.2).

Step 2: Definition of the initial spill

The initial volume of the spilled oil (V_o), its density (ρ_o) and the location of the accident (X,Y) are defined first. The oil density depends on the oil type (see Chapter 3.3.2.1), the initial volume varies according to the examined accident scenario whereas the accident location has already been defined via an accident frequency model, as an assumption of the researcher, from

historical data etc (see Chapter 3.3.2.5). The number, N, of the particles, that the oil spill is divided into, is defined at this step.

Step 3: Weathering processes
The new volume, V_{oil}, and density, ρ_{oil}, of the oil spill are calculated at each time step with the use of the empirical models described in Chapter 2. The weathering processes are taken into account with the following order:

(a) the area, A_s, of oil spill is calculated via equation 2.4-1 by Lehr et al. (1984).
(b) the evaporated oil volume fraction, F_e, is calculated via equation 2.4-4 by Mackay (1980).
(c) the dissolution rate, S_D, is calculated via equation 2.4-12 by Cohen et al. (1980).
(d) the emulsified volume fraction, F_w, is calculated via equation 2.4-14 by Mackay (1980).

V_{oil} and ρ_{oil} of the current time step are then calculated via equations 2.5-3 and 2.5-4 by Buchanan and Hurford (1988) and Guo and Wang (2009), respectively.

Step 4: New oil Mass
The new total oil mass, M_{oil}, is calculated at each time step via inserting the updated values of oil spill volume, V_{oil}, and oil density, ρ_{oil}, in equation 3.3-3:

$$M_{oil} = V_{oil} \cdot \rho_{oil} \tag{3.3-3}$$

Step 5: Division of the oil mass into particles
The new total mass of the oil spill is then divided into a number of N particles of equal mass which advect and disperse in the fluid domain individually, each one having an oil mass that changes with time due to the weathering. The number of particles is assumed to be constant which implies that, for example, particles “don’t evaporate”; however their mass is reduced due to evaporation. The number N of particles is defined by the researcher; the higher the number N the more accurate is the representation of the oil mass as an ensemble of oil particles. The mass of each oil particle is equal to:

$$M_i = M_{oil} / N \tag{3.3-4}$$

In the present study, the oil mass is divided into N=10,000 particles.

Step 6: Displacement of oil particles
The displacement of each particle (DS_X and DS_Y) at each time step is the addition of the distances that each one travels due to advection ($DS_{X,adv}$ and $DS_{Y,adv}$) and dispersion ($DS_{X,disp}$ and $DS_{Y,disp}$), at each time step. The combination of equations 2.3-1 and 2.4-10 yield the following:

$$\text{and} \qquad \begin{aligned} DS_X &= DS_{X,adv} + DS_{X,disp} = U_{surf}\, Dt + DS\cos\varphi \\ DS_Y &= DS_{Y,adv} + DS_{Y,disp} = V_{surf}\, Dt + DS\sin\varphi \end{aligned} \tag{3.3-5}$$

where DS [m] is the distance that each particle travels due to horizontal dispersion and φ is an angle [rad] that denotes the randomness of the direction of each particle, at each time-step, due to dispersion. DS and φ are calculated by equations 2.4-8 and 2.4-9, respectively.

Thus, the new position (X,Y) of each particle at the end of each time step can be calculated:

$$X = X^o + DS_X \text{ and } Y = Y^o + DS_Y \tag{3.3-6}$$

where X^o, Y^o are the coordinates of a particle’s position in the current time level.

Step 7: Counting of the oil particles at each grid cell

At each time step, the total number of particles, N_i, is defined at each grid cell. The particles that reach the coast are "stored" in the land coastal cells whereas the particles that exit the computational domain through the open boundaries are not also taken into account in the further computations. Afterwards, the remaining oil mass, M, at each grid cell is calculated:

$$M = M_i \cdot N_i \qquad (3.3\text{-}7)$$

Steps 3 to 7 are repeated until the stopping criterion is fulfilled, i.e. until the 10% of the oil particles leave the computational domain by reaching the coast or passing through the open boundaries (see Chapter 3.3.3).

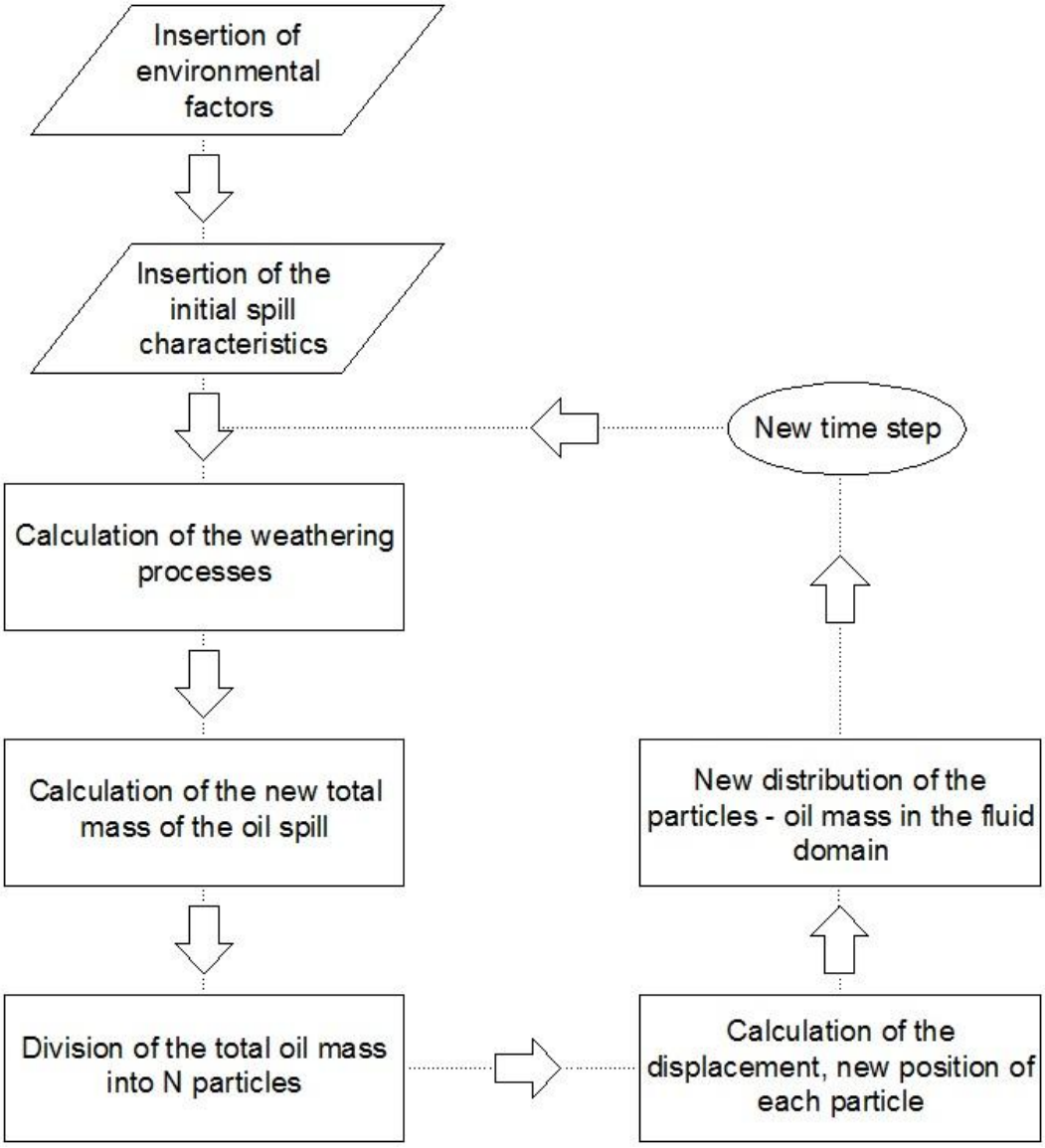

Figure 3.3-3. Steps of the OSM calculations

The time T*, i.e. the time needed for the 10% of the particles representing the spill to reach the coast (or the open boundary) is derived. Then the code can be reran and intermediate plots of the oil mass distribution can be extracted; in the present study plots were extracted at times T*/8, T*/4, T*/2 and T* to represent the trajectory of the oil spill.

3.3.4.2. A simple oil spill model

Before the development of the code in FORTRAN, preliminary calculations were performed to estimate the evolution of the weathering with time using an EXCEL spreadsheet. The particle tracking method was not applied in EXCEL due to the large computational memory needed to model the trajectories of each particle (here N=10,000 particles). However, the methodology of random walk procedure was tested considering that the total mass of the spill was concentrated in the one particle.

The mathematical models of the step 3 of the methodology (see Chapter 3.3.4.1) were employed for the calculation of the density, ρ_{oil}, and volume, V_{oil}, of the oil spill with time; an indicative initial oil volume V_o=500 barrels and density ρ_o=827.0 kg m^{-3} were considered, spilled in location (X_o,Y_o)=(0,0). Regarding the environmental factors, the air temperature and sea water density were considered to be equal to T=20 ° C and ρ_w=1026 kg m^{-3}, respectively, whereas the wind magnitude was taken equal to U_w=1.7 m s^{-1}, assuming that the wind velocity components were equal to (U_{wx}, U_{wy})=(0.8,-1.5) m s^{-1}. It was also assumed that the surface currents velocity was approximately equal to the 3% of wind velocity.

A time step equal to Dt=60 sec used. In each time step the procedure of the calculations was the same as described in Chapter 3.3.4.1 (see also Figure 3.3-3); the only difference was that the mass was not divided into N particles but considered to move as a single body. This was a preliminary stage of the computations to test the methods used and verify the results of the FORTRAN code regarding the weathering processes. More specifically, the order of the calculations at each time step was the following:

(a) a random number was considered in the interval [0,1].
(b) the distance DS and angle φ were calculated via equations 2.4-8 and 2.4-9, respectively,
(c) the displacement (DS_X, DS_Y) of the spill was calculated via equation 3.3-5,
(d) the new position of the spill was calculated via equation 3.3-6,
(e) the area, A_s, of oil spill was calculated first via equation 2.4-1,
(f) the evaporated oil volume fraction, F_e, was calculated via equation 2.4-4,
(g) the dissolution rate, S_D, was calculated via equation 2.4-12,
(h) the emulsified volume fraction, F_w, was calculated via equation 2.4-14,
(i) the new volume, V_{oil}, density, ρ_{oil}, and thickness $h=V_{oil}/A_s$ of the spill were calculated.

Figure 3.3-4 presents the results of the preliminary calculations in the EXCEL spreadsheet regarding the evolution of weathering with time. It can be observed that the oil slick thickness decreases rapidly during the initial 1 h. This means that the first stage of spreading occurs in a short time, due to gravity, inertia and viscous forces, and after this initial phase the surface tension the surface tension phase of spreading takes over and lasts for a longer time, until the oil slick becomes unstable and breaks up (Chao et al., 2001). The oil density, ρ_{oil}, increases as the volume fraction of emulsified oil, F_w, increases too. Regarding the volume of the oil spill, although it initially seems to increase, it then starts to decrease due to the evaporation and emulsification processes. The combined act of evaporation and dissolution mainly increases during the first 4 h; at time t=2 h an inflection point is noticed which coincides with the time that the oil spill volume takes its minimum value. After this point, the act of loss mechanisms, i.e. evaporation and emulsification, fades and the oil volume starts to increase again.

Qualitative agreement was observed between the results of this simple mathematical model and the results in the literature (Chao et al., 2001; Stiver and Mackay; 1984; Mackay et al., 1980). The results regarding the weathering processes were also used to validate the results of the FORTRAN code.

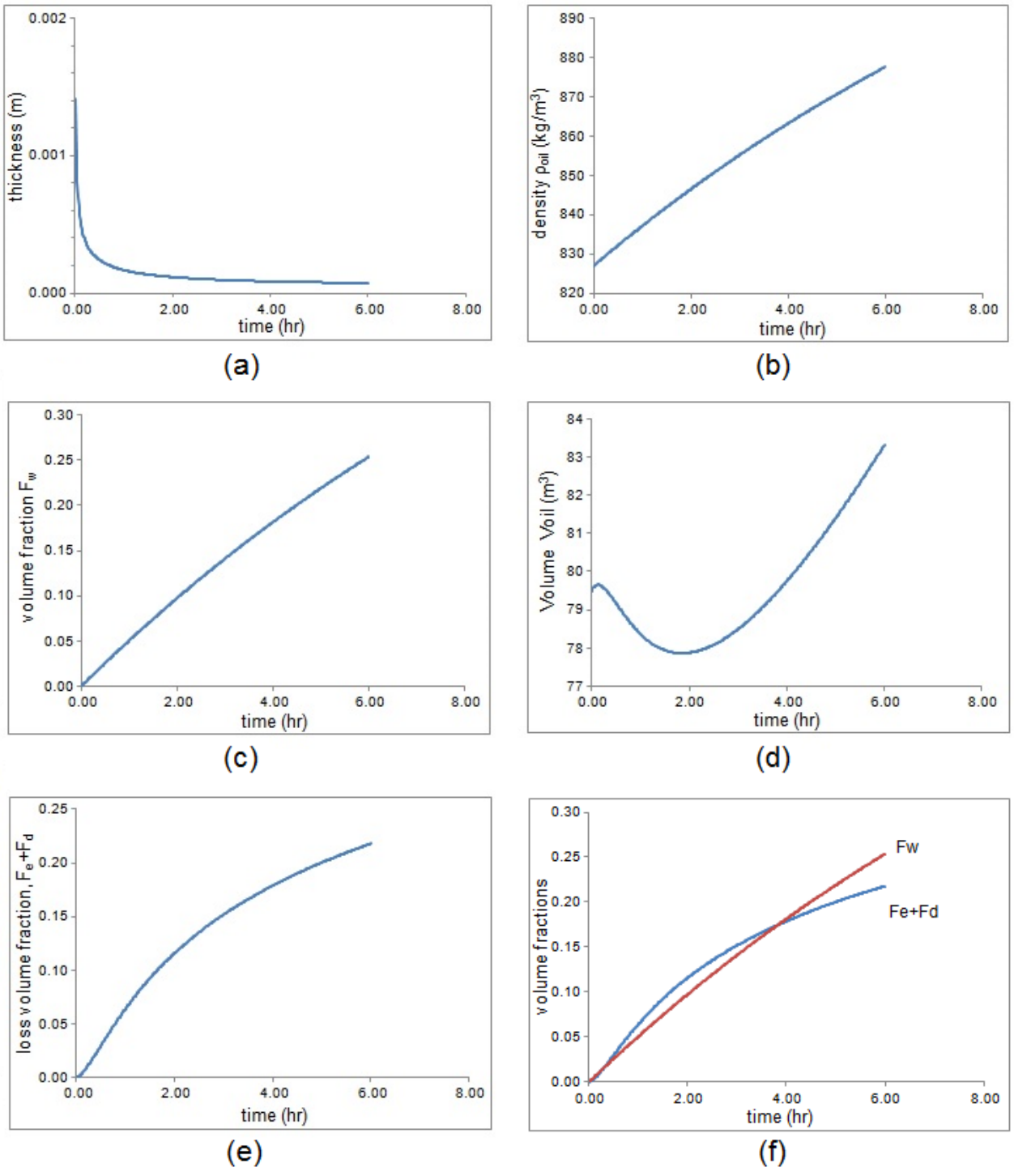

Figure 3.3-4. Evolution of (a) the spill thickness, h, (b) the oil density, ρ_{oil}, (c) the emulsified volume fraction, F_w, (d) the oil spill volume, V_{oil}, (e) the volume fraction of loss due to evaporation and dissolution, F_e+F_d, with time and (f) comparison.

Figure 3.3-5 depicts the trajectory of the spill using the simplified method described in this method. It is noted that this is not an accurate method for predicting the oil spill trajectory; it was tested is order to examine the random walk method to model the movement of a single particle. The effect of dispersion is obvious in the irregular pattern of the calculated trajectory.

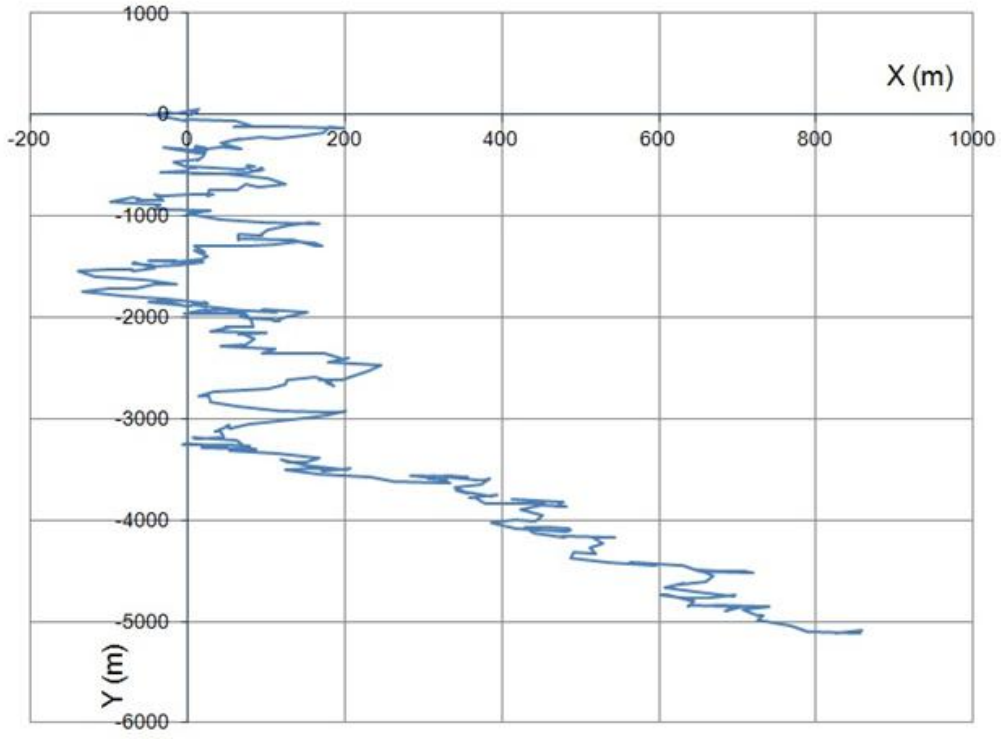

Figure 3.3-4. Trajectory of the oil spill

CHAPTER 4: CHARACTERISTICS OF THE APPLICATION AREA: THE SARONICOS GULF

4.1. Introduction

The Saronicos Gulf is located in east-central Greece, bounded by Attica and Peloponnesus coasts. The gulf is connected to the Aegean Sea to the south by an open boundary about 40 km long, extending from cape Sounion to the coast of Peloponnesus. At the west, Saronicos Gulf is connected to Corinthian Gulf through the Isthmus of Corinth, which is a narrow channel of about 8.0 m depth and 21.0-25.0 m width. The geometry of the gulf is complex including smaller gulfs, such as the Gulf of Elefsina. Several islands are also included with the largest ones being Aegina, Salamina, Poros and Agkistri. The Saronicos Gulf includes over 30 ports of different uses; the most important is the Port of Piraeus which is the largest and busiest port of Greece, handling mainly passenger ships. The Port of Piraeus, located in the vicinity of the capital of Greece, Athens, is a principal nautical and financial hub. An important port for the area is also the Port of Elefsina whereas the ports of Isthmia and Aegina are also busy enough.

Figure 4.1-1. Upper view of the Saronicos Gulf
(Source: http://www.google.com/earth/)

The Saronicos Gulf was chosen to be the application area of the present study due to its navigational traffic and thus increased probability of sea accidents. Moreover, an oil spill accident in Saronicos Gulf would have severe environmental impacts since several beaches and natural protected areas are located along its coasts. Thus, applying the Oil Spill Model (OSM) that was developed in the present study, in this area could be used for constructing Risk Maps and operational purposes.

4.2. Morphology and bathymetry

The water depth in Saronicos Gulf is highly variable; in the western part the depths reach up to 400 m whereas shallow areas are detected in the vicinity of the islands and the gulf of Elefsina (30-50 m depth). The gulf can be divided into four smaller basins, the western, the inner and outer eastern basins and the gulf of Elefsina. Figure 4.2-1 depicts the general bathymetry of the gulf whereas the sub-basins into which it is divided are also shown.

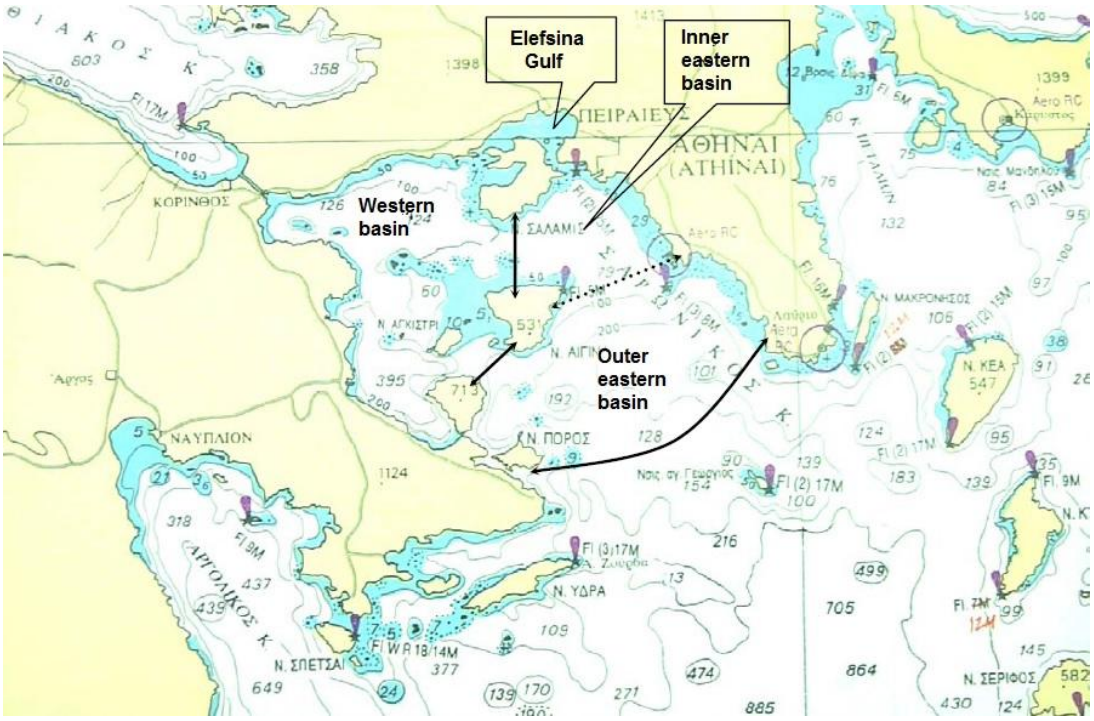

Figure 4.2-1. General bathymetry and morphology of the Saronicos Gulf (Obtained by Kalosakas, 2000)

4.3. Meteorological data

The wind data (wind direction and magnitude), which were used in the present study, were obtained from records of the Hellinikon weather station which is located in the vicinity of the gulf. Table 4.3-1 presents the annual frequency (%) observations of wind directions and magnitude in Beaufort scale in the area of study, at 15.0 m altitude. In Figure 4.3-1 a histogram of the most frequent winds in Saronicos Gulf, which are of magnitude of 1 to 6 Beaufort, are presented.

Table 4.3-1. Annual frequency (%) of wind direction and forces in Beaufort scale from observations 06h, 12h, 18h GMT (Station Hellinikon - Period 1955-1998)

BEAUF	N	NE	E	SE	S	SW	W	NW	CALM	S U M
0									18.109	18.109
1	0.953	0.668	0.482	0.362	0.603	0.482	0.646	0.635		4.831
2	4.82	3.396	1.917	2.607	3.966	3.856	2.859	3.013		26.434
3	5.752	4.404	1.632	1.994	4.174	3.232	1.972	2.531		25.691
4	5.390	4.875	1.435	0.920	1.873	0.909	0.668	1.775		17.845
5	1.775	1.687	0.296	0.208	0.471	0.186	0.208	0.548		5.379
6	0.493	0.416	0.088	0.044	0.110	0.055	0.066	0.153		1.425
7	0.077	0.055	0.011	0.011	0.011	0.011	0.011	0.022		0.209
8	0.022	0.011	0.011	0	0.011	0.011	0	0.011		0.077
9	0	0	0	0	0	0	0	0		0
10	0	0	0	0	0	0	0	0		0
>11	0	0	0	0	0	0	0	0		0
S U M	19.282	15.512	5.872	6.146	11.219	8.742	6.430	8.688	18.109	100

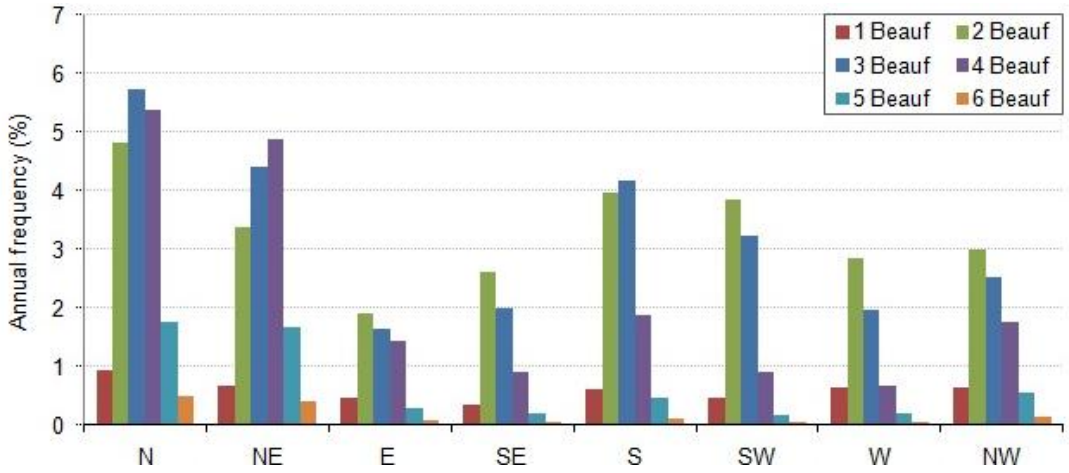

Figure 4.3-1. Histogram of the annual frequency (%) of wind direction and magnitude 1-6 Beaufort from observations 06h, 12h, 18h GMT (Station Hellinikon - Period 1955-1998)

From the wind data presented in Table 4.3-1 and Figure 4.3-1 the following are noticed:

(a) The prevailing winds are from northerly directions (N, NE and NW), with total annual frequency equal to 43.5%. The magnitude of these winds is mainly between 2-4 Beaufort (annual frequency 36.0%).

(b) The wind from the south (S, SE and SW) have a total annual frequency equal to 26.1%, with the 23.5% lying in the range 2-4 Beaufort wind magnitude.

(c) Calm prevails in the gulf for the 18.1% of the year.

4.4. Ports located in Saronicos Gulf

Saronicos Gulf includes over 30 ports of different uses which serve passengers, cargo ships and containers, industrial, port facilities and refineries, ship repairing and military facilities, leisure and fishing crafts and water sports facilities. Table 4.4-1 includes the 33 most important ports located in Saronicos Gulf together with their numbering and characterization of their uses; Figure 4.4-1 depicts the location of each port. The ports of Saronicos can be grouped into the following main categories according to their uses:

(a) Refineries, industrial, military and other facilities: The gulf of Elefsina includes 7 ports that mainly handle industrial and military facilities except leisure and fishery uses. Industrial, port facilities and refineries are also located at Isthmia and Agioi Theodori ports. Thus, these are the most suspected areas for oil leakage.

(b) Passengers: The Port of Piraeus is the busiest port in Greece and plays an important role in the country's economy since it handles the main Greek passenger coastal shipping. The biggest islands of Saronicos (Salamina, Egina, Poros, Agkistri) are connected to the Port of Piraeus via frequent services. Thus, the navigational traffic in the gulf is high.

(c) Leisure and sport facilities: Leisure crafts are sheltered in the majority of Saronicos ports. The eastern coasts of the gulf handle mainly leisure and sport facilities.

(d) Fishing crafts: Fishing ports are located all around the coasts of the gulf.

Table 4.4-1. The ports of Saronicos Gulf and their uses

	PORTS OF SARONICOS	USES							
		1	2	3	4	5	6	7	8
		Cargo	Containers	Military facilities	Passengers	Ship repairing, refineries, industrial etc facilities	Leisure	Fishing crafts	Sports
1	Poros - Galatas Trizinias						■		
2	Methana						■	■	
3	Kounoupitsa						■	■	
4	Agkistri				■		■	■	
5	Aegina				■		■	■	
6	Isthmia					■			
7	Ag. Theodori					■			
8	Pachi						■	■	
9	Nea Peramos						■	■	
10	Elefsina 1					■			
11	Elefsina 2	■	■				■	■	
12	Skaramagkas 1					■			
13	Skaramagkas 2			■					
14	Salamina 1			■					
15	Salamina 2 (Ampelakia harbour, Paloukia)				■		■	■	
16	Perama					■			
17	Neo Ikonio - Drapetsona		■						
18	Peiraeus Harbour				■				
19	Passalimani						■		
20	Mikrolimano						■	■	
21	Athens Marina								
22	NOTK (Nautikal club)								
23	Marina Floisvos						■		
24	Athens Sailing Academy								■
25	Marina Ag. Kosma								
26	Glyfada Leisure Crafts Harbour						■		
27	Glyfada Marina						■		
28	Glyfada Fishing Shelter							■	
29	Voula						■		
30	Vouliagmeni								■
31	Marina of Vouliagmeni						■		
32	Varkiza						■	■	
33	Palaia Fokaia						■	■	

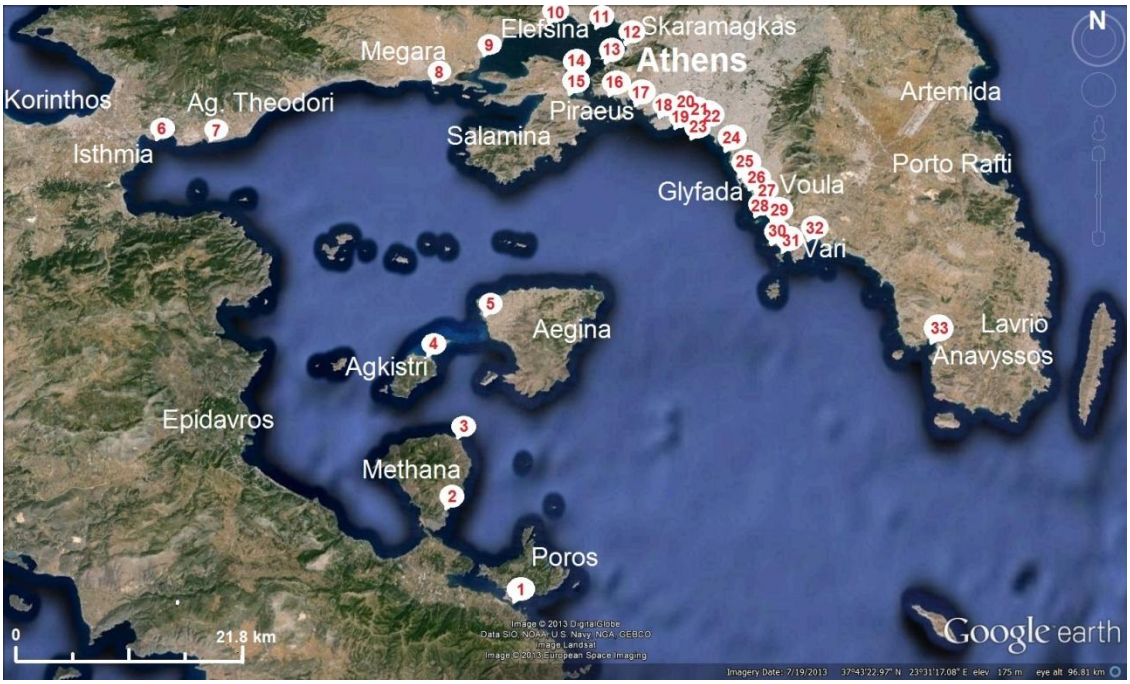

Figure 4.4-1. The ports of Saronicos Gulf and their uses
(Source: http://www.google.com/earth/)

4.5. Sea accidents in Saronicos Gulf

Increased navigational traffic, the existence of refineries, industrial facilities, ship repairing zones and ports are factors that increase the possibility of a spill accident, especially in a closed gulf like the Saronicos Gulf (Triantafyllou and Vergetis, 2004); this is verified by the statistics of Table 4.5-1 which was composed by Triantafyllou and Vergetis (2004) and includes the locations where oil spill accidents have occurred in the past (period 1979-1998), in the region of Saronicos Gulf.

Table 4.5-1. Locations of oil spill accidents in Saronicos Gulf - Data base span: 1979-1998 (Obtained by Triantafyllou and Vergetis, 2004)

Area	Accident Location	Number of accidents	Total
South of Aegina	Karavigka	1	18
	South Saronicos Gulf	12	
	Pappas Cape	1	
	Hydra	2	
	Poros	2	
From Sounio to Skaramagkas	Pireaus	88	97
	Drapetsona	3	
	Perama	2	
	Psitalia	2	
	Keratsini	2	
From Skaramagkas to Nea Peramos	Saronicos Gulf	5	72
	Megara	2	
	Elefsina	28	
	Aspropirgos	1	
	ELDA	18	
	Nea Peramos	1	
	MAMIDAKIS	3	
	TEXACO	2	
	PETROLA	6	
	TITAN A.E.	2	
	XALIBVEBORIKI A.E.	1	
	MOBIL	1	
	BAKOPOULOS SHIPYARDS	2	
From Nea Peramos to 20 km southern Isthmus, Korinthos	MOTOR OIL	33	42
	Isthmos, Korinthos	7	
	Kalamaki, Korinthos	1	
	Aghii Theodori	1	

From Table 4.5-1, based on the number of incidents, the regions stricken most by oil spills in Saronicos Gulf are the following:

- The greater region of the Port of Piraeus (38.4% of the incidents).
- The refineries of MOTOR OIL (14.4% of the incidents).
- The sea region of Elefsina (12.2% of the incidents).
- The refineries of ELDA (7.9% of the incidents).
- The region between Sounion and Hydra island (5.2% of the incidents).

(Triantafyllou and Vergetis, 2004)

Moreover, according to Triantafyllou and Vergetis (2004) and as it is depicted in Figure 4.5-1, it is concluded that the most risky regions for a sea accident in the gulf are the following:

(a) The greater region of the Port of Piraeus.
(b) The region between the Isthmus of Corinth, Megara, Salamina island and Kalamaki bay.
(c) The gulf of Elefsina (-Skaramagkas) due to the existence of several ship repairing and refinery facilities.
(d) The region between cape Sounion and the islands Hydra and Aegina, due to the increased navigational movement towards the Port of Piraeus.
(e) The region of Laurion in case of an upgrade of the Port, which lies outside the examined sea region.

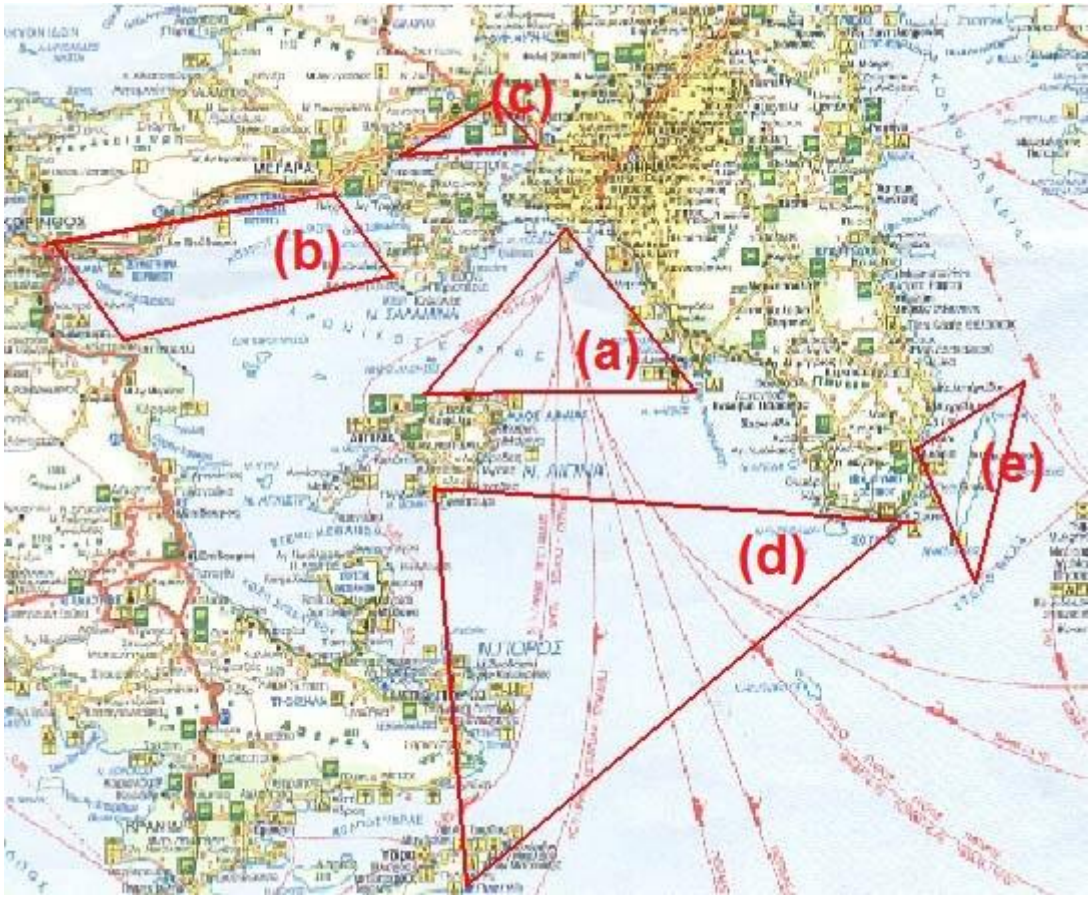

Figure 4.5-1. Map of possible locations of oil spill accidents in Saronicos Gulf (Obtained by Triantafyllou and Vergetis, 2004)

Regarding the type of the ships and according to the analysis by Triantafyllou and Vergetis (2004), "tankers" are the most hazardous ship type since they were involved in the 37% of the past incidents in Saronicos Gulf. The "general cargo" ships come next, having been involved in the 23.1% of the past incidents. Unknown ship types have caused 17.9% of the past sea casualties whereas the involvement possibility of "barge" ships was calculated equal to 8.7%. Finally, the "passenger" ships have been involved in the 7% of the ship accidents that have taken place in Saronicos Gulf.

Regarding the spilled oil quantities in the past, Figure 4.5-2 presents the relation between the number of incidents, the type of accident and the oil quantity spilled into the sea. It is noticed that in the majority of oil spill incidents the quantity spilled was less than 7 tons and were mainly due to operation or unknown reasons.

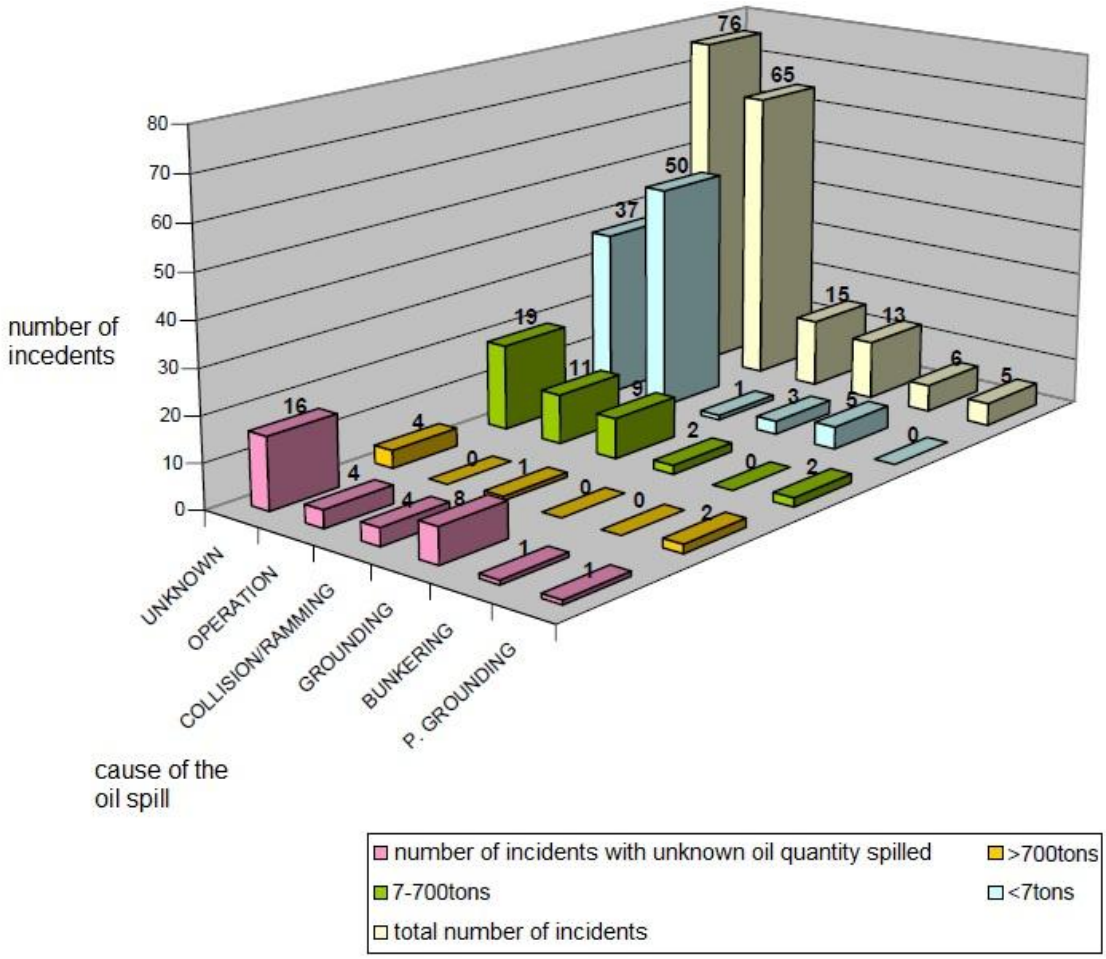

Figure 4.5-2. Distribution of the number of incidents according to the type of accident and the oil quantity spilled
(Obtained by Triantafyllou and Vergetis, 2004)

4.6. Special natural areas in Saronicos Gulf

Several areas of outstanding beauty and natural importance are included in the Saronicos Gulf. Figure 4.6-1 depicts the beaches of Saronicos Gulf that have been awarded with the eco-label of "Blue Flag" for their high water quality; these are tested beaches that comply with the Blue Flag requirements for physical, chemical, microbiological etc parameters. This also means that no industrial, waste-water or sewage-related discharges affect the beach area.

Figure 4.6-2 depicts the areas of outstanding natural beauty (AONB), in the vicinity of Saronicos Gulf, as they are reported in the data base for the Greek nature named "Filotis"; AONB are the areas which are considered to have significant landscape value and whose distinctive character and natural beauty are so precious that it is in the nation's interest to safeguard them.

Several areas characterized as NATURA and CORINE biotopes are noticed in Figures 4.6-3 and 4.6-4, respectively. NATURA biotopes are areas with rich flora and fauna, of recognized high importance, that are legally protected whereas CORINE biotopes denote vulnerable ecosystems, habitats and species.

Figure 4.6-1. Blue flag beaches in Saronicos Gulf

Figure 4.6-2. Areas of outstanding beauty in Saronicos Gulf
(Obtained from: http://filotis.itia.ntua.gr, Map data ©2013 Google Imagery ©2013 TerraMetrics)

Figure 4.6-3. NATURA biotopes in Saronicos Gulf
(Obtained from: http://filotis.itia.ntua.gr, Map data ©2013 Google Imagery ©2013 TerraMetrics)

Figure 4.6-4. CORINE biotopes in Saronicos Gulf
(Obtained from: http://filotis.itia.ntua.gr, Map data ©2013 Google Imagery ©2013 TerraMetrics)

It is concluded that there are several areas of high importance in the coastal region of Saronicos Gulf. Thus, the impacts on individual organisms and ecosystems in case of an oil spill accident would be severe. For this reason, the application of the present oil spill model aims to provide information regarding the operation area for the retention-purification of oil spill in case of an oil spill occurrence in the gulf.

CHAPTER 5: APPLICATION OF THE MODEL TO SARONICOS GULF - RESULTS

5.1. General

In this chapter the application of the HYM and OSM models is presented. The hydrodynamic field was reproduced first by the hydrodynamic model FLOW-3DL (Stamou et al., 1999; 2007a; 2007b) which was extended to calculate the surface current velocities; the hydrodynamic data were used as input by the Oil Spill Model (OSM) which was developed in the present study. The OSM was applied next to calculate the trajectory of an oil spill, the evolution of oil mass with time due to the weathering and the time needed for the spill to reach the coast once an oil leakage accident happens. The results of the computations are presented in this chapter.

The dimensions of the greater area of study, i.e. the Saronicos Gulf, which is depicted in Figure 5.1-1, are equal to 80.0 km X 60.0 km. At the South, the 40 km long open boundary was taken into account whereas land bounded the rest of the computational domain; these boundary conditions were inserted in the mathematical models applied.

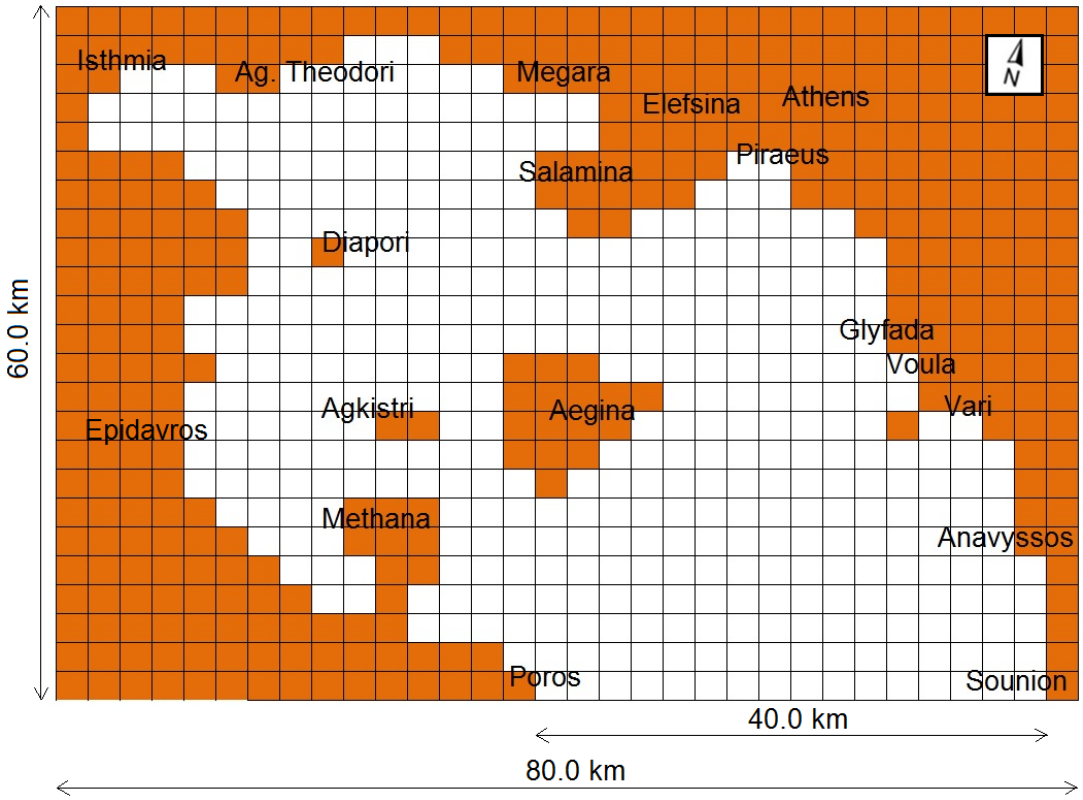

Figure 5.1-1. The computational domain

5.2. The hydrodynamic field of Saronicos Gulf

As described in Chapter 3.2.5, the hydrodynamic model FLOW-3DL (Stamou et al., 1999; 2007a; 2007b) was modified in the present study and applied in a single layer in order to calculate the flow field and, specifically, the surface sea currents in the Saronicos Gulf. The necessary inputs for the hydrodynamic model were the following:

1) The computational grid was constructed and boundary conditions were defined.
2) The bathymetry was specified.
3) The wind scenarios were defined.
4) The sea water characteristics and other input parameters for the HYM were defined.

5.2.1. The computational grid - Boundary conditions

The computational grid used was orthogonal; the x and y dimensions were equal to 2500 m. The selection of the grid dimensions was based on the study of Koutitas (1989), who used the same mesh quality to reproduce the hydrodynamic field of the Saronicos Gulf. Thus, a comparison was made with the reproduced flow field of Saronicos Gulf by Koutitas (1989) to verify the present results.

The boundary conditions included (a) land boundaries, where the no-slip condition for horizontal velocity was applied, and (b) one open sea boundary, where the radiation condition was used for velocities (Krestenitis, 1987). The largest islands of the gulf, i.e. Salamina, Aegina, Poros, Agkistri and the island cluster Diapori were included in the computational domain. The gulf of Elefsina was ignored since the objective of the study was to examine the greater region of Saronicos Gulf.

A 15° rotation of the grid was applied so that the axis of the open boundary would be parallel to the x axis. The computational grid used is shown in Figure 5.2-1. The boundaries of the computational domain were defined as follows:

1) In the vertical direction a single layer was considered, which had varying depth and was bounded by the bottom.
2) In the open boundary at the south, the radiation condition was used for velocities.
3) In the case of calm condition in the gulf, the open boundary condition was modified; a relative water level variation equal to 1.0 cm between the cape Sounion and the coast of Peloponnesus was considered (Christodoulou, 1989).
4) In the land boundaries the no-slip condition for horizontal velocity was applied whereas the velocity components normal to the coastal boundaries were set equal to zero.

It is noted that the computational grid used was relatively coarse but represented the greater area of study satisfactorily. The time step used was equal to Dt=30.0 sec.

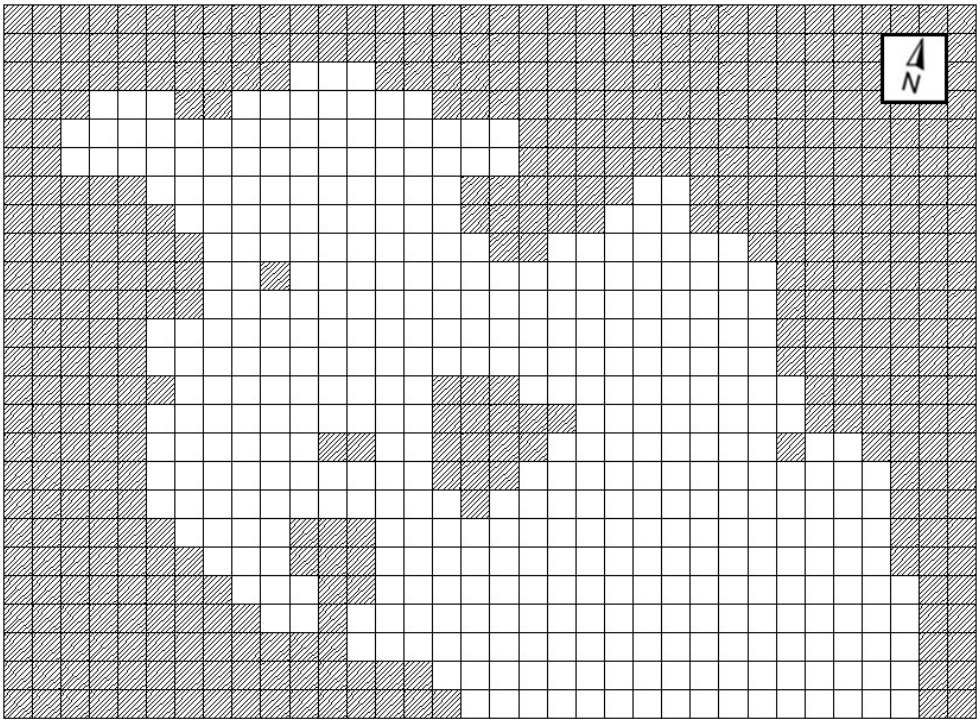

Figure 5.2-1. The computational grid

5.2.2. The bathymetry

The bathymetry of the Saronicos Gulf was defined and each cell of the computational grid was characterized by a number representing its depth (see Figure 5.2-2). The fluid domain was represented by a single layer of specific depth that varied for each grid cell. Moreover, the definition of the gulf's bathymetry was exploited to detect the shallow water areas that are most risky in oil spill occurrence due to a sea accident.

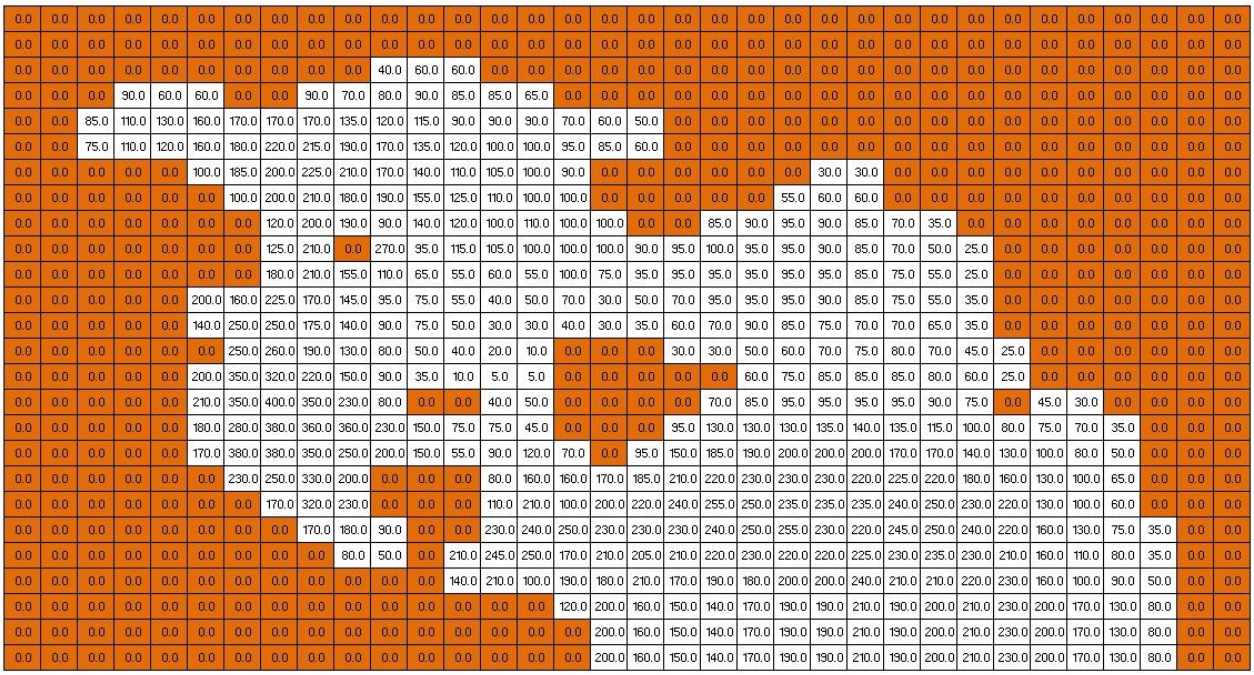

Figure 5.2-2. The bathymetry of the gulf

5.2.3. The wind scenarios

As presented in Chapter 4.3, the most frequent winds in the area of study are from northerly directions. In this study, the 49 most frequent winds in Saronicos Gulf were examined; these were of magnitude from 1 to 6 Beaufort. The eight geographic sectors {N, NE, E, SE, S, SW, W, NW} and six wind categories given in Beaufort (bf) {1 to 6+} lead to a total number of 48 wind scenarios; the 49th wind scenario corresponded to the no wind condition in the gulf.

5.2.4. Sea water characteristics and other parameters

The necessarily known sea water data for the HYM were (i) the sea water density, ρ_w, (ii) the kinematic viscosity, v_w, (iii) the horizontal dispersion coefficient, D_h, and (iv) the Coriolis parameter, f, which depends on the latitude, φ, of the application site. The sea water density and the kinematic viscosity were taken equal to ρ_w=1026 kg m^{-3} and v_w=1.1·10^{-6} m^2 s^{-1}, respectively. After a series of tests and in accordance with Koutitas (1989), the horizontal dispersion coefficient, D_h, was taken equal to 100.0 m^2 s^{-1}. The Coriolis parameter, f=2ω sinφ, was calculated for a latitude equal to φ=37.70 for the case of the Saronicos Gulf; ω is the rotation rate of earth (7.2921 · 10^{-5} rad s^{-1}).

5.2.5. The HYM results

Indicative results of the HYM regarding the surface currents of Saronicos Gulf are presented in this chapter, and, more specifically, the 8 most probable scenarios of hydrodynamic field, according to the wind annual frequency data (see Table 4.3-1). These are the following wind scenarios: N - 2, 3 and 4 bf; NE - 3 and 4 bf, S - 2 and 3 bf and the calm condition. The HYM results for all 49 wind scenarios are included in Appendix A.

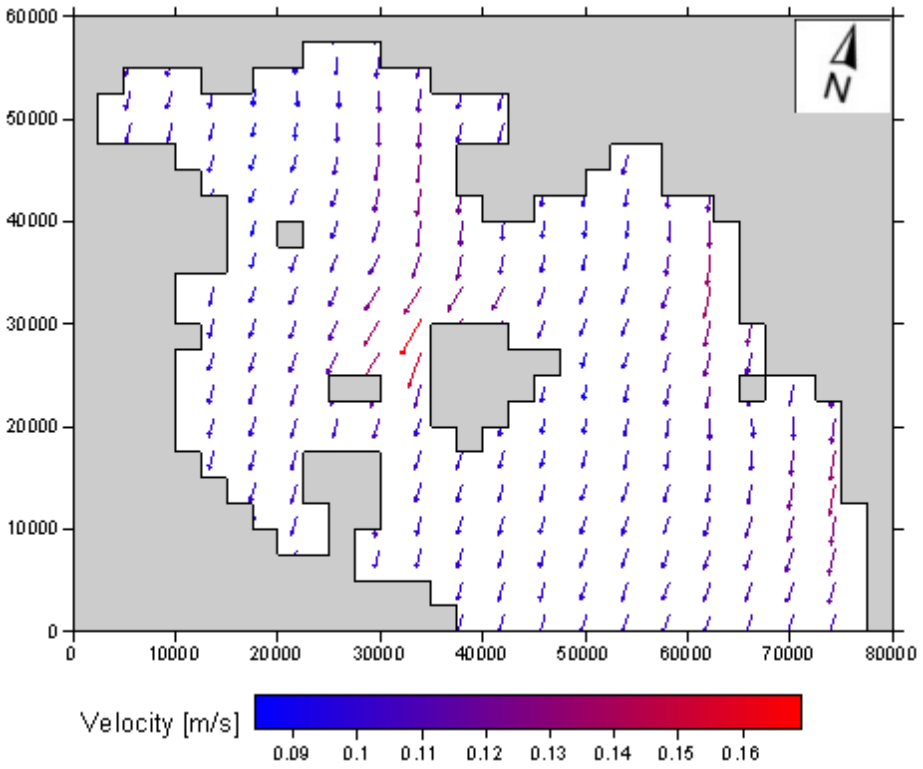

Figure 5.2-3. Surface currents for North wind - 2 bf

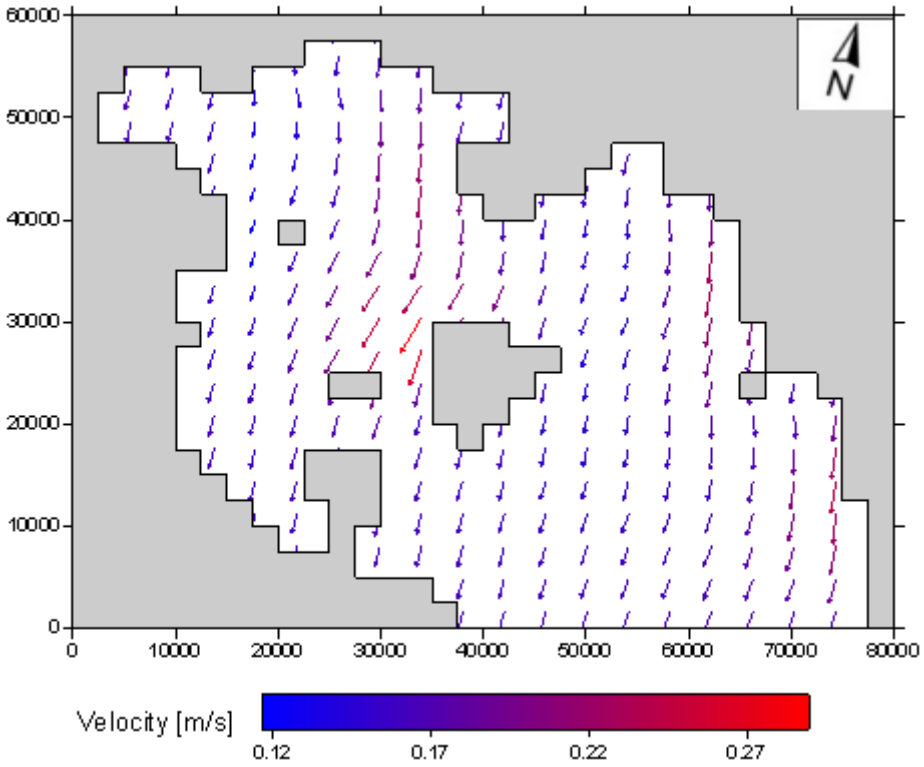

Figure 5.2-4. Surface currents for North wind - 3 bf

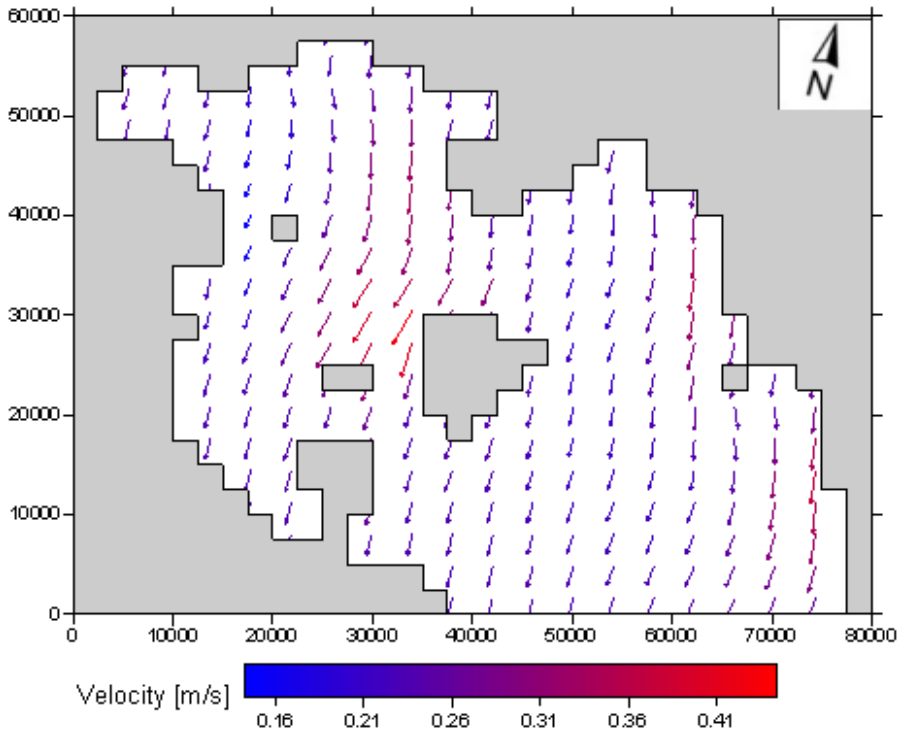

Figure 5.2-5. Surface currents for North wind - 4 bf

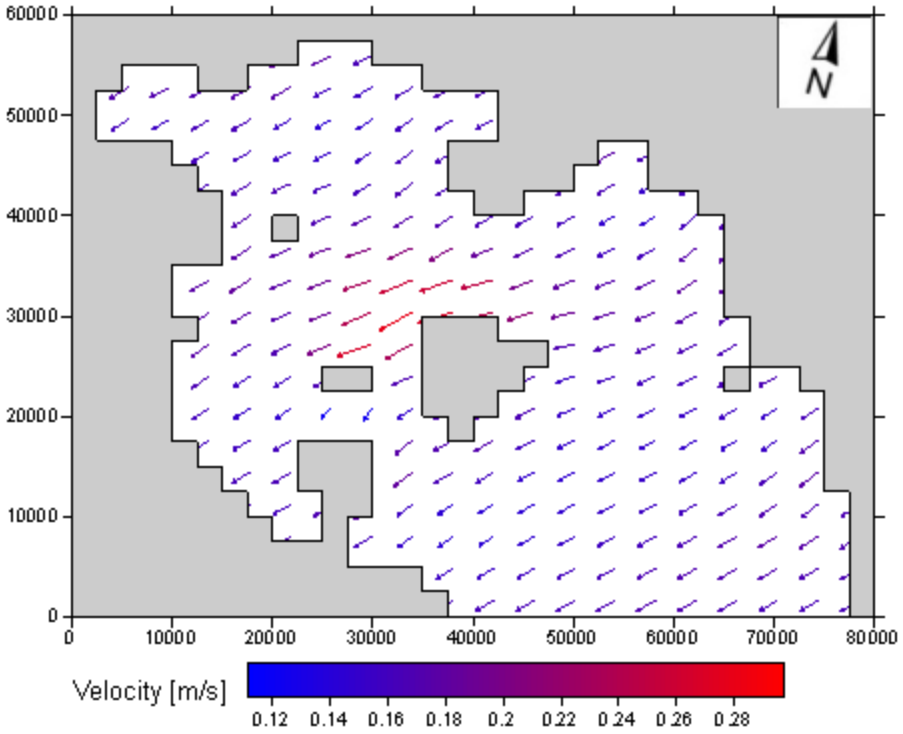

Figure 5.2-6. Surface currents for North-East wind - 3 bf

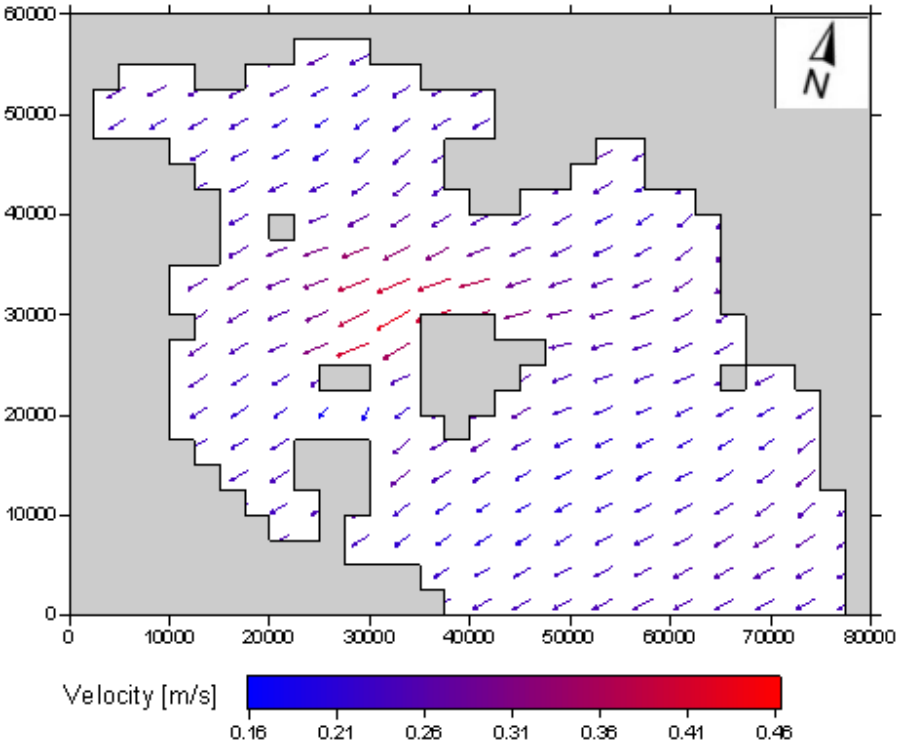

Figure 5.2-7. Surface currents for North-East wind - 4 bf

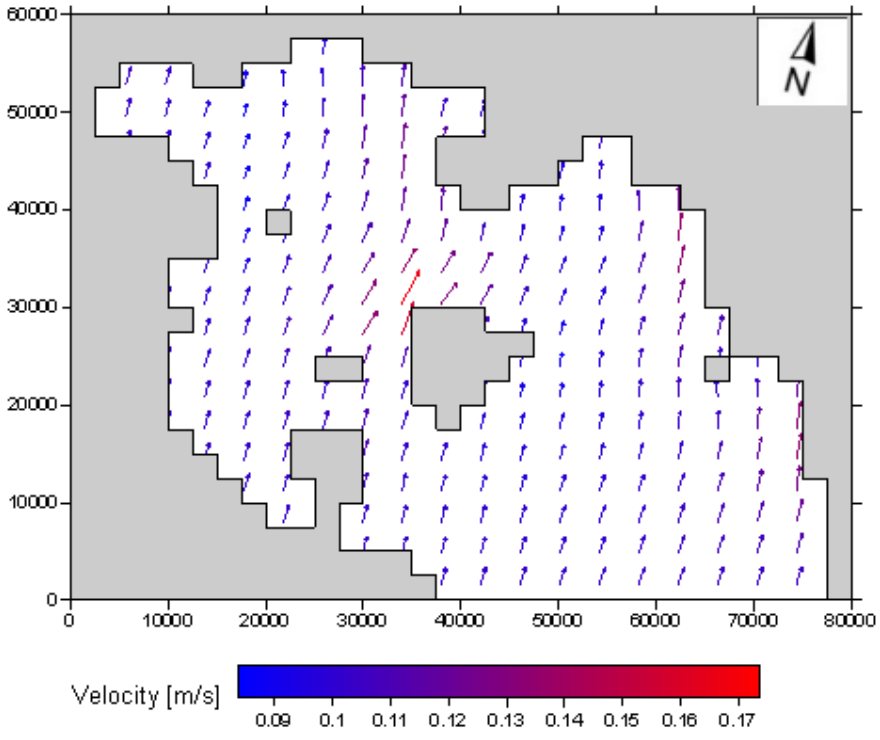

Figure 5.2-8. Surface currents for South wind - 2 bf

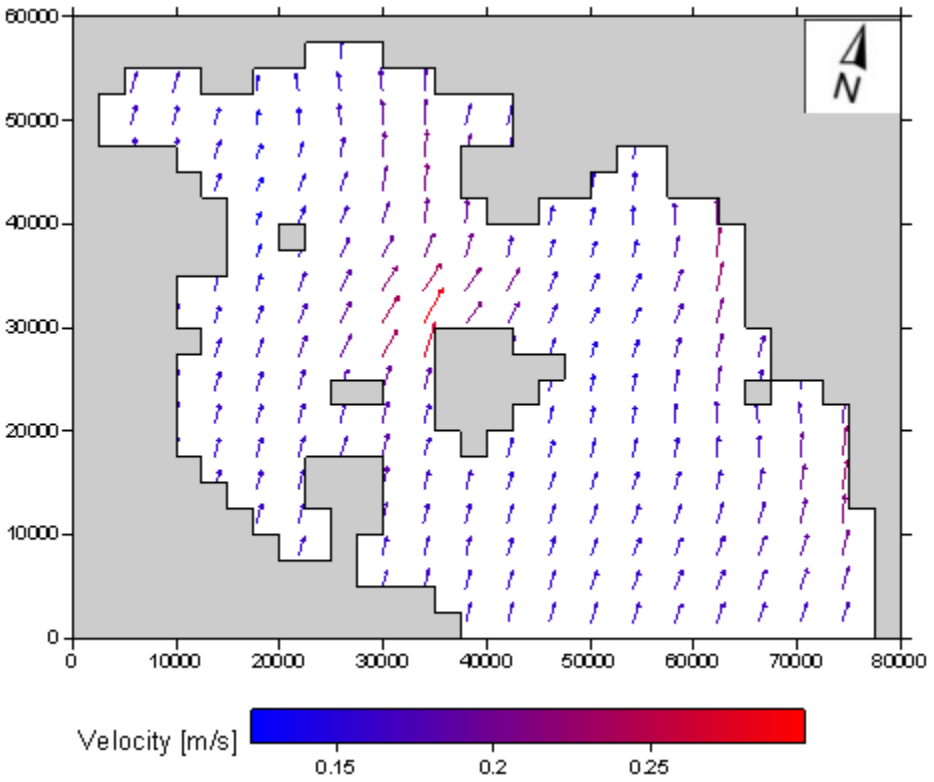

Figure 5.2-9. Surface currents for South wind - 3 bf

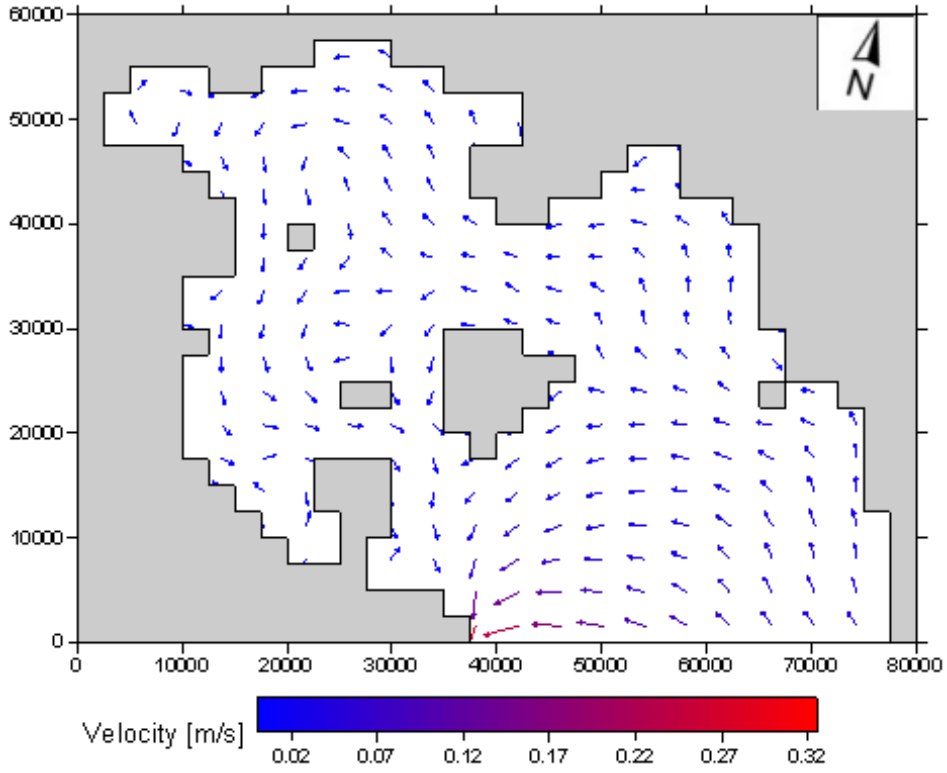

Figure 5.2-10. Surface currents for no wind condition

5.3. Application of the Oil Spill Model

The Oil Spill Model (OSM) employs the computational grid constructed for the calculation of the flow field by the HYM. Each grid cell is characterized by a number, N_i, which counts the number of oil particles that move within its boundaries, at the end of each time step. As already mentioned in Chapter 3.3.2, the necessary input data for the OSM are the following:

(i) The accident locations.
(ii) The initial spill characteristics (quantity, properties).
(iii) The hydrodynamic data, i.e. velocity components of the surface currents, which were reproduced by the HYM.
(iv) The wind characteristics (magnitude and direction).
(v) The sea water characteristics (density and temperature).

5.3.1. Definition of the most probable accident locations in Saronicos Gulf

Four probable accident locations were chosen for applying the OSM; the selection was based on the high accident risk of some regions with high navigational traffic due to their proximity with the busiest ports of Saronicos Gulf. The locations most at risk were considered to be the coastal areas near Piraeus Port, the north-western coasts of the island of Aegina, where shallow waters are also noticed, and the north-western part of the Gulf near the town of Isthmia. The selected accident locations are depicted in Figure 5.3-1; location 3 is also very close to the entrance of the Gulf of Elefsina which includes several industrial facilities and has a high probability of oil spill accident. Moreover, the selection of the accident locations was based on the historical data regarding oil spill accidents in Saronicos Gulf (see Chapter 4.5).

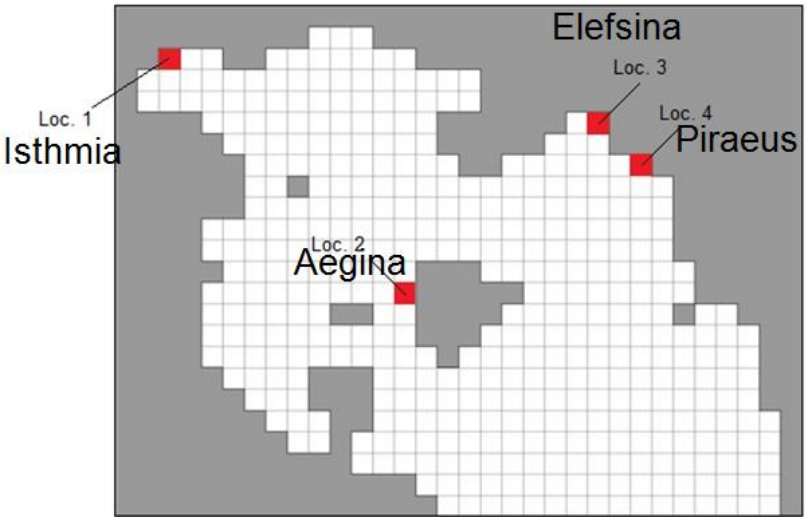

Figure 5.3-1. The 4 most probable accident locations in Saronicos Gulf

5.3.2. Initial spill characteristics

The initial volume of the fictitious oil spill was considered equal to V_o =1500 barrels =197 tons, having a density equal to ρ_o = 827 kg m^{-3}. Typical values of the various parameters, used in the equations describing the weathering processes, were also considered (see Table 3.3-1 for oil=Diesel):

- Initial boiling point for oil, T_o =517 K,
- Gradient of the distillation curve of oil, T_G =139.8 K,
- A = 20.274 and
- B = 18.052.

5.3.3. Hydrodynamic data

The surface current velocities in the x and y directions (U_{surf} and V_{surf} respectively) were calculated by the HYM and inserted in the OSM as an input.

5.3.4. Wind data

The wind magnitude, U_w, is a necessary input for the OSM; 49 wind scenarios were examined in accordance with the hydrodynamic calculations.

5.3.5. Sea water characteristics

The sea water characteristics used by the HYM were also inserted in the OSM as inputs; ρ_w=1026 kg m^{-3}, v_w=1.1·10^{-6} m^2 s^{-1} and D_h=100.0 m^2 s^{-1}. The environmental temperature was considered equal to 15 °C.

5.3.6. The OSM results

5.3.6.1. Oil spill trajectories

A total of 49x4=196 cases were examined since the OSM was run for the 49 chosen wind scenarios, for each one of the 4 selected accident locations. Indicative results of the OSM regarding the oil spill trajectories are presented in this section, and, more specifically, the 8 most probable scenarios according to the wind annual frequency data (see Table 4.3-1). These are the following wind scenarios: N - 2, 3 and 4 bf; NE - 3 and 4 bf, S - 2 and 3 bf and the calm condition, which are in accordance with the HYM results presented in section 5.2. The OSM results for all 49 wind scenarios are included in Appendix B.

Regarding location 1, near Isthmia, it is noticed the oil spill is trapped in all scenarios due to the morphology of the coasts. For northern winds, which are the most probable, the spill moves to the south towards the coasts of Almiri and Katakalion. Since a Blue flag beach is located near Isthmia, an oil spill accident in the region would certainly affect its use except the cases of northern and northern-western winds; in the other cases the oil spill is trapped in the area of Isthmia and Ag. Theodori. Regarding location 2, the oil spill is trapped in the region between Aegina, Agkistri and Methana in the most probable scenarios of northern and northern-western winds. Since the Methana Peninsula and Agkistri Island have been characterized as regions of outstanding natural beauty and vulnerability, respectively, an oil spill accident in the region would not only affect the human activities and the uses of the area, but would also sever and harmful impacts on the area's ecosystems. Regarding locations 3 and 4, which are in the vicinity of the busiest port of Greece, in the most probable scenarios of northern and northern-western winds, the oil spill exits the gulf. In location 3, the oil spill is also easily trapped due to the morphology of the coast.

It is noticed that the areas most at risk are the coastal areas near Piraeus Port, the north-western coasts of the island of Aegina, and north-western end of the Gulf near the town of Isthmia. This is due to their proximity with the chosen accident locations which are considered to be the most probable accident locations in the Saronicos Gulf. The proximity of the western coast of Aegena with the CORINE biotope of Agkistri and the areas of outstanding beauty in the coasts of Peloponnesus, makes the scenario of an accident in this region probably the worst one.

Generally, the wind direction strongly determines the trajectory of the spill. For example, if the wind direction is towards the land, the oil spill moves towards the coast with a speed depended on the wind speed. For low wind magnitudes, the effect of dispersion is more important than in the high wind scenarios. The results of the OSM are reasonable and the affected coasts in case of a spill can be well predicted. However, a significant information for the retention-purification of an oil spill, once an accident happens, is the time needed for the spill to reach the coasts and, thus, affect them. This parameter (T*) is also presented in this chapter.

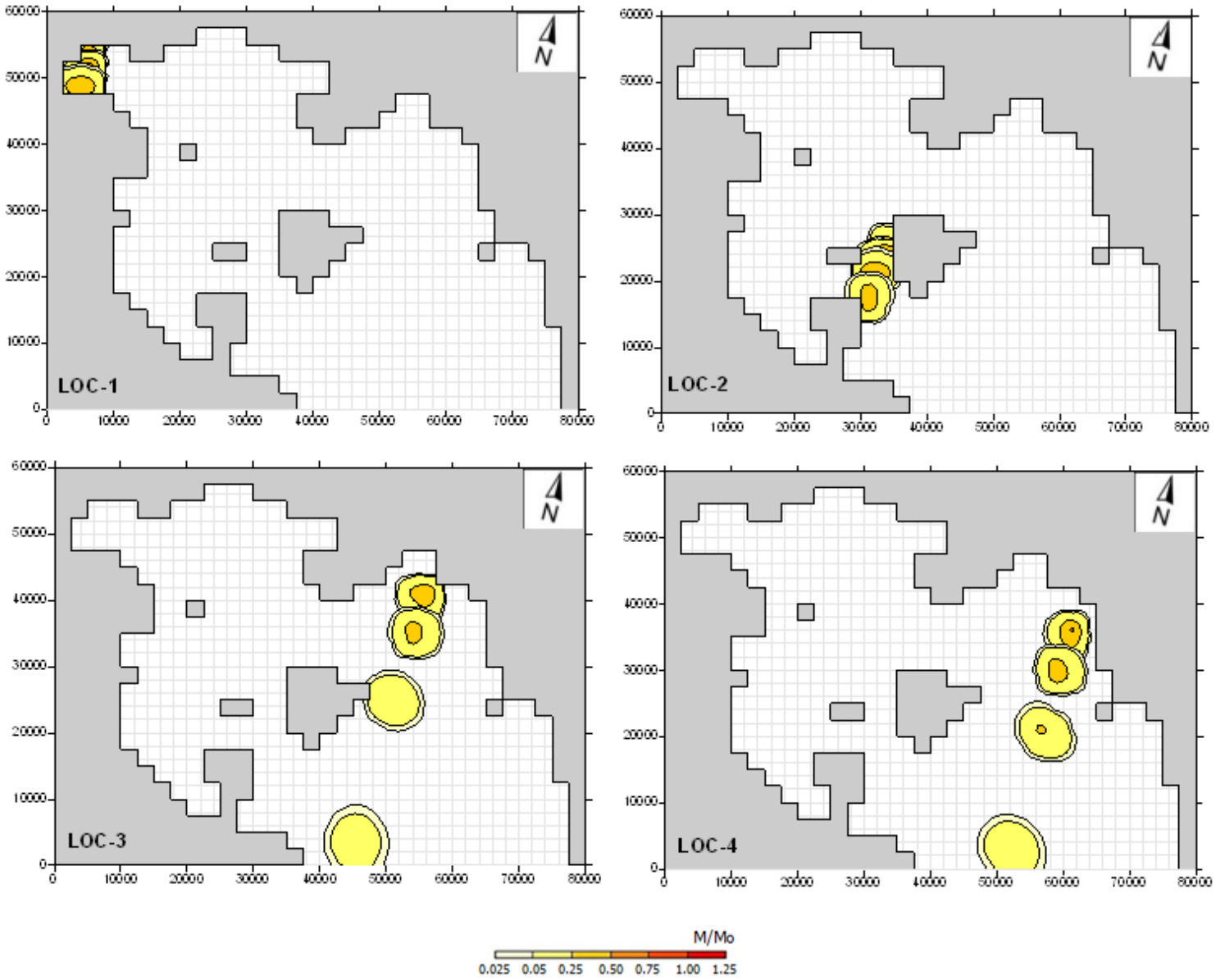

Figure 5.3-2. Trajectory of the oil spill at the 4 locations examined for North wind - 2 bf

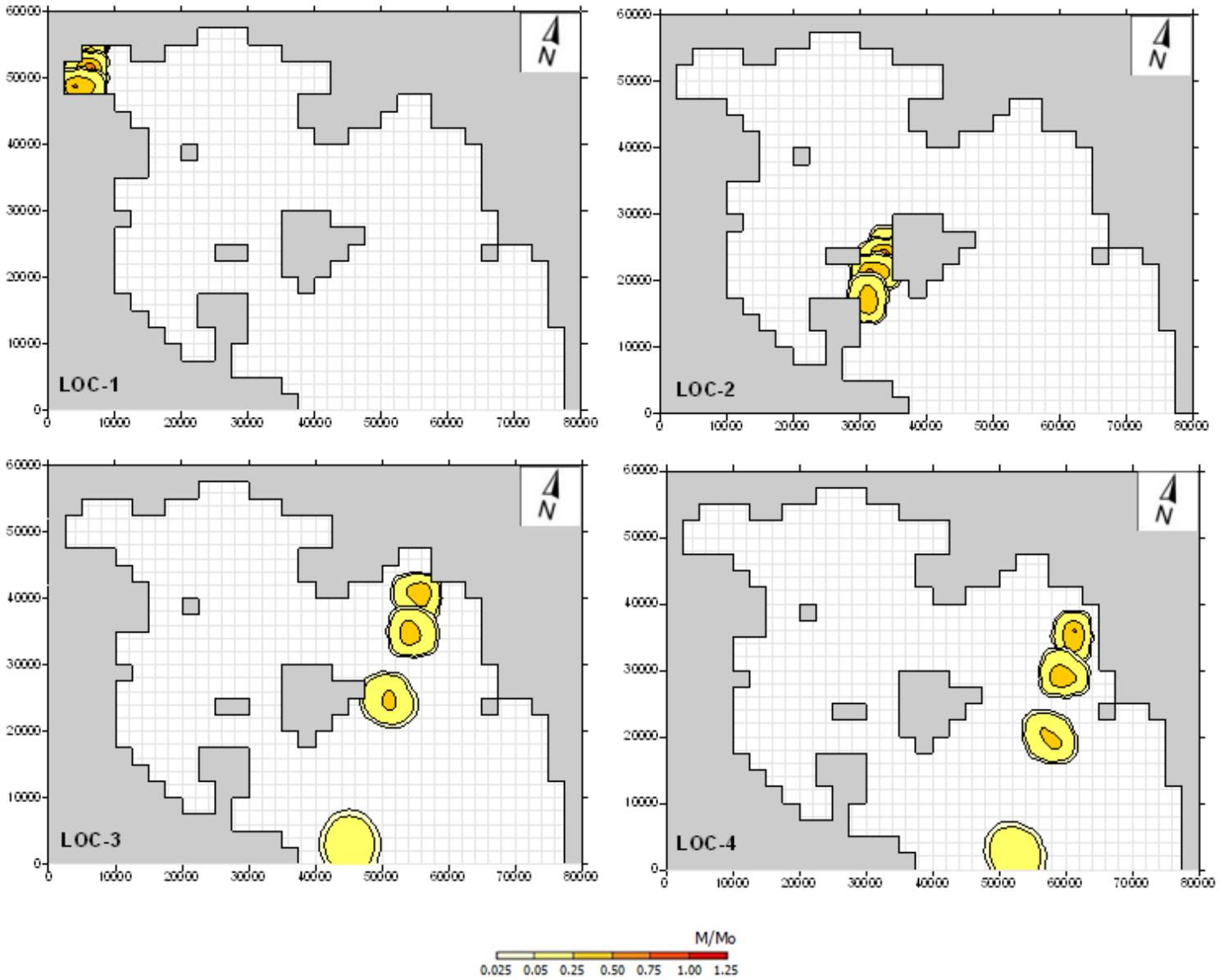

Figure 5.3-3. Trajectory of the oil spill at the 4 locations examined for North wind - 3 bf

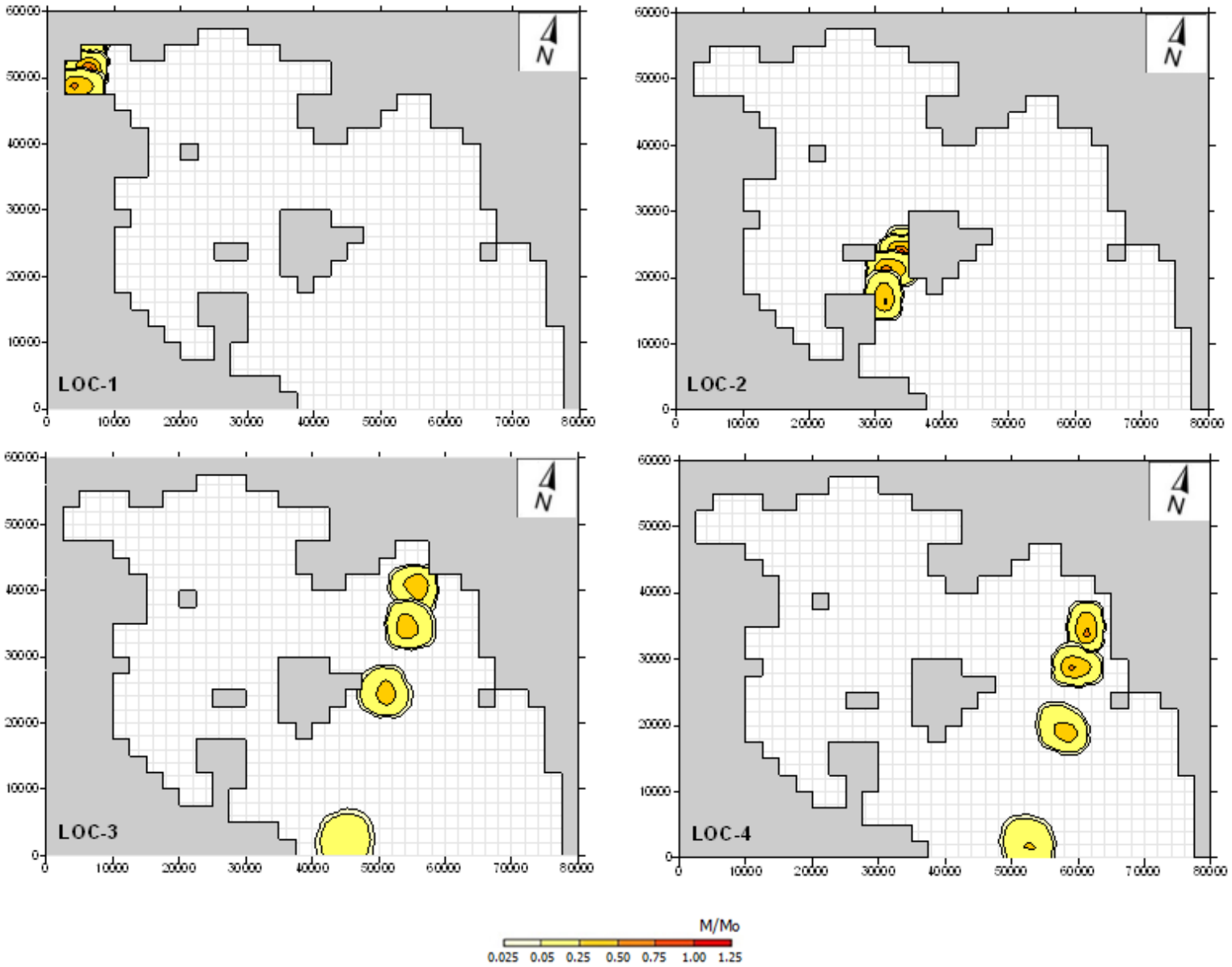

Figure 5.3-4. Trajectory of the oil spill at the 4 locations examined for North wind - 4 bf

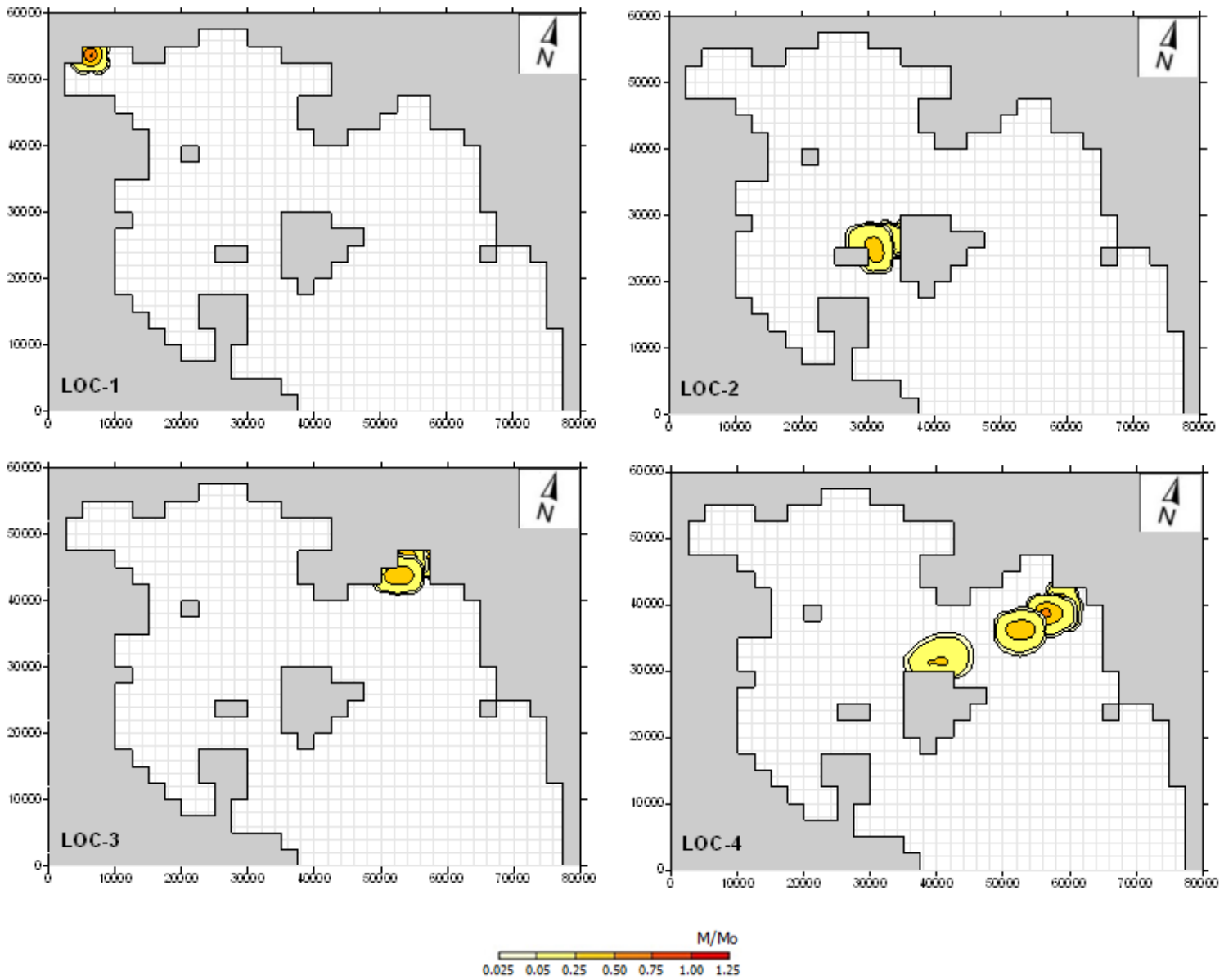

Figure 5.3-5. Trajectory of the oil spill at the 4 locations examined for North-East wind - 3 bf

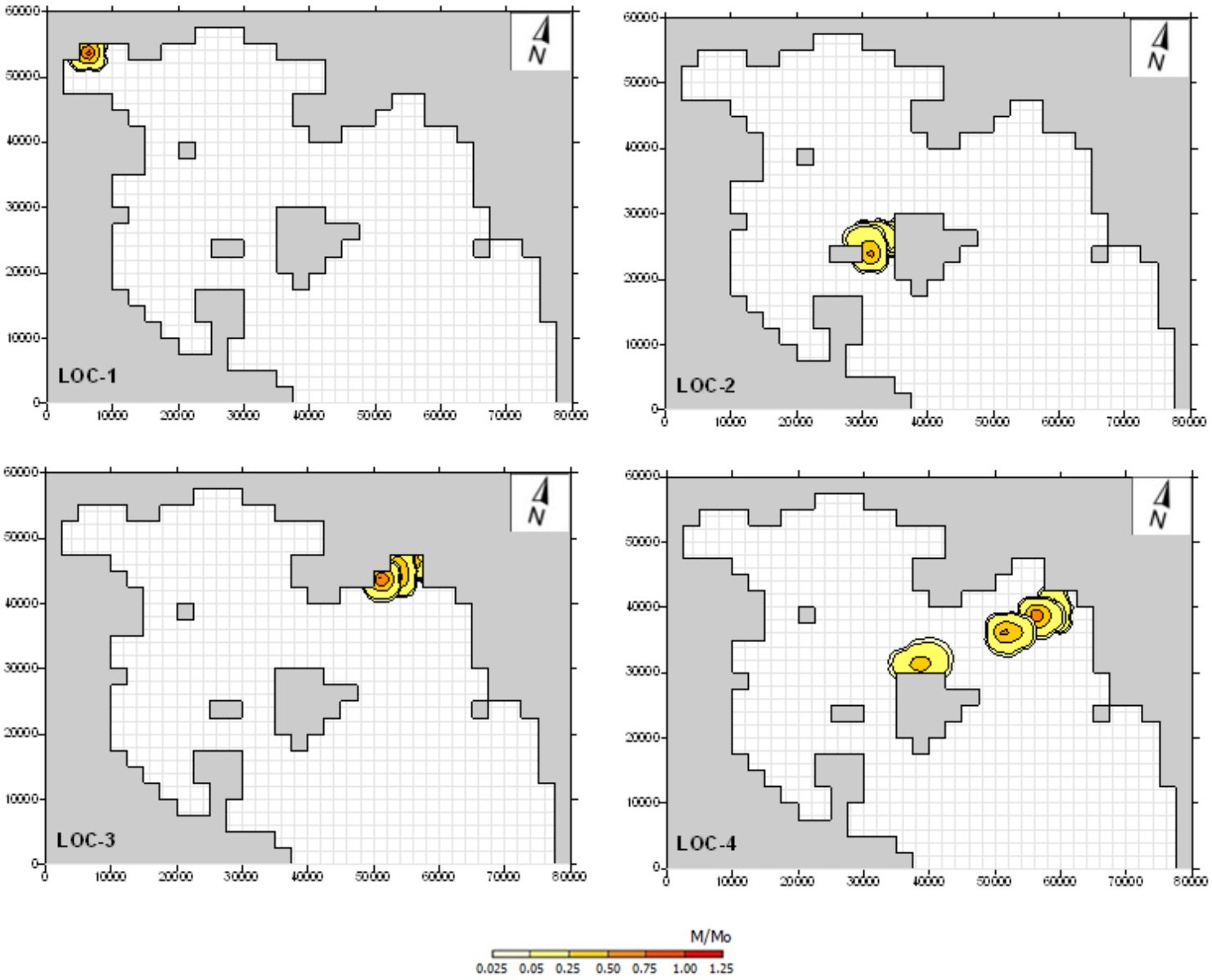

Figure 5.3-6. Trajectory of the oil spill at the 4 locations examined for North-East wind - 4 bf

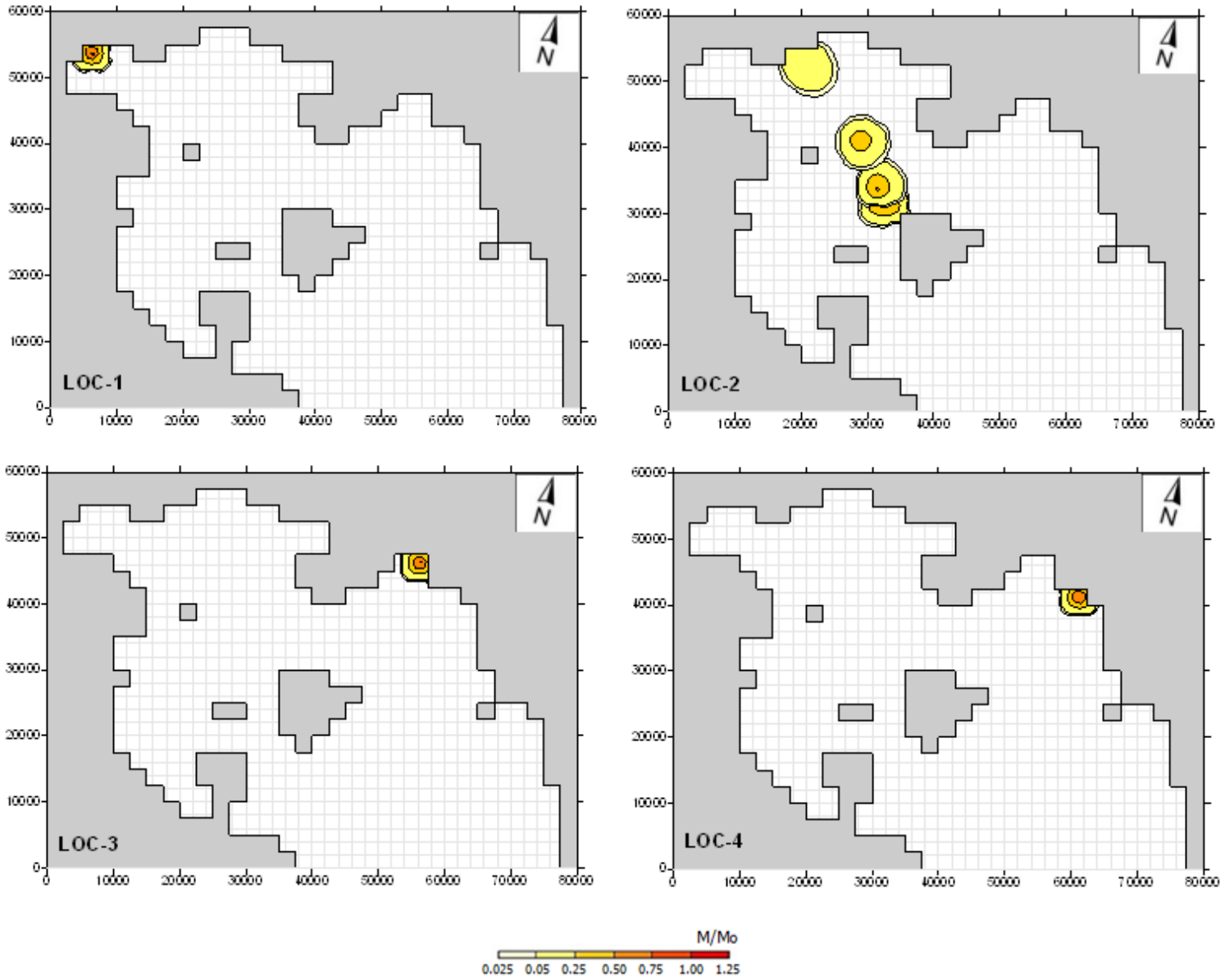

Figure 5.3-7. Trajectory of the oil spill at the 4 locations examined for South-East wind - 2 bf

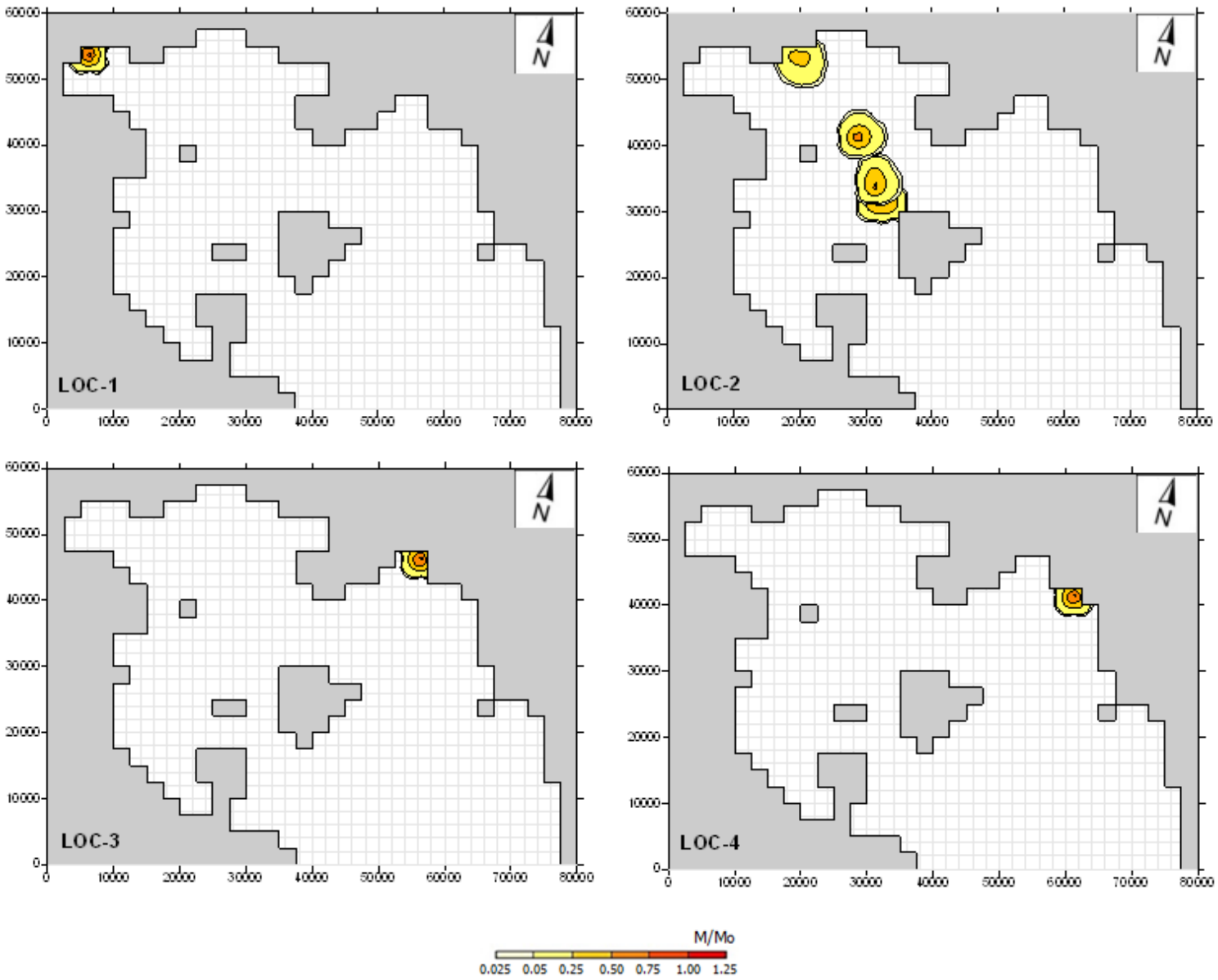

Figure 5.3-8. Trajectory of the oil spill at the 4 locations examined for South-East wind - 3 bf

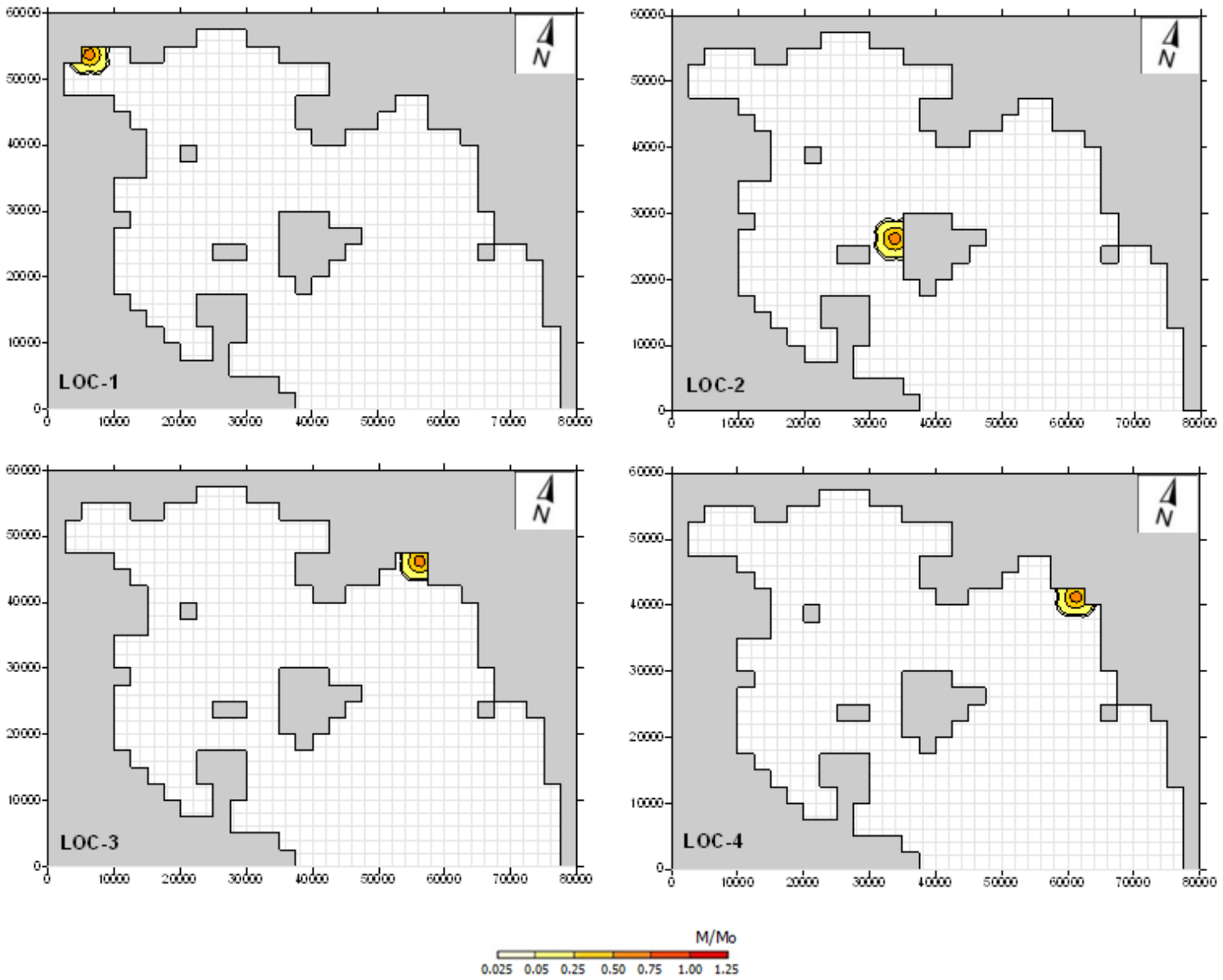

Figure 5.3-9. Trajectory of the oil spill at the 4 locations examined for the no wind condition

5.3.6.2. Time to reach the coast

As described in the assumptions of the OSM (see Chapter 3.3.3), the spill was considered to reach the coast (or the open boundary) at time T*, which corresponded to the time when the 10% of the oil particles reached it. The time T* for each scenario examined are presented in Table 5.3-1.

Table 5.3-1. Time for the oil spill to reach the open or land boundaries

			LOC. 1		LOC. 2		LOC. 3		LOC. 4	
			T* (hr)		T* (hr)		T* (hr)		T* (hr)	
WIND SCENARIO	WIND DIRECTION	WIND FORCE (bf)	TIME TO REACH THE COAST (hr)	TIME TO EXIT THE GULF(hr)	TIME TO REACH THE COAST (hr)	TIME TO EXIT THE GULF (hr)	TIME TO REACH THE COAST (hr)	TIME TO EXIT THE GULF (hr)	TIME TO REACH THE COAST (hr)	TIME TO EXIT THE GULF (hr)
1	N	1	8.3		39.2		117.3			227.0
2		2	13.4		22.6			127.8		102.2
3		3	9.1		14.1			82.8		64.9
4		4	6.5		9.5			57.7		45.1
5		5	4.8		6.9			42.8		33.9
6		6	3.5		4.8			30.4		24.6
7	NE	1	4.1		15.8		18.7		117.3	
8		2	2.3		6.7		9.9		55.7	
9		3	1.6		4.0		6.8		36.4	
10		4	1.2		2.7		6.3		25.9	
11		5	0.9		2.1		4.9		19.7	
12		6	0.7		1.6		3.6		14.3	
13	E	1	3.8		111.2		7.3		6.8	
14		2	2.2		52.9		4.9		4.4	
15		3	1.5		34.2		3.9		3.1	
16		4	1.1		23.6		3.1		2.4	
17		5	0.8		17.3		2.4		1.9	
18		6	0.6		12.1		1.8		1.4	
19	SE	1	3.9		157.9		4.1		3.8	
20		2	2.4		69.0		2.4		2.1	
21		3	1.7		42.1		1.6		1.4	
22		4	1.3		28.2		1.2		1.0	
23		5	1.0		20.6		0.9		0.8	
24		6	0.7		14.6		0.7		0.6	
25	S	1	3.8		5.8		3.8		3.5	
26		2	2.2		3.5		2.2		1.9	
27		3	1.5		2.5		1.6		1.3	
28		4	1.1		1.9		1.2		1.0	
29		5	0.8		1.5		0.9		0.7	
30		6	0.6		1.2		0.7		0.6	
31	SW	1	5.4		3.4		3.8		3.9	
32		2	3.4		1.8		2.3		2.5	
33		3	2.4		1.2		1.6		1.8	
34		4	1.8		0.9		1.1		1.3	
35		5	1.4		0.7		0.9		1.0	
36		6	1.1		0.5		0.6		0.8	
37	W	1	26.3		3.3		3.8		3.8	
38		2	14.3		1.7		2.1		2.1	
39		3	9.1		1.2		1.4		1.4	
40		4	5.8		0.8		1.0		1.0	
41		5	4.6		0.6		0.8		0.8	
42		6	3.3		0.5		0.6		0.6	
43	NW	1	32.3		5.2		5.4		5.3	
44		2	16.2		3.0		3.3		3.2	
45		3	10.6		2.2		2.4		2.4	
46		4	7.5		1.6		1.7		4.8	
47		5	5.7		1.3		1.3		4.0	
48		6	4.1		1.0		1.0		3.0	
49	CALM	0	8.4		13.5		8.3		8.3	

It is noticed that only in 11 out of 196 wind scenarios, the oil spill exits the gulf; this would not take less than one day, according to the results presented in Table 5.3-1. Thus, retention-purification could be done in time.

For northern winds, it takes no sooner than 3.5 hours, in the case of 6 bf wind, for the spill to reach the coast. In the most probable wind scenario, which corresponds to the Northern wind of 3 bf magnitude, it takes more than 9.0 hours for the spill to reach the coast. The next most probable wind scenario is that of the Northern wind of 4 bf magnitude; in this case there are about 5.0 hours available for the proper services to take actions to deter the damage of the coast.

In the worst scenarios where the wind blows towards the land and the oil particles reach the coast relatively fast, the time T* is equal to 0.5 hours, i.e. 30 minutes. In this case, impacts to the coasts are not easily prevented; however, this scenario is not included in the most probable wind scenarios.

CHAPTER 6: CONCLUSIONS – PROPOSED FUTURE WORK

6.1. Summary and conclusions

A 2D physics-based mathematical model for the calculation of the behaviour of oil spills (Oil Spill Model, OSM) was developed in the present study. The present OSM provides the oil spill trajectory, oil density, mass and volume of the spill with time. Apart from advection, the processes taken into account were dispersion, spreading, evaporation, dissolution and emulsification, which are the most frequently used in the literature. The oil mass was divided into a large number of particles and the random walk procedure was employed to model the trajectories of each particle; thus, the stochastic factor of dispersion was taken into account.

Information about the time needed by the oil spill to reach the coast for each scenario are also given by the present OSM; this is a determinant information for the retention-purification of oil spill by the proper services aiming at the avoidance-mitigation of pollution impacts. It is noted that the objective of the present study was to provide indicative-qualitative technical answers rather than reliable scientific results.

The developed methodology of the present study was applied in the region of Saronicos Gulf; this application site was chosen due to its importance for the country's economy, since it includes the largest and busiest port of Greece, i.e. the Port of Piraeus. Moreover, the high navigational traffic of the Saronicos Gulf was considered to increase the probability of an oil spill accident. The results of the model show that the areas most at risk are the coastal areas near Piraeus Port, the north-western coasts of the island of Aegina, and north-western end of the Gulf near the town of Isthmia, due to their proximity with the busiest ports of the Saronicos Gulf. Indicative results for the time needed for a spill, occurred in the chosen accident locations of Saronicos Gulf, to reach the coast show that in the most probable cases of a spill accident, retention of the impacts of the spill is feasible if the alarming is immediate.

6.2. Proposed future work

In the present study a simplified, 2D mathematical model was developed to predict the oil spill behaviour in case of an oil spill accident at the sea. The present OSM accounts only for the behaviour of the oil spill in the water and thus can be used only for calculating the oil spill risk in the fluid domain (for example the coastal regions); calculations are stopped when the 10% of the particles reached the coast (or the open boundary).

A proposed improvement of the code could be the alteration of the stopping criterion in order to account for the modified weathering processes, once an oil particle reaches the land, and also monitor the evolution of the oil spill at the coast. Moreover, 3D calculations should be performed to include the rest of the weathering processes in the OSM model and, especially sedimentation. The determinant act of waves on the spill should also be taken into account since they strongly contribute to the breaking of the spill and dispersion of the oil particles.

Finally, given the difficulty of predicting future oil spill accident locations and the high level of uncertainty in the definition of the prevailing weather conditions, the modeling procedure should be formulated within a stochastic framework.

CHAPTER 7: REFERENCES

1) Al-Rabeh, A.H., Cekirge, H.M., and Gunay, N. (1989). A stochastic simulation model of oil spill fate and transport. Applied Mathematical Modelling, 13, pp. 322–329.
2) Atlas, R.M. (1981). Microbial degradation of petroleum hydrocarbons: an environmental perspective. Microbiological Reviews, 45, pp. 225-266.
3) Boyd, J.N., Kucklick, J.H., Scholz, D.K., Walker, A.H., Pond, R.G., and Bostrom, A. Health and Environmental Sciences Department, Scientific and Environmental Associates, inc. Cape Charles, Virginia, May 2001.
4) Bobra, M. (1992). A study of the evaporation of petroleum oils, Environment Canada EE-135, Ontario, Canada.
5) Buchanan, I., and Hurford, N. (1988). Methods for predicting the physical changes in oil spilt at sea, Oil & Chemical Pollution, 4, pp. 311–328.
6) Brutsaert, W., and Yeh, G.T. (1970). A power wind law for turbulent transfer computations, Water Resource Research, 6, pp. 1387- 1391.
7) Chao X., Shankar, N.J., and Cheong, H.F. (2001). Two- and three-dimensional oil spill model for coastal waters, Ocean Engineering, 28, pp. 1557-1573.
8) Christodoulou, G. Mathematical modeling of the hydrodynamics of the Saronicos Gulf, Part 2, Final Technical Report, School of Civil Engineering, National Technical University of Athens, Athens 1989. (in greek)
9) Cohen, Y., MacKay, D., and Shiu, W.Y. (1980). Mass Transfer Rates Between Oil Slicks and Water. The Canadian Journal of Chemical Engineering, 58, pp. 569-574.
10) Delvigne, G.A.L., and Sweeney, C.E. (1988). Natural dispersion of oil. Oil and Chemical Pollution, 4, pp. 281-310.
11) Exxon Corporation (1985). Fate and effects of oil in the Sea. Exxon Background Series, December 1985.
12) Gundlach, E.R., and Boehm, P. (1981). Fates of several oil spills in coastal and offshore waters. Report to NOAA/Seattle. NOAA Grant No.NA80RAD00060, RPI/R/81/12/31-30.
13) Guo, W.J., and Wang, Y.X. (2009). A numerical oil spill model based on a hybrid method, Marine Pollution Bulletin, 58, pp. 726-734.
14) Harrison, W., Winnik, M.A., Kwong, P.T.Y., and MacKay, D. (1975). Disappearance of aromatic and aliphatic components from small sea-surface slicks. Environmental Science and Technology, 9, pp. 231-234.
15) Huang, J.C., and Monastero, F.C. (1982). Review of the State-of-the-Art of Oil Spill Simulation Models, Final Report Submitted to the American Petroleum Institute, Raytheon Ocean Systems Company, East Providence, Rhodes Island.
16) ITOPF, Handbook 2010/11, Technical report, The Iternational Tanker Owners Pollution Federation Limited, 2010.
17) ITOPF (1987). Response to Marine Oil Spills. International Tanker Owners. Pollution Federation Ltd., London.
18) Jokuty, P., Whiticar, S., Wang, Z., Fingas, M., Fieldhouse, B., Lambert, P., and Mullin, J. Properties of crude oils and oil products, Technical report, Environment Canada, 2000.
19) Jones, R. (1997). A simplified Pseudo-component Oil evaporation Model, NOAA, USA, Proceedings of the Twentieth Arctic and Marine Oil spill Program, Technical Seminar, 1, 43-60, Vancouver, Canada.
20) Kalosakas, D. The consequences of navigation to Saronic's Gulf maritime environtment, considering the moderntechniques of integrated coastal zone management, Master thesis, National Technical University of Athens, April 2000. (in greek)
21) Koutitas, C.G., and O' Connor, B. (1980). Modelling 3-D wind induced flows. Journal of the Hydraulics Division, 106, pp. 1843-1865.
22) Koutitas, C.G. (1985). Mathematical Models in Coastal Engineering (Application with micro-PC), Thessaloniki.

23) Koutitas, C.G. Mathematical modeling of the hydrodynamics of the Saronicos Gulf, Part 3, Final Technical Report, School of Civil Engineering, Democritus University of Thrace, Athens 1989. (in greek)
24) Krestenitis Y.N. (1987), Numerical study of the wind-induced circulation and examination of open-sea boundary conditions — Case study of Thermaikos Gulf, Technical Report, Aristotle University, Thessalonika, Greece.
25) Lacaze, J.C., and Villedon de Naide, O. (1976). Influence of illumination on phototoxicity of crude oil. Marine Pollution Bulletin, 7, pp. 73-16.
26) Lehr, W.J., Cekirge, H.M., Fraga, R.J., and Belen, M.S. (1984). Empirical studies of the spreading of oil spills. Oil and Petrochemical Pollution, 2(1), pp. 7–11.
27) Lehr, W.J. (2001). Review of modeling procedures for oil spill weathering behavior, in: C.A. Brebbia (Ed.), Oil Spill Modeling and Processes, WIT Press, Southampton, UK, 2001, pp. 5190.
28) MacKay, D., and Matsugu, R.S. (1973). Evaporation rates of liquid hydrocarbon spills on land and water, Canadian Journal of Chemical Engineering, 51, pp. 434-439.
29) MacKay, D., Paterson, S., and Trudel, K. (1980). A mathematical model of oil spill behaviour. Report EE-7, Environmental Protection Service, Fisheries and Environment, Canada, Ottawa, Ontario.
30) Mackay, D. (1980). Oil Spill Processes and Models, Environmental Protection Service, Canada.
31) Neff, J.M. (1990). Composition and Fate of Petroleum and Spill Treating Agents in the Marine Environment. In: J.R. Geraci and D.J. St. Aubin (eds.), Sea Mammals and Oil: Confronting the Risks. Academic Press, New York, NY, pp. 1-33.
32) Novelli, G. (2011). Numerical simulation of oil spills in coastal areas using shallow water equations in generalised coordinates, Doctoral Thesis, Department of Mechanical Engineering, Universitat Rovira I Virgili.
33) Payne, J.R., and Phillips, C.R. (1985). Petroleum Spills in the Marine Environment-the Chemistry and Formation of Water-in Oil Emulsions and Tar Balls, Lewis, Chelsea, Michigan.
34) Reed, M., Gundlach, E., and Kana, T. (1989). A coastal zone oil spill model: Development and sensitivity studies, Oil and Chemical Pollution, 5(6), pp. 411–449.
35) Reinhart, R., and Rose, R. (1982). Evaporation of crude oil at sea. Water Research, 16, pp. 1319-1325.
36) Smagorinsky, J. (1963). General circulation experiments with the primitive equations: I. The basic experiment. Monthly Weather Review, 91, pp. 99-164.
37) Stamou, A.I., Noutsopoulos, C., Pipilis, K.G., Gavalaki, E., and Andreadakis, A. (1999). Hydrodynamic and water quality modelling of Southern Evoikos Gulf – Greece, Global Nest the International Journal, 1(2), pp. 131-141.
38) Stamou, A.I., Memos, C.D., and Spanoudaki, K. (2007a). Estimating water renewal time in semi-enclosed coastal areas with complicated geometry using a hydrodynamic model, Journal of Coastal Research, 50, pp. 282-286.
39) Stamou, A.I., Memos, C.D., and Kapetanaki, M.E. (2007b). Modelling water renewal in a coastal embayment, Proceedings of the ICE - Maritime Engineering, 160(MA3), 93-104.
40) Stiver, W., and MacKay, D. (1984). Evaporation Rate of Spills of Hydrocarbon and Petroleum mixtures. Environmental Science and Technology, 18, pp. 834-840.
41) Stolzenbach, K.D., Madsen, O.S., Adams, E.E., Pollack, A.M., and Cooper, C.K. (1977). A review and evaluation of basic techniques for predicting the behaviour of surface oil slicks, Report No. 22, MIT: Cambridge, Massachusetts, USA.
42) Triantafyllou, G., and Vergetis, M. Chapter: Oil Spills. School of Naval Architecture and Marine Engineering, National Technical University of Athens, Athens 2004. (in greek)
43) Venosa, A. D., Suidan, M. T., Wrenn, B. A., Strohmeier, K. L., Haines, J. R., Eberhart, B. L, King, D.W., and Holder, E. (1996). Bioremediation of experimental oil spill on the shoreline of Delaware Bay. Environmental Science and Technology, pp. 30, 1764-1775.

44) Vos, R.J. (2005). Comparison of 5 oil-weathering models. Project: Calprea Werkdocument: RIKZ.ZD/2005.011.
45) Wang, S.D., Shen, Y.M., Guo, Y.K., and Tang, J. (2008). Three-dimensional numerical simulation for transport of oil spills in seas. Ocean Engineering, 35, pp. 503-510.
46) Xie, H., Yapa, P.D., and Nakata, K. (2007). Modeling emulsification after an oil spill in the sea. Journal of Marine Systems, 68, pp. 489–506.
47) Zadeh, E.S., and Hejazi, K. (2012). Eulerian Oil Spills Model Using Finite-Volume Method with Moving Boundary and Wet-Dry Fronts, Modelling and Simulation in Engineering, 2012(33), Article ID 398387, 7 pages, doi:10.1155/2012/398387.
48) http://abbeydufoe.wordpress.com/2013/04/23/earth-week-2013-bp-oil-spill-update/
49) http://www.fastcompany.com/1659822/infographic-day-physics-oil-spills
50) http://filotis.itia.ntua.gr
51) http://forbesindia.com/article/on-assignment/who-do-oil-companies-turn-to-when-theres-a-spill/17352/1
52) http://www.google.com/earth/
53) http://www.itopf.com/marine-spills/fate/weathering-process/
54) http://www.noaanews.noaa.gov
55) http://www.offshore-environment.com/accidents.html
56) http://www.oilspillsolutions.org/evaluation.htm

APPENDIX A: THE HYM RESULTS

The results of the hydrodynamic model (HYM) are concentrated in Appendix A; Figures 1 to 49 depict the hydrodynamic field of Saronicos Gulf for the 49 wind scenarios examined (the 49th wind scenario correnponds to the no wind condition).

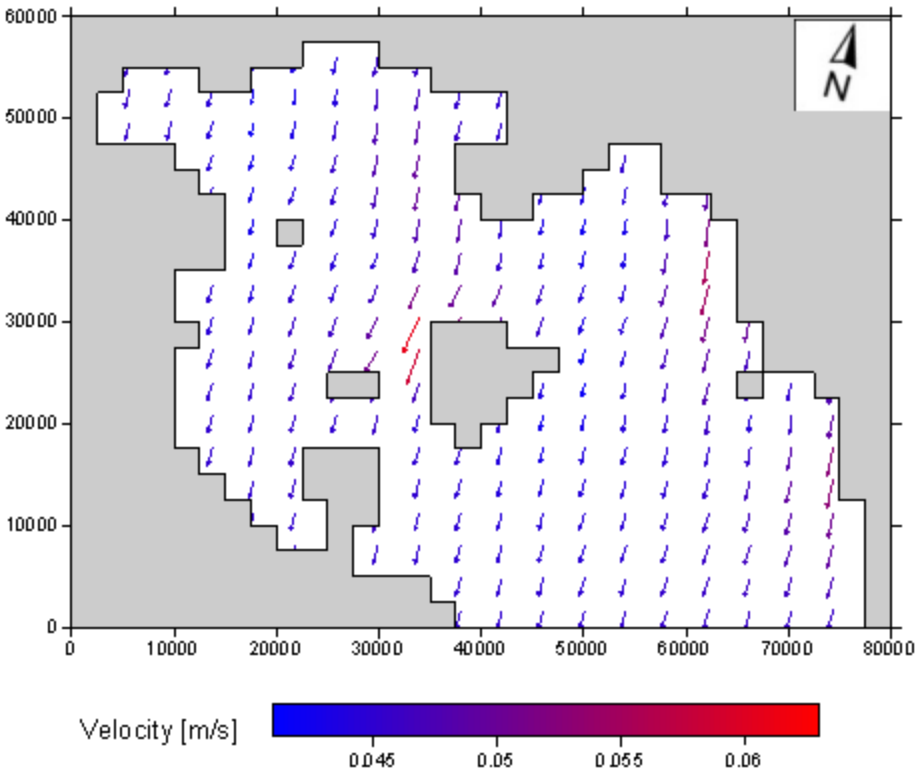

Figure AA1. Surface currents for North wind - 1 bf

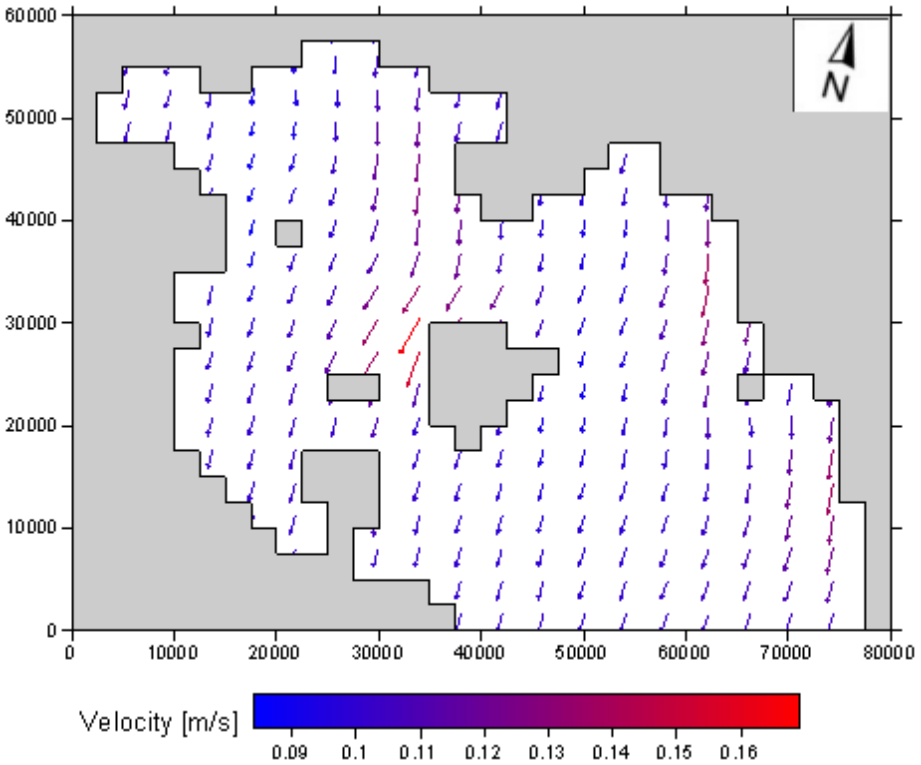

Figure AA2. Surface currents for North wind - 2 bf

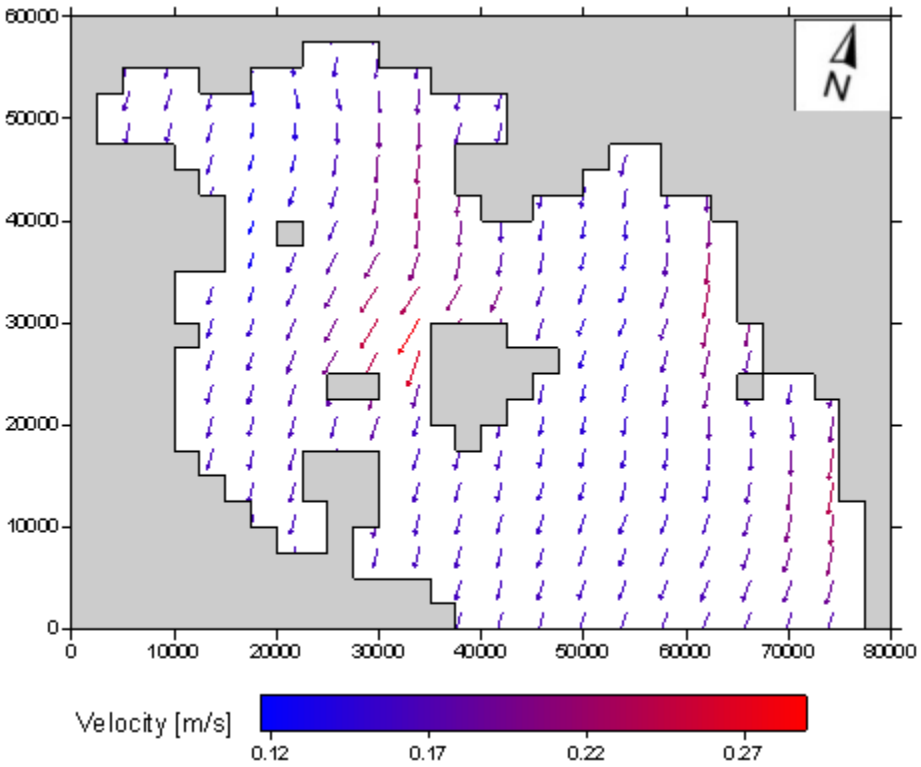

Figure AA3. Surface currents for North wind - 3 bf

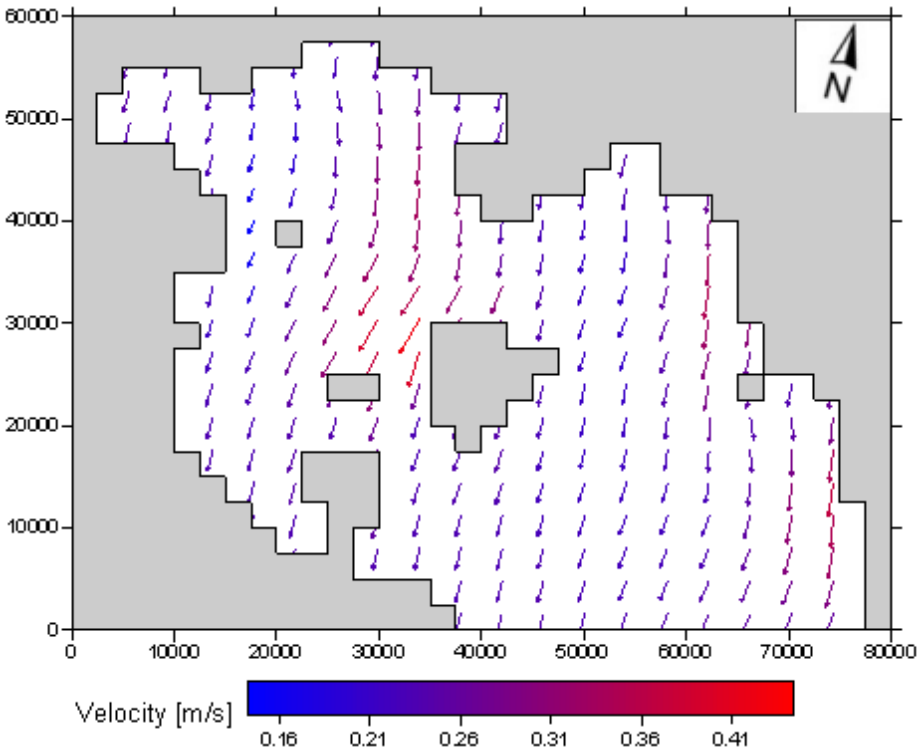

Figure AA4. Surface currents for North wind - 4 bf

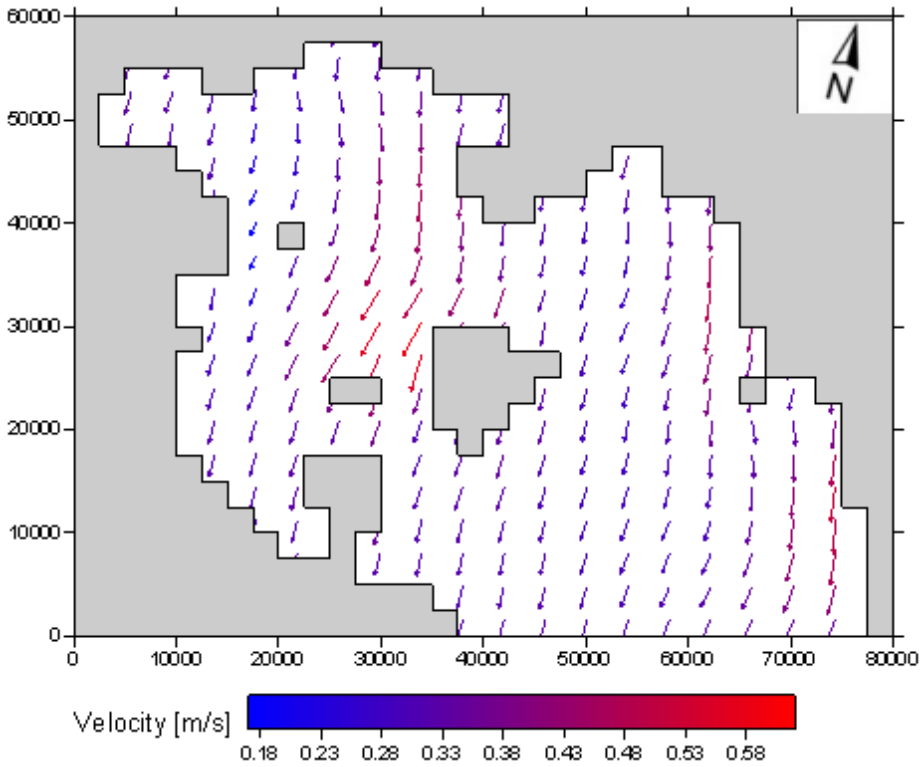

Figure AA5. Surface currents for North wind - 5 bf

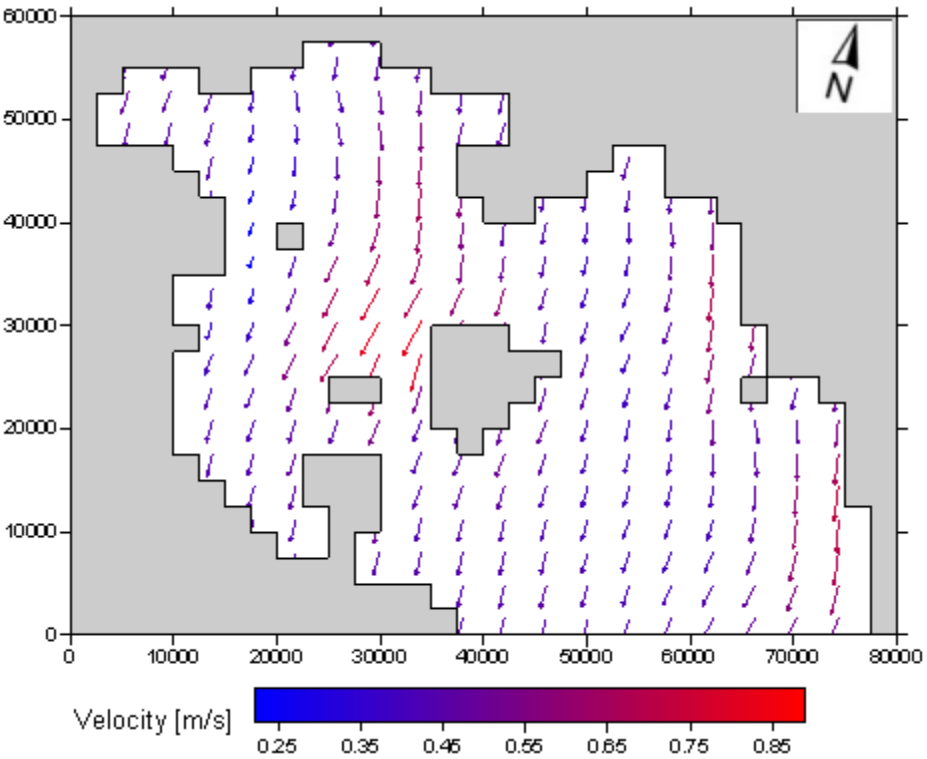

Figure AA6. Surface currents for North wind - 6 bf

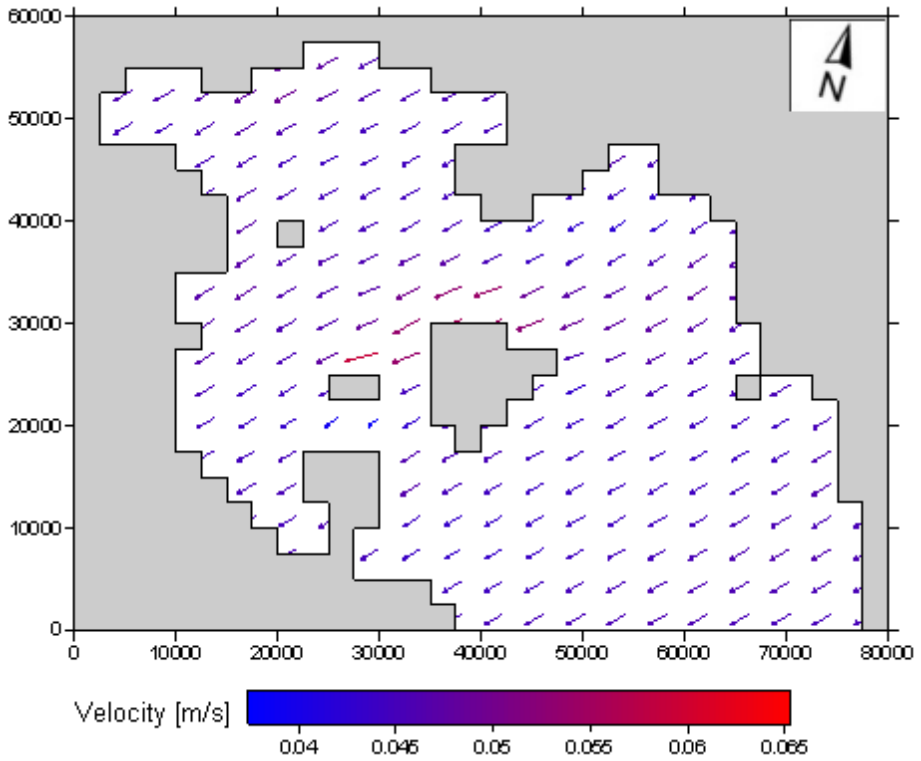

Figure AA7. Surface currents for North-East wind - 1 bf

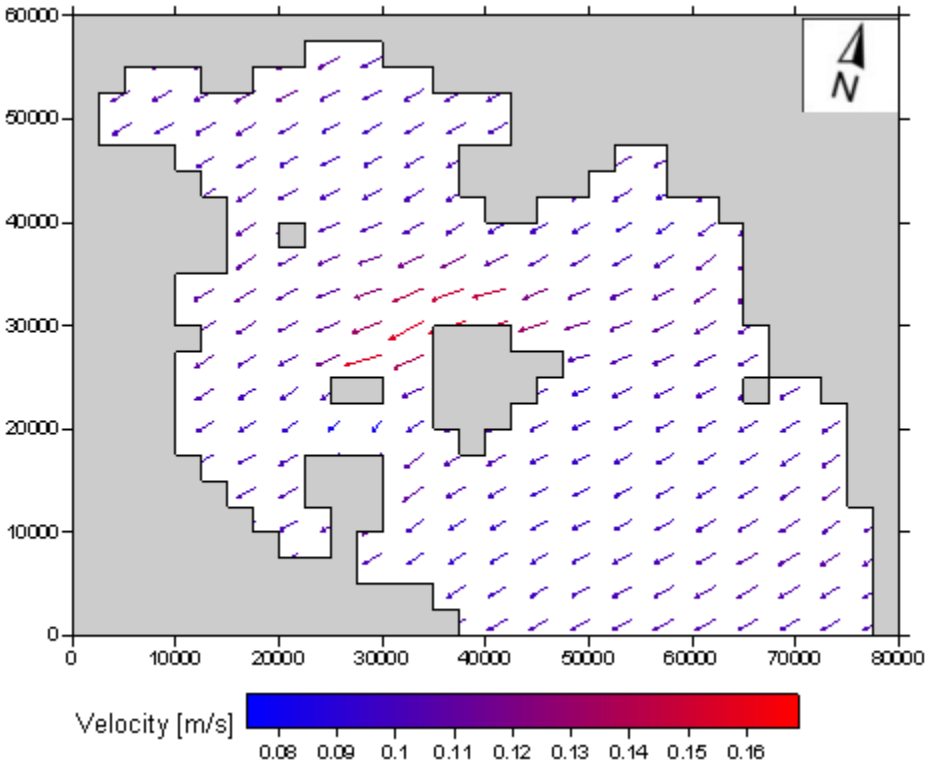

Figure AA8. Surface currents for North-East wind - 2 bf

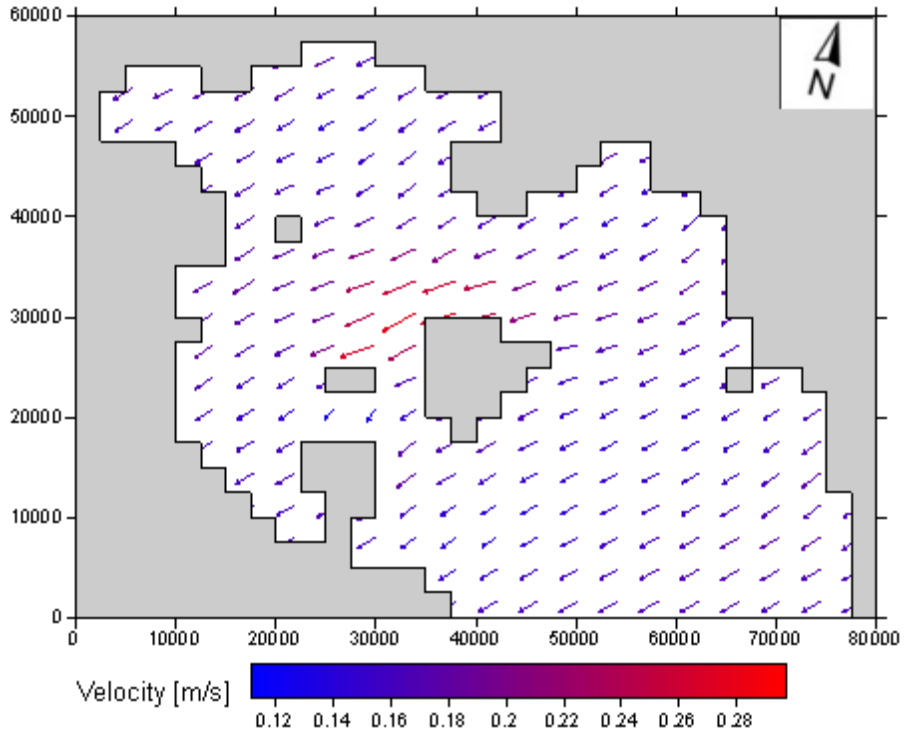

Figure AA9. Surface currents for North-East wind - 3 bf

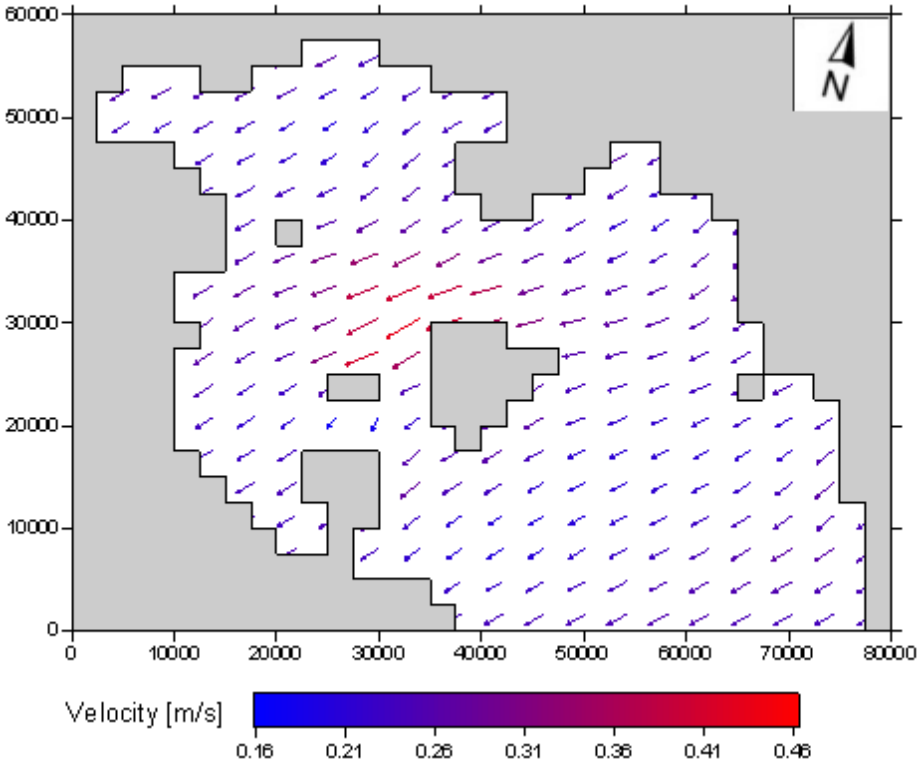

Figure AA10. Surface currents for North-East wind - 4 bf

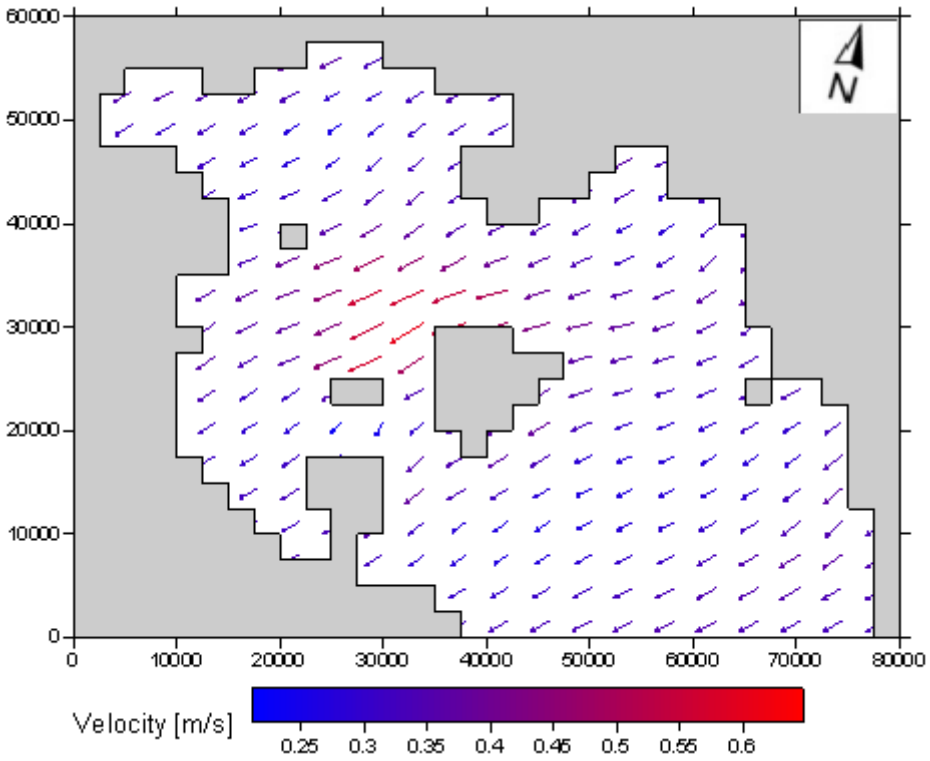

Figure AA11. Surface currents for North-East wind - 5 bf

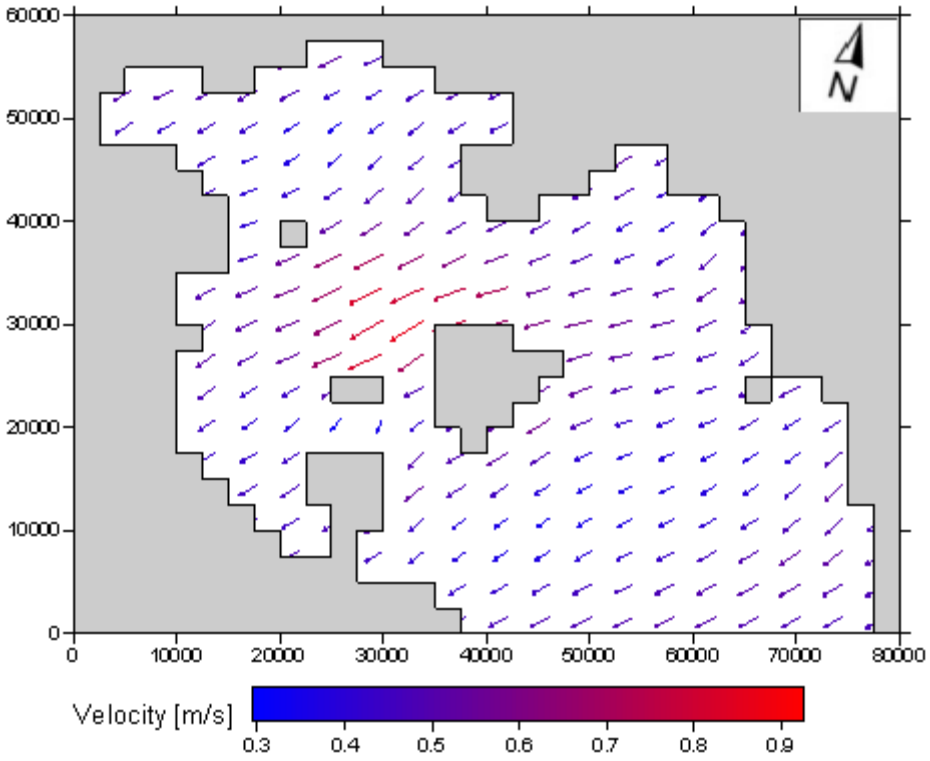

Figure AA12. Surface currents for North-East wind - 6 bf

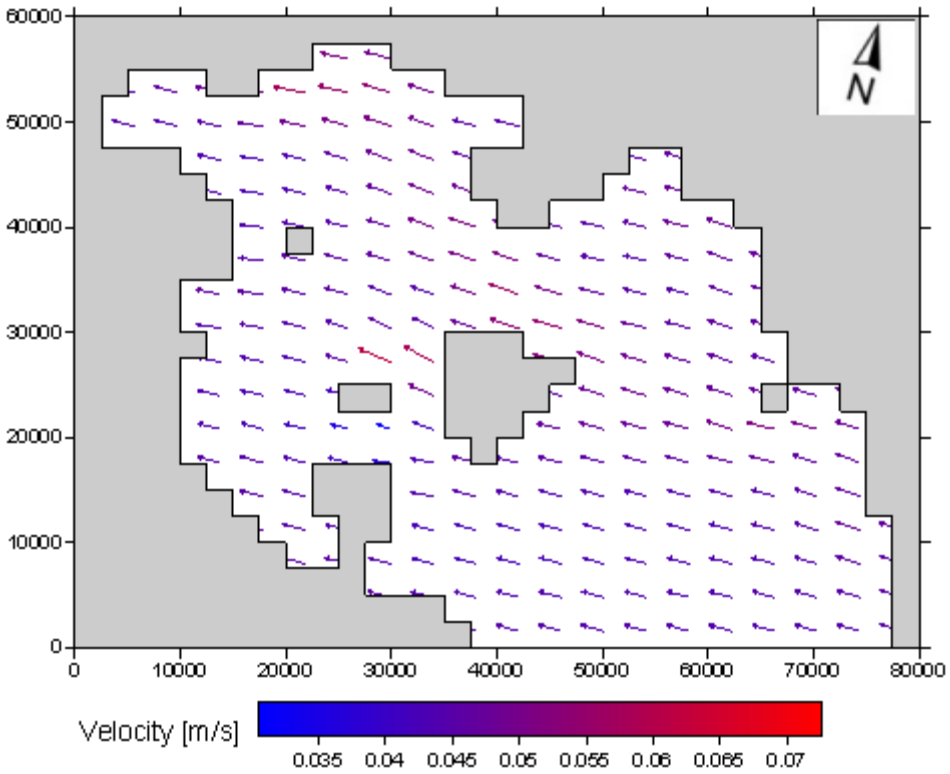

Figure AA13. Surface currents for East wind - 1 bf

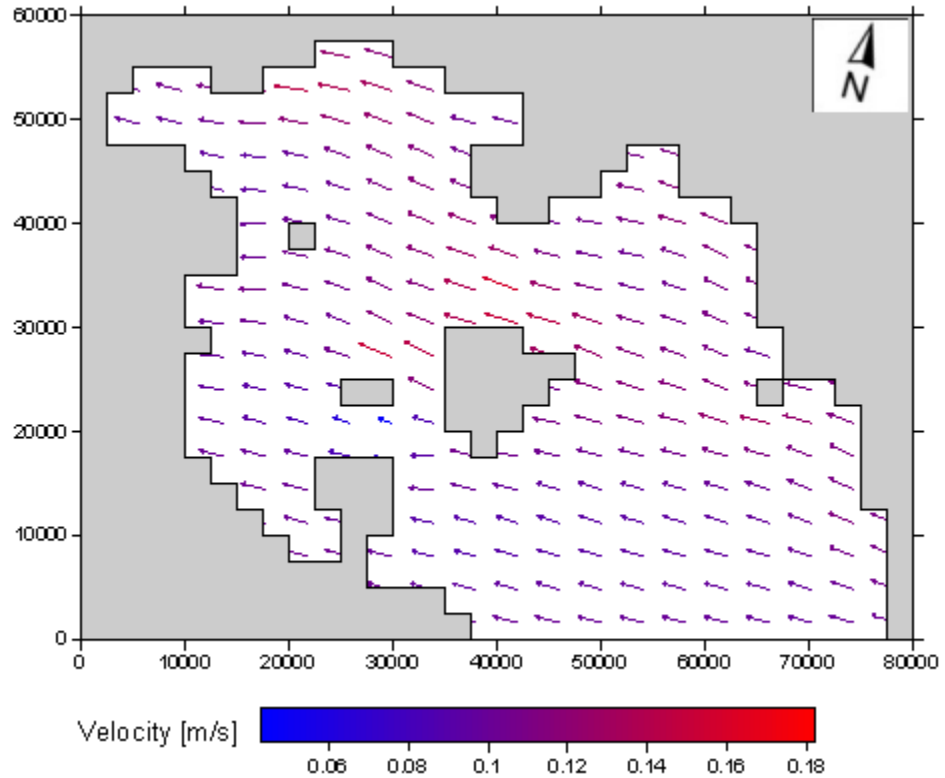

Figure AA14. Surface currents for East wind - 2 bf

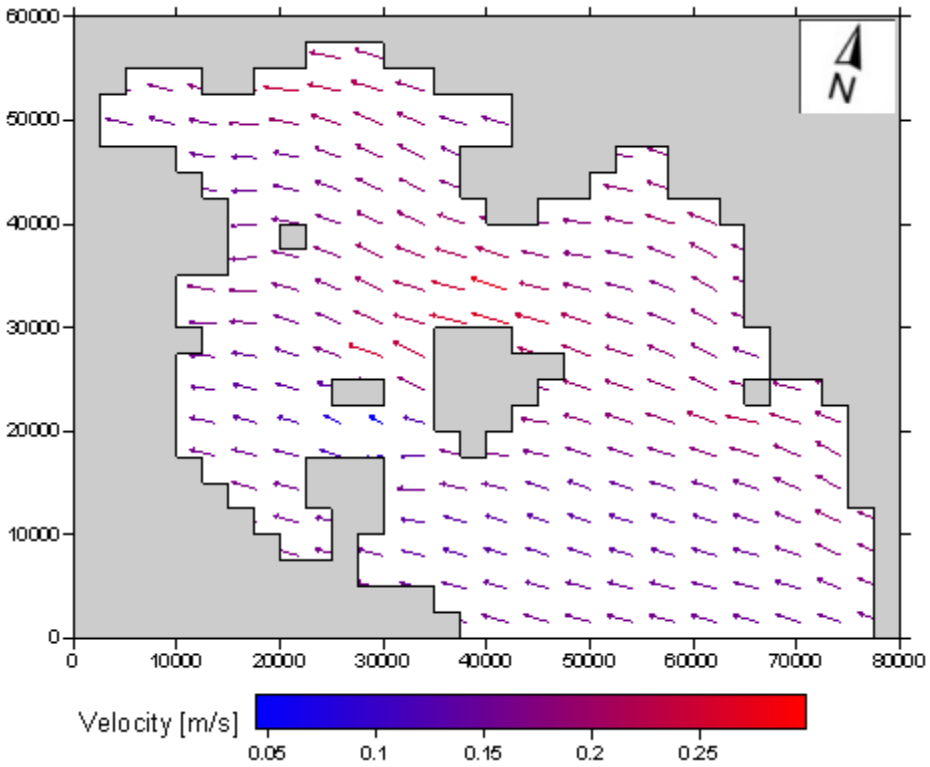

Figure AA15. Surface currents for East wind - 3 bf

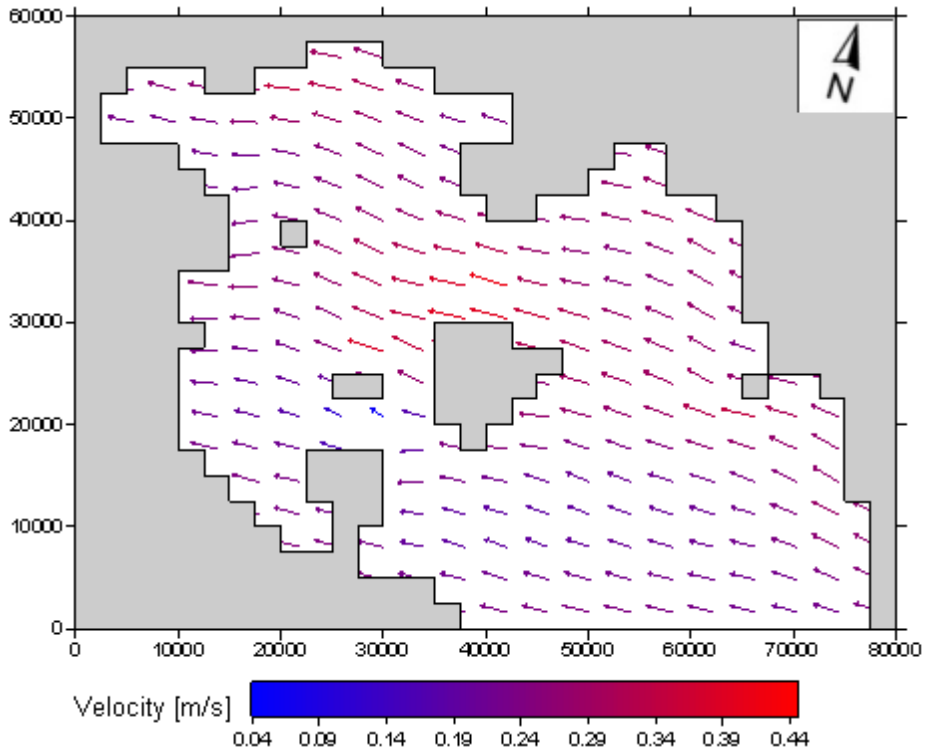

Figure AA16. Surface currents for East wind - 4 bf

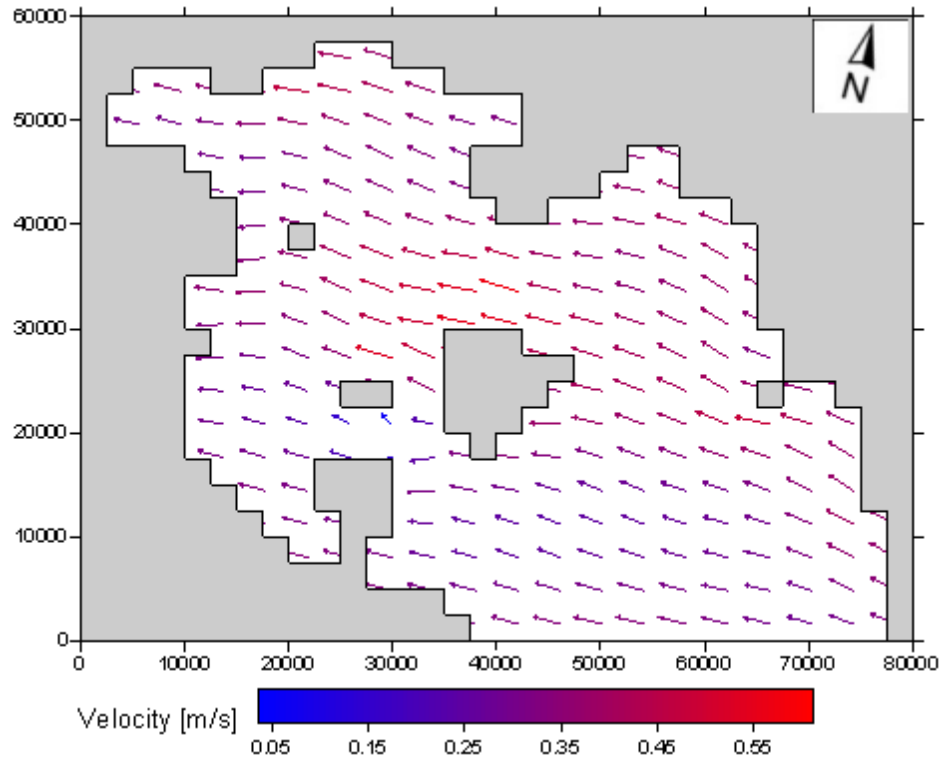

Figure AA17. Surface currents for East wind - 5 bf

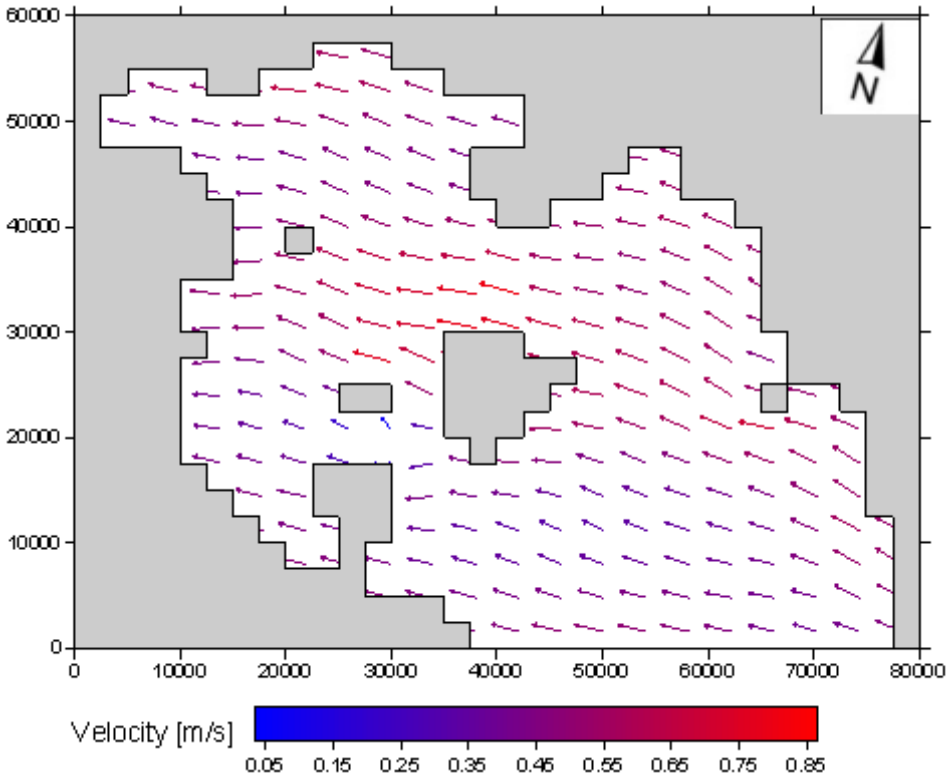

Figure AA18. Surface currents for East wind - 6 bf

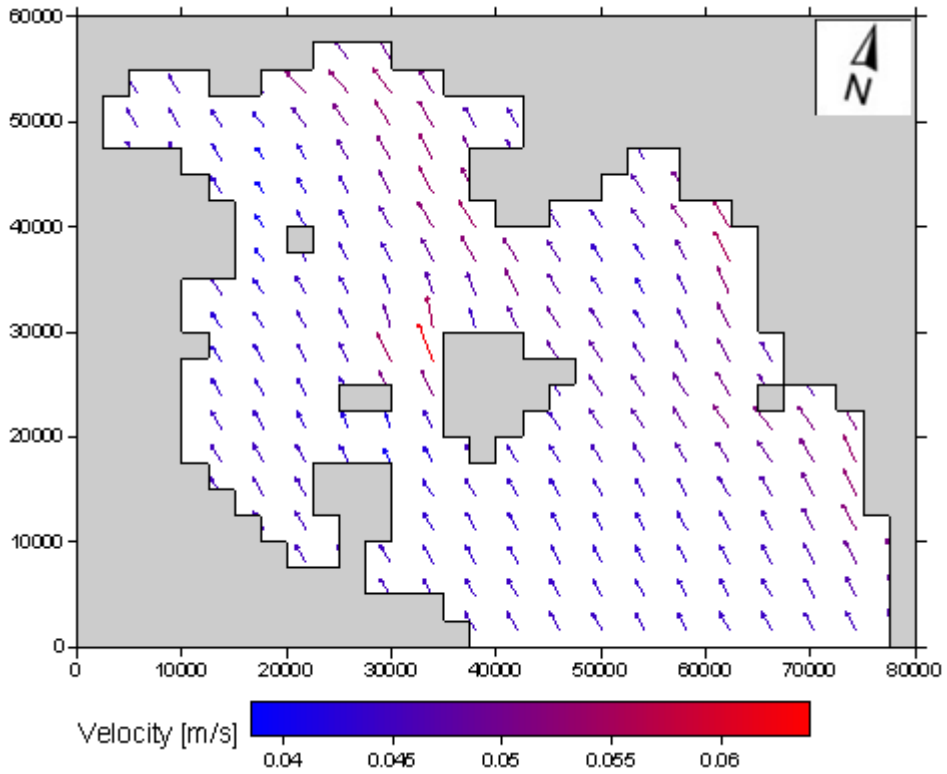

Figure AA19. Surface currents for South-East wind - 1 bf

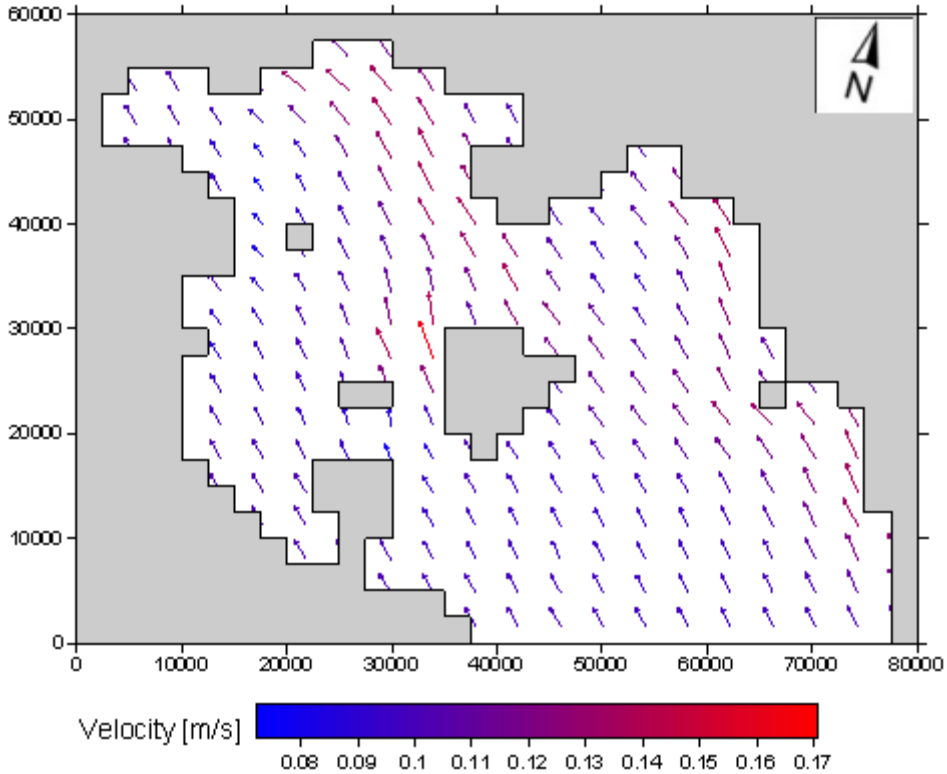

Figure AA20. Surface currents for South-East wind - 2 bf

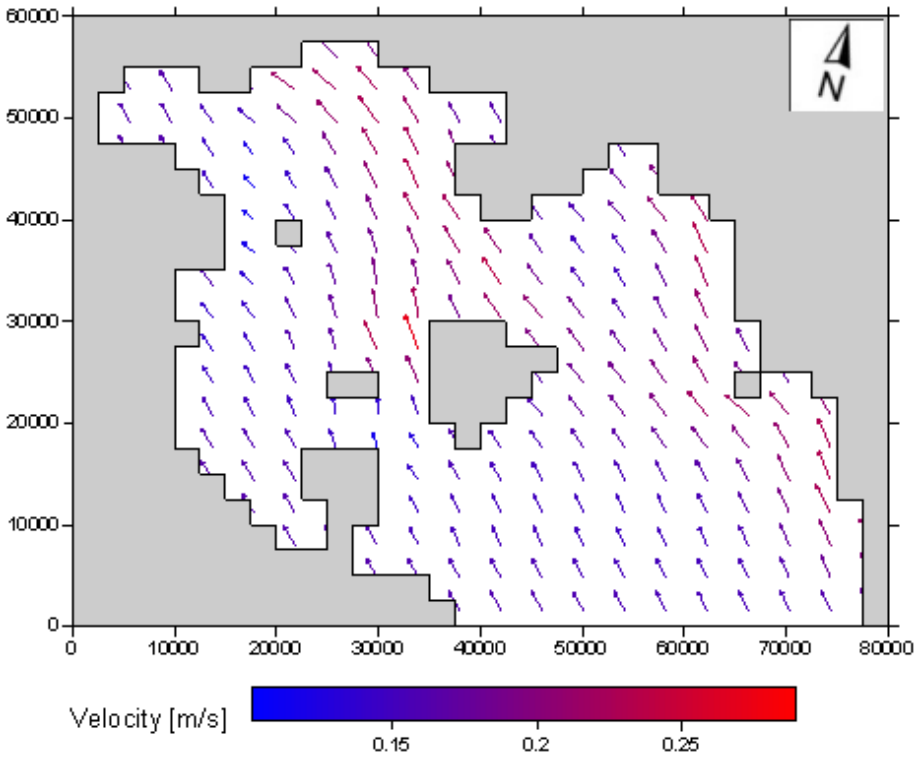

Figure AA21. Surface currents for South-East wind - 3 bf

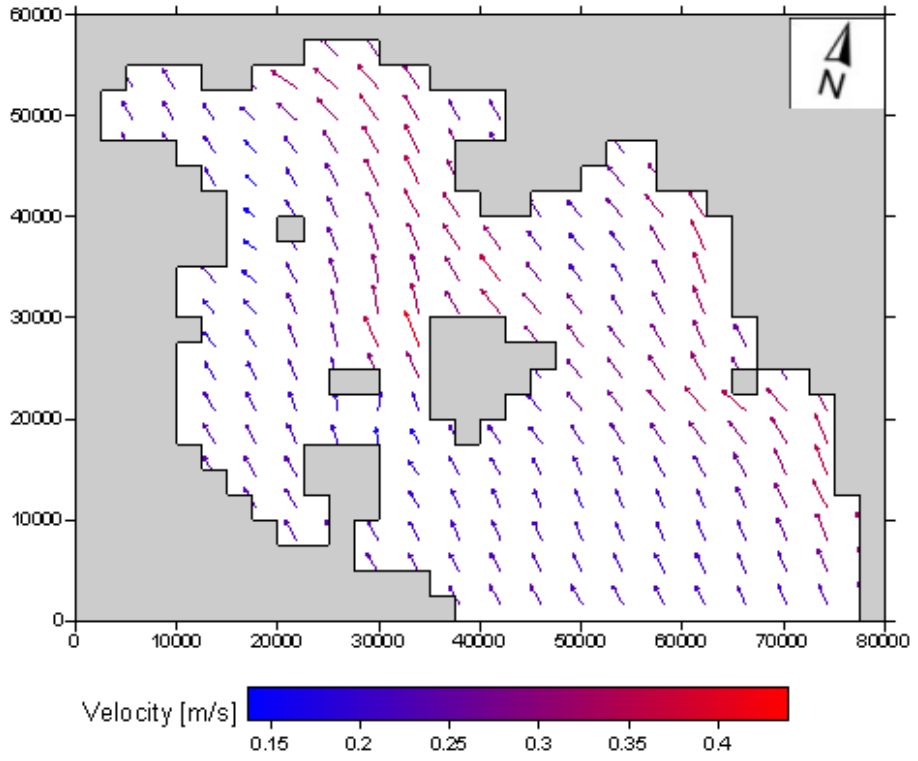

Figure AA22. Surface currents for South-East wind - 4 bf

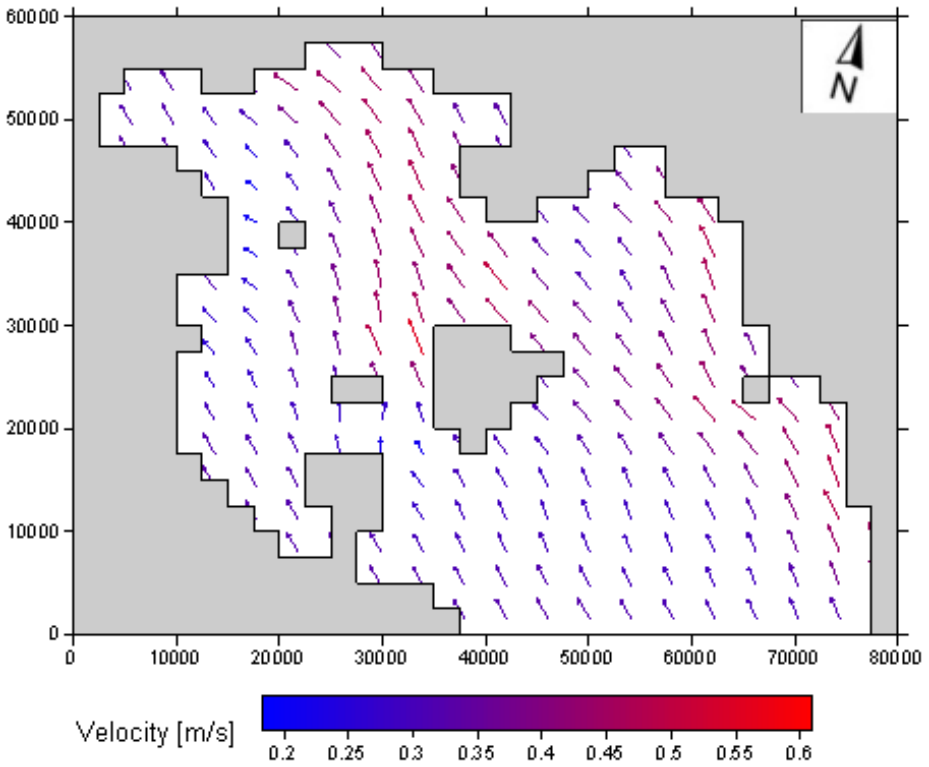

Figure AA23. Surface currents for South-East wind - 5 bf

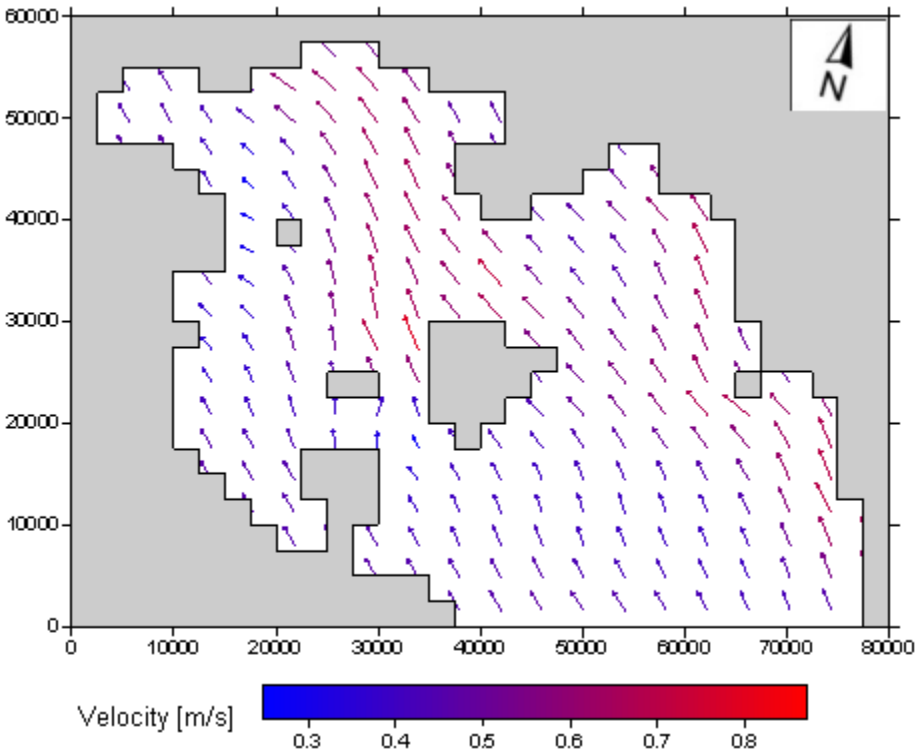

Figure AA24. Surface currents for South-East wind - 6 bf

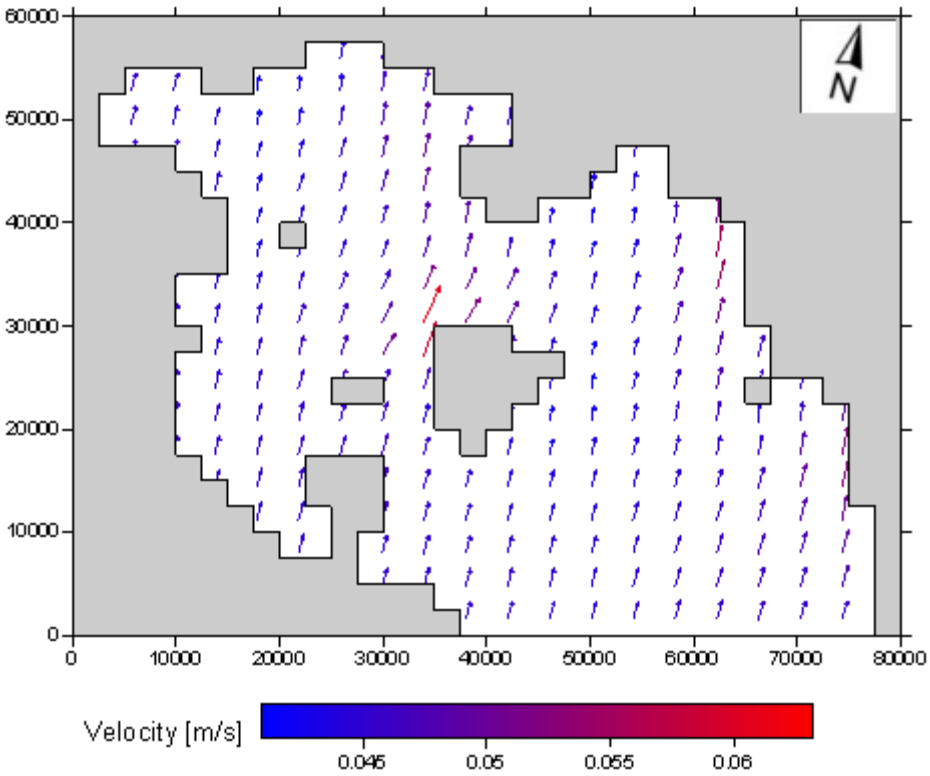

Figure AA25. Surface currents for South wind - 1 bf

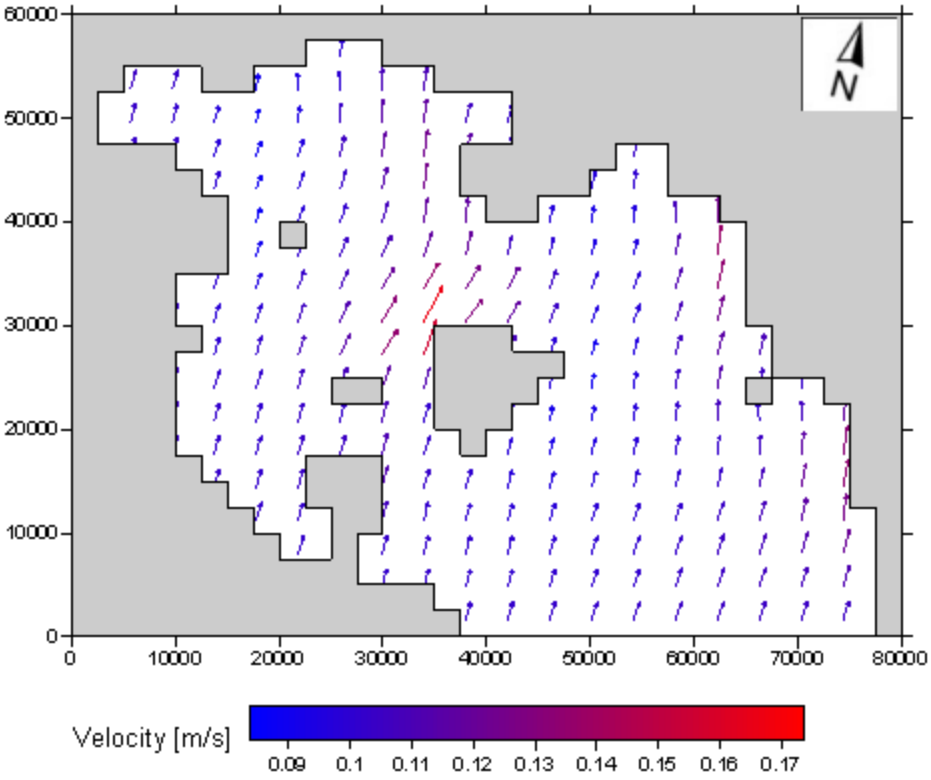

Figure AA26. Surface currents for South wind - 2 bf

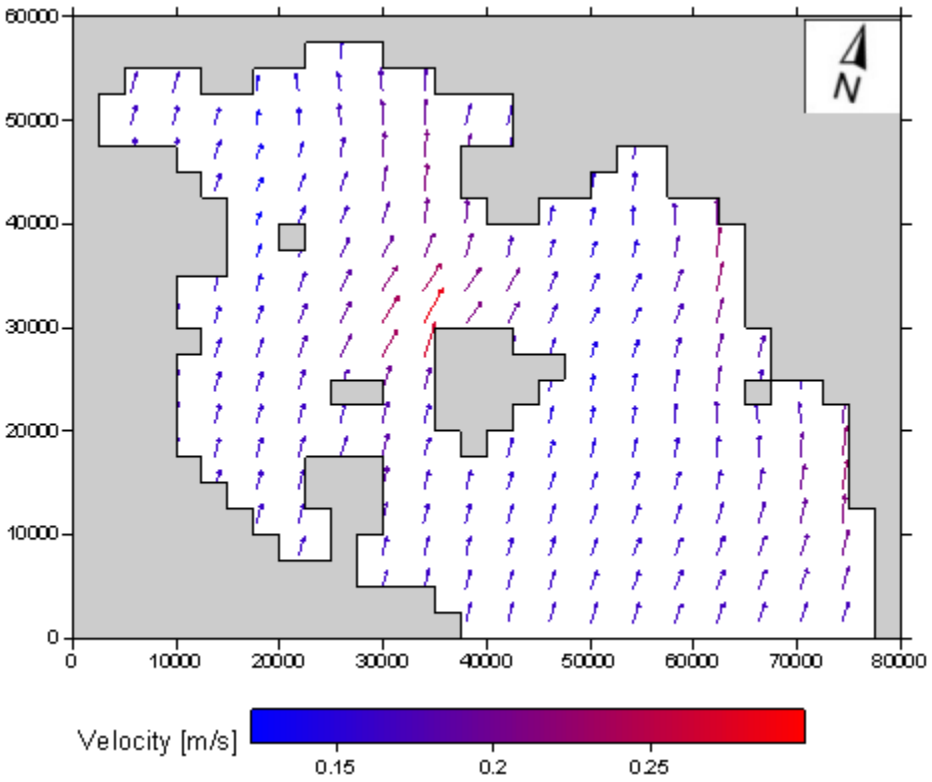

Figure AA27. Surface currents for South wind - 3 bf

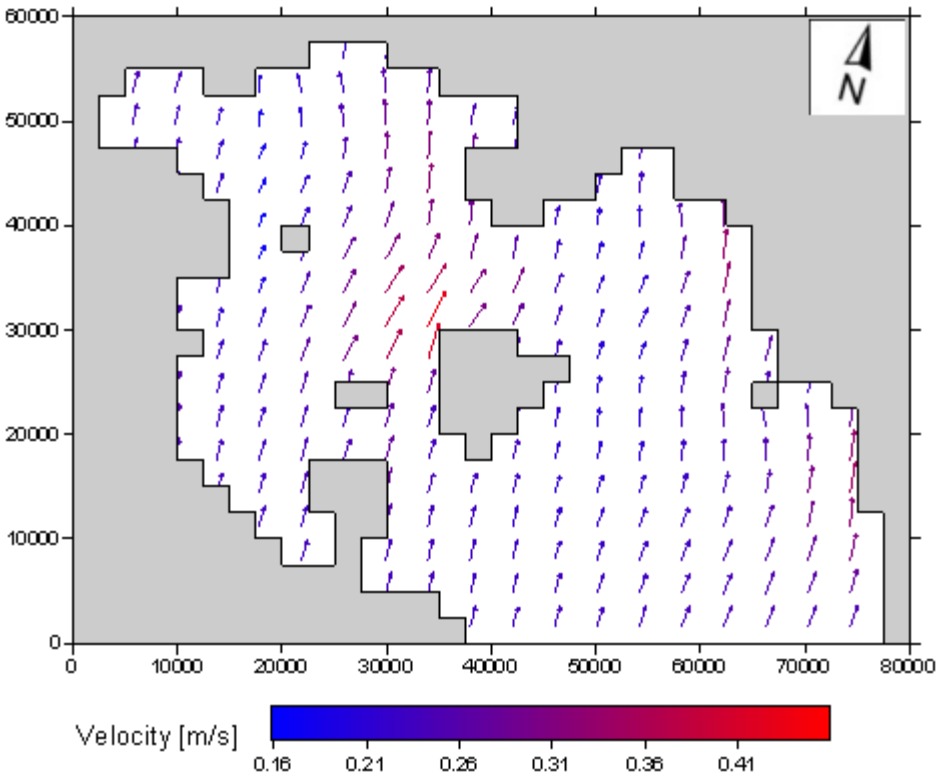

Figure AA28. Surface currents for South wind - 4 bf

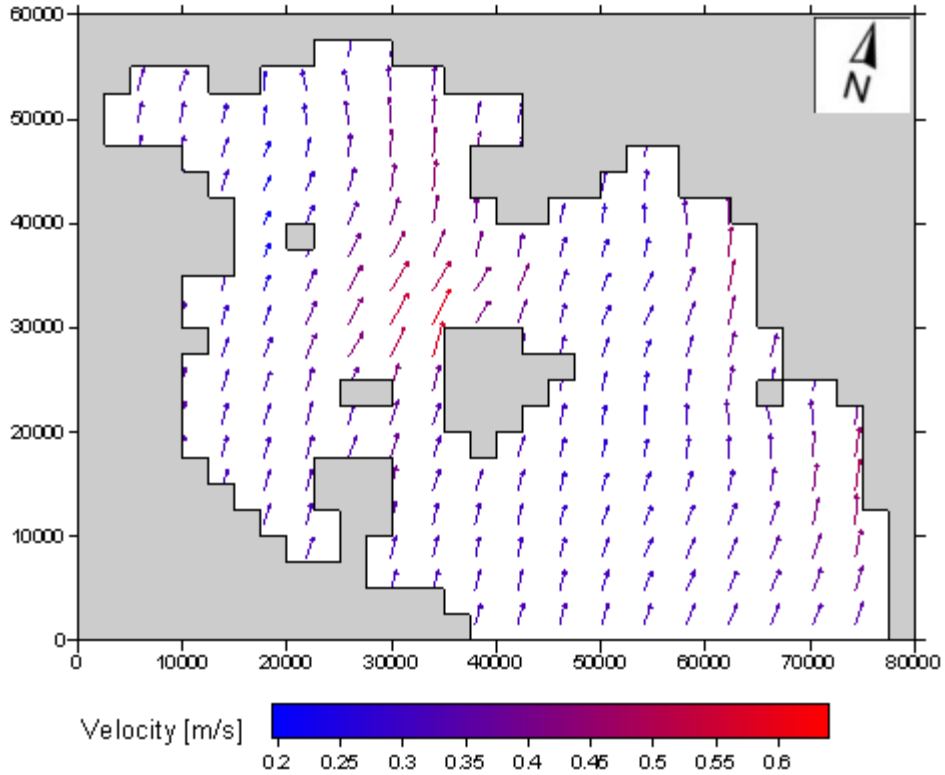

Figure AA29. Surface currents for South wind - 5 bf

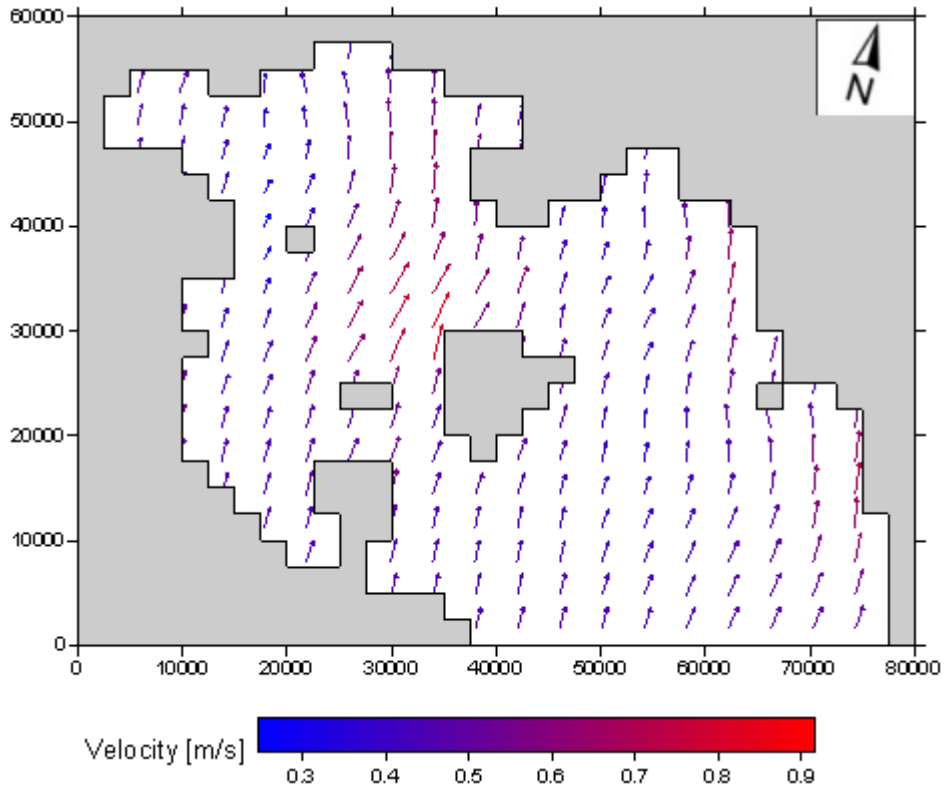

Figure AA30. Surface currents for South wind - 6 bf

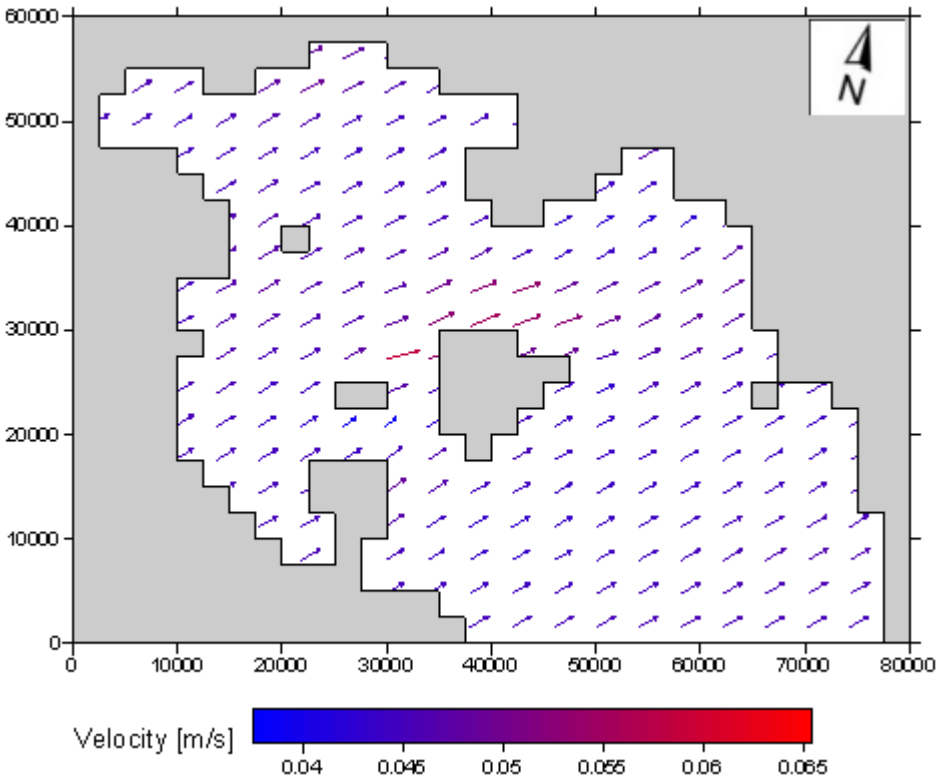

Figure AA31. Surface currents for South-West wind - 1 bf

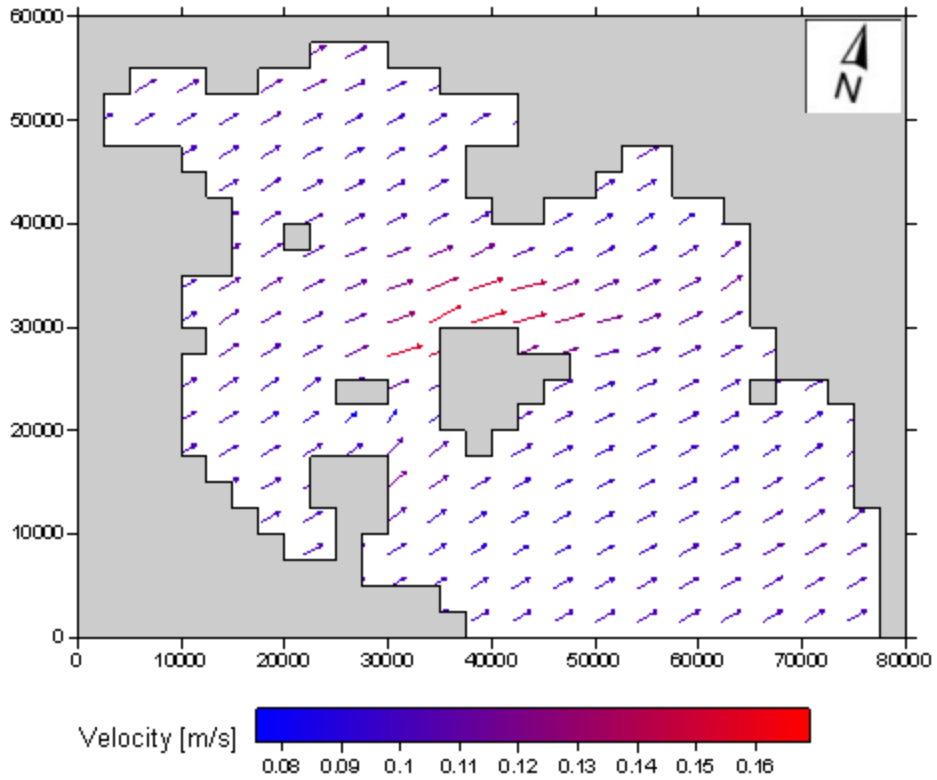

Figure AA32. Surface currents for South-West wind - 2 bf

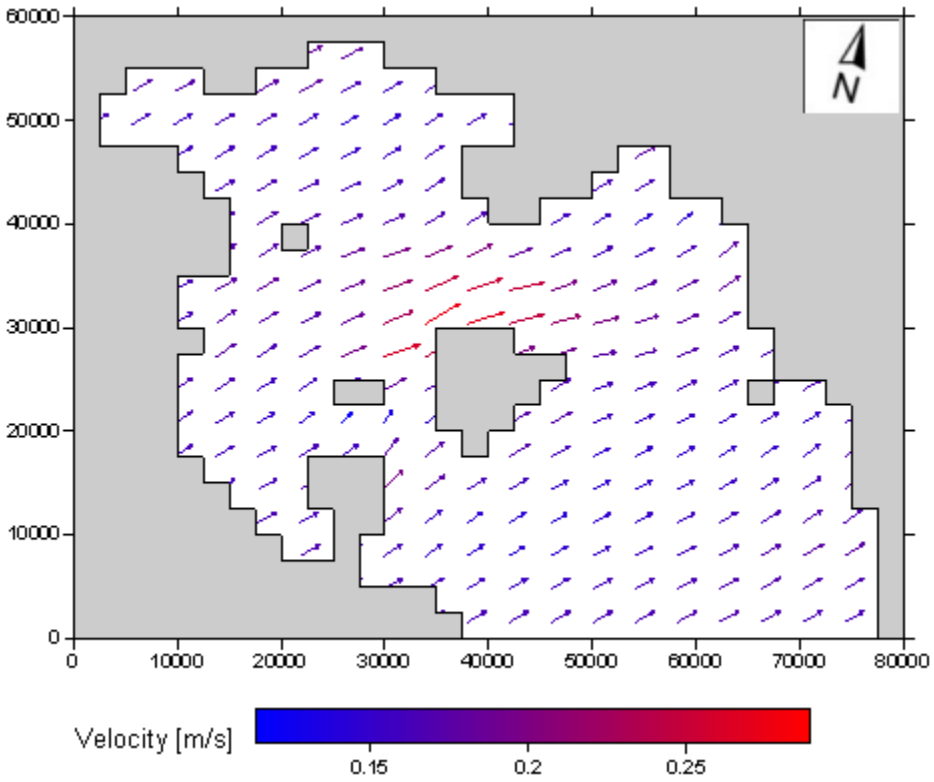

Figure AA33. Surface currents for South-West wind - 3 bf

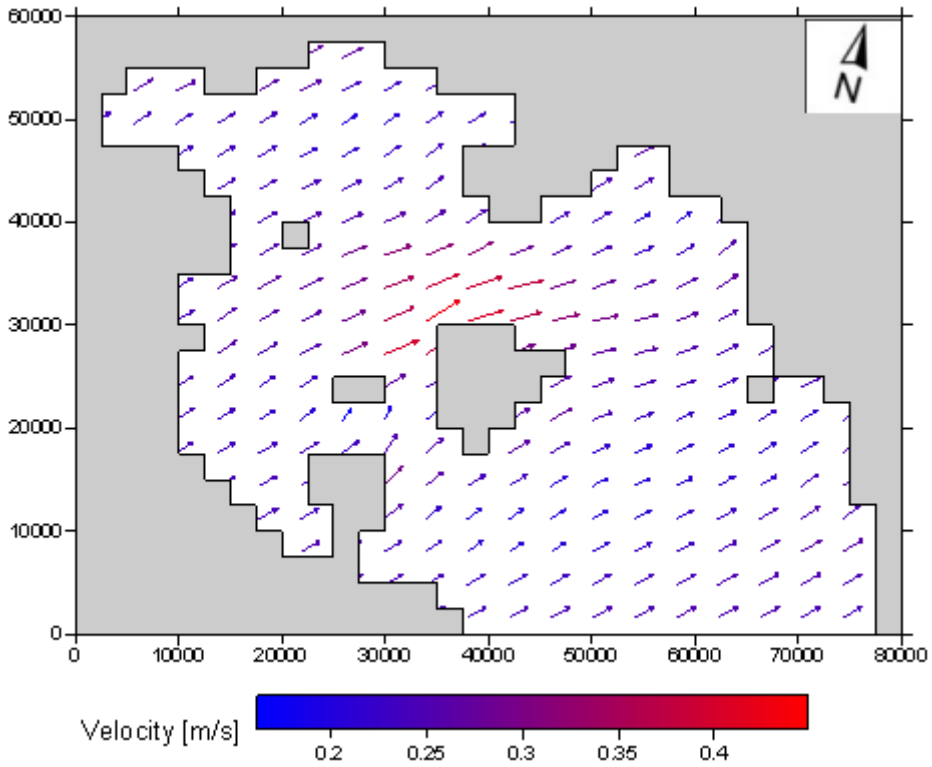

Figure AA34. Surface currents for South-West wind - 4 bf

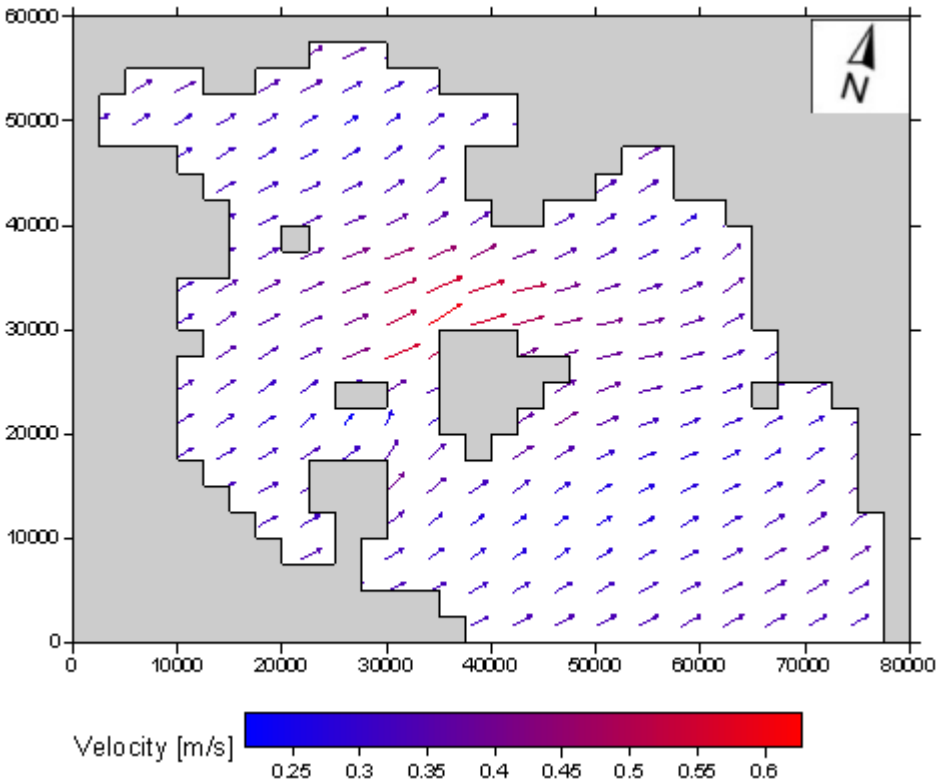

Figure AA35. Surface currents for South-West wind - 5 bf

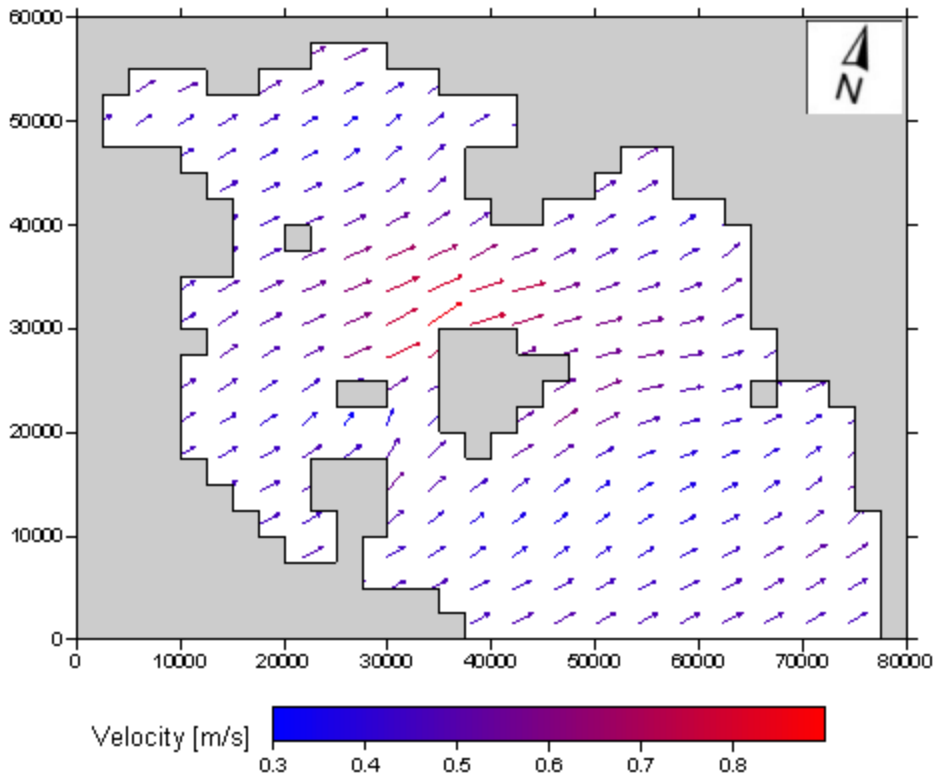

Figure AA36. Surface currents for South-West wind - 6 bf

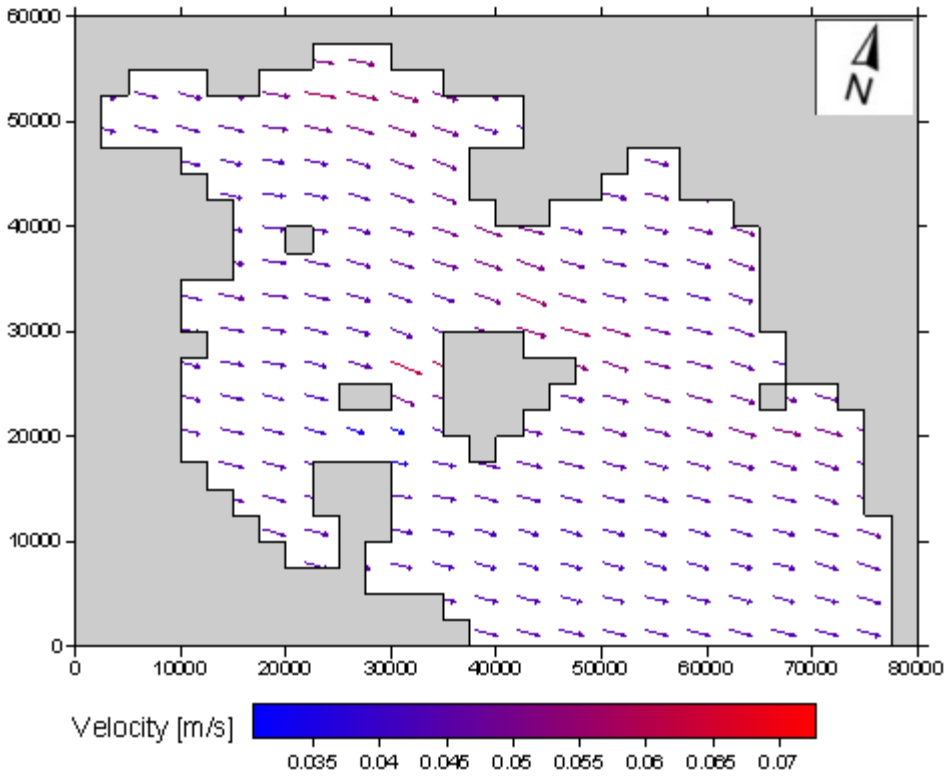

Figure AA37. Surface currents for West wind - 1 bf

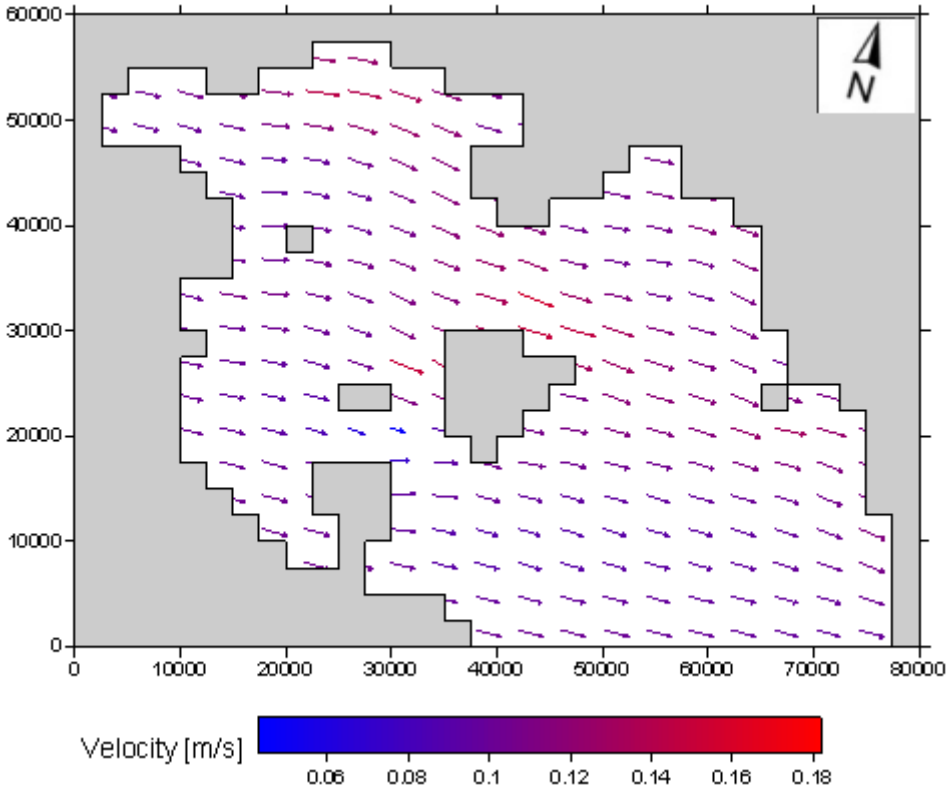

Figure AA38. Surface currents for West wind - 2 bf

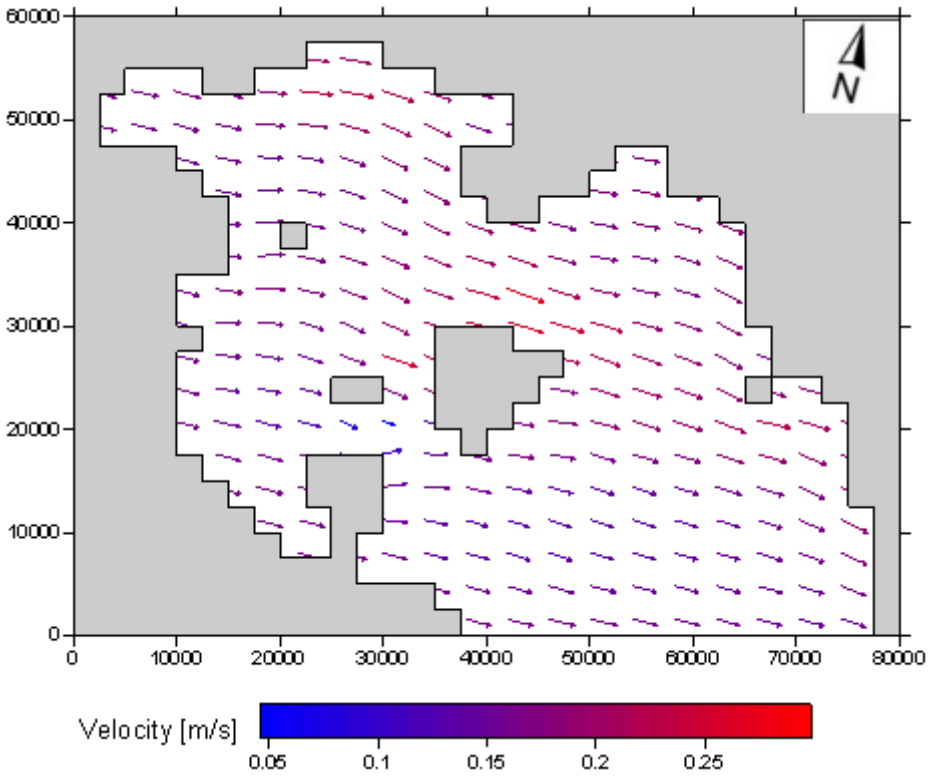

Figure AA39. Surface currents for West wind - 3 bf

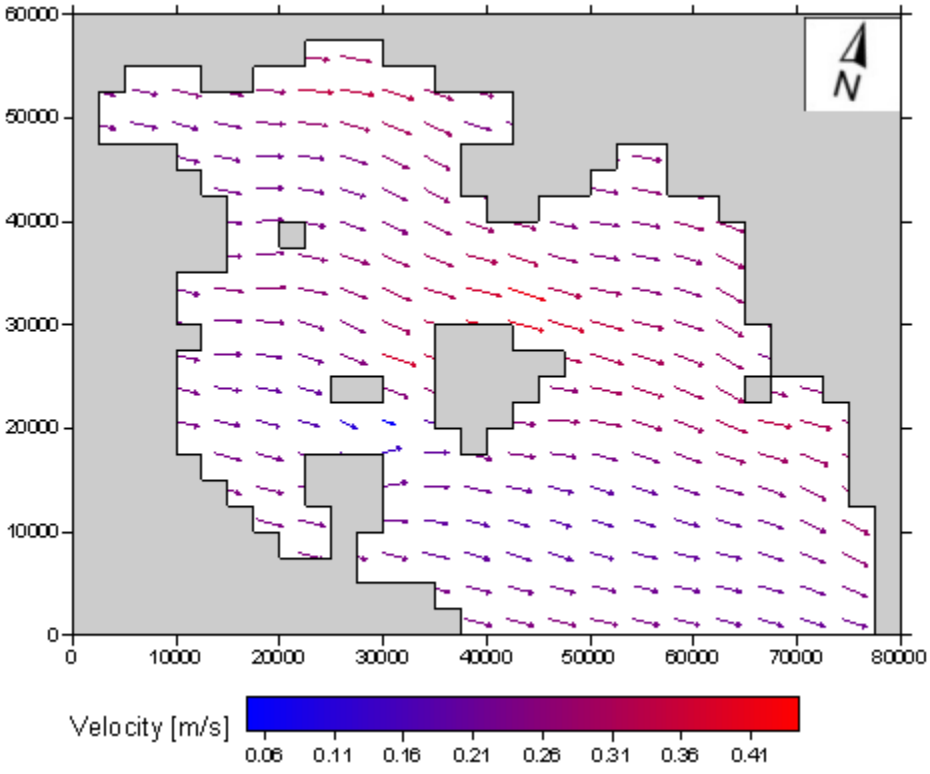

Figure AA40. Surface currents for West wind - 4 bf

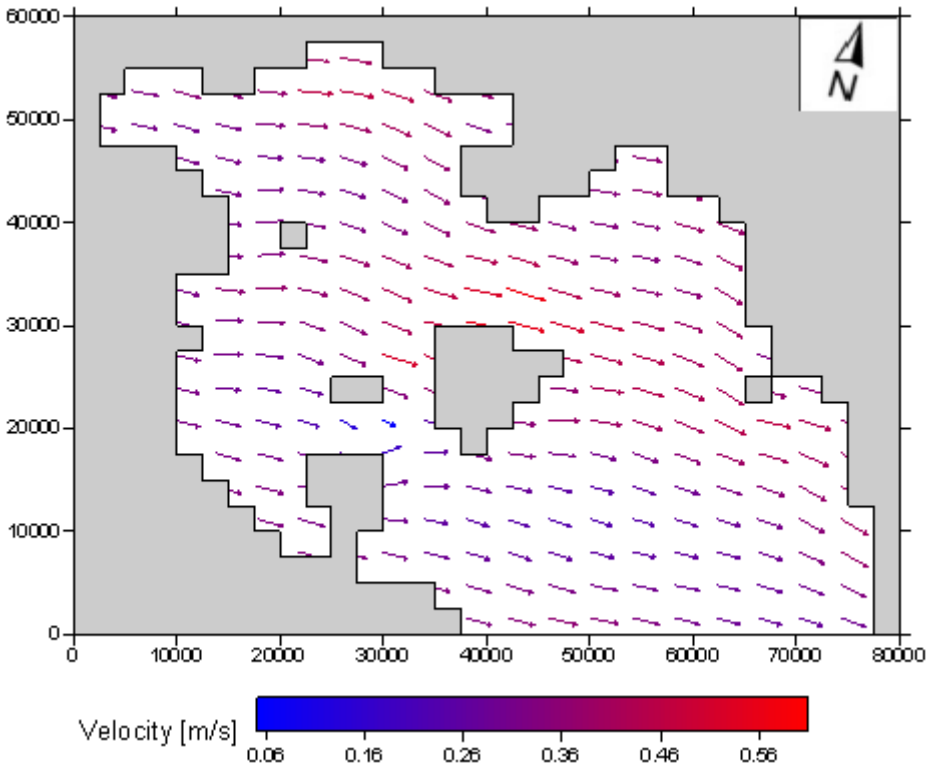

Figure AA41. Surface currents for West wind - 5 bf

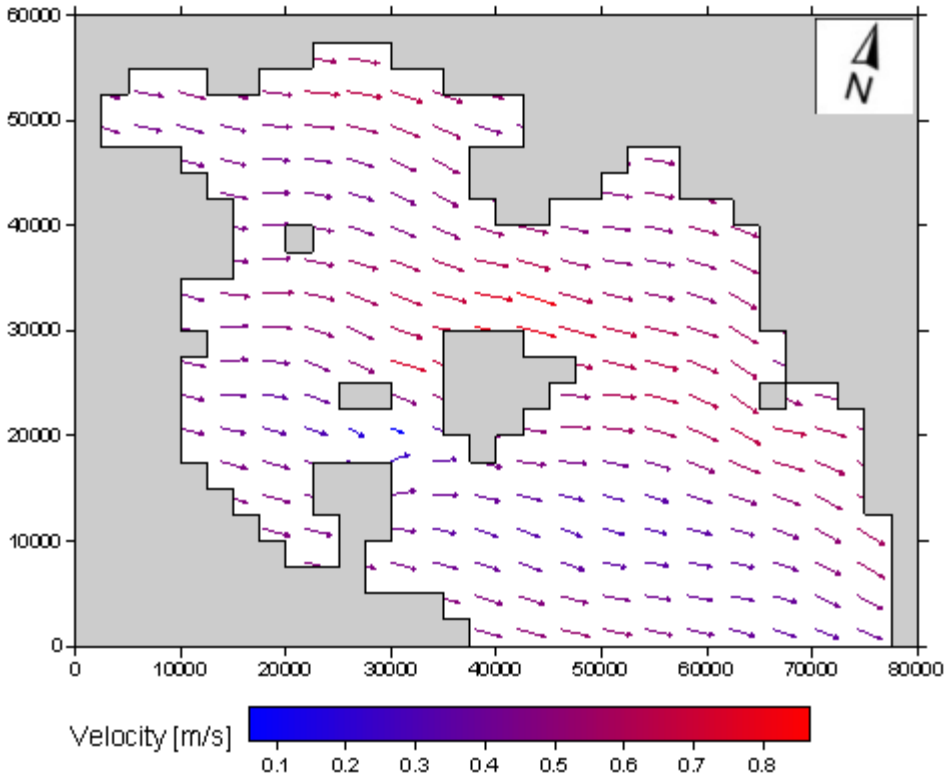

Figure AA42. Surface currents for West wind - 6 bf

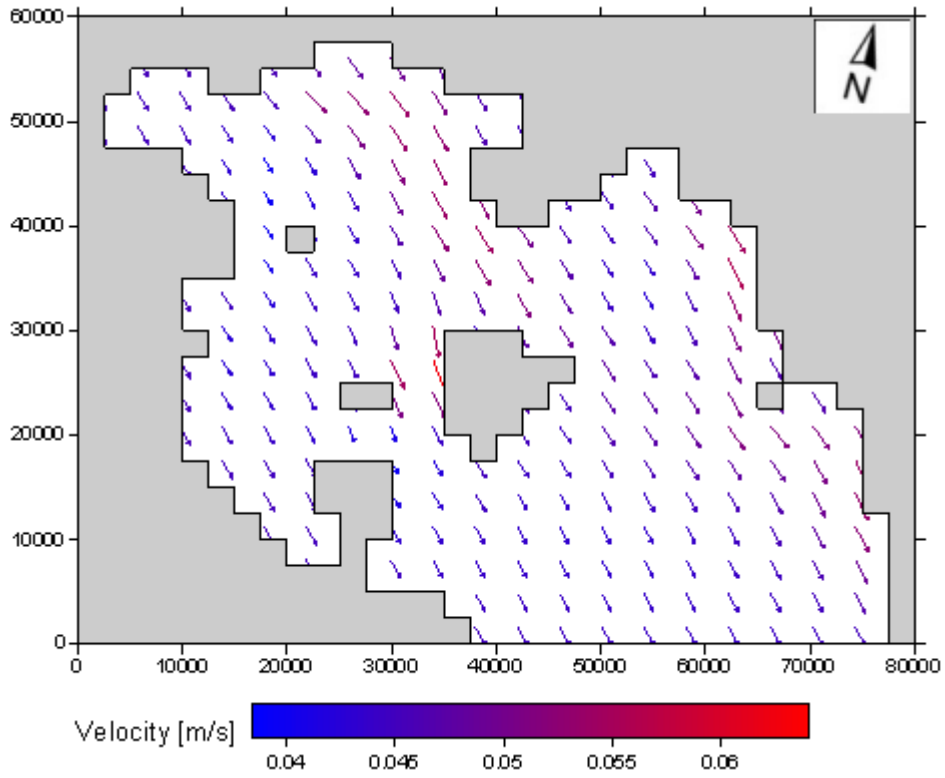

Figure AA43. Surface currents for North-West wind - 1 bf

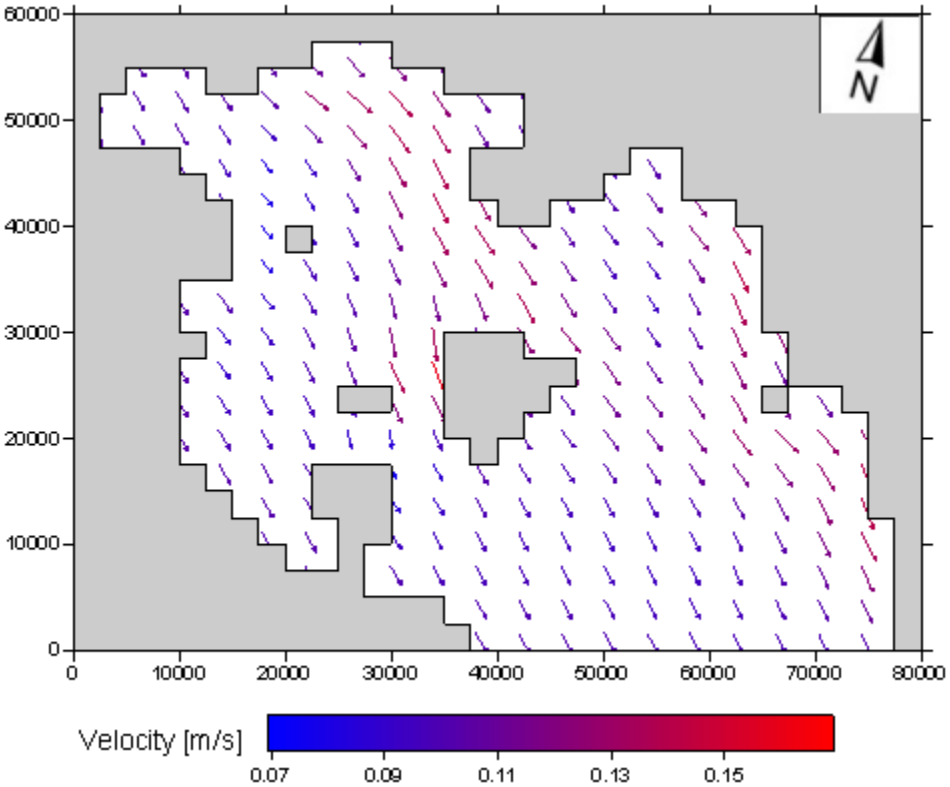

Figure AA44. Surface currents for North-West wind - 2 bf

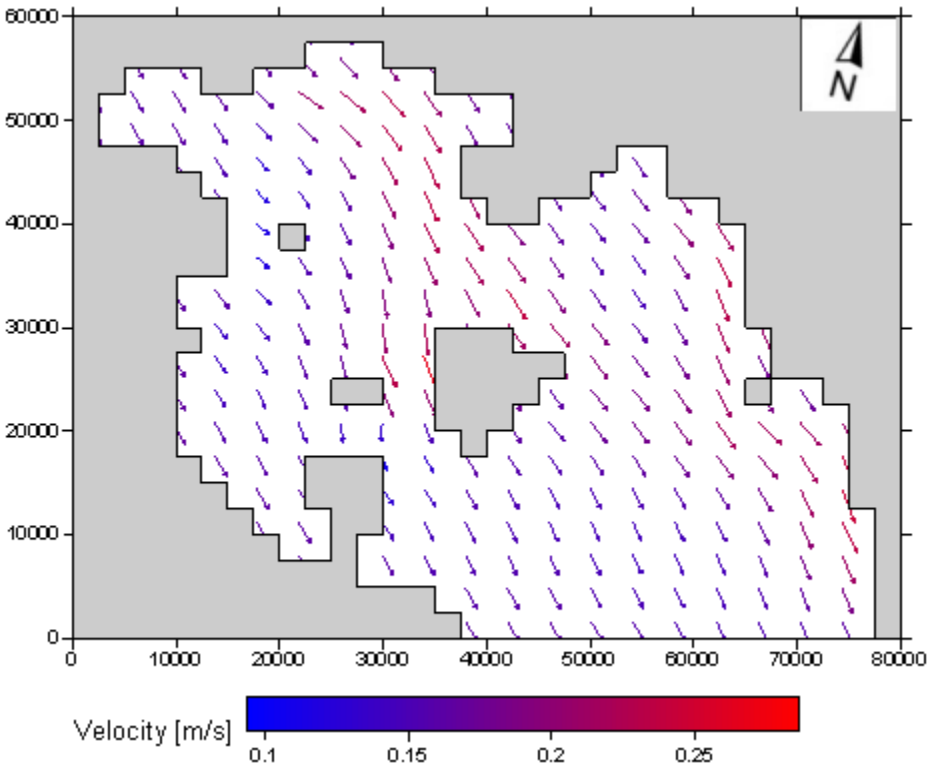

Figure AA45. Surface currents for North-West wind - 3 bf

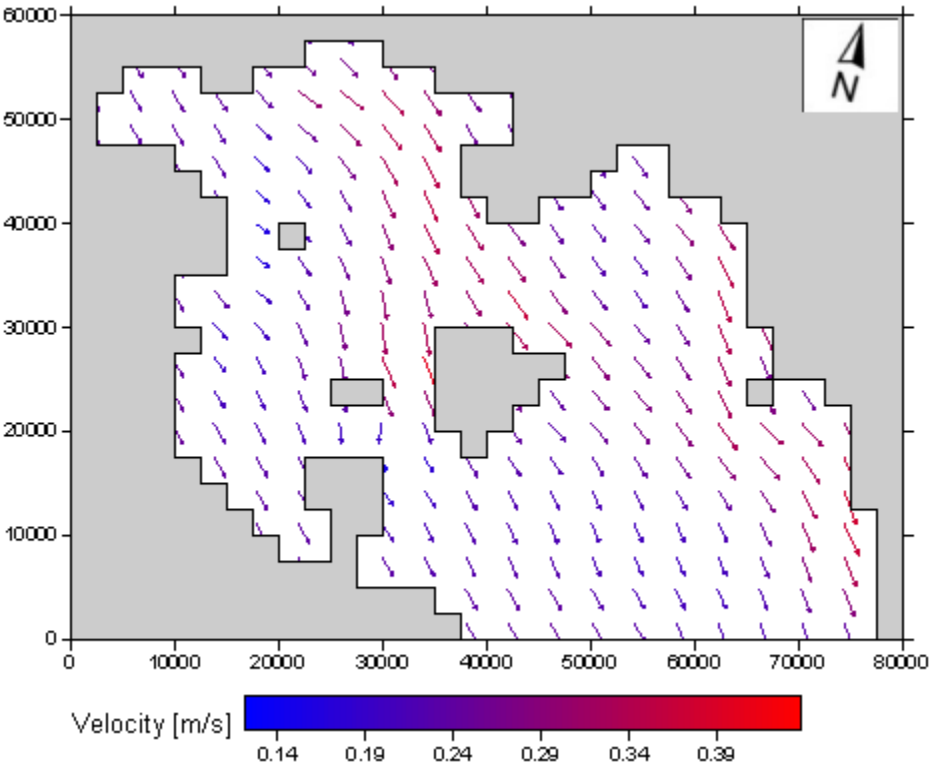

Figure AA46. Surface currents for North-West wind - 4 bf

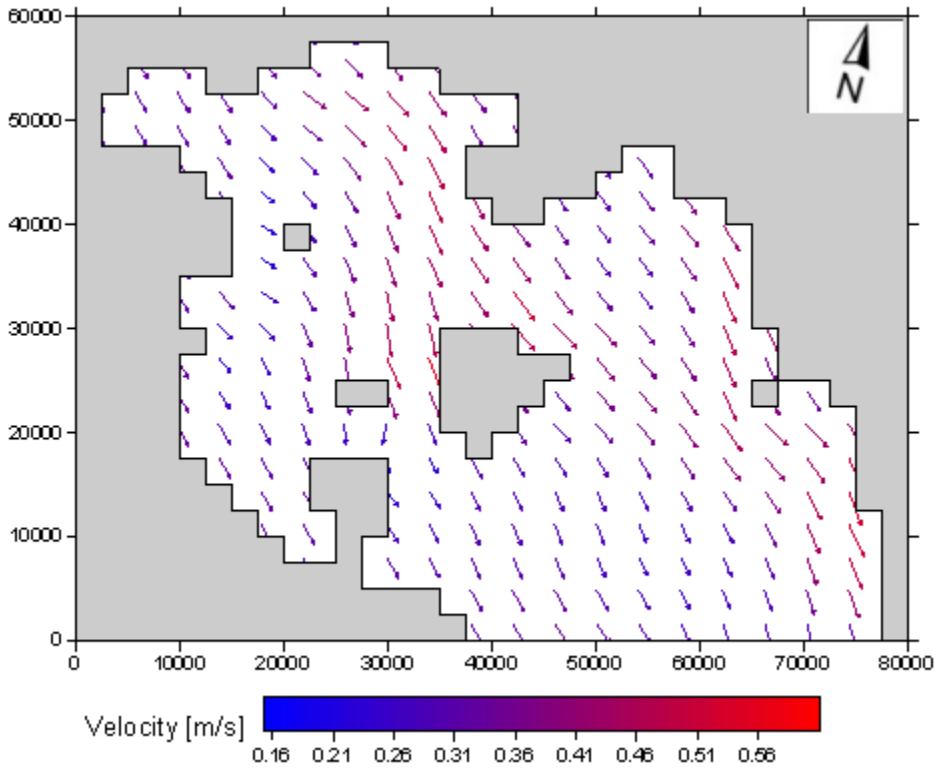

Figure AA47. Surface currents for North-West wind - 5 bf

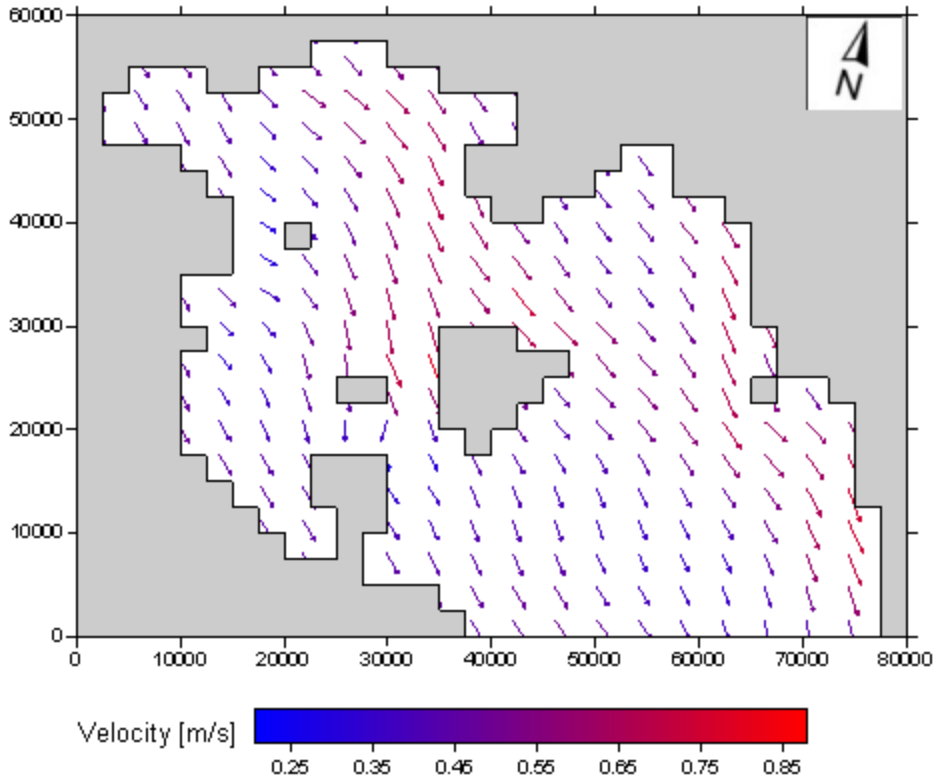

Figure AA48. Surface currents for North-West wind - 6 bf

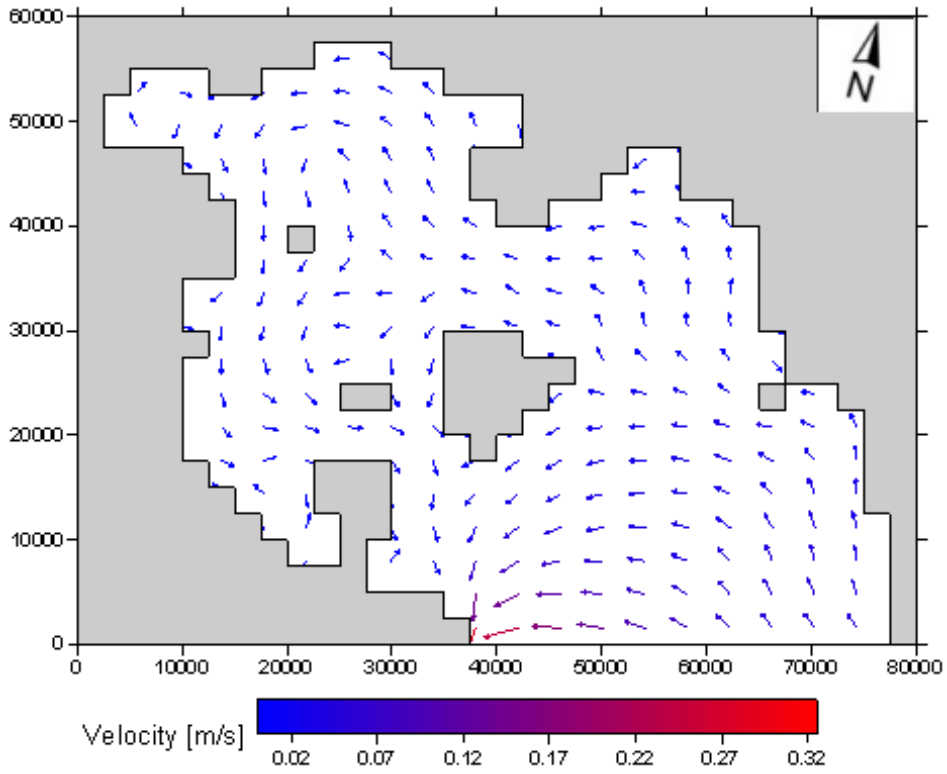

Figure AB49. Surface currents for no wind condition

APPENDIX B: THE OSM RESULTS

The results of the Oil Spill Model (OSM) are concentrated in Appendix B; Figures 1 to 49 depict the trajectory of the oil spill at the 4 locations for each one of the 49 scenarios examined (48 wind scenarios plus the no wind condition) for the case of Saronicos Gulf. M/Mo is the ratio of the current (remaining) oil mass and the oil mass of the initial spill.

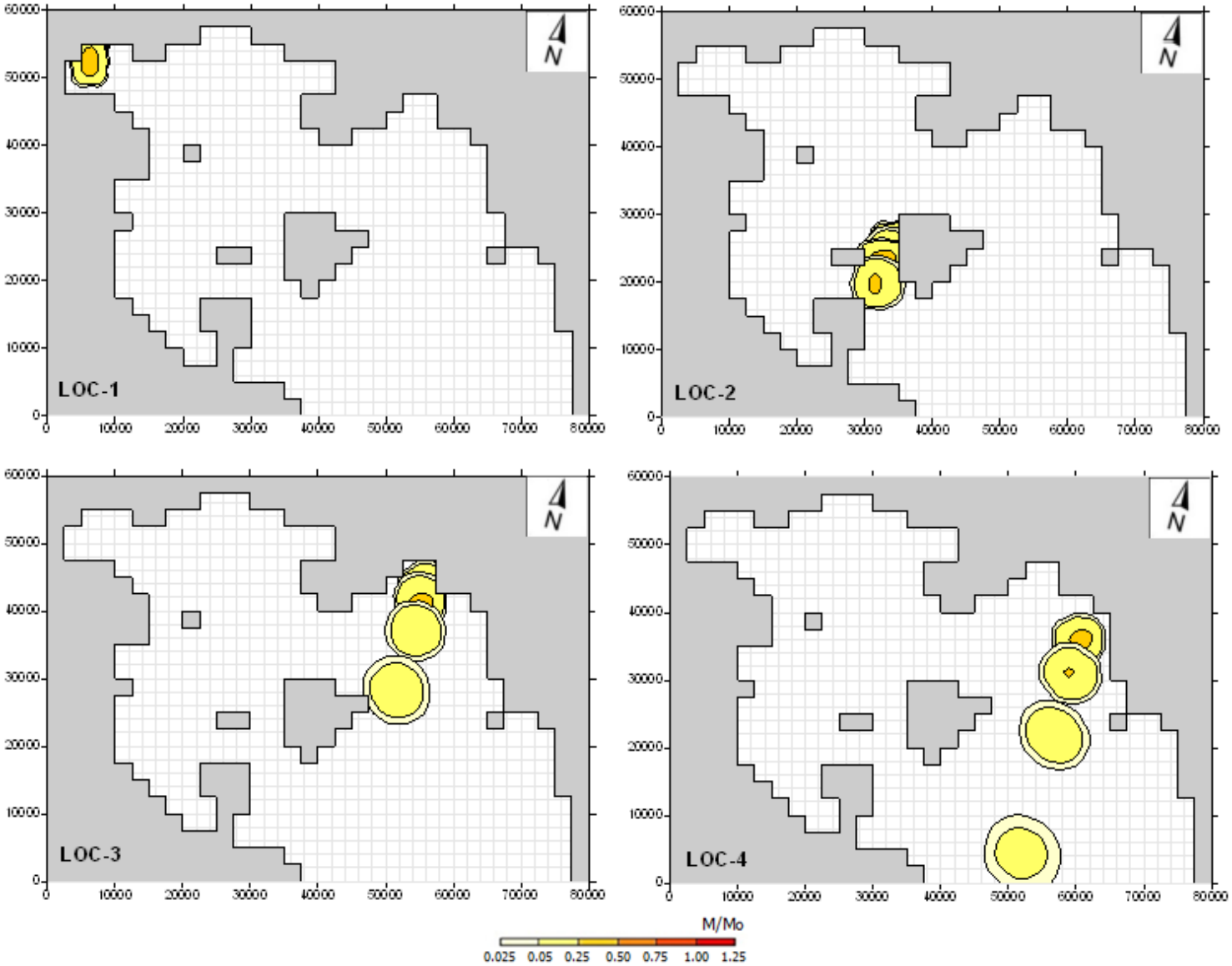

Figure AB1. Trajectory of the oil spill at the 4 locations examined for North wind - 1 bf

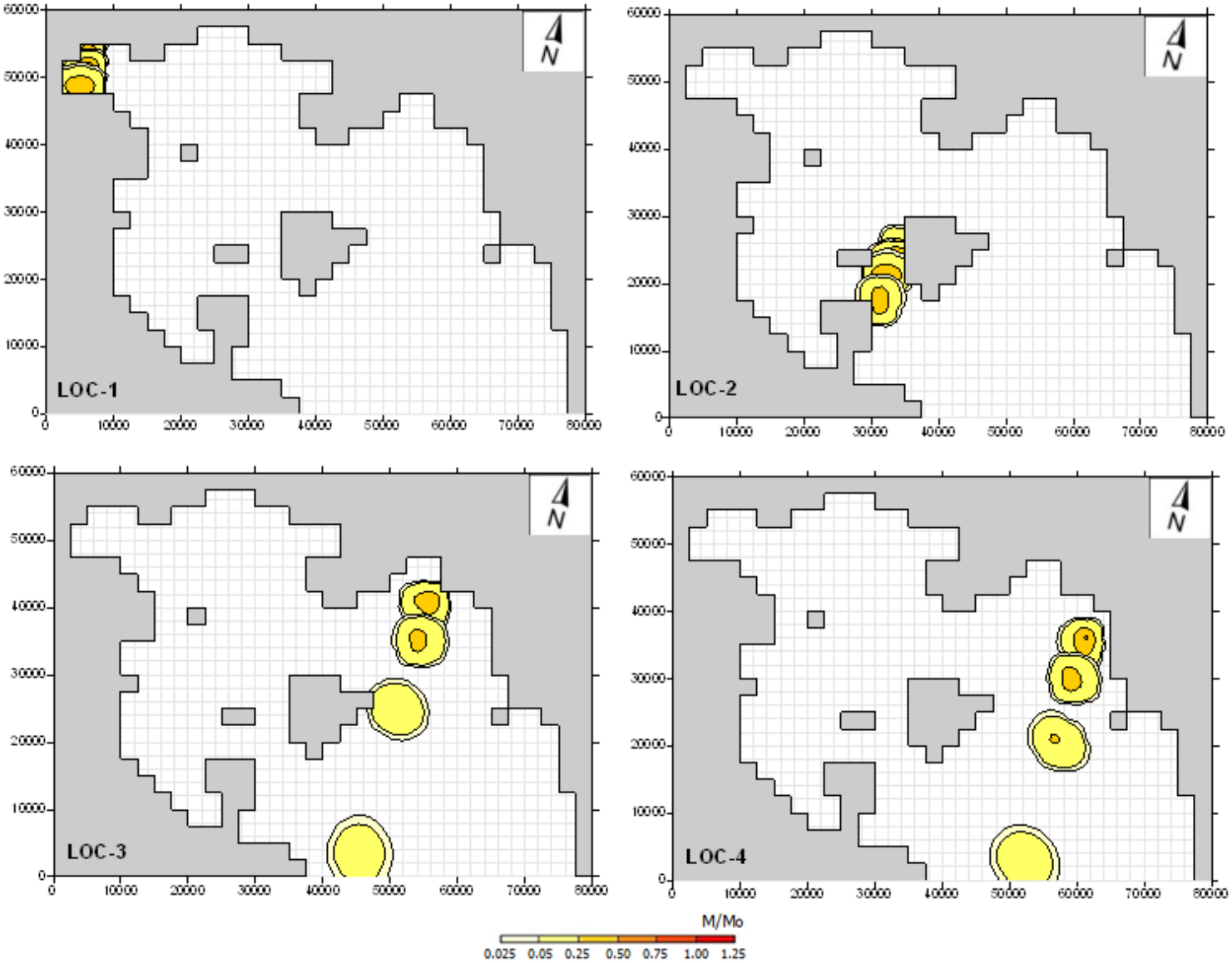

Figure AB2. Trajectory of the oil spill at the 4 locations examined for North wind - 2 bf

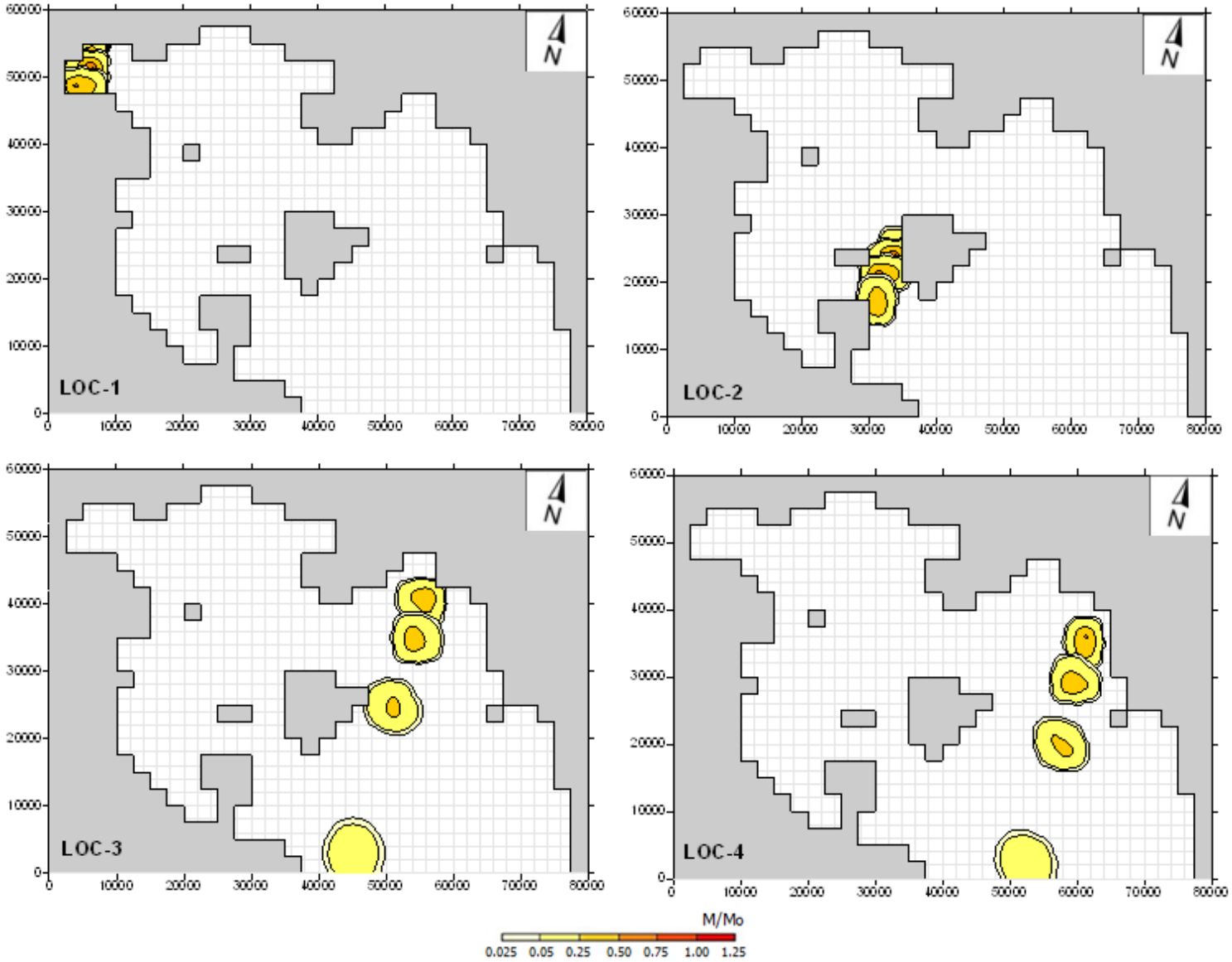

Figure AB3. Trajectory of the oil spill at the 4 locations examined for North wind - 3 bf

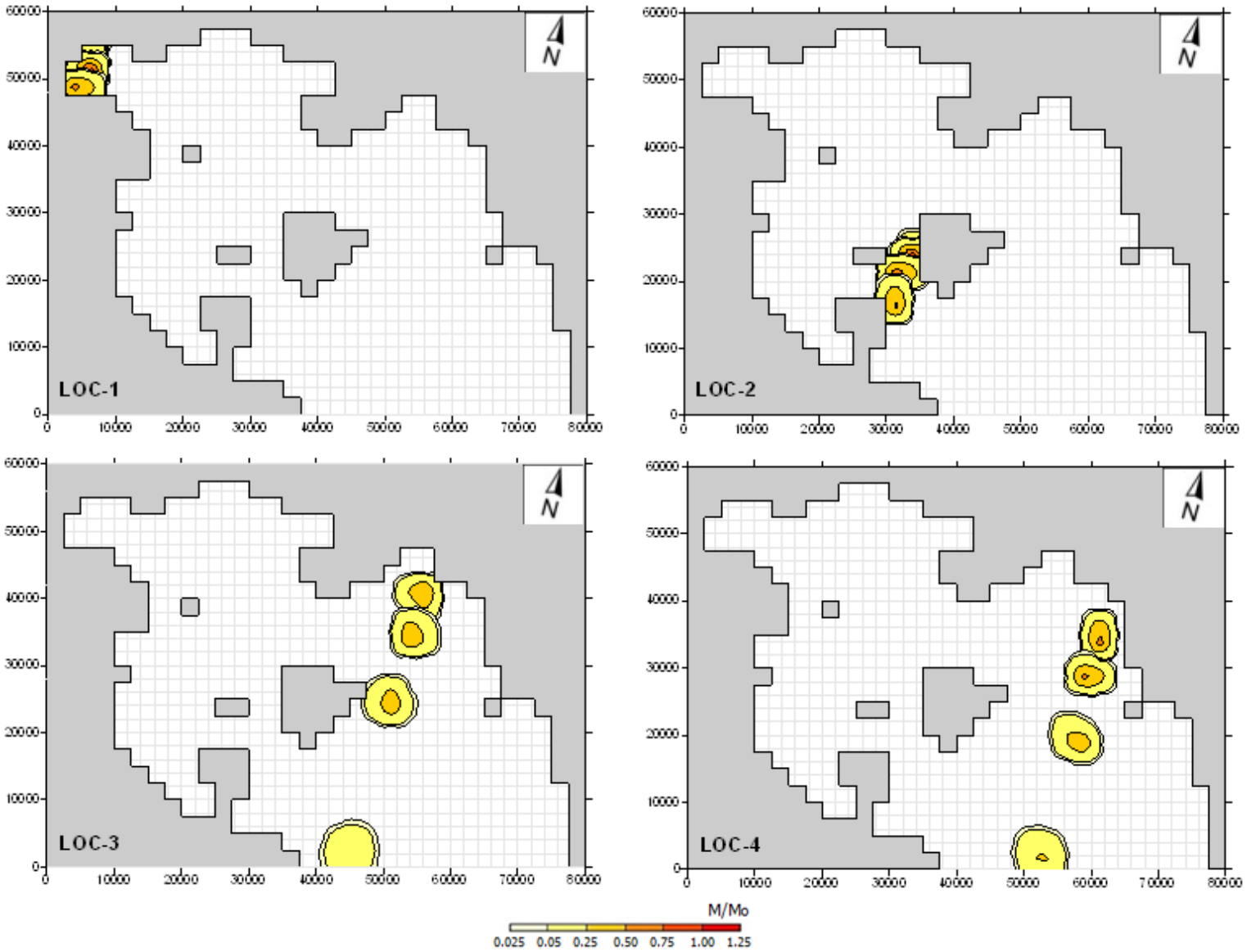

Figure AB4. Trajectory of the oil spill at the 4 locations examined for North wind - 4 bf

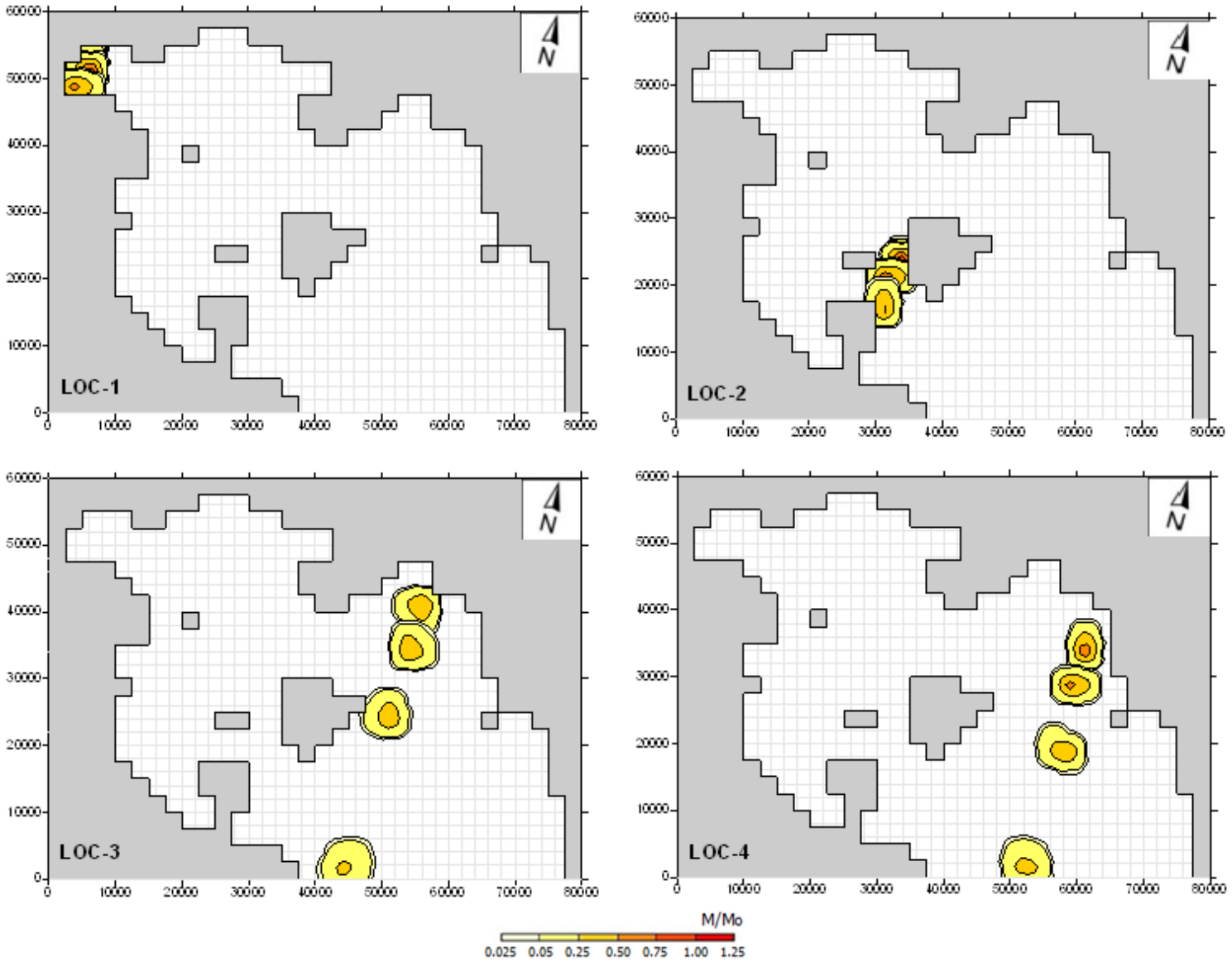

Figure AB5. Trajectory of the oil spill at the 4 locations examined for North wind - 5 bf

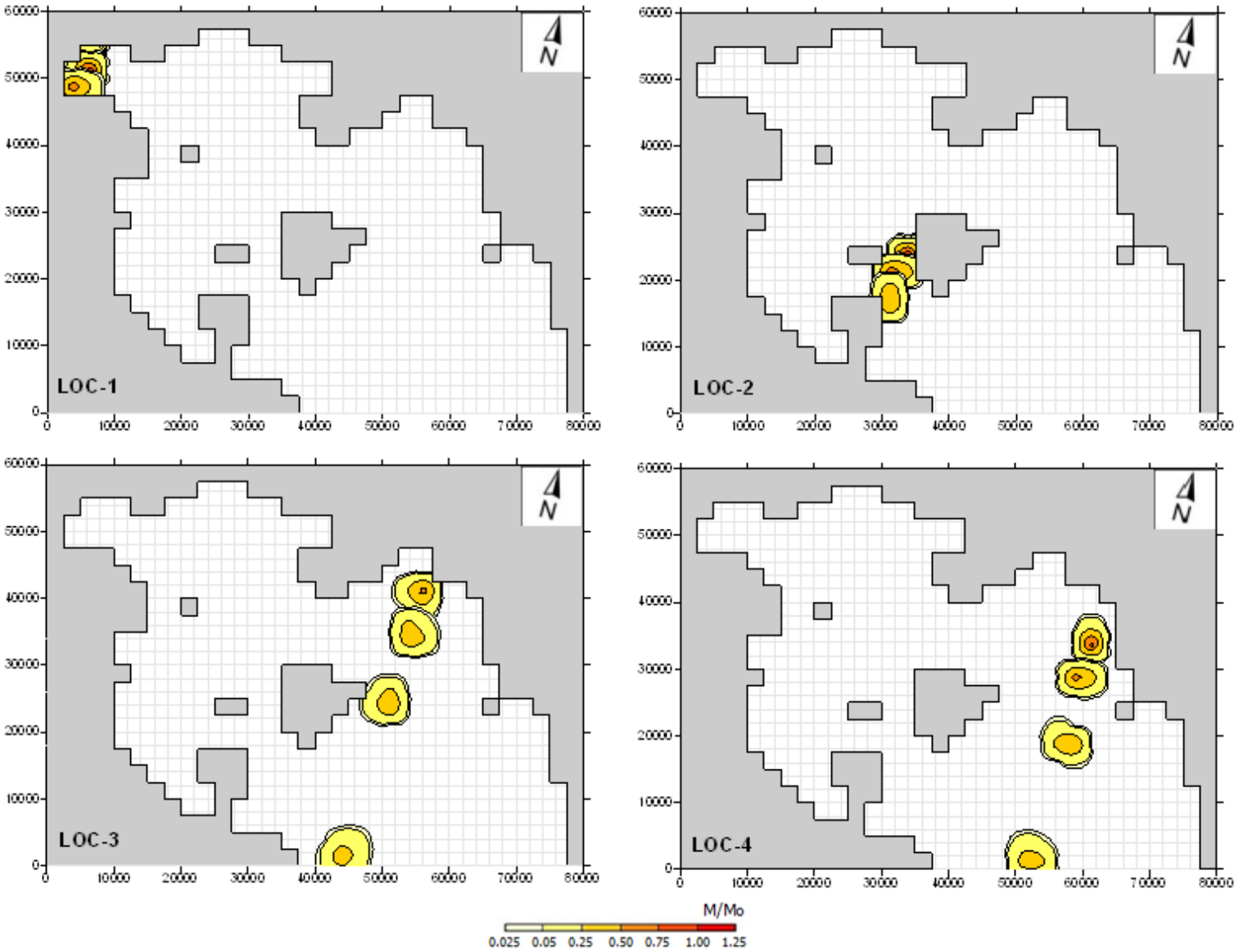

Figure AB6. Trajectory of the oil spill at the 4 locations examined for North wind - 6 bf

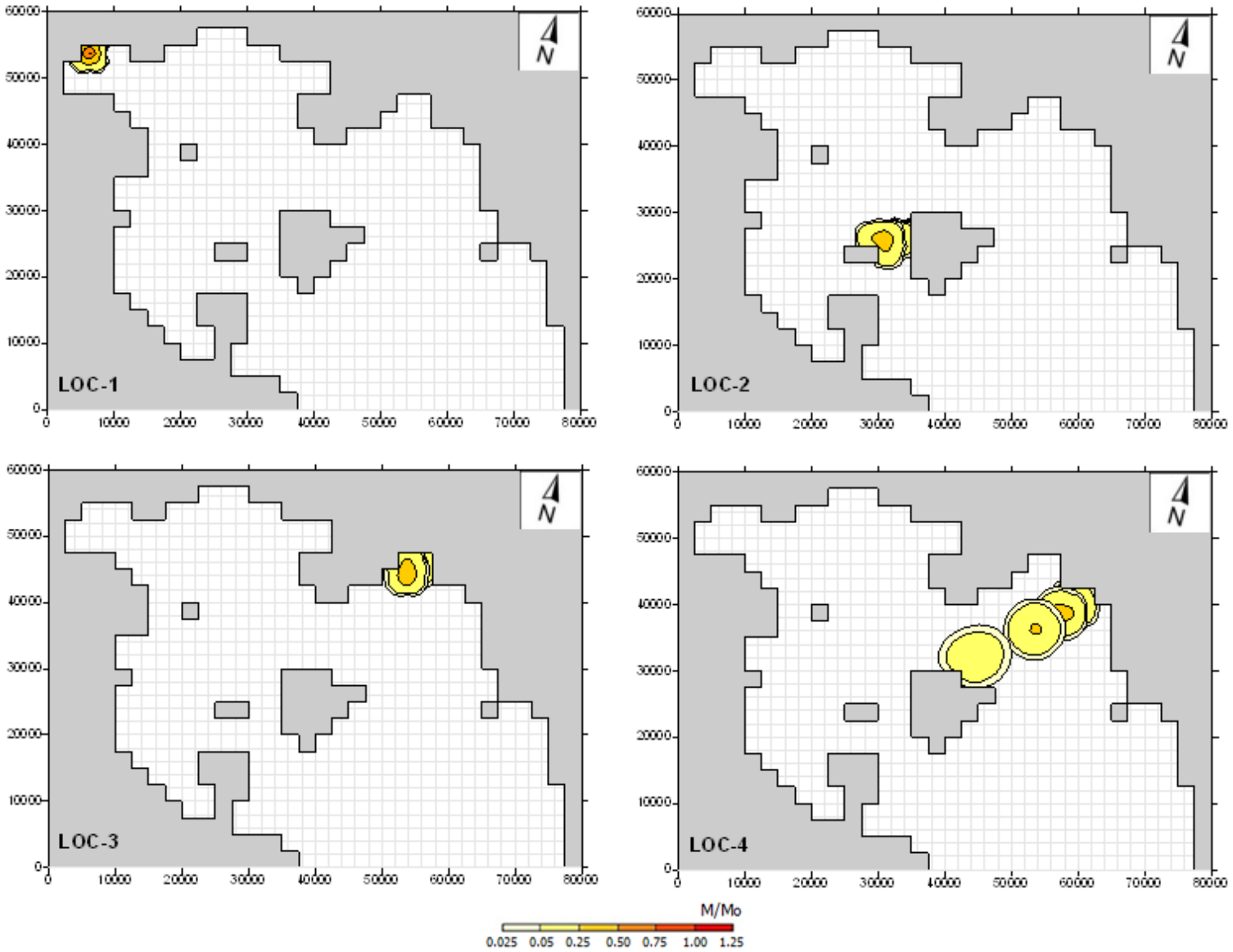

Figure AB7. Trajectory of the oil spill at the 4 locations examined for North-East wind - 1 bf

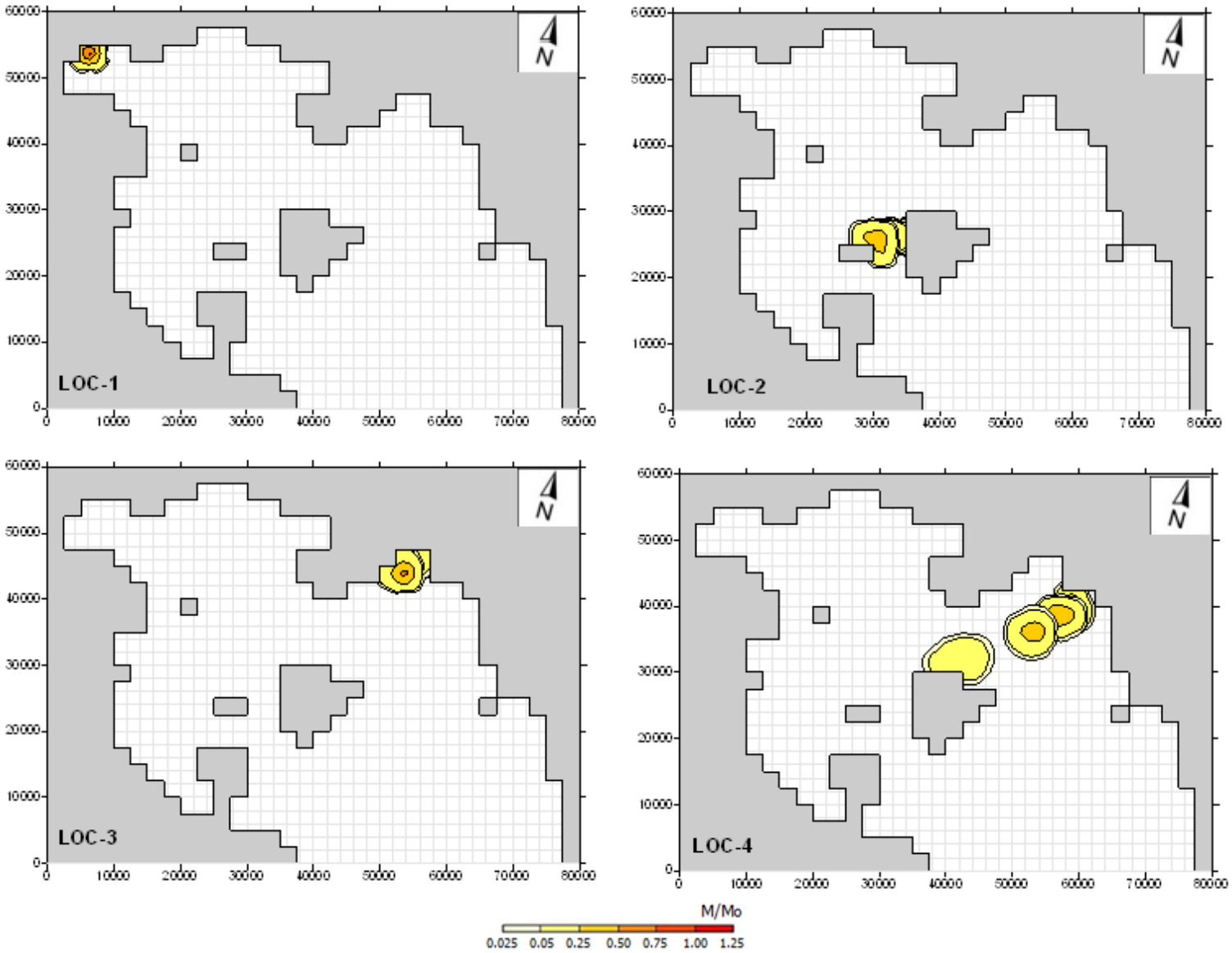

Figure AB8. Trajectory of the oil spill at the 4 locations examined for North-East wind - 2 bf

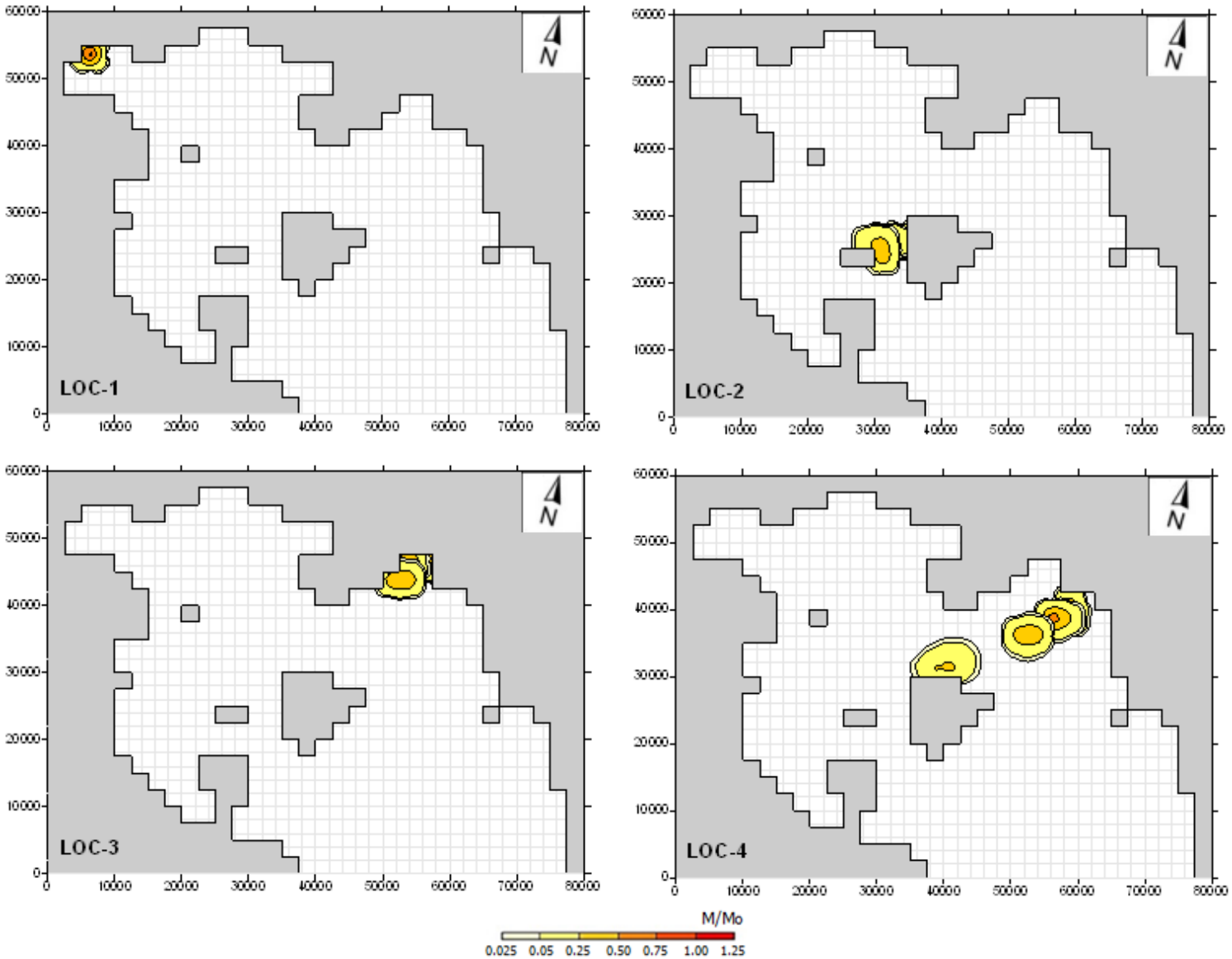

Figure AB9. Trajectory of the oil spill at the 4 locations examined for North-East wind - 3 bf

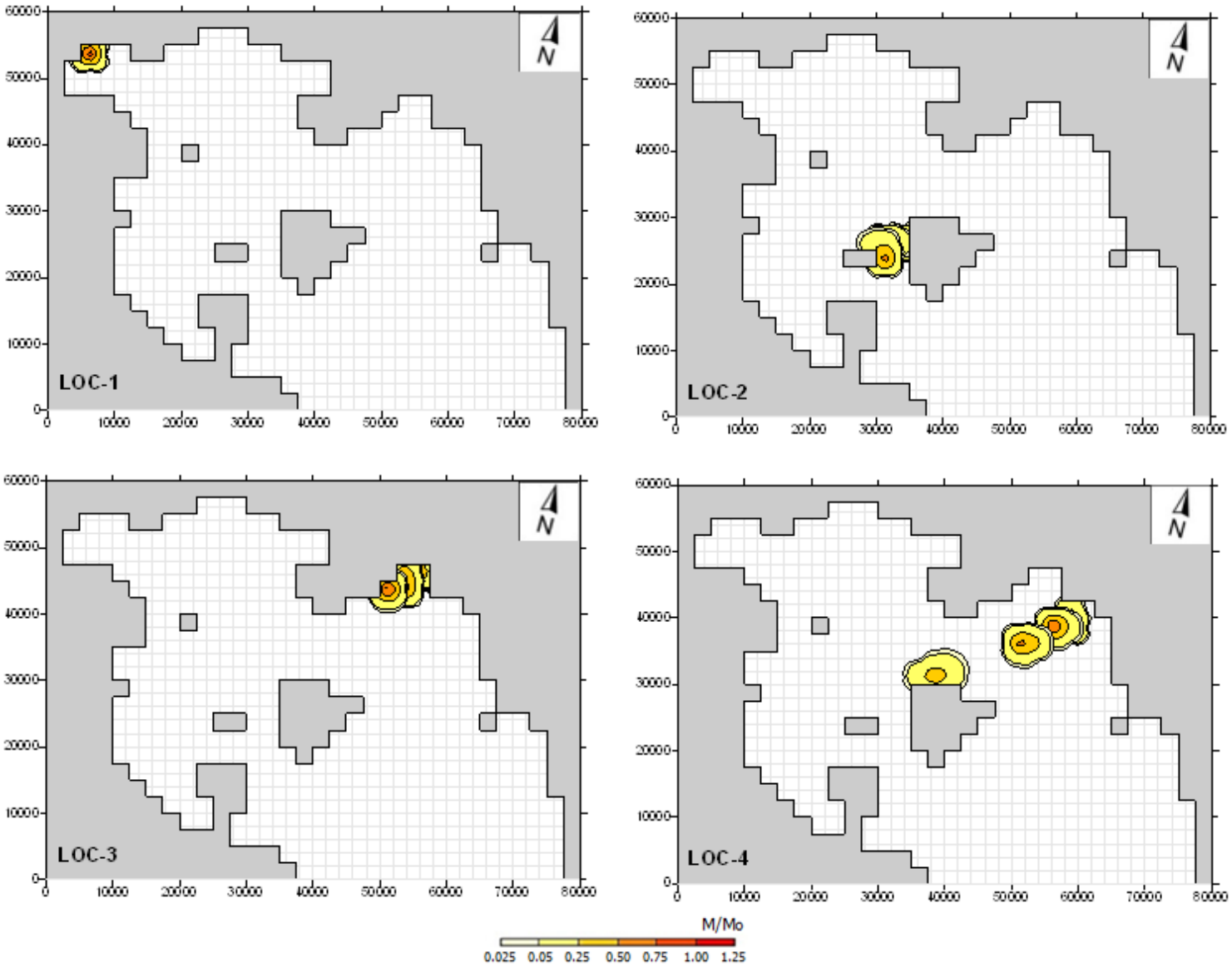

Figure AB10. Trajectory of the oil spill at the 4 locations examined for North-East wind - 4 bf

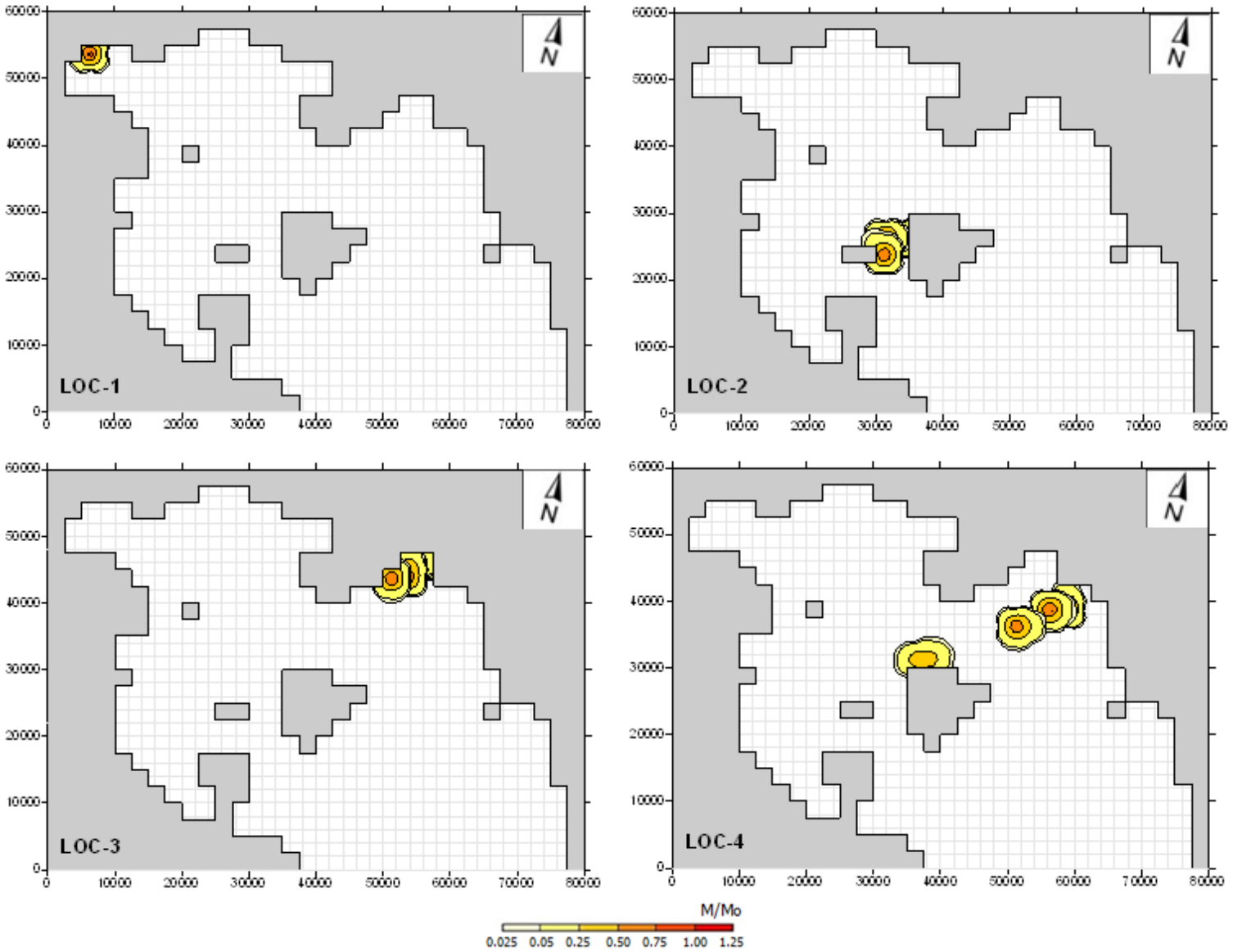

Figure AB11. Trajectory of the oil spill at the 4 locations examined for North-East wind - 5 bf

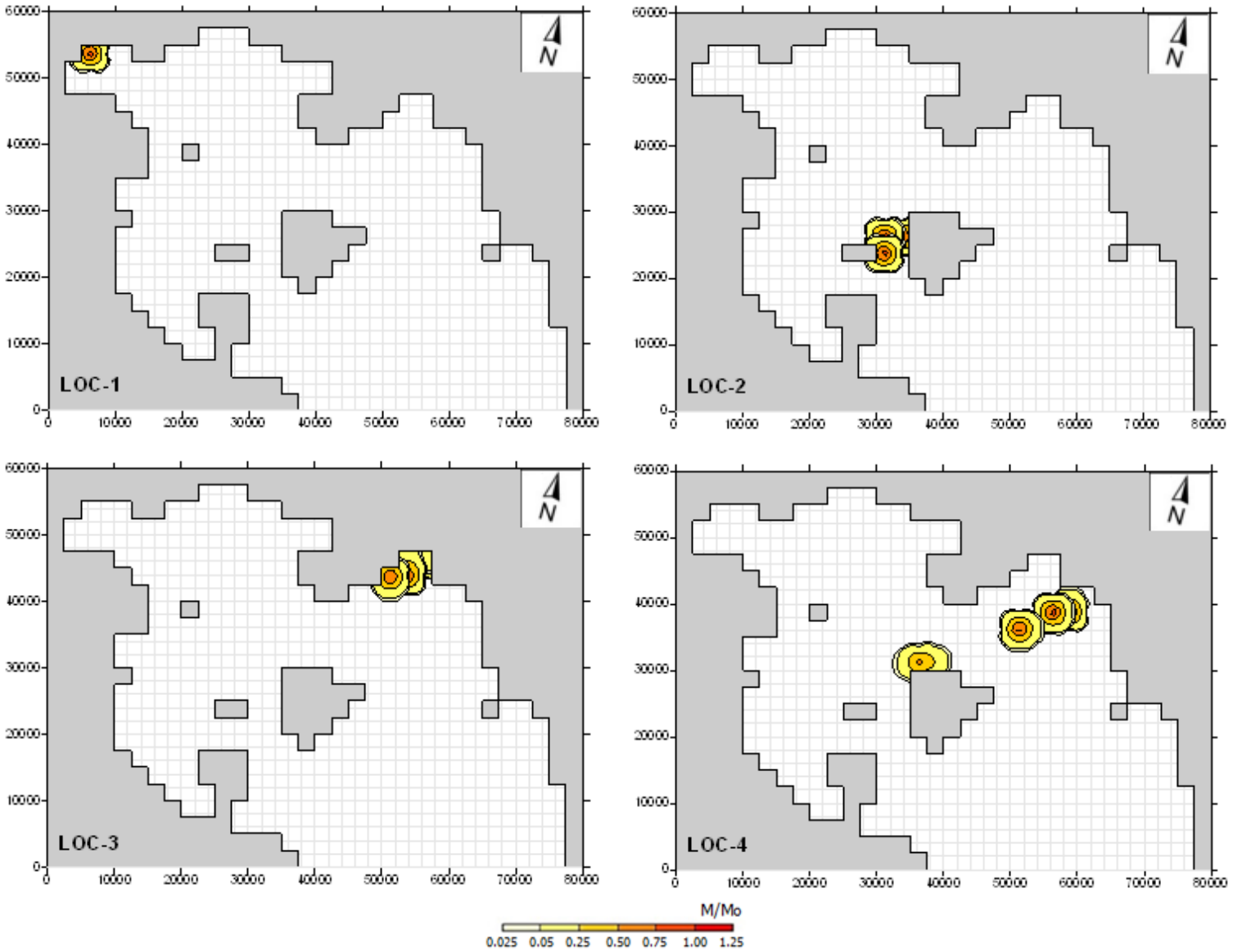

Figure AB12. Trajectory of the oil spill at the 4 locations examined for North-East wind - 6 bf

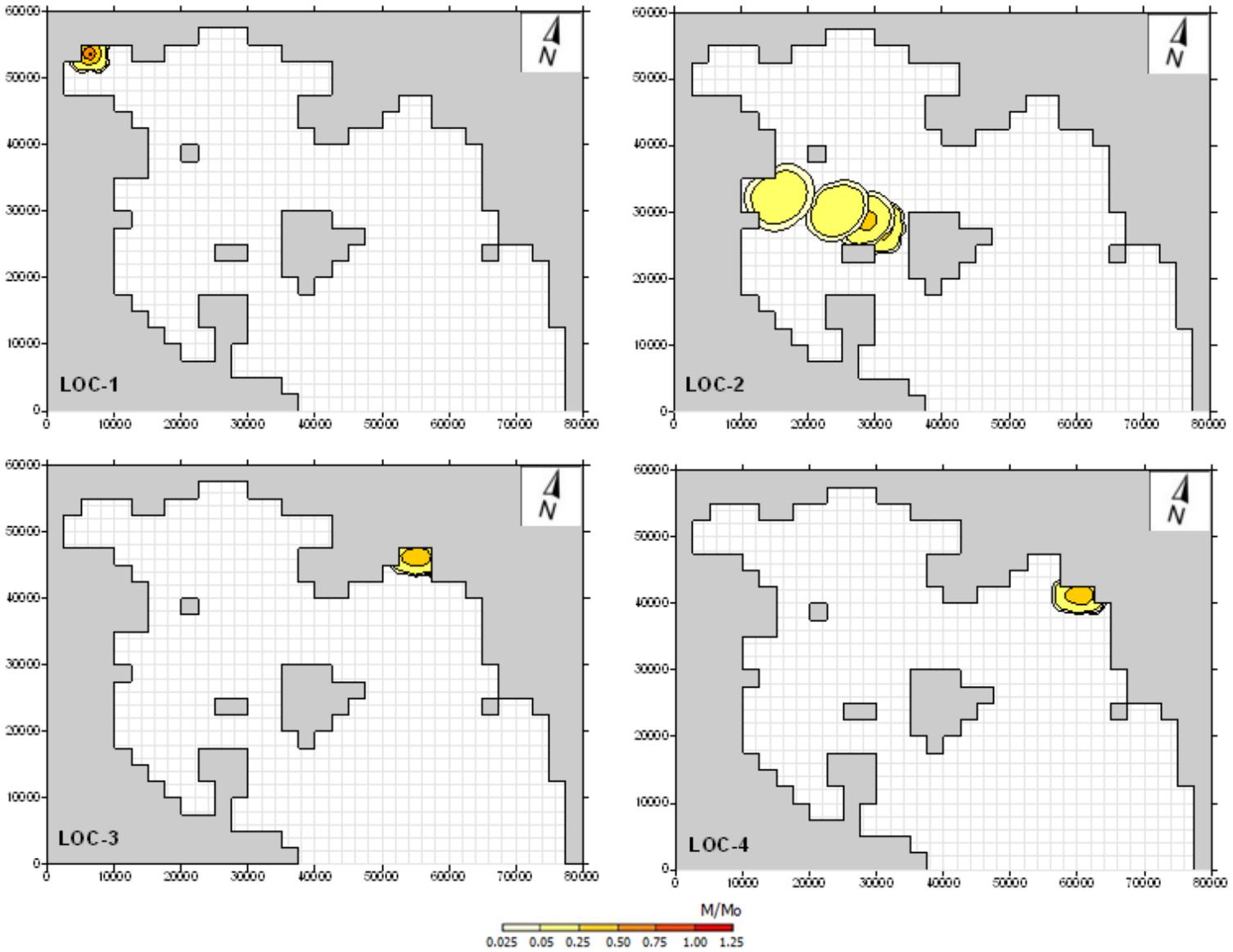

Figure AB13. Trajectory of the oil spill at the 4 locations examined for East wind - 1 bf

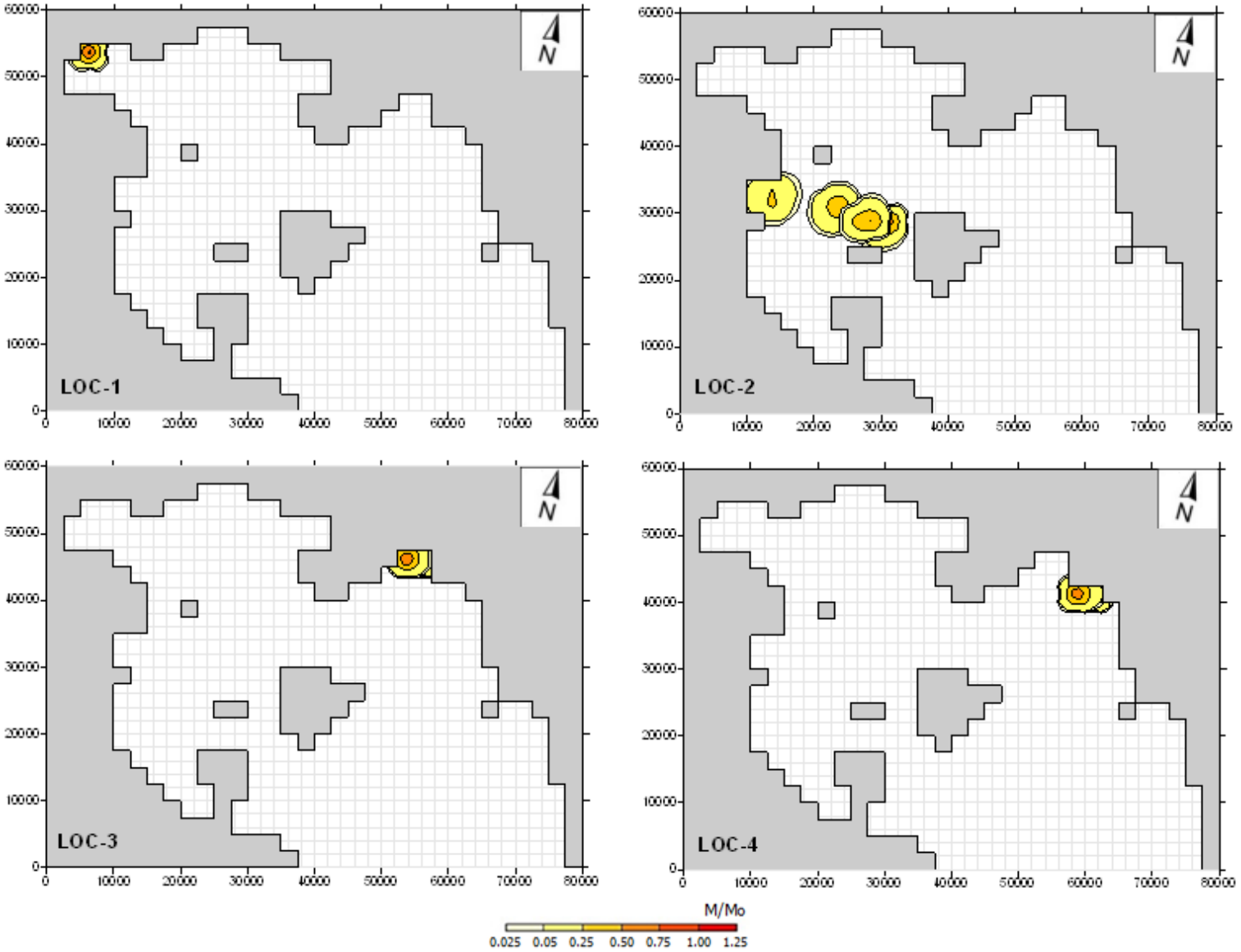

Figure AB14. Trajectory of the oil spill at the 4 locations examined for East wind - 2 bf

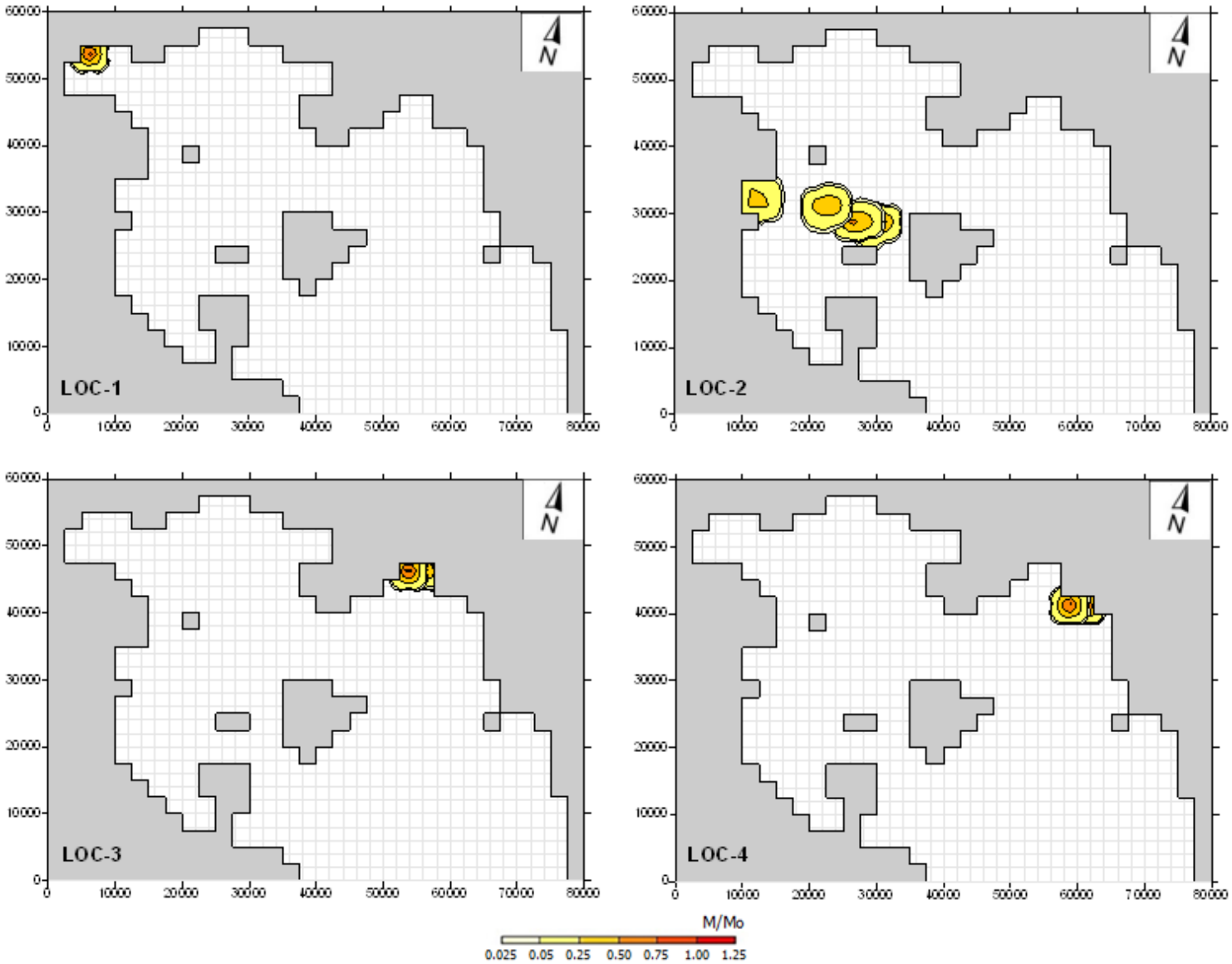

Figure AB15. Trajectory of the oil spill at the 4 locations examined for East wind - 3 bf

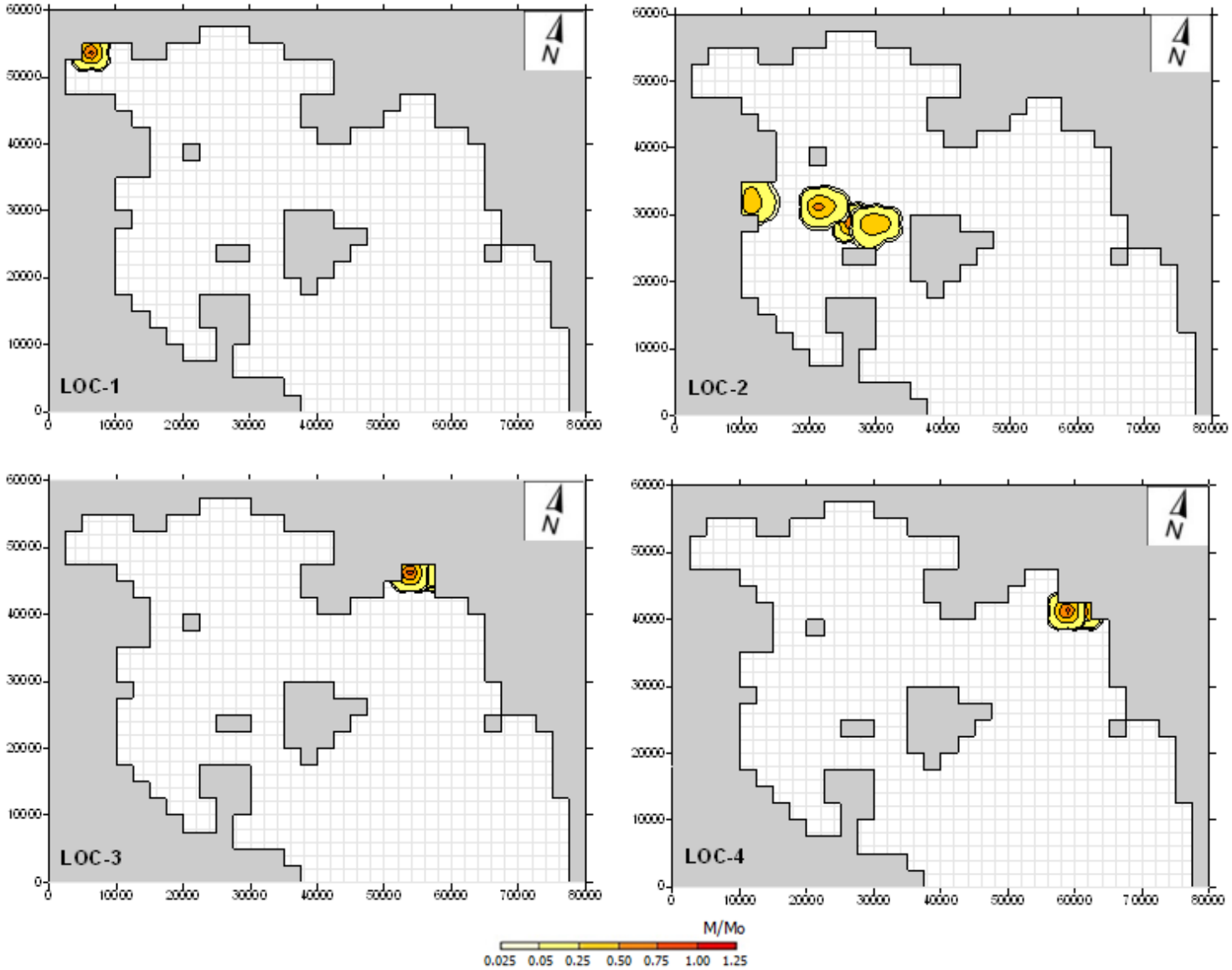

Figure AB16. Trajectory of the oil spill at the 4 locations examined for East wind - 4 bf

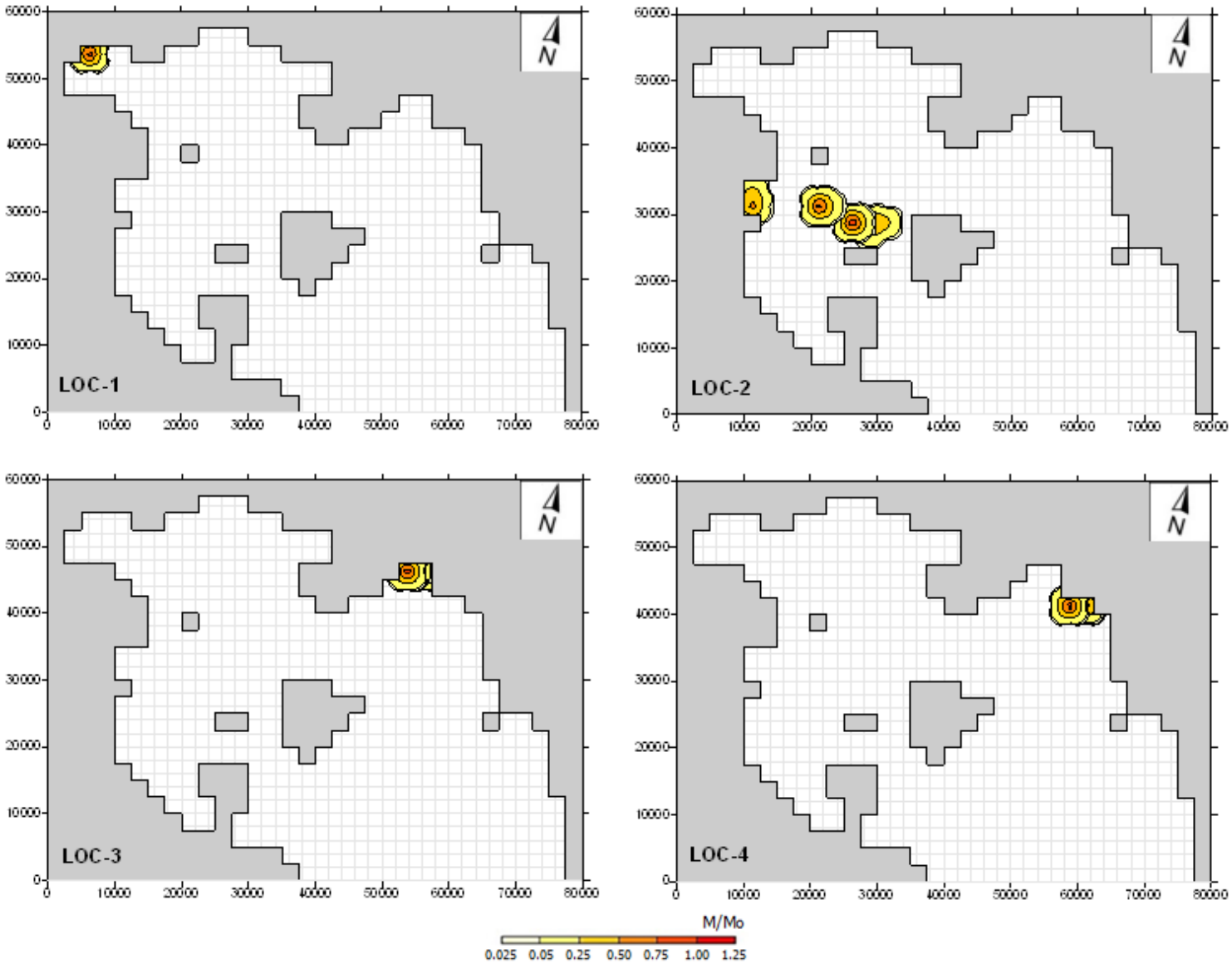

Figure AB17. Trajectory of the oil spill at the 4 locations examined for East wind - 5 bf

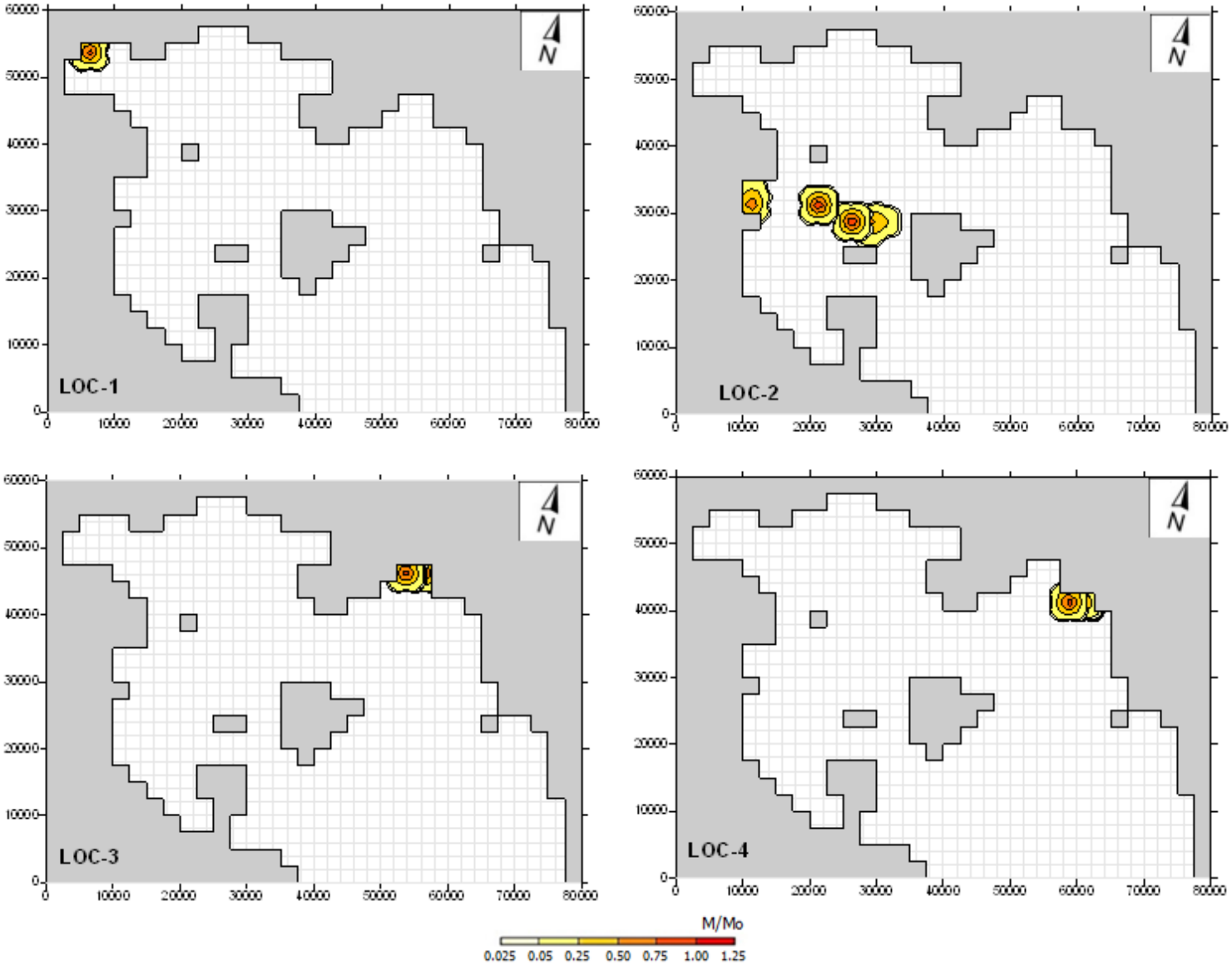

Figure AB18. Trajectory of the oil spill at the 4 locations examined for East wind - 6 bf

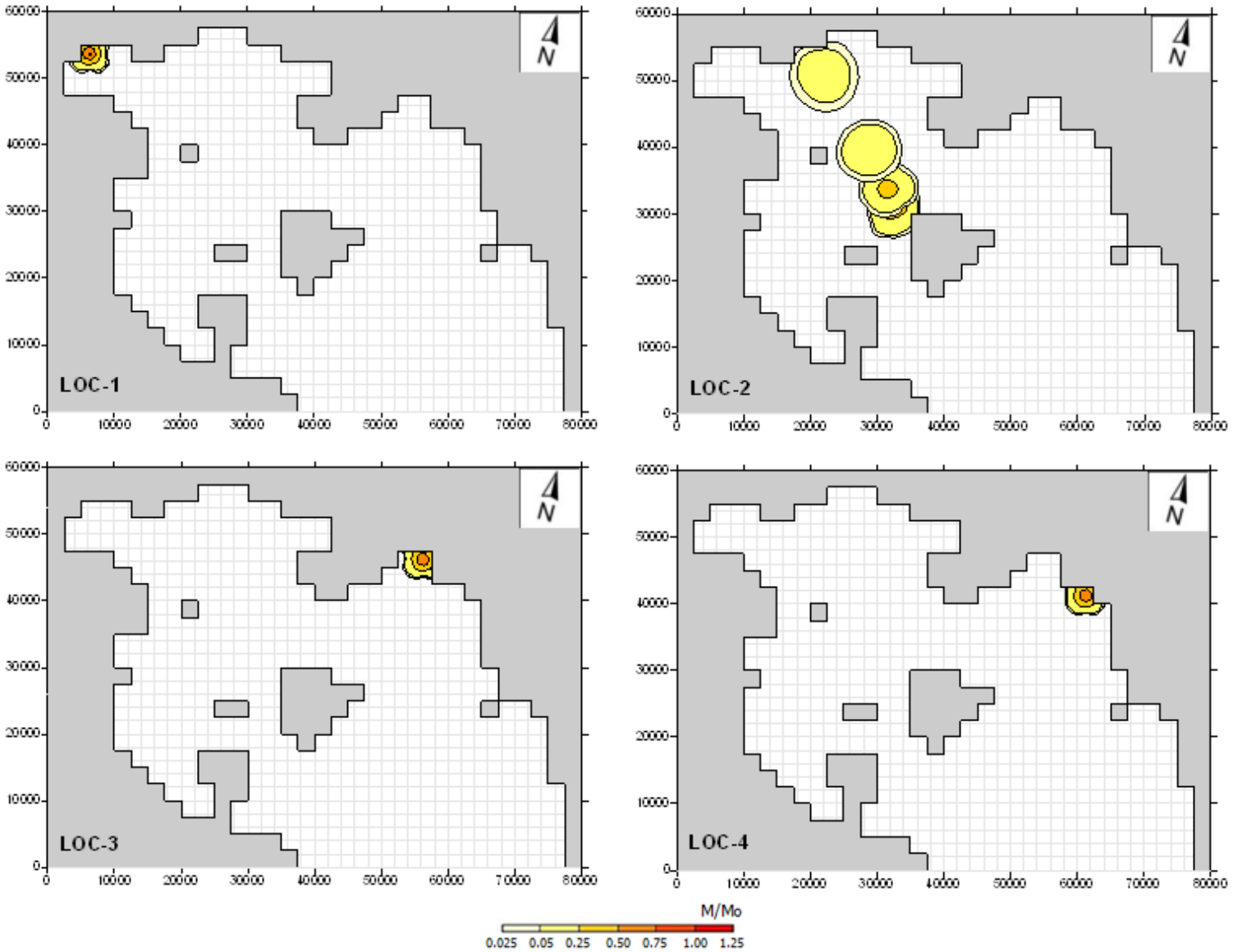

Figure AB19. Trajectory of the oil spill at the 4 locations examined for South-East wind - 1 bf

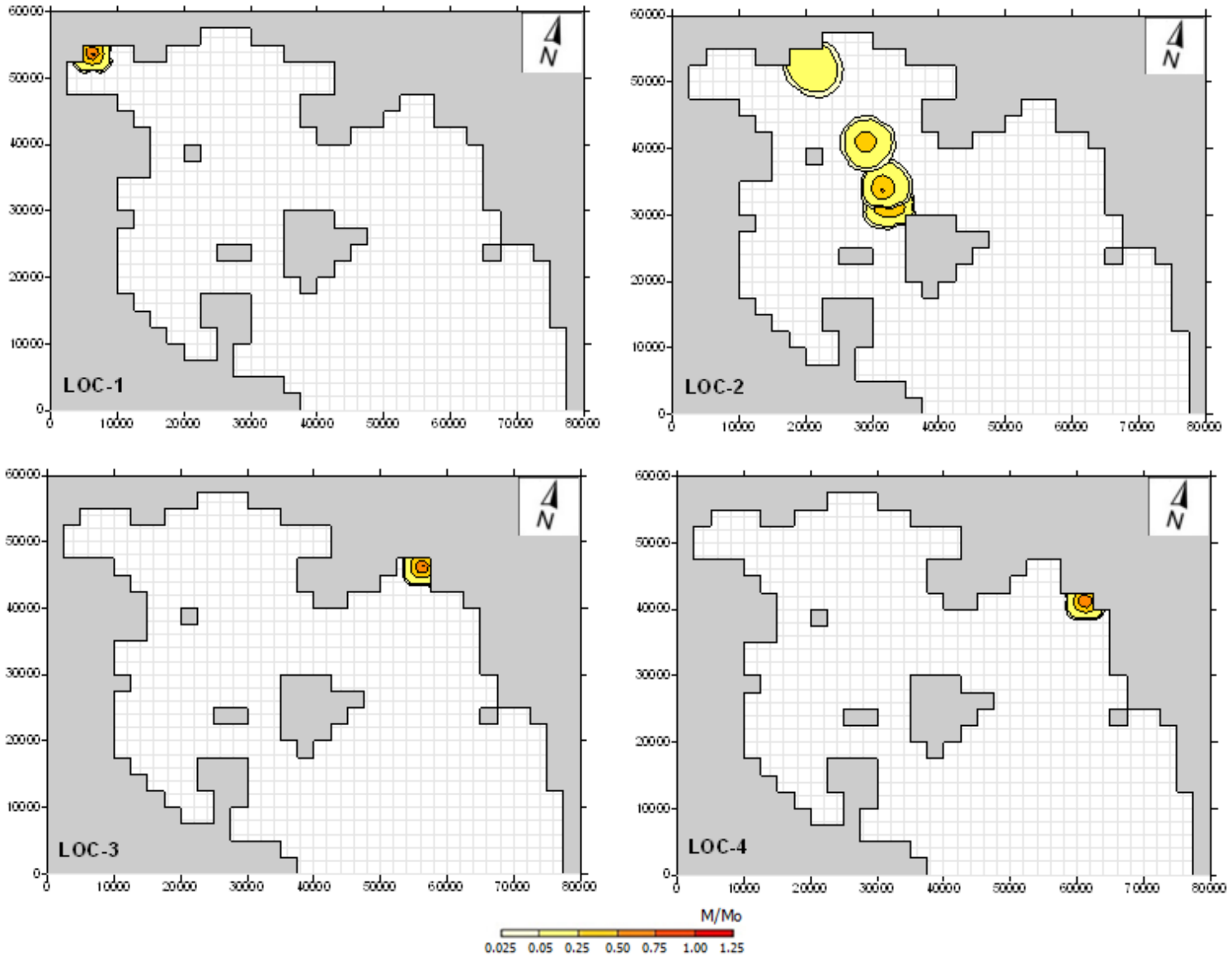

Figure AB20. Trajectory of the oil spill at the 4 locations examined for South-East wind - 2 bf

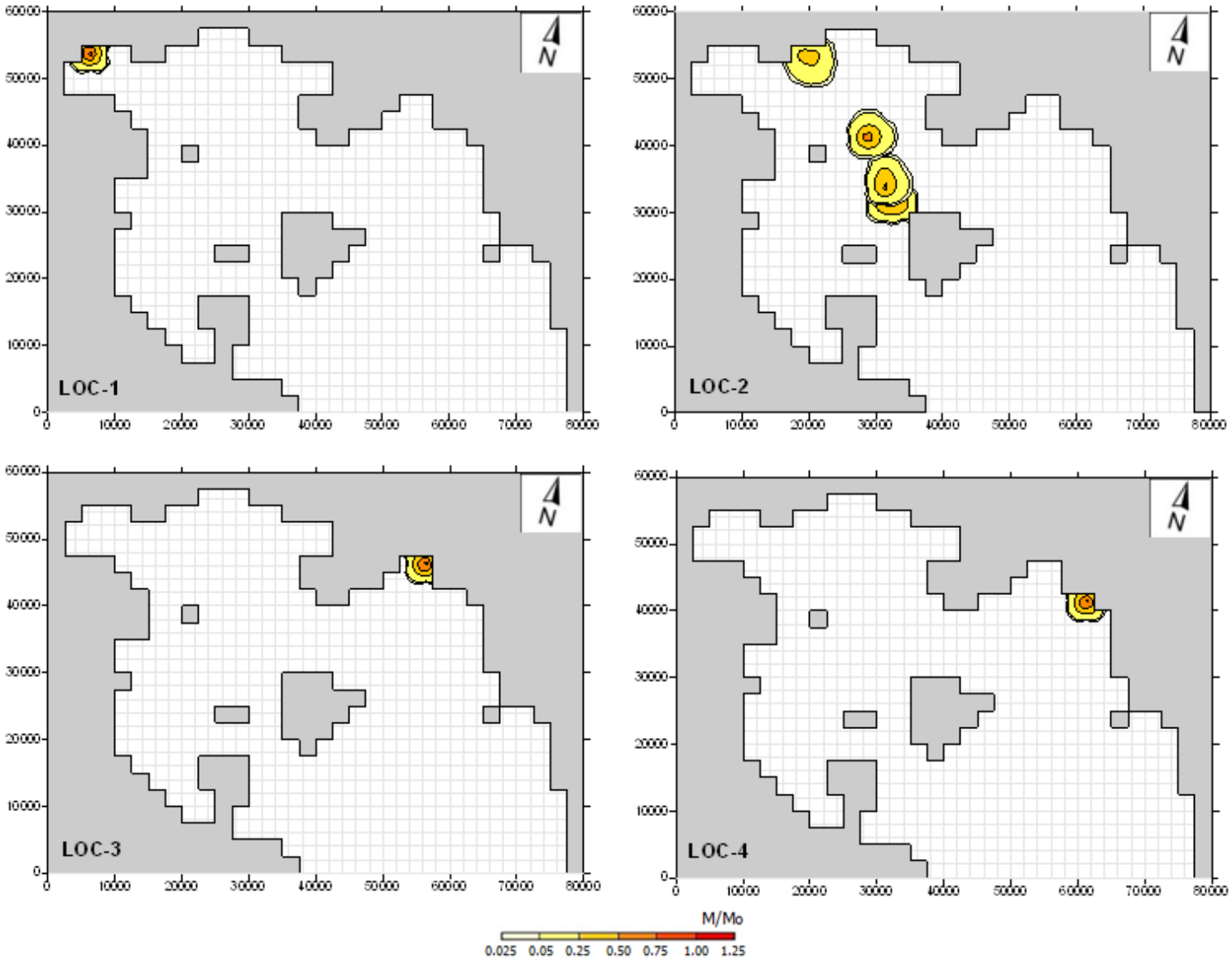

Figure AB21. Trajectory of the oil spill at the 4 locations examined for South-East wind - 3 bf

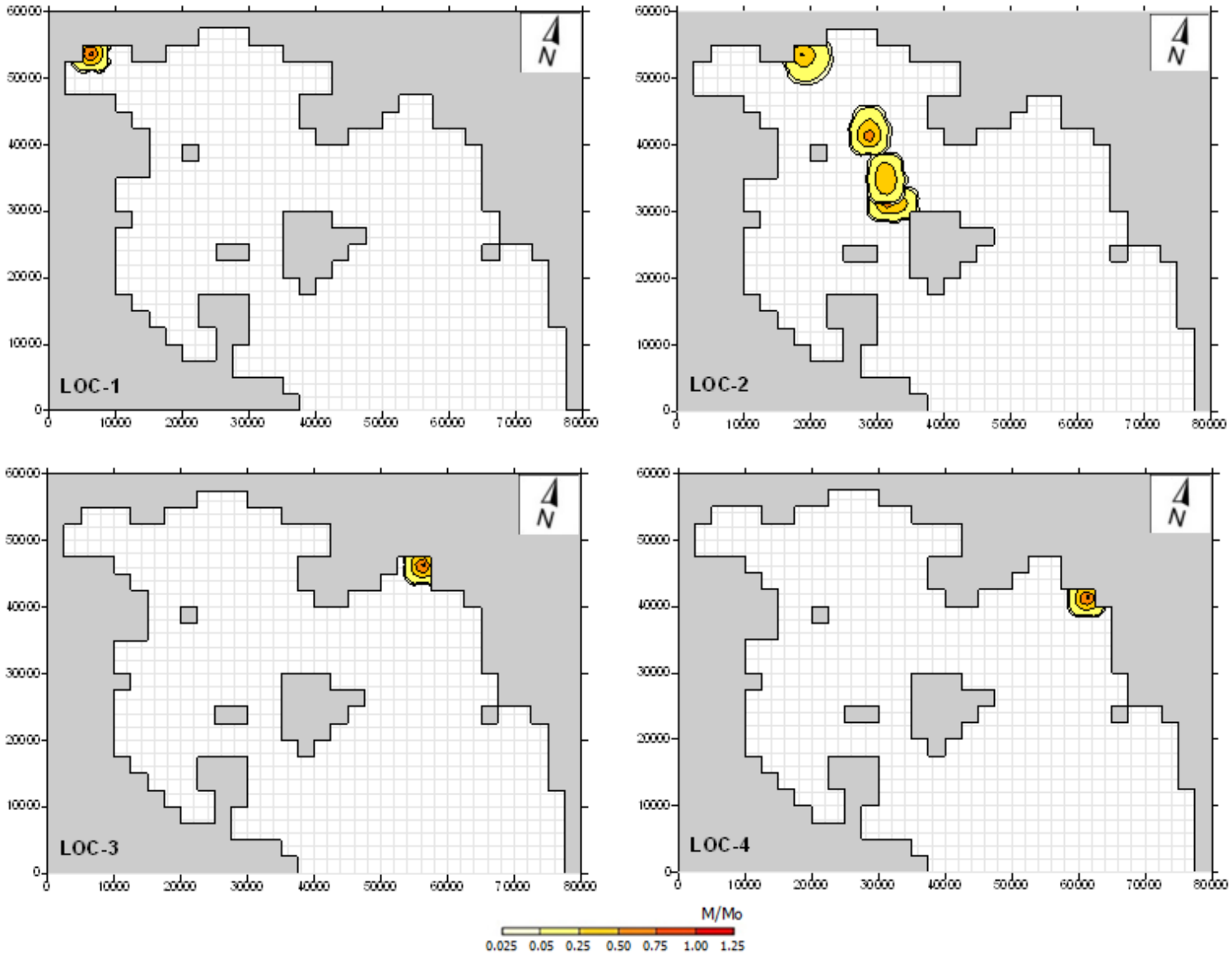

Figure AB22. Trajectory of the oil spill at the 4 locations examined for South-East wind - 4 bf

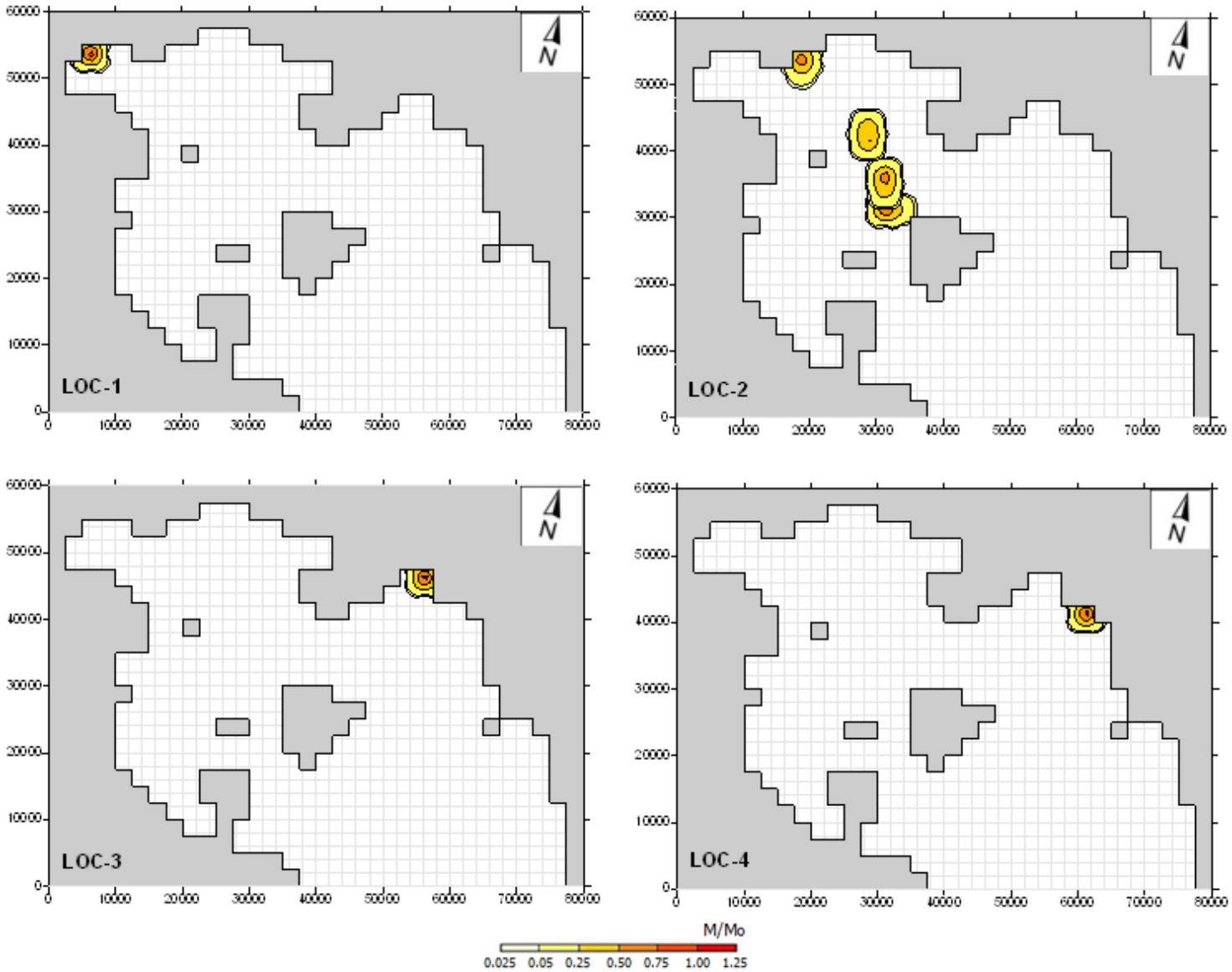

Figure AB23. Trajectory of the oil spill at the 4 locations examined for South-East wind - 5 bf

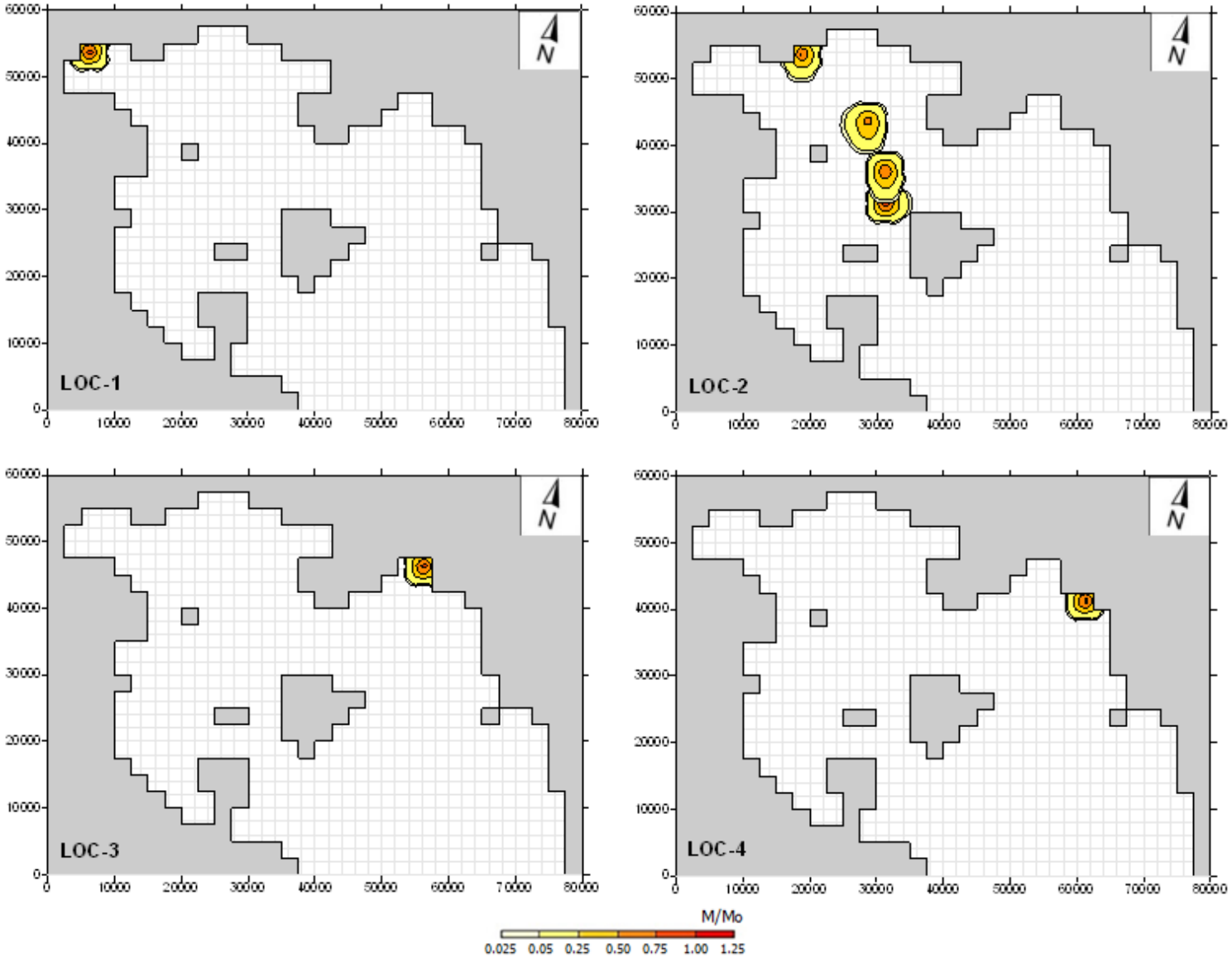

Figure AB24. Trajectory of the oil spill at the 4 locations examined for South-East wind - 6 bf

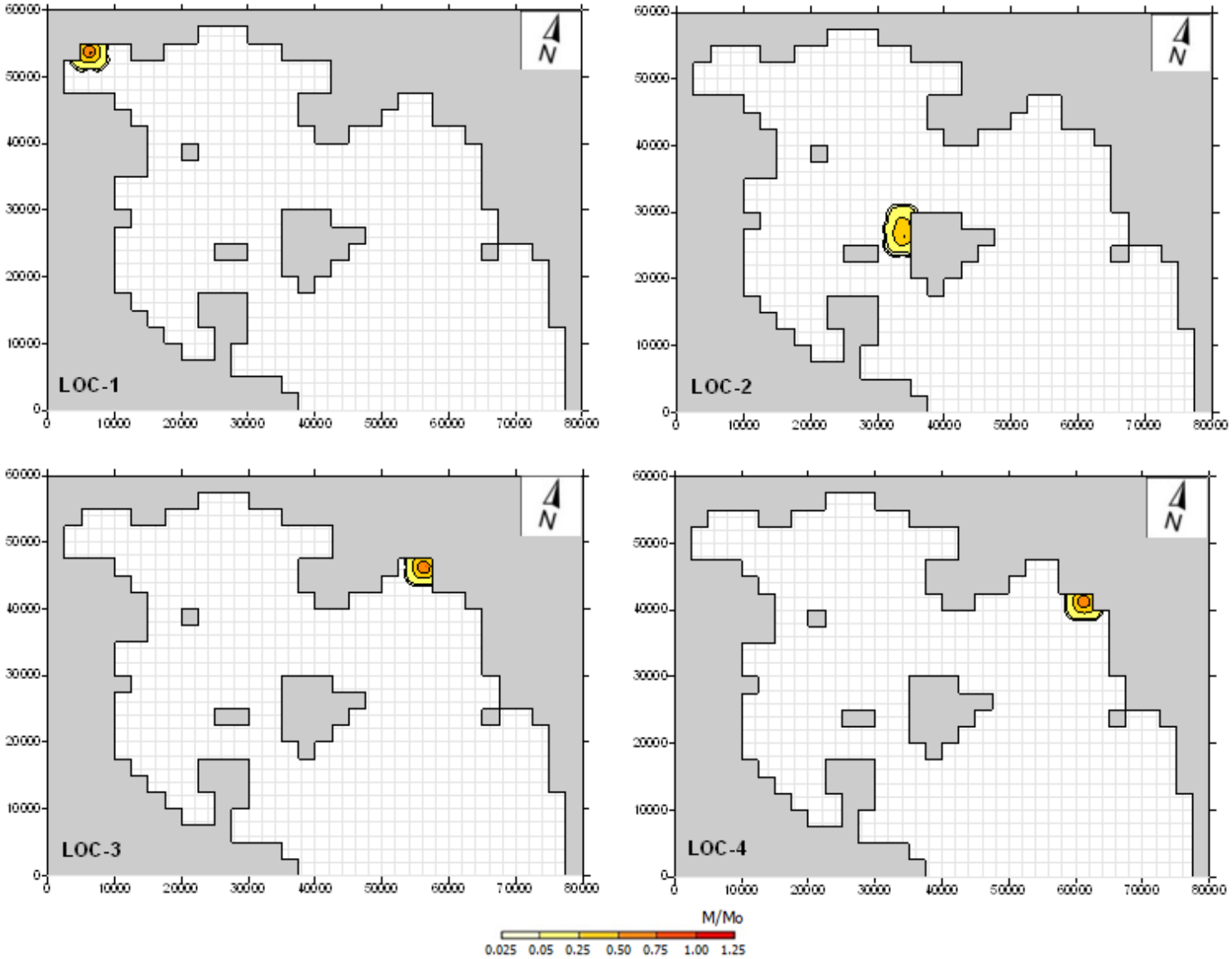

Figure AB25. Trajectory of the oil spill at the 4 locations examined for South wind - 1 bf

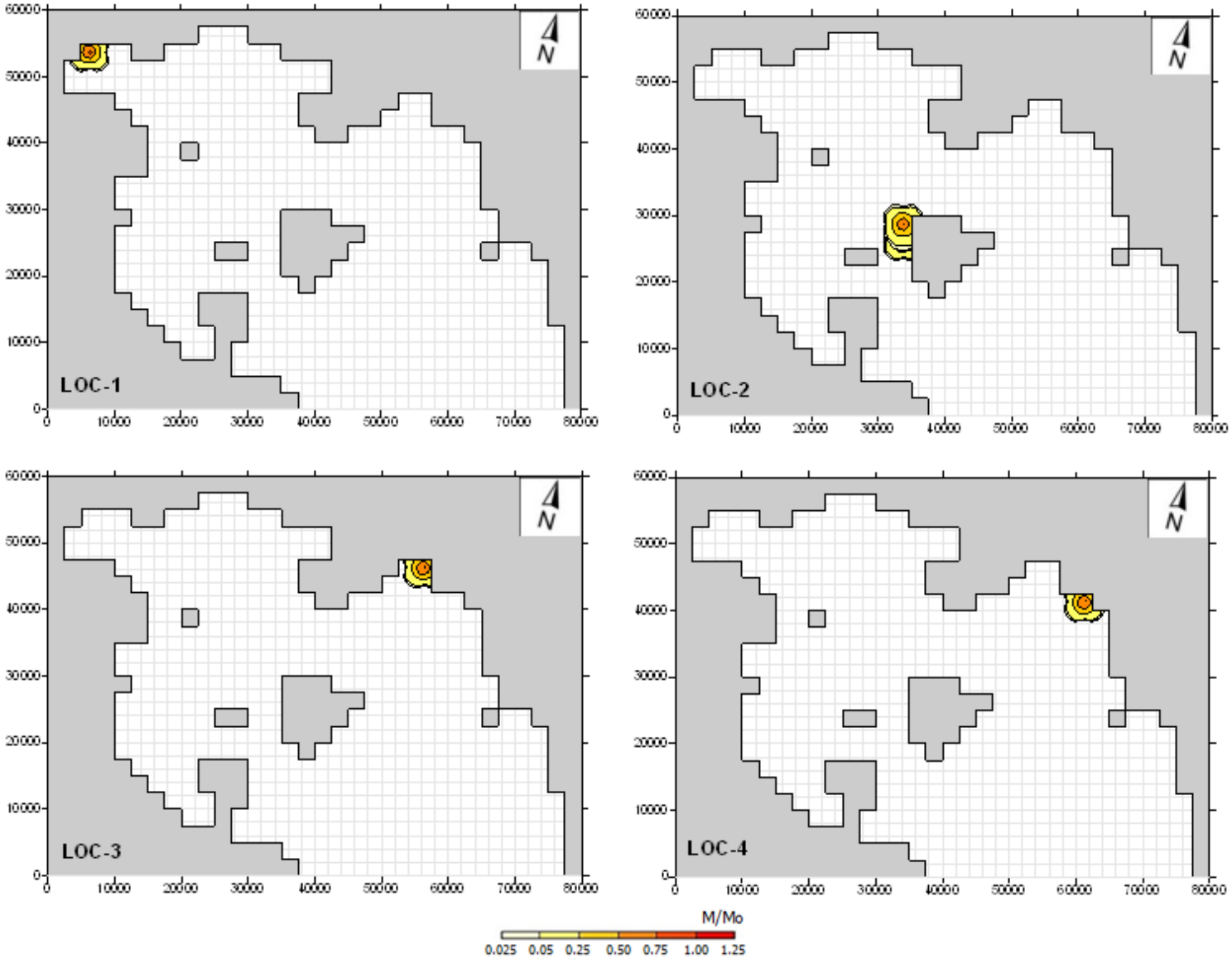

Figure AB26. Trajectory of the oil spill at the 4 locations examined for South wind - 2 bf

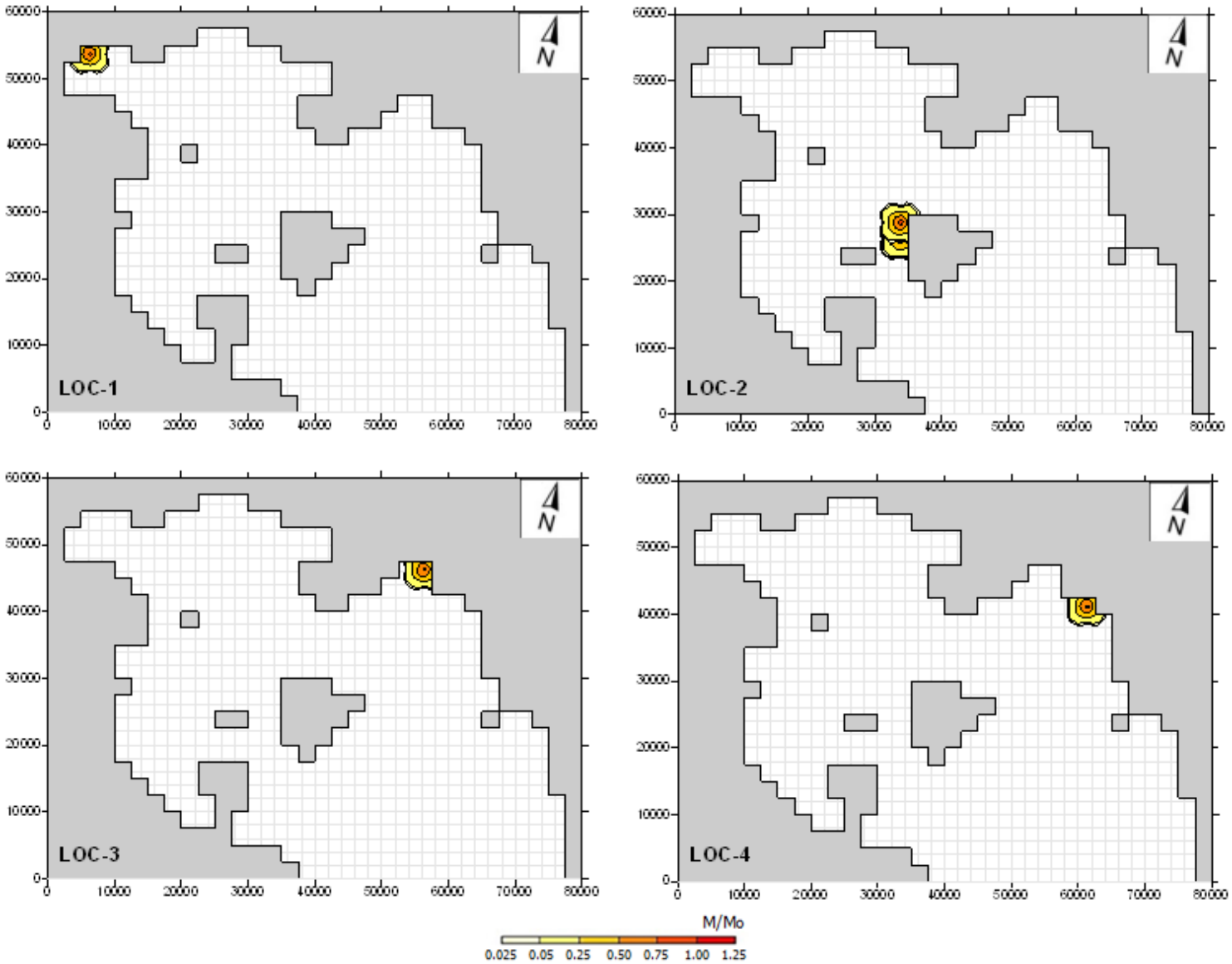

Figure AB27. Trajectory of the oil spill at the 4 locations examined for South wind - 3 bf

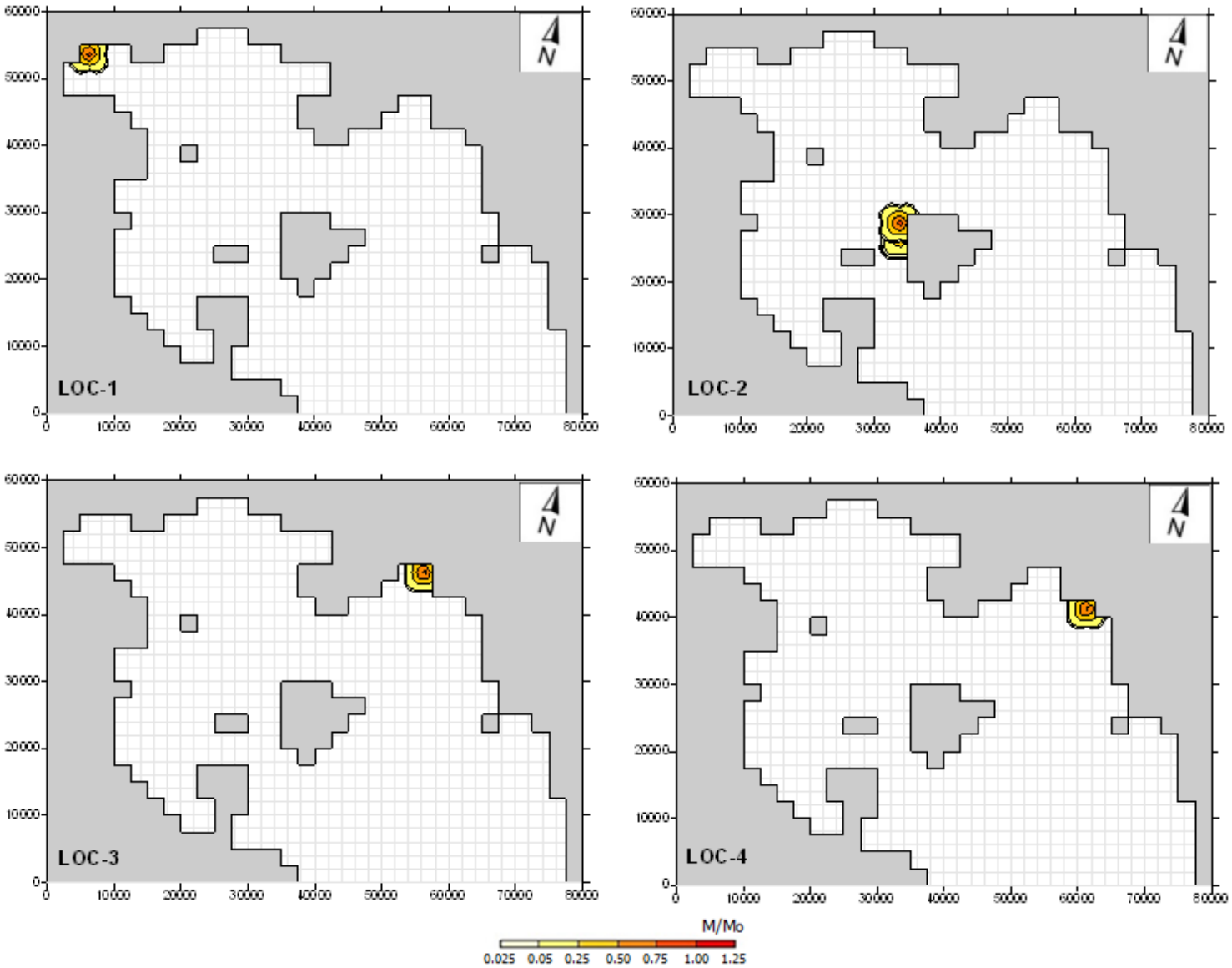

Figure AB28. Trajectory of the oil spill at the 4 locations examined for South wind - 4 bf

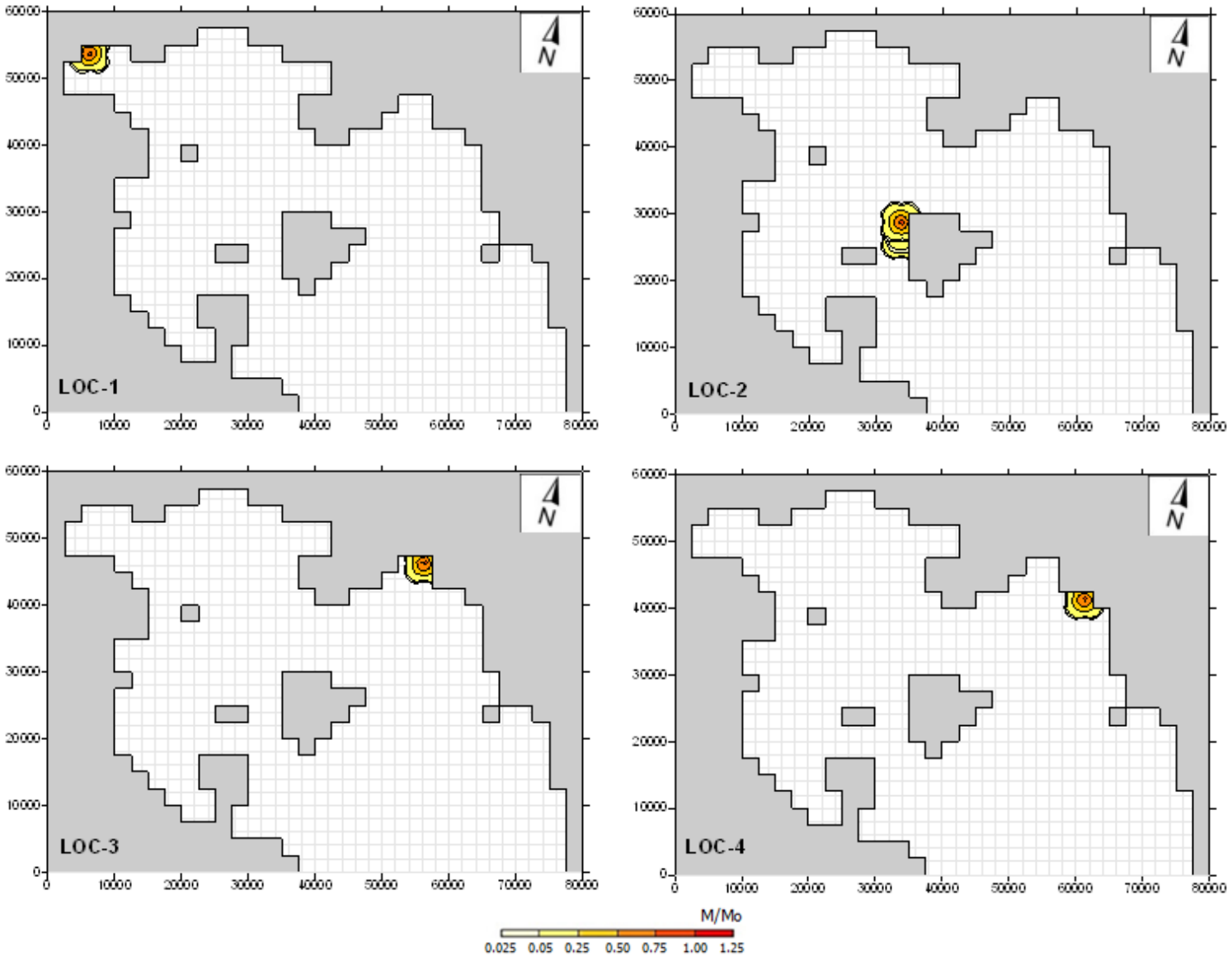

Figure AB29. Trajectory of the oil spill at the 4 locations examined for South wind - 5 bf

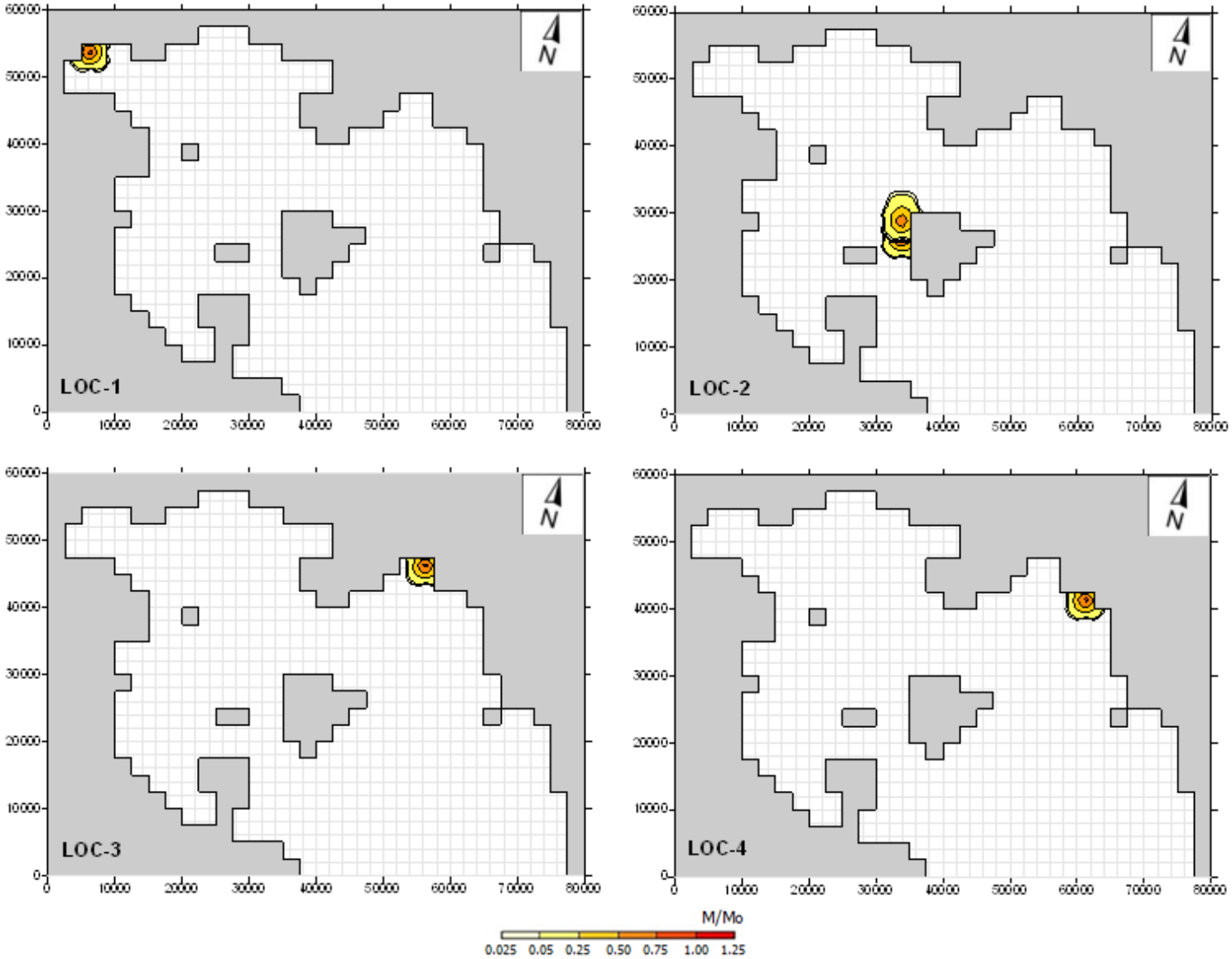

Figure AB30. Trajectory of the oil spill at the 4 locations examined for South wind - 6 bf

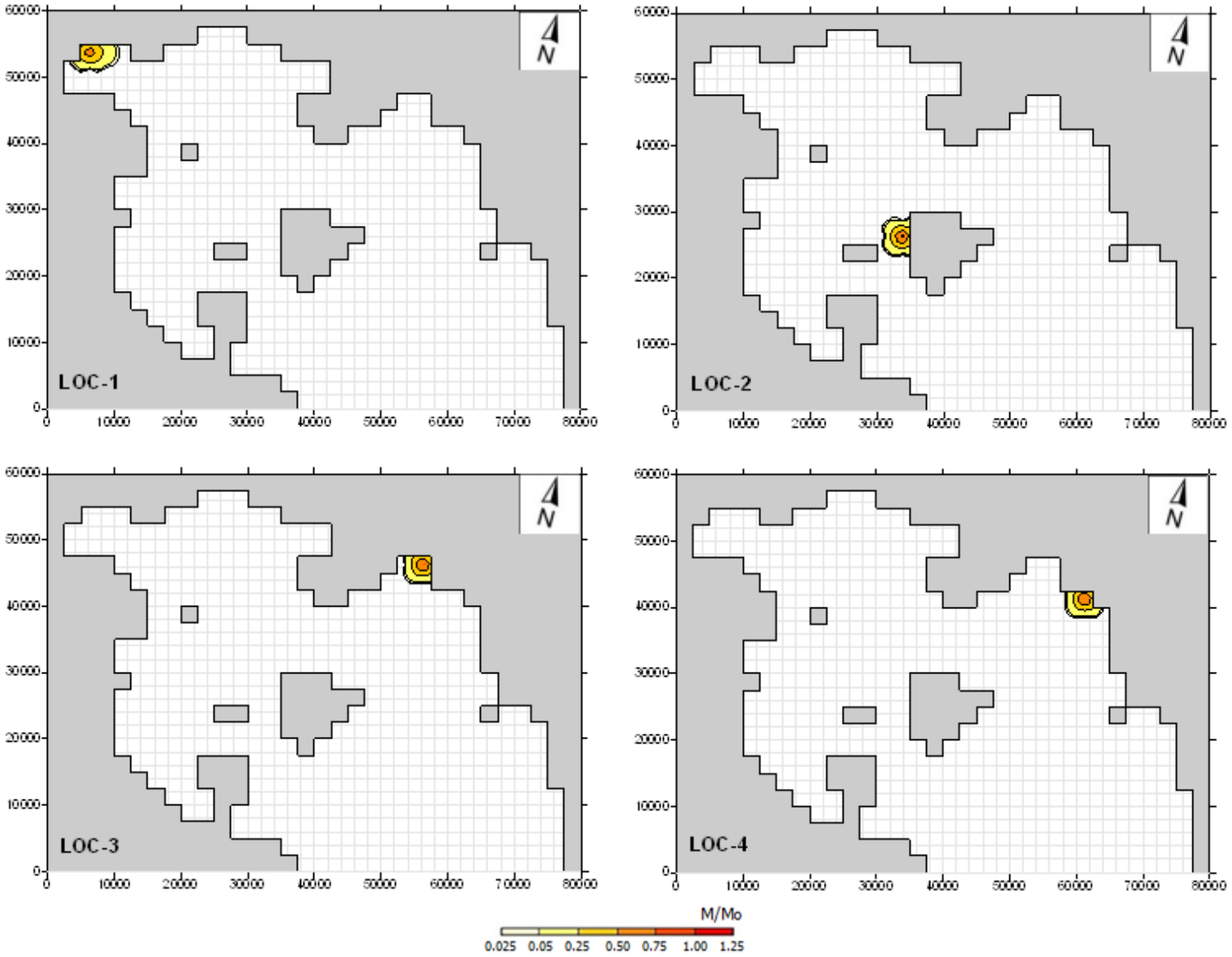

Figure AB31. Trajectory of the oil spill at the 4 locations examined for South-West wind - 1 bf

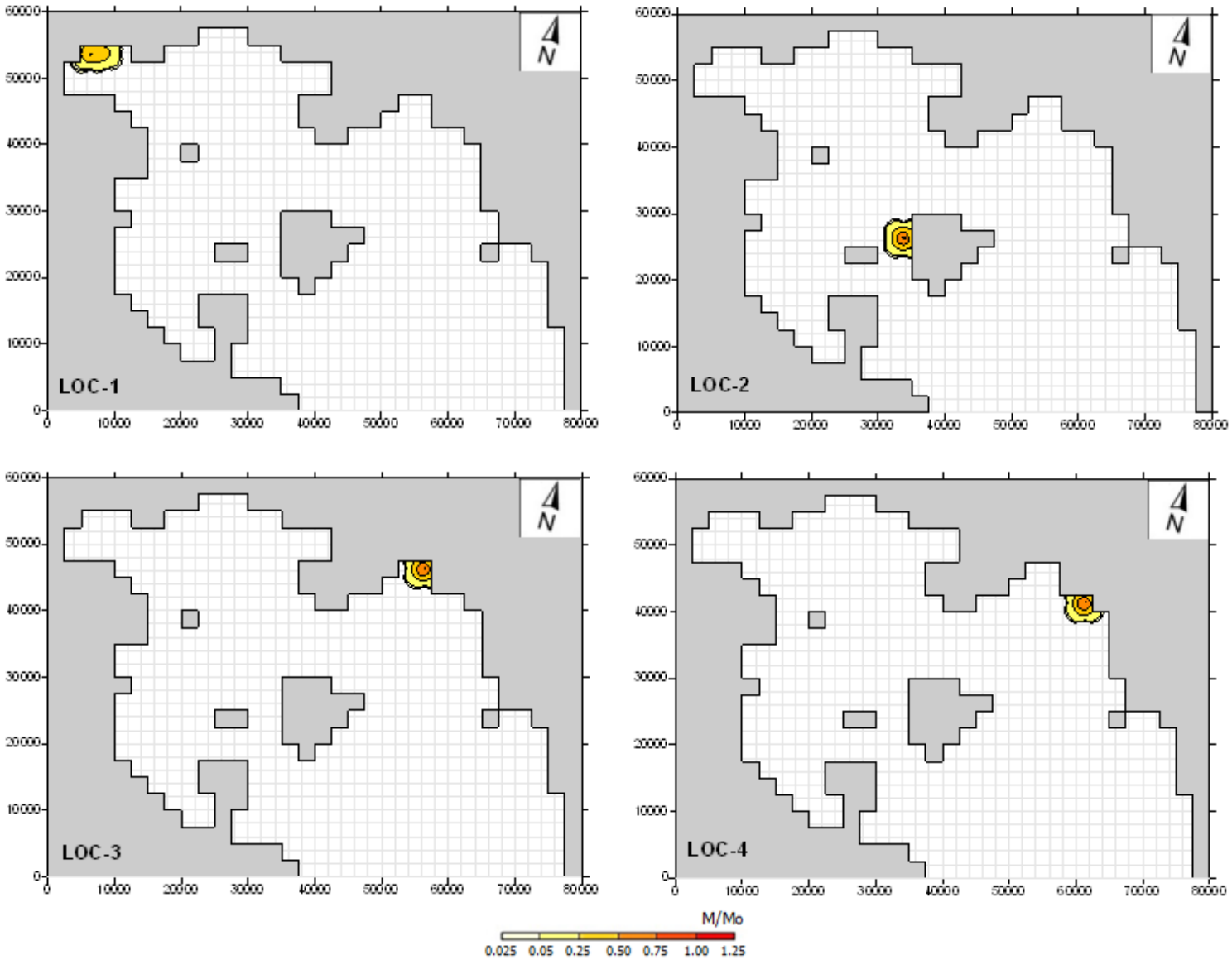

Figure AB32. Trajectory of the oil spill at the 4 locations examined for South-West wind - 2 bf

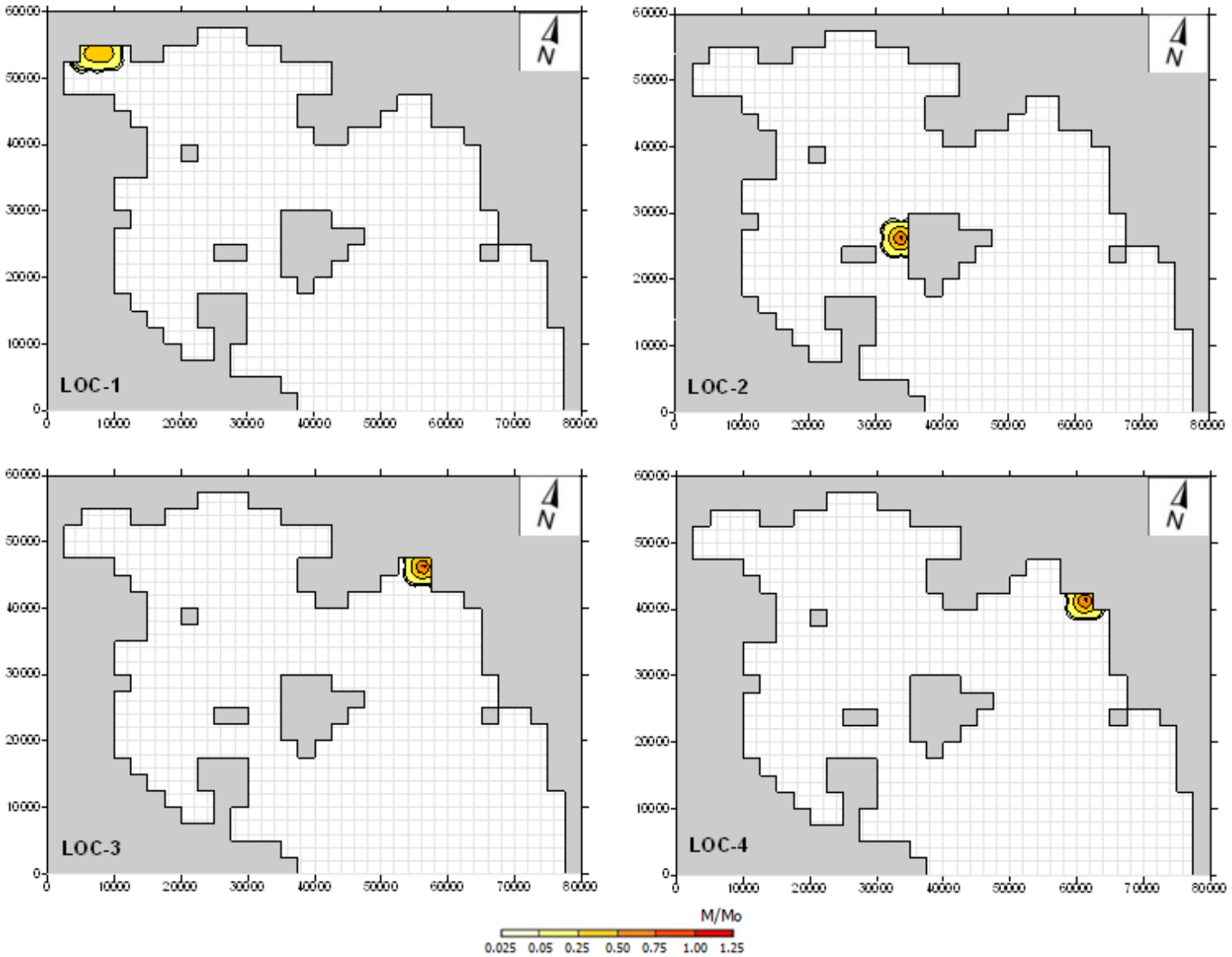

Figure AB33. Trajectory of the oil spill at the 4 locations examined for South-West wind - 3 bf

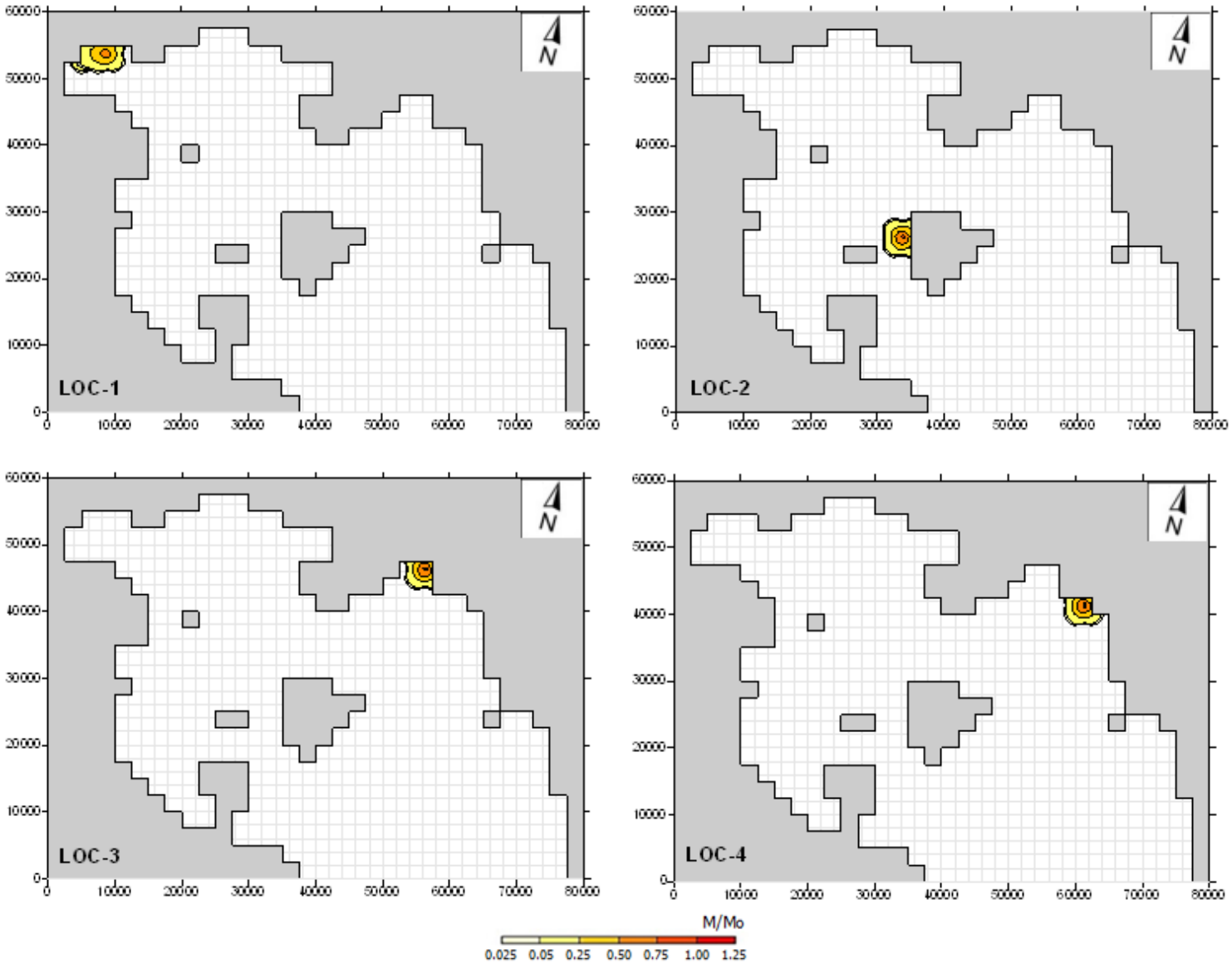

Figure AB34. Trajectory of the oil spill at the 4 locations examined for South-West wind - 4 bf

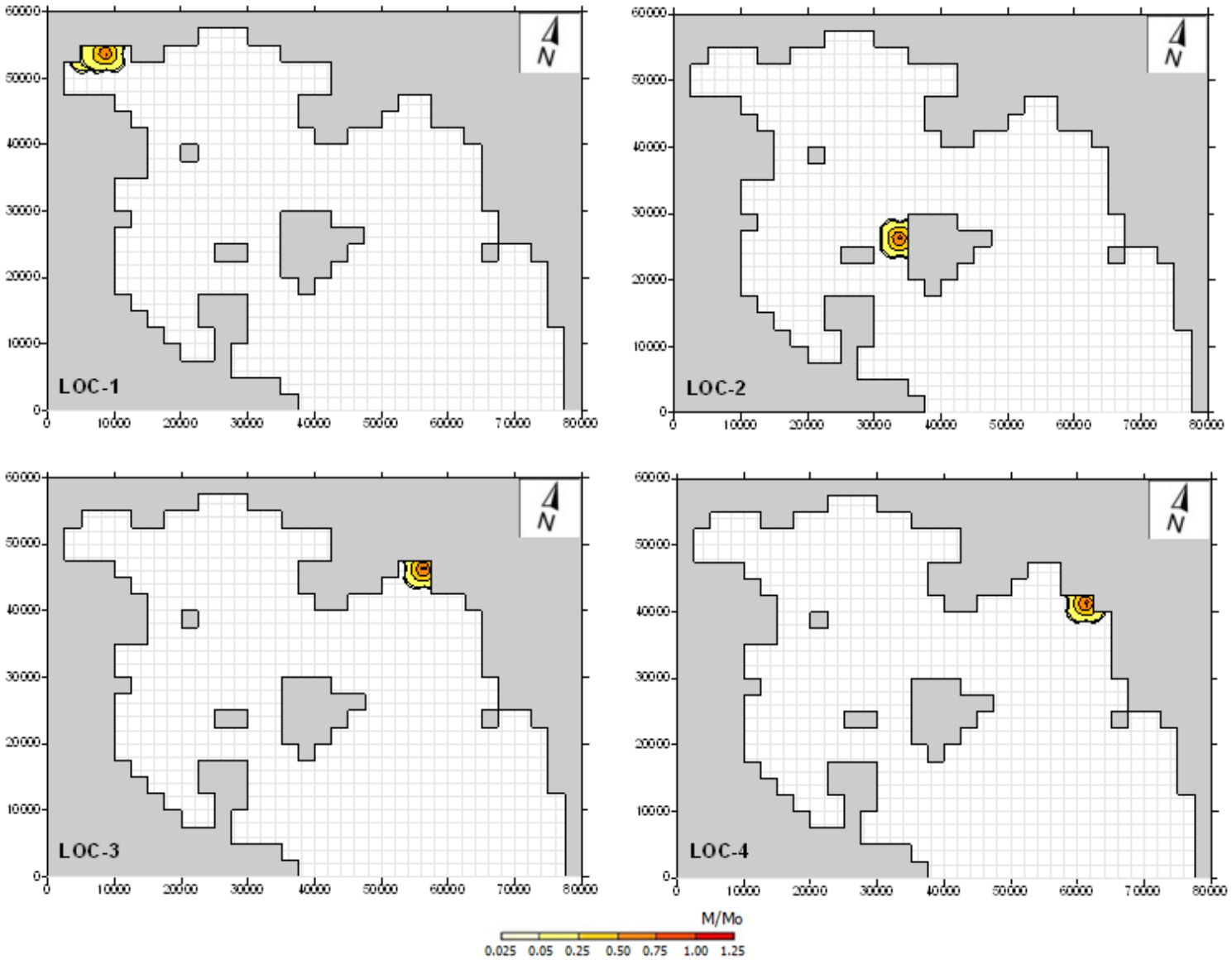

Figure AB35. Trajectory of the oil spill at the 4 locations examined for South-West wind - 5 bf

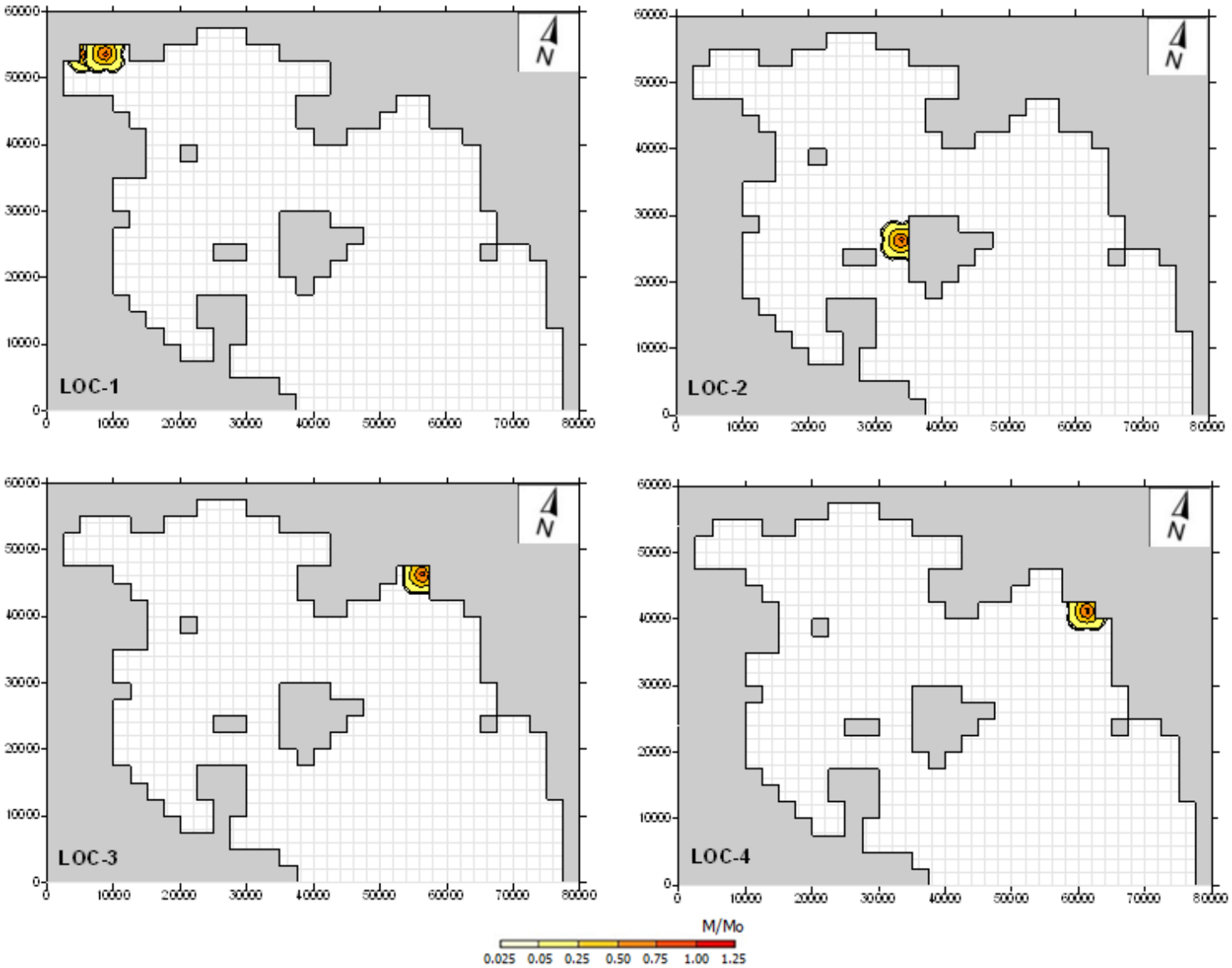

Figure AB36. Trajectory of the oil spill at the 4 locations examined for South-West wind - 6 bf

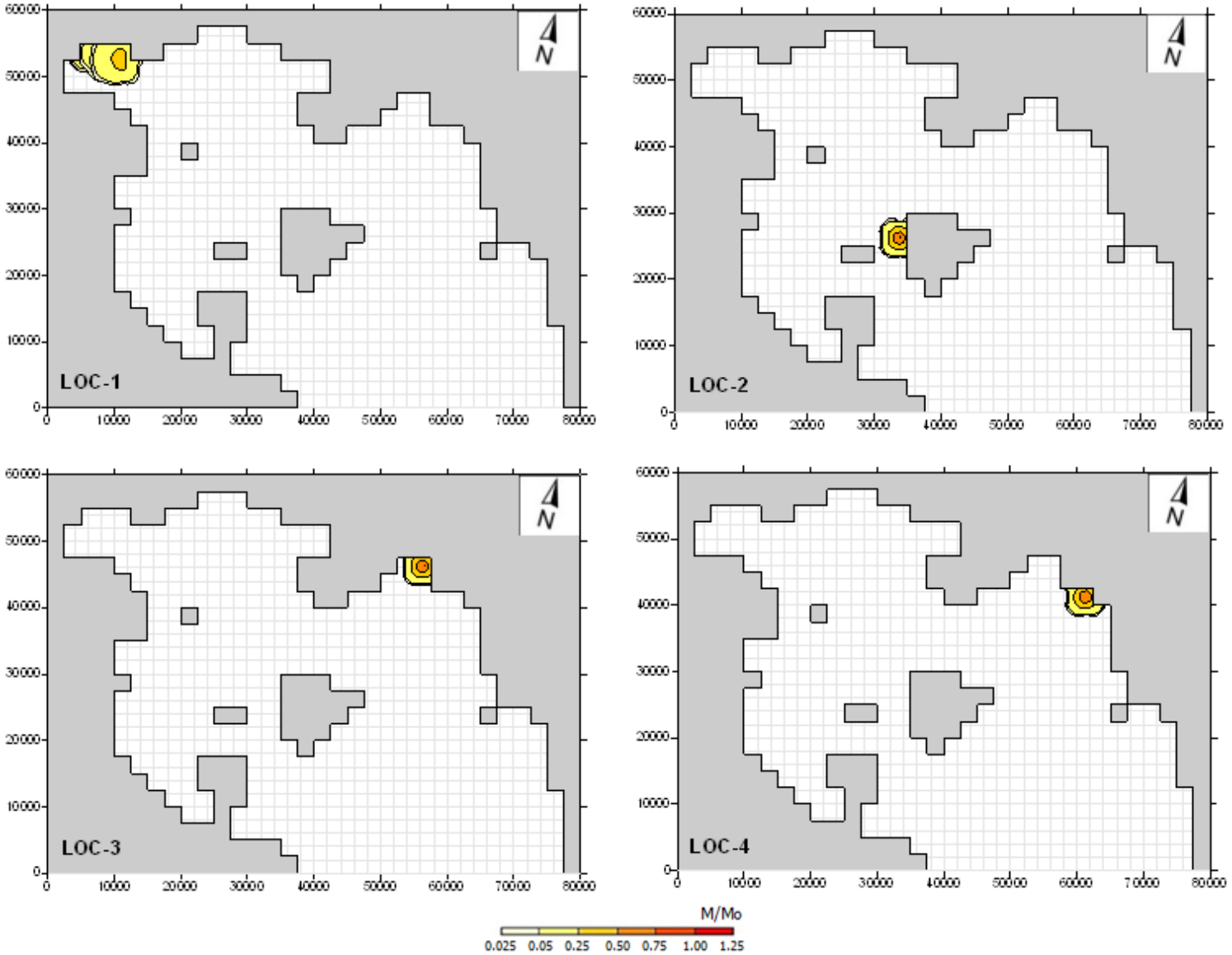

Figure AB37. Trajectory of the oil spill at the 4 locations examined for West wind - 1 bf

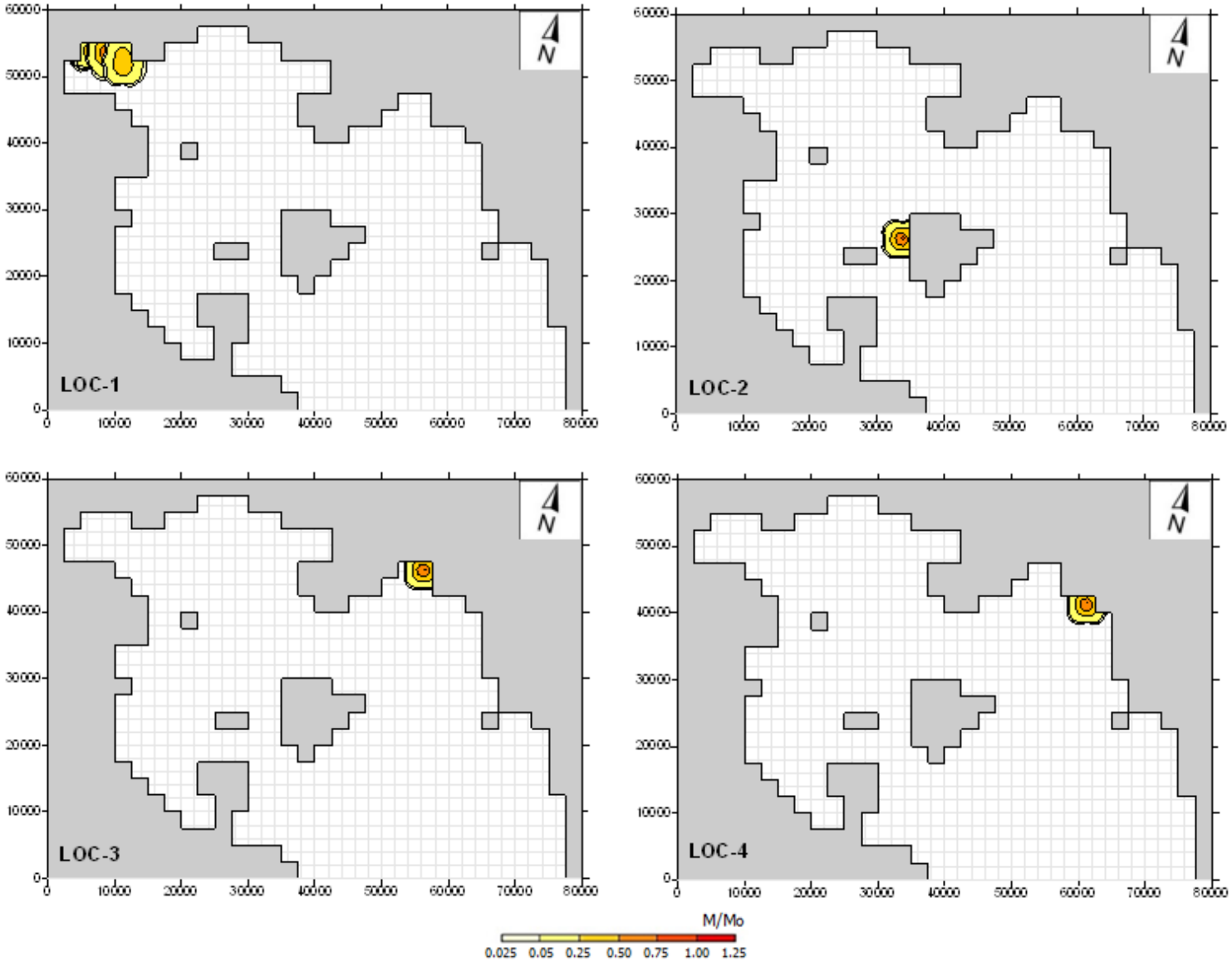

Figure AB38. Trajectory of the oil spill at the 4 locations examined for West wind - 2 bf

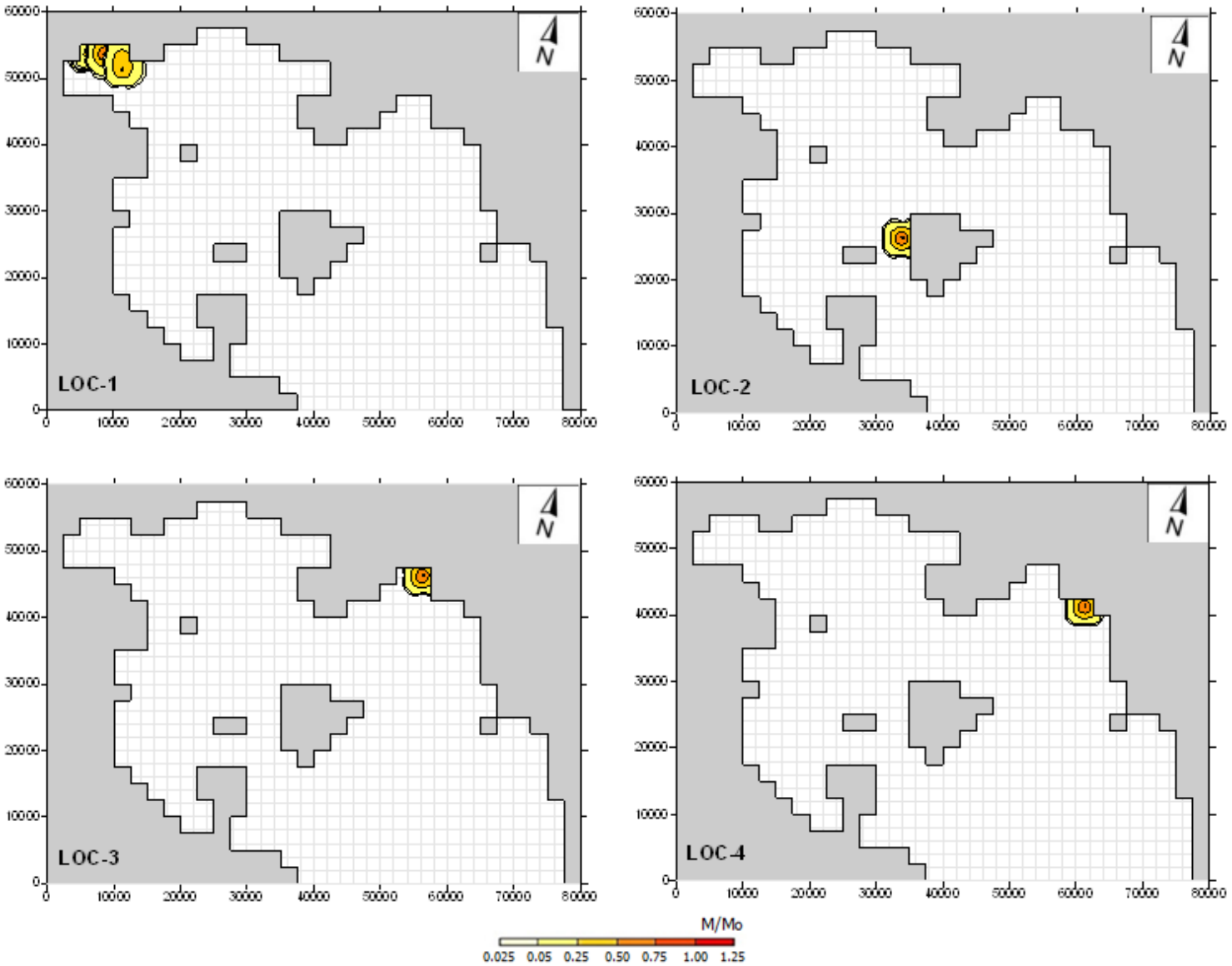

Figure AB39. Trajectory of the oil spill at the 4 locations examined for West wind - 3 bf

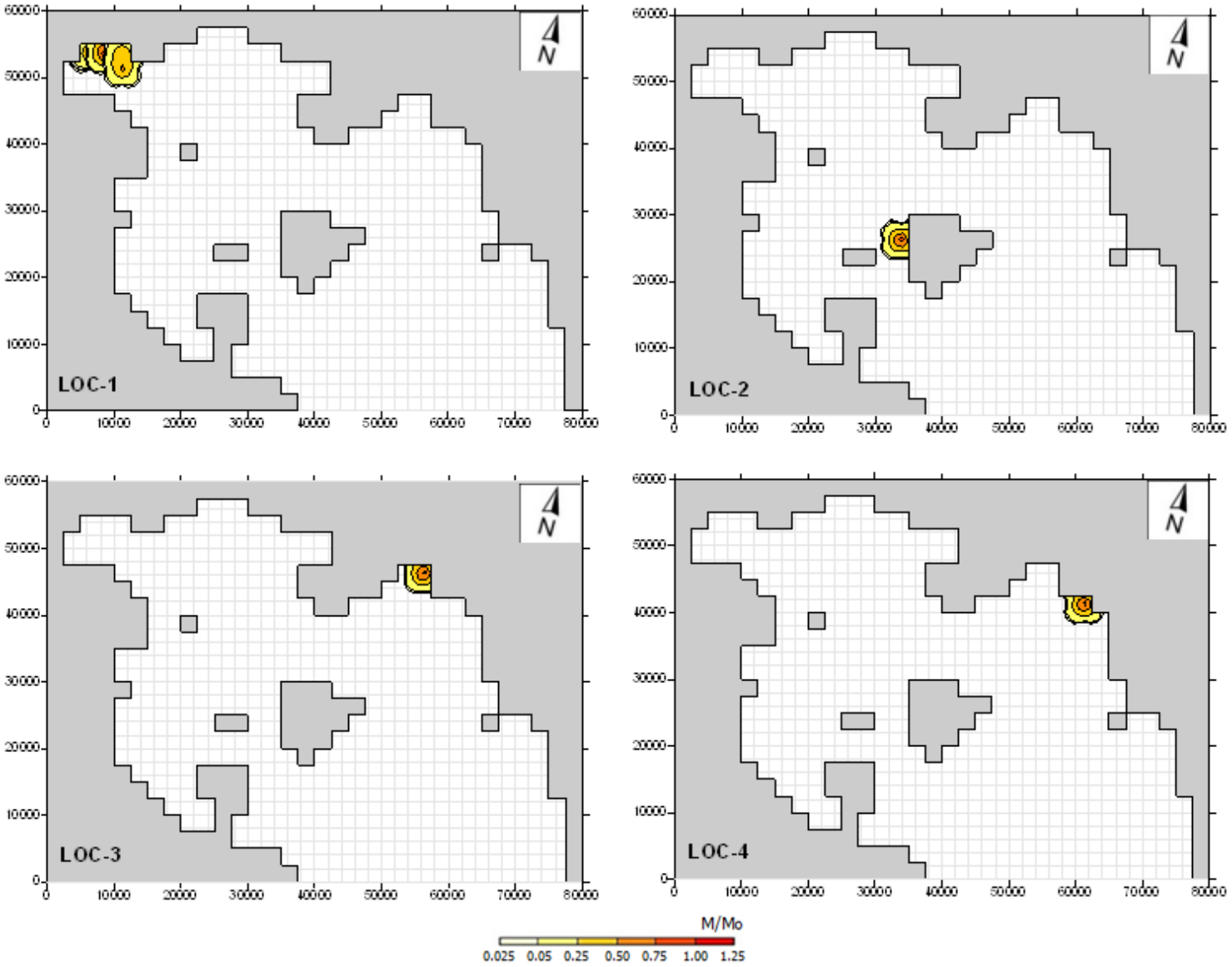

Figure AB40. Trajectory of the oil spill at the 4 locations examined for West wind - 4 bf

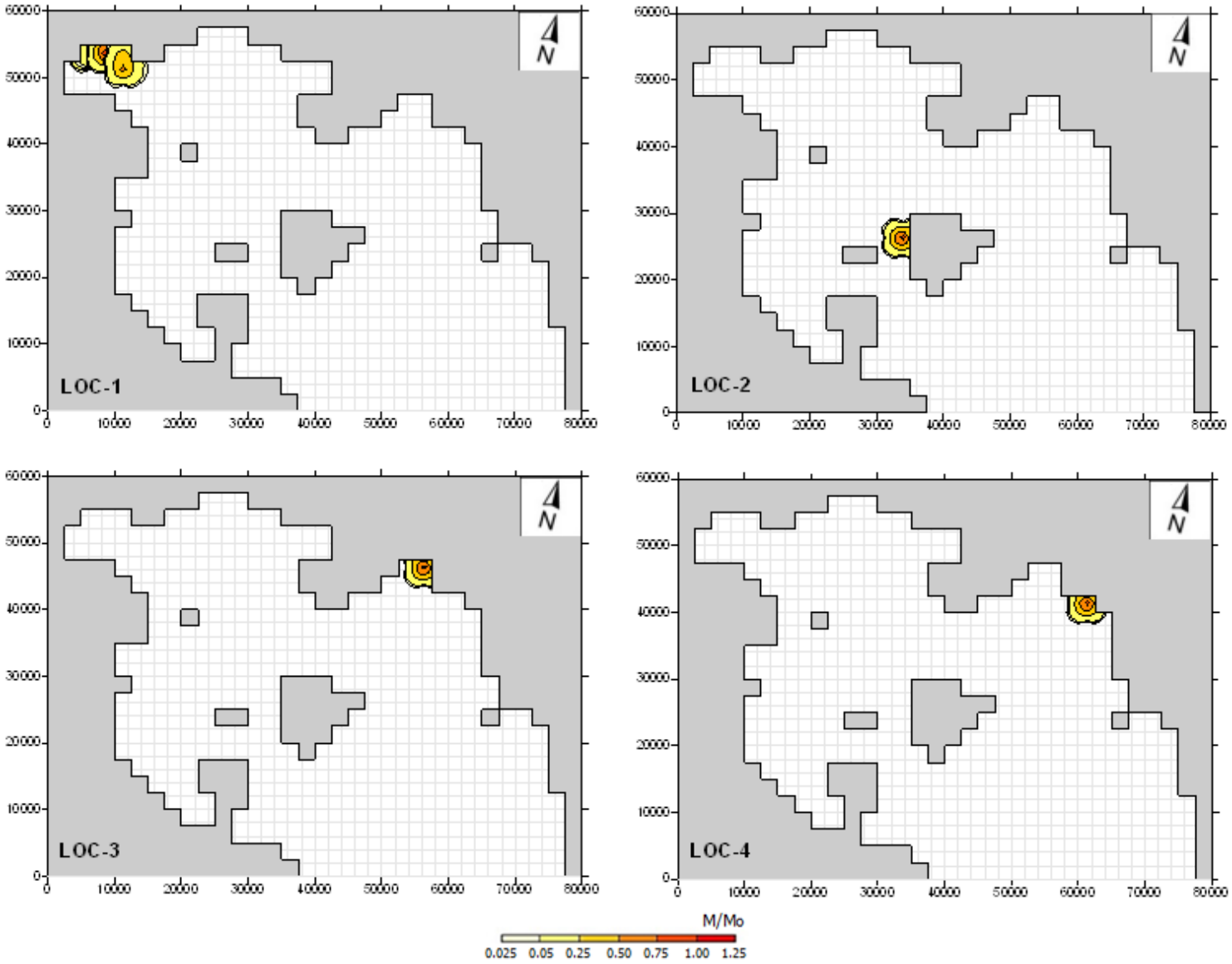

Figure AB41. Trajectory of the oil spill at the 4 locations examined for West wind - 5 bf

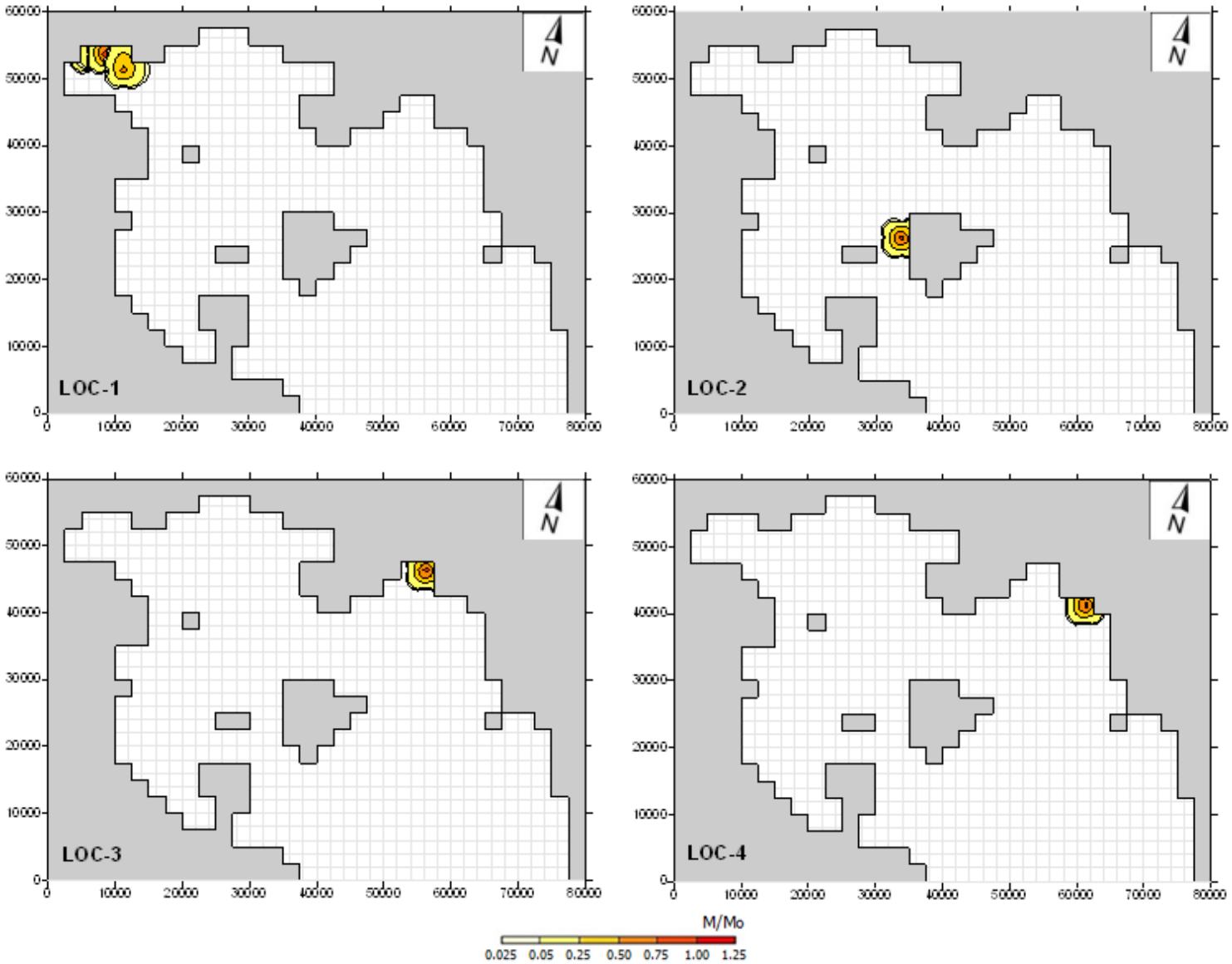

Figure AB42. Trajectory of the oil spill at the 4 locations examined for West wind - 6 bf

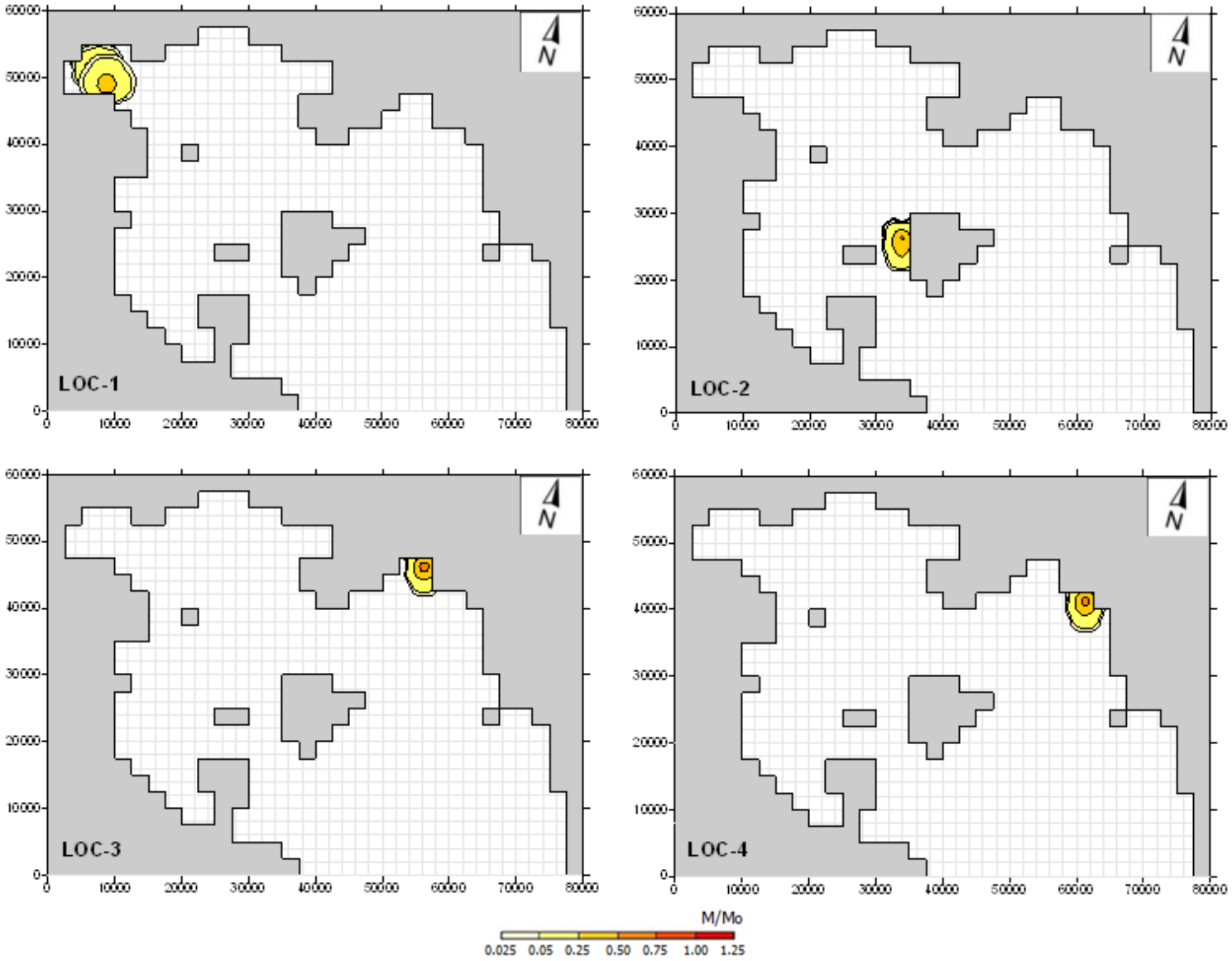

Figure AB43. Trajectory of the oil spill at the 4 locations examined for North-West wind - 1 bf

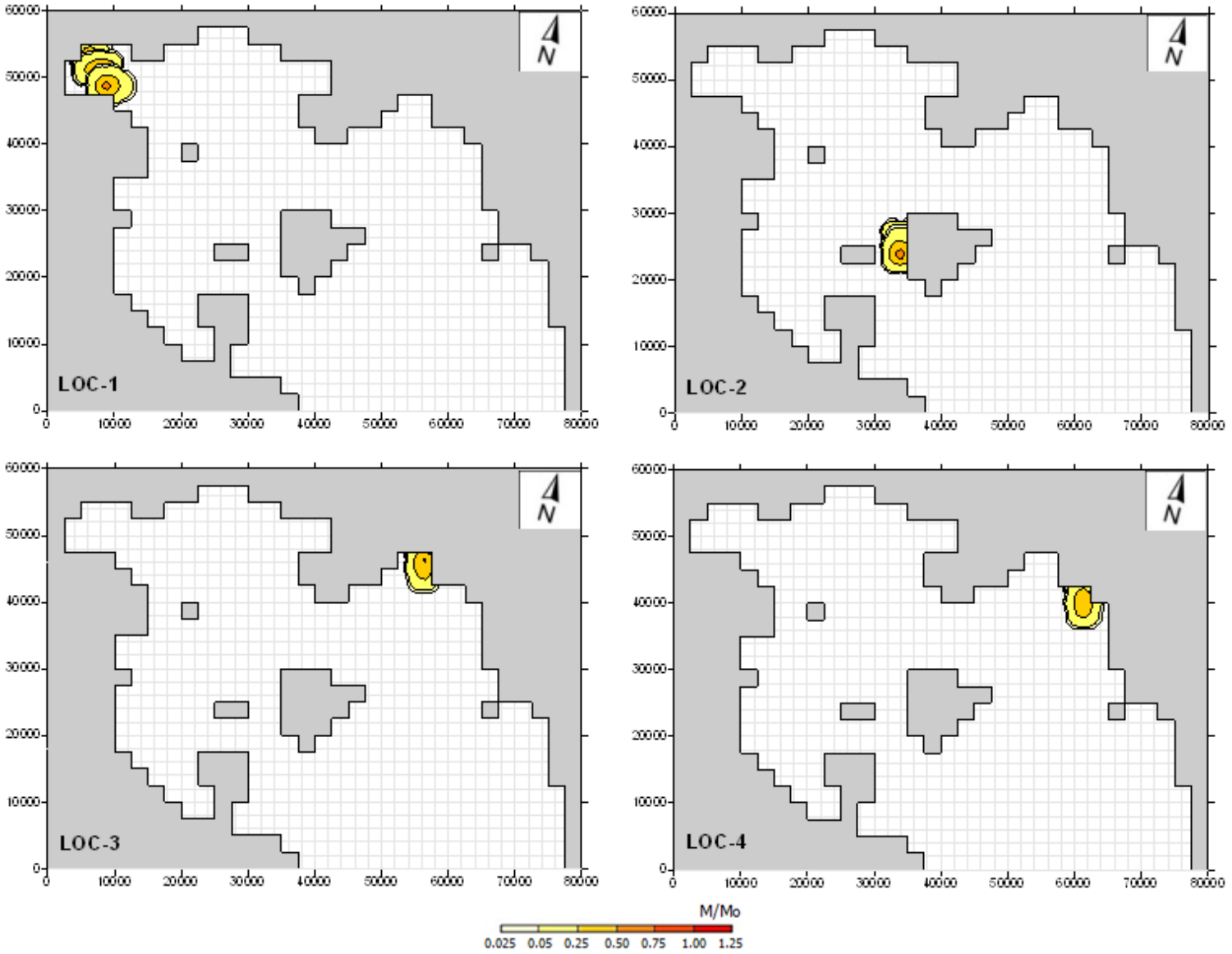

Figure AB44. Trajectory of the oil spill at the 4 locations examined for North-West wind - 2 bf

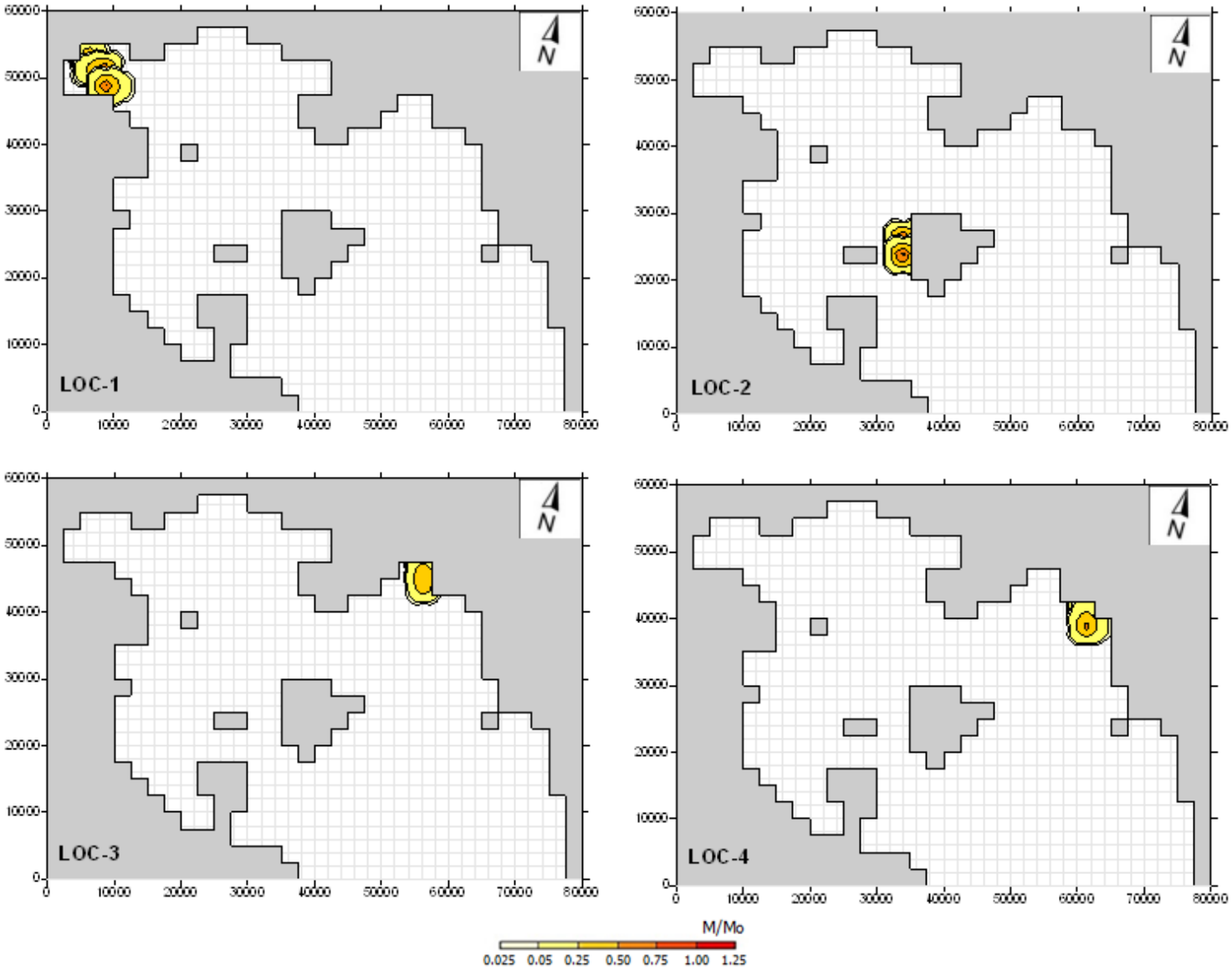

Figure AB45. Trajectory of the oil spill at the 4 locations examined for North-West wind - 3 bf

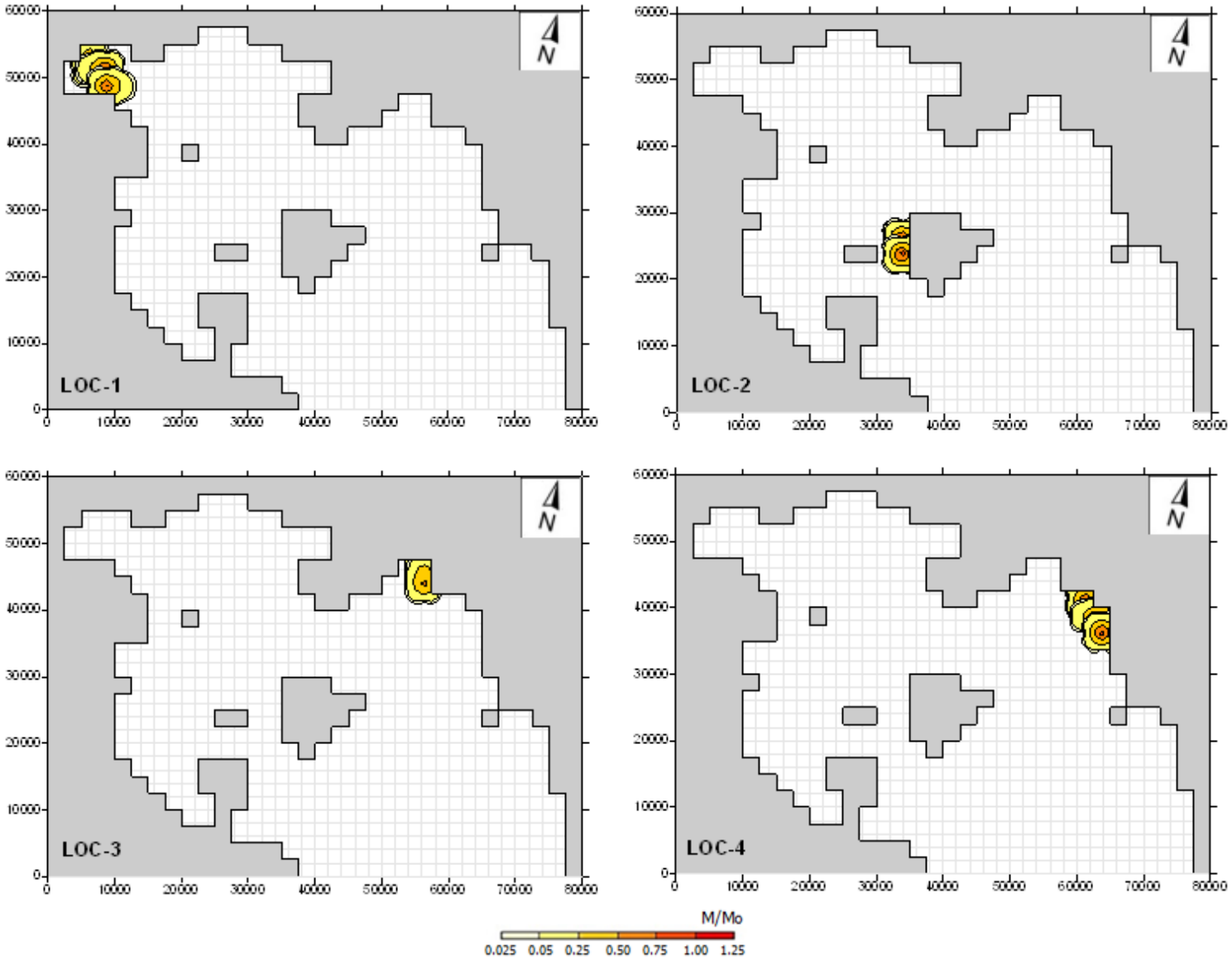

Figure AB46. Trajectory of the oil spill at the 4 locations examined for North-West wind - 4 bf

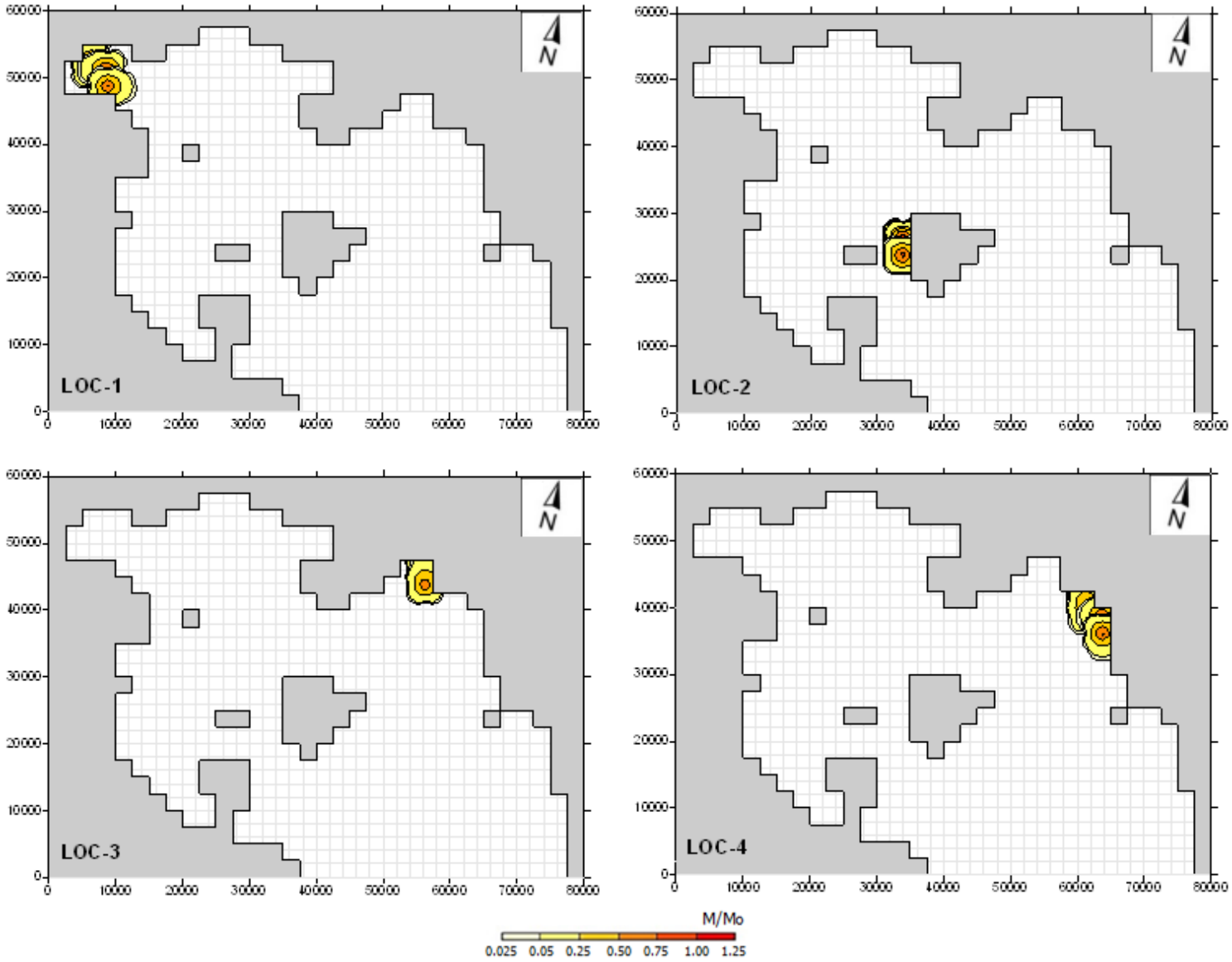

Figure AB47. Trajectory of the oil spill at the 4 locations examined for North-West wind - 5 bf

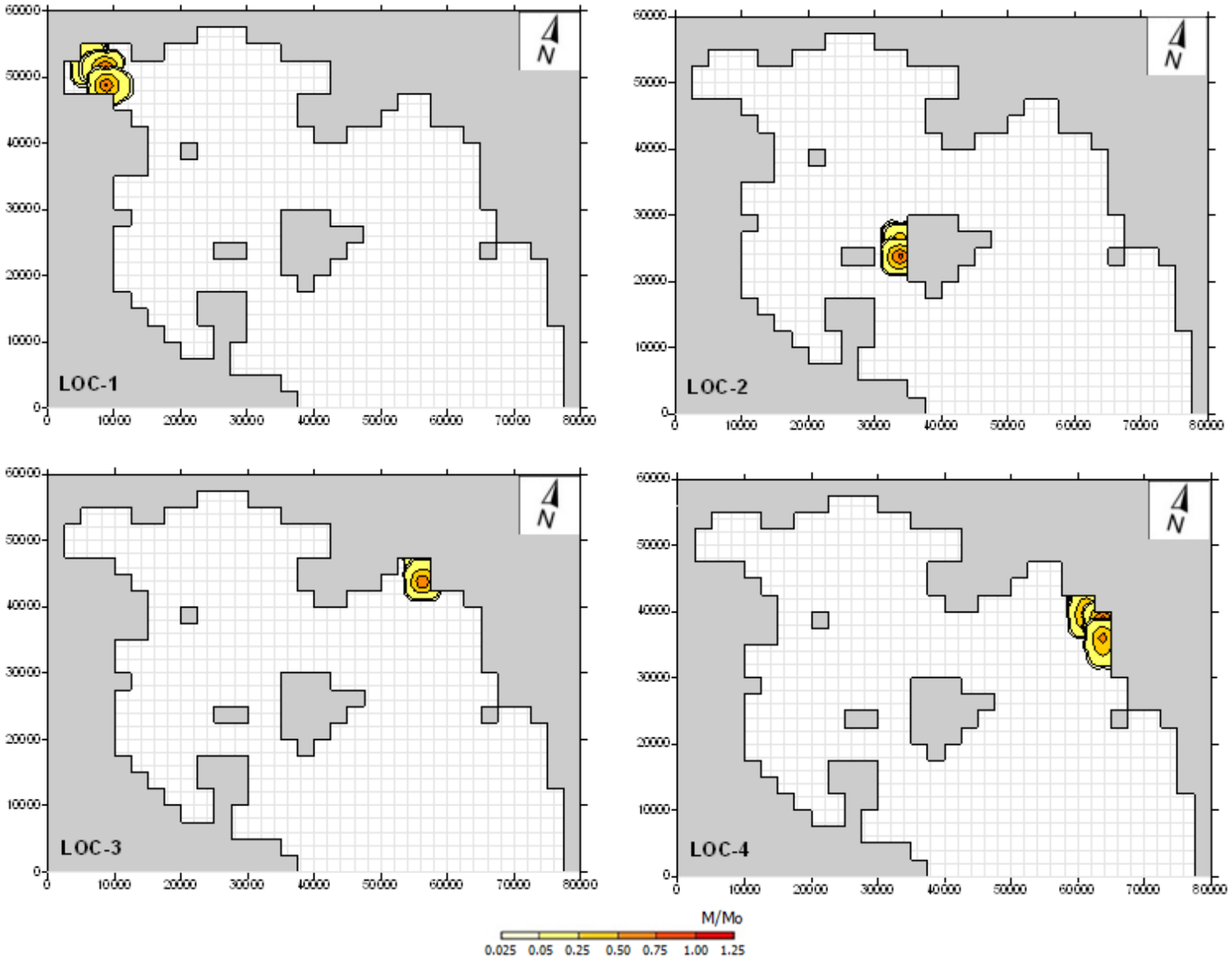

Figure AB48. Trajectory of the oil spill at the 4 locations examined for North-West wind - 6 bf

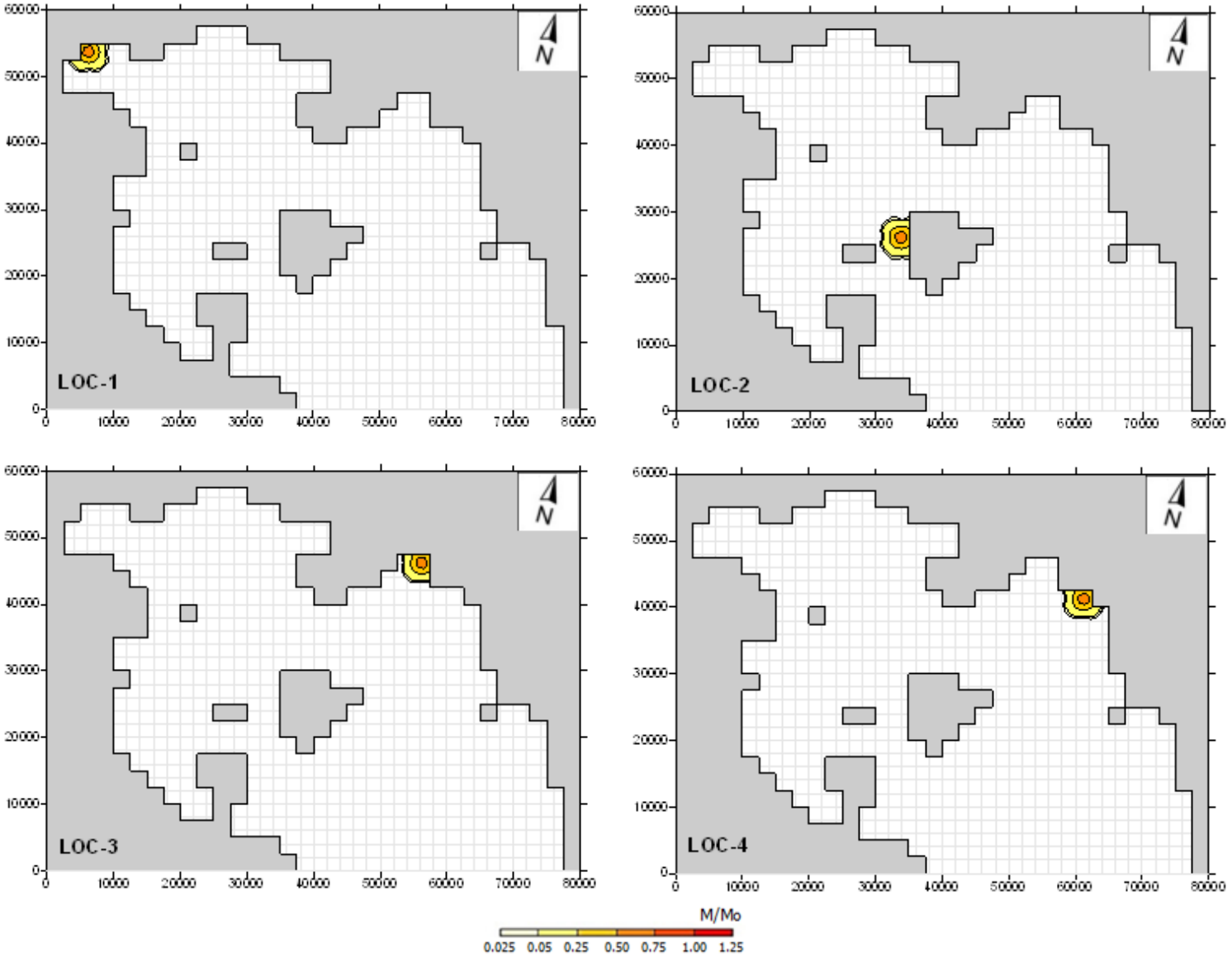

Figure AB49. Trajectory of the oil spill at the 4 locations examined for the no wind condition